2003

The Wind Effects on the Evaluation of Proposed Craney Island Expansions in the Lower James and Elizabeth Rivers

Momo Chen
College of William and Mary - Virginia Institute of Marine Science

The Wind Effects on the Evaluation of Proposed Craney Island Expansions in the Lower James and Elizabeth Rivers

---

A Thesis

Presented to

The Faculty of the School of Marine Science

The College of William and Mary in Virginia

In Partial Fulfillment

Of the Requirements of the Degree of

Master of Science

---

by

Momo Chen

2003

APPROVAL SHEET

This thesis is submitted in partial fulfillment of

the requirements for the degree of

Master of Science

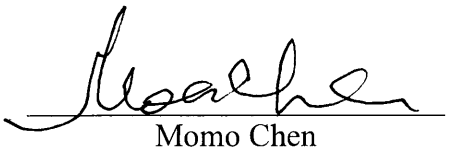

Momo Chen

Approved, April 2003

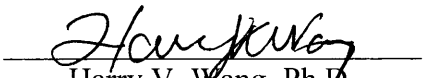

Harry V. Wang, Ph.D.
Committee Chairman/Advisor

Carl Hershner, Ph.D.

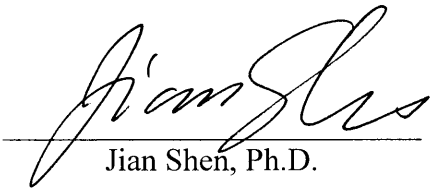

Jian Shen, Ph.D.

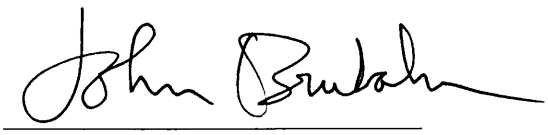

John Brubaker, Ph.D.

TABLE OF CONTENTS

Page

ACKNOWLEDGEMENTS

The majority of the data for this study were obtained from the Virginia Institute of Marine Science's Craney Island Eastward Expansion (CIEE) project field program. Appreciation is extended to all the members of the CIEE team. Through this CIEE study, I learned many techniques and skills, which contributed a lot to this thesis. Specifically, I would like to thank Mr. Mac Sisson for his inputs to this study and review of the manuscript. I also wish to thank my Advisory Committee members for their helpful suggestions and constructive reviews of this manuscript. Finally, one individual has been most influential in my academic and non-academic career: I would like to thank my advisor, Dr. Harry V. Wang, who taught me and broadened my knowledge about physical oceanography and numerical modeling.

LIST OF TABLES

LIST OF FIGURES

ABSTRACT

The hydrodynamic features in the lower James and Elizabeth River estuarine system are affected by a combination of effects from river discharge, tides, and winds. An analysis of field data from the VIMS CIEE field project and NOAA CO-OPS program reveal that wind can play an important role in regulating the estuarine system during episodic wind events. Different wind direction, magnitude and duration will have different impacts on the main hydrodynamic characteristics including water level, salinity, and circulation pattern. To further examine the cause-and-effect of wind forcing on this system, a three dimensional numerical model, HEM-3D, was applied to the James River and Elizabeth River system to investigate the dynamic aspects of wind-driven circulation and evaluate its impact in the proposed Craney Island expansion.

The three-dimensional model domain spans the entire James River (coarse grid), including the Elizabeth (fine grid). The dynamic features included are three-dimensional velocity field, water elevation, salinity and state of mixing. The model simulation period was from March through August, 2000. The VIMS CIEE measurement data was used as initial and open boundary conditions. The model was calibrated and verified, and proved to be able of reproducing the basic features that were observed from the field data.

Two sets of model experiments (Experiment I and Experiment II) were then conducted in order to perform sensitivity analyses. Experiment I focuses on the effects by single variable. Under conditions of no wind and no river discharge, tidal range proves to be the most important factor in controlling water level, the state of mixing, stratification, and resulting patterns of water circulation. Under variable river flow condition, the most impacted characteristic is surface salinity level, and thus the strength of stratification and gravitational circulation. When wind forcing was added on, extreme changes in water level, current, mixing, and circulation pattern emerged. Wind direction and magnitude appear to be factors in controlling the extent of those changes. Thus, the Experiment II was conducted to further investigate the effects of winds with different magnitudes and directions. Northeasterly and northwesterly winds induced greatest water level changes, causing water level rises/drop within several hours. Southeasterly and southwesterly winds can also raise/drop water levels in this lower James River estuarine system, but the changes are not strong and rapid as that caused by northeasterly and northwesterly. Downstream winds enhance estuarine circulation, and strengthen stratification. Conversely, an upstream wind might be able to reverse the circulation pattern. Also, wind serves as a strong mixing factor.

Finally, evaluations of two proposed Craney Island Expansion Designs (Option 7 and 7/5a) under wind events were conducted using global analysis and local analysis. It was found that the East Expansion (Option 7) produced less change among those global analysis variables than that caused by the East/West Expansion (Option7/5a). Local changes in the residual current field are not significant except in the vicinity of Craney Island.

The Wind Effects on the Evaluation of Proposed Craney Island Expansions in the Lower James and Elizabeth Rivers

CHAPTER 1

Introduction

1-1. Background Review

Previous studies have shown that wide estuaries respond to atmospheric forcing in addition to buoyancy and tidal forcing (Wang, 1979a, b). Wind can raise or lower the level of surface waters and occasionally reverse the direction of flow. For instance, the first major study of this was a one-year-long series of current measurement in the Potomac Estuary by Elliott (1978). His study shows that a downstream wind would enhance the surface outflow and increase the vertical mixing and the bottom inflow; when the wind blows upstream, the classical estuarine circulation may be reversed, with inflow on the surface and outflow on the bed. Van de Kreeke and Robaczewska (1989) show that, for the Volkerak estuary, a down-estuary wind increases the vertical exchange of momentum and decreases the gravitational circulation. Wind-induced current amplitude is typically larger than the gravitational (density-driven) component and can be of the same order as the tidal current during the wind events (Wang and Elliott, 1978).

Changes in water level and surface slope along the estuary are strongly correlated to local winds (Elliott, 1978). Observation of currents in the Potomac

showed that this estuary responded baroclinically to local meteorological forcing: a downstream wind blew surface water out of the estuary causing a reduction in the mean water level and setting up a surface slope from head to mouth. These were accompanied by a strengthened return flow at mid-depth and near the bottom. In contrast, an upstream wind could increase the water level in the estuary and reverse the direction of estuarine circulation (Elliott, 1978). Similar wind effects have been observed on many other estuaries (Wang and Elliott, 1978; Wang, 1979 a, b).

Wind direction and magnitude can affect the salinity distribution as well as water level. During a study in the York River, it was found that wind stress factors correlated most strongly with salinity difference were those axial to the upper and lower York River Basins from the north and northeast (Hayward et al., 1986). If wind blew in the upstream direction, it would force high salinity water from the lower estuary towards the upper estuary, increasing salinity at up-estuary locations. Downstream winds would force freshwater from the upper estuary toward the lower estuary, decreasing the salinity there. Wind is also a contributing factor to induce greater mixing between surface and subsurface layers, as well as leading to a less vertically stratified system. The magnitude of these effects would increase with increasing wind magnitude and duration.

Wind-induced mixing is neither local nor confined to surface waters. Synoptic observations from five current meter arrays in autumn 1981 (Goodrich, 1985) show that well-mixed conditions could extend over a distance of 130 km and to a depth of 29 m. A homogeneous water column persisted during a one-

month period for at least one of these stations. Observations and modeling of periodic stratification in the upper York River (Sharples et al., 1994) show that a number of transitional mixing events caused by peaks in the surface wind stress are superimposed on the spring-neap tidal signal. Indeed, the wind-mixing events appear at least as important as strong tides in remixing the predominantly stratified water column.

Wind events may tend to alter stratification by this advective and mixing mechanism. A down-estuary wind would advect fresher surface water seaward while more saline bottom water would move up the estuary, increasing stratification. The analogous destratification effect would be achieved by an up-stream wind. With the relaxation of the wind events, self-adjustment of hydrodynamic features will take over. Surface slope setup by an upstream wind will induce barotropic flow, which will reinforce gravitational circulation. The homogeneous water column induced by a wind event will restratify, if the weakening of wind coincides with a relatively weak mixing forcing (i.e., neap tide), and enhanced stratification may occur (Valle-Levinson et al., 1998).

1-2. Study Area

The study area (Figure 1-1) spans from the James River entrance to the limit of tide at Richmond, including the major tributaries of the James River, and extends to the innermost reaches of the Norfolk Harbor and the Elizabeth River.

The James River estuary is the southernmost major tributary to the Chesapeake Bay. Pioneering works on estuarine dynamics in this partially mixed

estuary have been done here in the lower James (Pritchard, 1952, 1954, 1956). In the early studies, the direct influence from James River discharges and by tides subject to spring-neap modulation was extensively studied. Tides and tidal currents are predominantly semi-diurnal with a mean tidal range of about one meter. The three major constituents are, in order of importance, M_2, N_2, and S_2, with the M_2 bearing ~80% of the total energy of the signal (Browne and Fisher, 1988). Spring-neap variations for both tides and tidal current were reported and result in a periodic stratification-destratification in the estuary (Haas, 1977). The salinity stratification, principally governed by variation in tidal range at the mouth and fresh water discharge at the head of the river, is one of the main factors controlling the behaviors of three-dimensional circulation and material transport in the lower James River (Kuo et al., 1988, 1990; Shen et al., 1999).

The special geomorphological features also play an important role here. Near the Hampton Roads area, the lower James River displays a bathymetry that consists of a deep channel, the Newport News channel, and a shallow area, Hampton Flats. Shen and Kuo (1999) suggested that the higher friction on the shoal is the primary factor for the phase lead of the current on the Hampton Flats, and that, in turn, contributes to the formation of the estuarine front and its associated eddy. Geyer (1993) and Chant and Wilson (1997), however, suggested that the sharp bend in orientation of the estuary around Newport News possibly induces centrifugal accelerations that could influence the dynamics in the vicinity of the headland. These effects could be manifested in the form of secondary flows consisting of near-surface normal flow away from (and near-bottom normal flows

towards) the headland. This eddy and front are believed to be the main factors that contribute to the James River's success in seed oyster production (Hargis, 1966, 1969; Marshall, 1954; Pritchard, 1952; Wood and Hargis, 1971; Haven et al., 1978; Shen et al., 1999).

The Elizabeth River is a highly branched tributary of Hampton Roads, which includes the cities of Norfolk, Portsmouth, and Chesapeake. It receives little fresh water and has a modest tidal circulation. The tide in the Elizabeth River behaves much like a standing wave, with inflow (flood current) being directly related to a rise in tidal height. The surface circulation in the Elizabeth River, controlled by tide, wind, and freshwater inflow, is highly weather dependent. Wind can drive circulation, in addition to the tidal circulation, in its predominant direction. The exchange of water between the Elizabeth and Hampton Roads depends on tides and the non-tidal circulation set up by density gradients and wind-driven circulation. During periods of low freshwater inflow, a relatively homogeneous water mass exists in the Elizabeth River system.

Craney Island is a dredged material containment area located near the entrance of the Elizabeth River, which has received maintenance and permitted dredged material from numerous dredging projects in Hampton Roads and the Lower Chesapeake Bay region since the 1950's (U.S. Army Engineer District, Norfolk 1974). To increase the Craney Island capacity and extend its useful life, several expansion design options (i.e., to the east, north, west, and northeast of the Craney Island) were proposed. These are shown in Figure 1-2.

1-3. Objective

To examine the cause-and-effect of wind forcing on the lower James estuary, a series of field data will be employed first to describe the wind effect on the estuarine system. The primary data to be used in this study are the long-term current meter records obtained from fixed time series measurement and slack water surveys in conjunction with river discharge, water level, and wind data (Wang et al., 2001).

After the field data analysis, numerical model experiments will be conducted. First, an isolated, single wind event of seven days will be investigated relating wind forcing to tidal elevation, salinity, and the circulation pattern. Then a longer period (six months, from March – August, 2000) will be simulated to examine the wind effect with and without the wind forcing. Here, all the set up for the numerical model remains the same, except for the wind forcing.

VIMS conducted the study using a rational technique for evaluation of these Craney Island expansions (Wang et al., 2001). The technique is based on analyzing the results from a three-dimensional numerical model, HEM-3D, applied in the James/Elizabeth River system. The criteria used for the evaluation consist of (1) physical parameters (tidal elevation, velocity, salinity, and sediment potential), (2) flushing and transport capability, and (3) special features (frontal and eddy systems). To assess the effects of each expansion, they first conducted a global analysis under a quasi-periodically stationary process, comprised of measuring root mean square differences throughout a broad area. Then, they performed a local analysis for the effects in more localized areas. The GIS

software package ArcView was extensively used. Event-driven processes were also considered.

Based on the above efforts, we know that the hydrodynamic characteristics (i.e., water level, salinity, and velocity) of this estuarine system are strongly affected by the external forcing from river discharge, tides, and wind events. In the VIMS CIEE study, the single variable approach was used extensively. This approach, sometimes also called "one-at-a-time" approach in the context of statistical experiment design, examines the effect of a single variable by varying levels of this variable while holding other independent variables fixed. This process continues until the effect of each variable on the response has been examined while holding other independent variables constant. The single variable run approach works well with the forcing by tide and river discharge, but not for wind. Tides and river discharge have only a limited number of degrees of freedom. In contrast, the wind is composed of different magnitudes and directions. Furthermore, the wind effect is not confined to the local region, but also extends to the far field.

The overall objective of this study is to demonstrate a fundamental understanding of the wind effect on the Elizabeth and lower James estuarine hydrodynamics, and to evaluate its effects on the proposed expansions of Craney Island. A descriptive approach will be employed first to examine the cause-and-effect of wind forcing, next to analyze the wind consequences, and, finally, to conclude with results from the numerical model on both long and short time scales.

This thesis is composed of six chapters:

Chapter 1 – a review of the former studies on wind effects on estuarine systems and a description of the study area and objective of this thesis.

Chapter 2 – a description of the phenomenon observed from field program data analysis.

Chapter 3 – an application of a three-dimensional model to the Lower James and Elizabeth River system.

Chapter 4 – a model sensitivity analysis to evaluate the role of individual external forcing.

Chapter 5 – a description of the methods for evaluation of Proposed Craney Island Expansion under Wind Events.

Chapter 6 – a summary discussion and conclusions of this study.

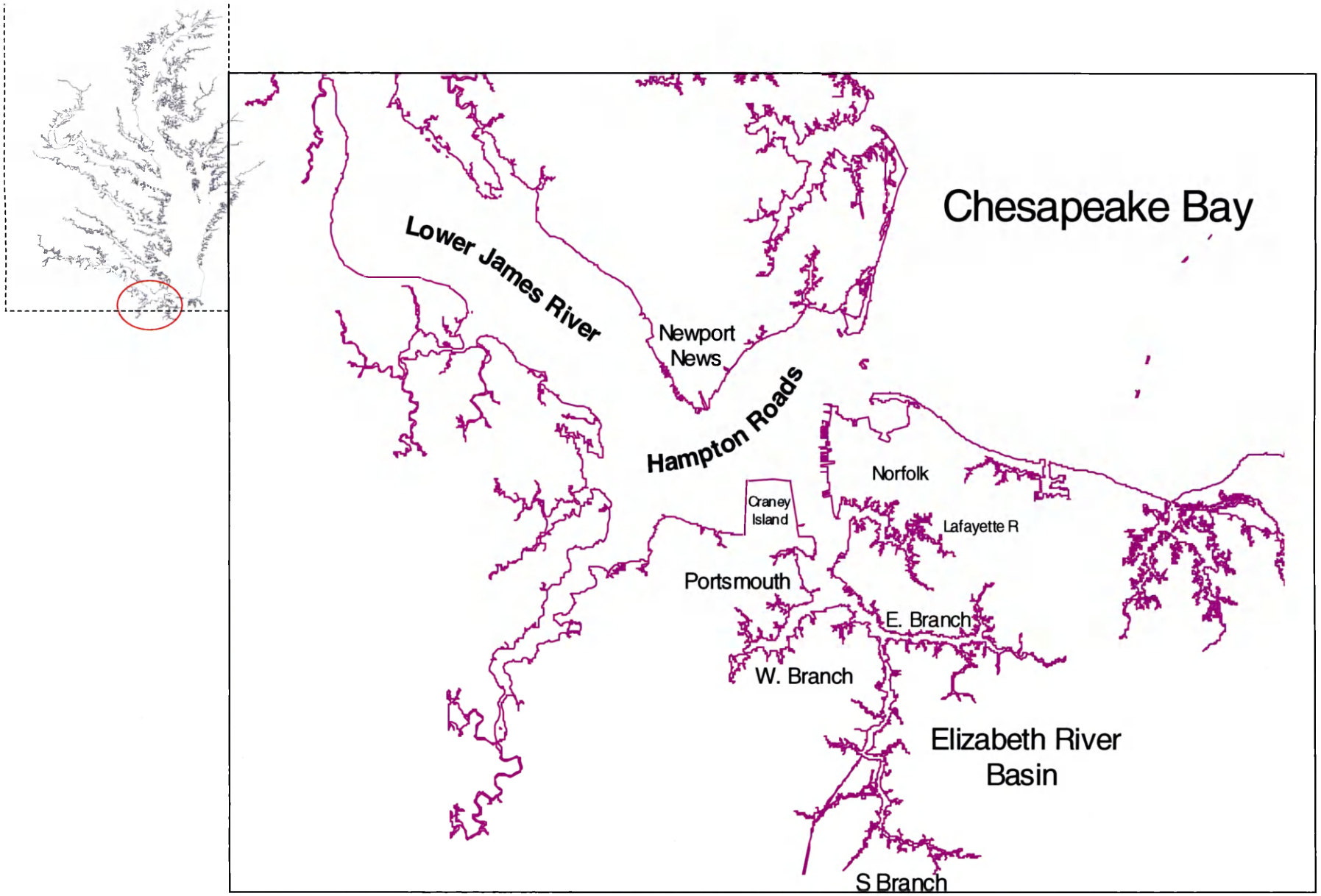

Figure 1-1. Study area-The lower James River and Elizabeth River system

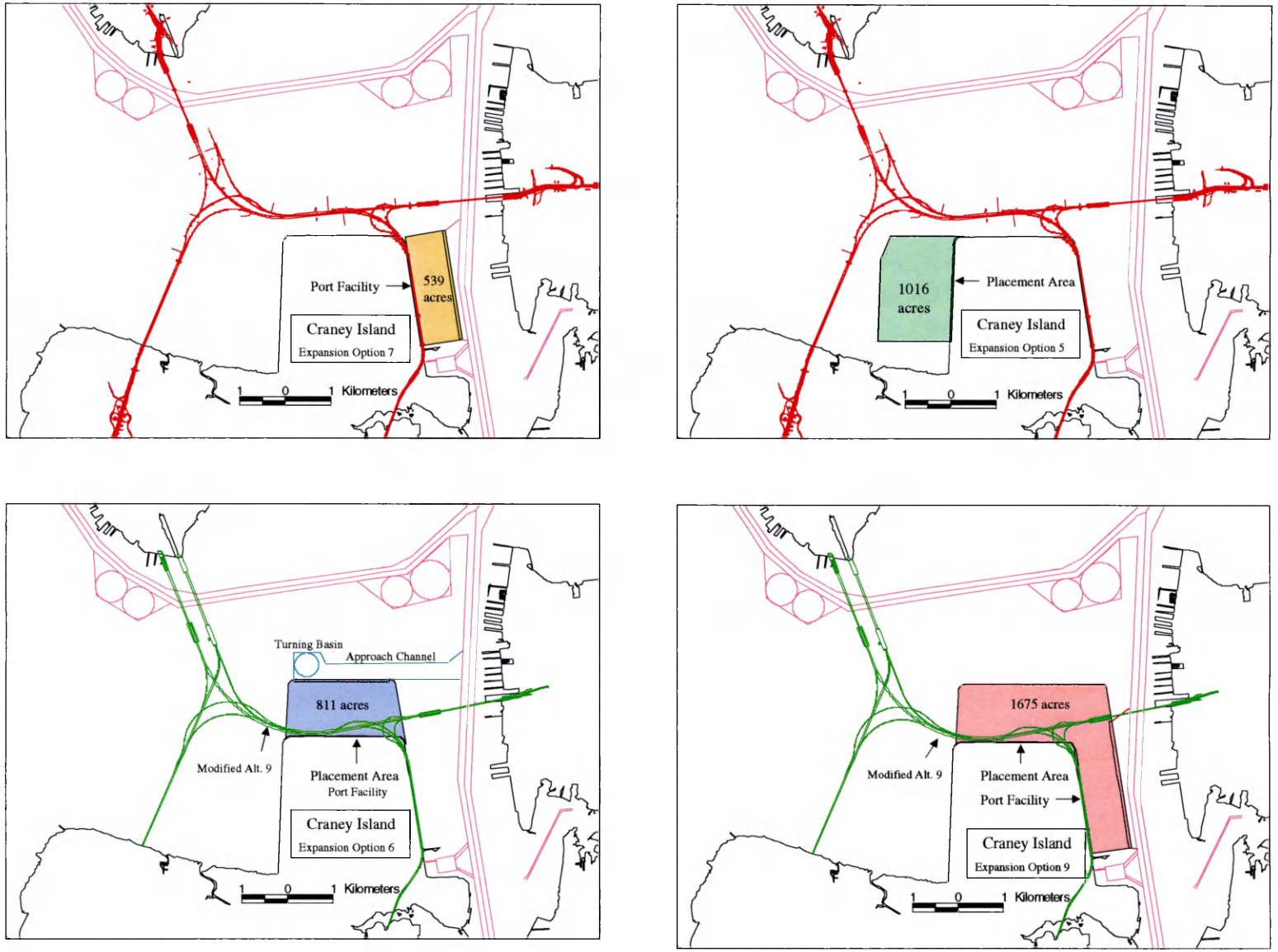

Figure 1-2. Expansion design options for CIEE

CHAPTER 2

Field Observations

A set of field programs was conducted during the VIMS CIEE project study. Time series of currents were obtained at three locations. A fixed (bottom mounted) ADCP unit was installed on the eastern side of the Norfolk Harbor Channel within the Craney Island Reach in the Elizabeth River. A moored current meter array was deployed, consisting of three InterOcean Systems S4 current meters mounted at surface, middle, and bottom depths on a taught-wire submerged buoy platform near Hospital Point between Port Norfolk Reach and Town Point Reach. Additionally, two InterOcean S4 current meters with CTD sensors were installed near Thimble Shoal Light outside the entrance to Hampton Roads. These two S4 meters provided time series of temperature and salinity at near-surface, mid-depth, and near-bottom positions in the water column from April 15 to June 8, 2000, for input to the model at its open boundary.

To discern the along-channel distribution feature of physical characteristics (i.e., salinity and temperature), a total of 12 slack water surveys were conducted from April 24 to October 18, 2000, using a cable-mounted CTD probe for measuring temperature and salinity along the longitudinal axis of the Elizabeth River. Twenty stations along the Elizabeth River main-stem and several stations in its branches (2 in the Eastern Branch, 3 in the Western Branch, 3 in the

Lafayette River, and 3 in Deep Creek) were selected as the slack water survey sampling locations. At each location, continuous over depth, salinity and temperature were collected.

Episodic wind events do occur. These range from day-to-day weather fronts, winter extra-tropical storms, to tropical hurricanes. The winds generated by the atmospheric circulation are random motions, which exert wind stress on the water surface. The water moved by the wind depends on its direction, magnitude, and the characteristics of the adjacent landscape. In order to obtain information of the wind effects on water levels and the circulation pattern during episodic wind event in the lower James system, a set of observation data from NOAA recorded for the September 15-18, 1999 storm events will be discussed in this chapter.

2-1. VIMS CIEE Field Program

In this section, time series of water level observed at Sewells Point, and salinity and current profiles (surface and bottom) observed from Thimble Shoal Light and Hospital Point in the Elizabeth River, will be presented. In order to gain insight into the wind forcing consequences on these hydrodynamic characteristics, an initial data processing will be conducted for records of water level, salinity, and current using a low-pass filter to remove diurnal, semidiurnal, and other high frequency fluctuations.

2-1-1. Wind Data

The hourly recordings of wind speed and direction measured at Sewells Point were obtained from NOAA, as shown in Figure 2-1. A plot of frequency

distribution of hourly values for each 15° interval of wind direction is shown in Figure 2-2. Based on Figures 2-1 and 2-2, it appears that strong wind events occur quite frequently, and the most frequent wind is from the south (southwest or southeast). Although the northeasterly wind doesn't blow as often as the southwardly wind during this period, it could cause significant changes in water level (setup), salinity, and current structures.

2-1-2. Water Level

The hourly recorded water level from March 1 – August 1, 2000 at Sewells Point is shown in Figure 2-3, which is the low-pass filtered water level. Extreme water level events (rising or falling by 0.25 m) were highlighted with arrows. By correlating this series with wind velocity data, it can be seen that:

a) The largest water level rise (greater than 0.3 m) directly corresponds to the northeasterly wind. For instance, the northeasterly wind events occurred on Julian days 82, 110, 116, 150. A weaker event, for instance, on Julian days 62, 72, 77, 132, and 159, increased water levels by 0.15 m to 0.23 m. Even a short period northeasterly wind event, limited to a one-day duration, was shown to cause a rapid water level rise within several hours.

b) The greatest water level drop is associated with northwesterly wind (i.e., on Julian days 96 and 100).

c) Southwesterly wind drops the water level, too (i.e., on Julian days 140, 180, and 122). Usually, southwesterly wind with a duration of 2-3 days causes a larger water level variation, but not as rapidly as does a northeasterly wind.

d) Southeasterly wind could raise water level as well, but only on the order of 0.1 m - 0.15 m (i.e., on Julian days 165, 112, and 78-80).

In summary, strong upstream wind (i.e., northeasterly/southeasterly wind) pushes Bay water into the lower James, producing an exceptionally high water level. In contrast, strong downstream wind (i.e., northwesterly/ southwesterly wind) pushes the water out of the James, and drops the water level in the estuary. For a southeasterly/ southwesterly wind, a relatively longer duration is required to produce a response compared to the winds from the north; a possible explanation is due to the land effects (Paraso and Valle-Levinson, 1996).

2-1-3. Salinity

Fixed salinity measurements at Thimble Shoals (TSCW) and Hospital Point (HSPT) were conducted during the period from April 15 to June 8, 2000. At both stations, surface, middle, and bottom salinities were measured at an interval of half an hour. In this analysis, the surface and bottom salinity are plotted in two time series, as shown in Figure 2-4.

At both stations, a significant bottom salinity decrease on Julian day 150 is associated with a strong northeasterly wind that day. At station HSPT, the water column is less stratified than that at station TSCW, indicating more active vertical mixing in the Elizabeth River than in the Lower James and/or reduced influence of buoyant water. Surface to bottom salinity difference at HSPT is lower than at station TSCW, which is a consequence of stronger vertical mixing. Also, it should

be noted that local vertical mixing tends to have a greater effect on bottom salinity than on surface salinity.

When the surface to bottom salinity difference was taken, the stratification -destratification pattern emerges at both stations. One can see on Julian days 150-160, the water column was well mixed, while on Julian days 115 and 122, the water column was strongly stratified. This pattern was also independently verified by the slack water survey along the Elizabeth River, shown as an example in Figures 2-5a to 2-5b, during this period. On one hand, there is the longitudinal salinity difference that provides a source of baroclinic pressure gradient force, and thus sets up the stratification by the gravitational circulation. On the other hand, turbulent mixing from tides and atmospheric forcing tends to homogenize the water column in both the vertical and horizontal directions.

In order to have a depiction of the longitudinal and vertical trend in salinity, data received from slack water surveys were plotted in Figures 2-5a to 2-5f.

From these plots, an alternately stratified and de-stratified salinity pattern was observed along the Elizabeth River, which maybe coincides with the tidal spring-neap cycle. In addition to tides, winds also contribute to the mixing process. The mixing process in the Elizabeth is sufficiently strong to overcome the vertical and longitudinal salinity gradients. Strong stratification in Hampton Roads can be caused by sharp increases in the freshwater flow upstream, and the strong stratification will extend into the Elizabeth River. As an example, Figure 2-5a shows the longitudinal salinity structure on Julian day 122 after the passage of

the peak flow at Richmond on Julian day 110. Water columns, at both Hampton Roads and Elizabeth, are strongly stratified.

One noteworthy point is that this longitudinal variation might be caused by a net transport between Hampton Roads and the Elizabeth. During periods of stratification, there is a very substantial net non-tidal flow, which is set up by the density gradients, and flushing of specific water masses is enhanced. The water masses include both saltier water moving into the Elizabeth near the bottom and freshwater moving out to Hampton Roads near the surface. During periods of homogeneous or well-mixed conditions, this non-tidal flow does not exist. Therefore, the flushing of the Elizabeth is poorest during these periods and the residence time of water in the Elizabeth is increased.

Also, during the slack water surveys, a reversed salinity gradient in the mouth region of the Elizabeth River was consistently observed. The simultaneous measurement of ADP profile indicated that, when the reversed surface salinity occurred, a significant portion of the non-tidal velocity profile was also reversed, and the surface flow changed direction from outflow to inflow. Also, the velocity profile there showed that a three-layered circulation pattern prevails in the mouth region, but gradually transitioned to a two-layer circulation. The reverse salinity and velocity does not seem to be permanent, rather it is transient feature. The primary mechanism responsible for the reversal points to the fact that freshwater from the James River is being driven into the Elizabeth through a combination of surface slope and the baroclinic pressure force during the high flow season.

2-1-4. Current

The wind exerts stress on the surface of the water. This stress imposes a forced motion at the surface layer, as opposed to the free surface motion driven by tide. The direction, magnitude, and duration of the wind stress are all important in determining the wind-driven motion. If the wind stress can move the water, causing either setup or set down, as discussed in the previous section, it must also be associated with the momentum, and hence, the velocity.

Simultaneous measurement of CTD and current data was carried out at two stations: Thimble Shoal (TSCW) and Hospital Point (HSPT). Measured current was decomposed into principal axis and cross-principal axis components using least square analysis for the tidal current. The orientation of the principal axis was determined from the semi-major axis of the M_2 ellipse, which will tend to follow the bathymetry of the region. The principal axial current components at these two stations were shown in Figures 2-6 and 2-7.

As previously reported in the water level section, strong northeasterly wind on Julian days 82, 110, 116, 150 and 226 could cause a water level setup larger than 0.28 m. We expect these strong wind events will have impacts on current in corresponding days. Here it can be shown how the northeasterly winds on Julian days 116 and 150 affect the current pattern. The low-pass filtered residual currents along the principal axes are shown in Figure 2-6b for both stations. At the TSCW station, strengthened surface flood current (flow into the lower James River) occurred during these three days, indicating that a northeasterly wind will force water flow into the James. At station HSPT, a

similar pattern is observed: a strong wind reverses the ebb surface flow to flood into the Elizabeth.

In terms of tidal inequality, the ebb and flood show an asymmetric pattern. At station TSCW, the flow is quite rapid (>1 m/s). The magnitude of ebb speed (~1.2 m/s) is larger than that of flood (~0.8 m/s). Except for a few days (i.e., Julian days 116 and 150), this ebb-flood asymmetry is evident in almost the whole record at this station. During this period, the landward advection of water at flood periods is small. Throughout the record, surface flow is ebb dominant, while bottom flow is flood dominant. The phase of the near bottom current leads that of the near surface by about 45 minutes due to bottom friction. At station HSPT, the flow was slower (<0.6 m/s) than that observed at station TSCW. The phase lead of bottom current to surface current is about 30 minutes. Stratification tends to be greater during neap tides than during spring tides as will be seen in the following analysis of low-pass records.

Throughout the record, ebb residual current (seaward to the Bay) dominants the surface current, which is consistent with surface outflow of gravitational circulation. However, on Julian days 116 and 150, flood residual current can reach 10 cm/s, which is abnormal for this station. The increased flooding is due to the northeaster wind that pushes the Bay water into the lower James and Elizabeth, and overcomes the normal gravitational circulation pattern. When the surface current reversal occurs, we also observe that bottom flow tends to reduce the landward movement. In other words, the basic structure of the gravitational circulation was disrupted. This contradicts the classical theory of

steady gravitational circulation. In reality, the gravitational circulation is frequently modified by the wind driven circulation and thus it is unsteady in nature.

Since Hospital Point is located between Sewells Point and Money Point, dynamically speaking, the current measured at Hospital Point during the wind event can be related to the gradient between the two stations based on the shallow water equation, where u is the along shore current velocity, η is the water surface elevation, and g is gravity.

$$\frac{\partial u}{\partial t} + g\frac{\partial \eta}{\partial x} = 0$$

In other words, the time rate of current at Hospital Point can be inferred from the tidal elevation difference between Sewells Point and Money Point. The analysis shows that a difference of 2 cm in surface elevation corresponds to a 16.9 cm/sec change in velocity.

2-2. NOAA September 15 –18, 1999 Tropical Storm Data

Meteorological forcing can cause water to move vigorously. Under severe weather, both water level and current velocity can undergo significant changes, even to the extent of affecting astronomical tidal cycles. The mid-Atlantic region in the east coast of US is located in the temperate latitude where severe meteorological conditions frequently encountered include cyclonic systems which create the day-to-day weather fronts, extra-tropical storms during the winter and spring, and tropical storms like hurricanes during the summer and fall seasons. From September 15-18, 1999, a category 4 tropical-storm Floyd swept by the Atlantic Coast carrying strong wind and heavy rainfall. The hardest hit area was

in North Carolina, and before reaching Virginia, it became a category 1 storm. On September 16, Hurricane Floyd passed by the lower Chesapeake Bay, where sea level data were collected in several stations including Chesapeake Bay Bridge Tunnel, Sewells Point, and Money Point, as shown in Figure 2-8. Also collected were ADCP data in Hampton Roads and Craney Island (Zervas et al., 2000). This provides valuable information to study the wind effect on the water level and the circulation.

2-2-1. Wind Data

Figures 2-9a and 2-9b show wind speed and direction from 08/26/99 – 09/30/99 at Sewells Point and Money Point. Two strong wind events occurred during this period. The first one occurred from August 30th to September 4th. Wind directions varied mostly from northeast to north and maximum wind speeds reached to 12 m/s at Sewells Point and 10 m/s at Money Point. The second one was related the passage of Hurricane Floyd off the lower Bay during September 15 – 18, 1999. Wind direction changed from northeast on 15th to southeast during the 16th, and then to northwest at the end of the 16th and through the 17th. Magnitudes of wind speed were about 20 m/s, much stronger than that of the first storm event.

2-2-2. Water Level

The upper panel of Figure 2-10 shows the hurricane route and the sea level records at 7 stations in the lower Chesapeake Bay. In the lower panel, a detailed wind direction and sea level rise record at the Hampton Roads station were presented. The period between 9/15/12:00 to 9/16/00:00 is the first phase, when

the sea level began to rise in response to the modest easterly wind just over 5 m/sec. Between 9/15/16:00 to 9/15/16:06, when the easterly wind was over 10 m/sec, the rise of sea level intensified. Between 9/16/16:06 to 9/16/17:04, a second surge under the easterly wind developed. In the final stage, when the wind shifted from easterly to northwesterly, the sea level quickly dropped and that was when the surge began to die down. At 9/16/18:00, with the wind speeds approaching 20 m/sec, a maximum for this entire period, the water level actually fell because the wind direction changed. This suggests that the wind direction is extremely important in determining the water level variation in an estuary such as the lower James River. Figure 2-11 shows the record of wind speed, and the storm surge at Hampton Roads (in Lower James) and Money Point (in the Elizabeth River), respectively. In Figure 2-12, the predicted astronomical tide was superimposed on the real water level record at the same stations described above. It should be noted that the surge is higher and the deviation from the astronomical tide occurs earlier in Money Point than Hampton Roads. Given that Hampton Roads is in a progressive tidal regime while Money Point is in a standing wave regime, these different responses are not too surprising.

Figure 2-13 shows the water levels relative to MLLW at Sewells Point (upper panel) and Money Point (middle panel). The water elevation difference between Money Point and Sewells Point is shown in the lower panel. It appears that the water levels were setup these two storm events at both stations. The water level at Money Point is higher than that at Sewells Point. Due to the bigger magnitude of wind speed, the surface slope between Money Point and Sewells

Point is much bigger during Hurricane Floyd than that during the first storm event. This strong surface slope may cause strong ebb current in the Elizabeth River.

From this we concluded that the storm surge is sensitive to the wind direction, magnitude, and the duration that a persistent wind exerts on the water surface. This is consistent with the importance of the fetch distance and the required acceleration time for wind force to be effective. For the James River, a "setup" is most susceptible to the northeasterly or southeasterly wind, and a "set down" is caused by the northwesterly wind.

2-2-3. Velocity

Currents were also measured during this storm at two locations: Newport News in the James and Craney Island in the Elizabeth River. Velocity vectors recorded from Newport News station and Craney Island station, at different depths, were plotted in Figures 2-14a and 2-14b for the first storm event, and in Figures 2-15a and 2-15b for Hurricane Floyd. During the first storm event, August 30th to 31st, at Newport News, in Figure 2-14a, the regular ebb-flood (positive current is flood) signal displayed by the vector plots was totally disrupted. No ebb current appeared (at noon of August 30th) and water was advected upstream by the Northeasterly wind. At the end of the day, the ebb current came back, but its strength was degraded. This might be caused due to change of wind direction from Northeast to North. At the Craney Island station, as shown in Figure 2-14b, the ebb-flood signal (positive current is ebb) was also

affected. For example, the normal ebb current decreased at noon of August 30th, and the ebb signal was intensified at the end of the day.

During Hurricane Floyd, on September 16th to 17th, the ebb-flood signals at both stations were strongly affected, too. At Newport News, as shown in Figure 2-15a, a stronger than usual flood was shown during the first quarter of 16th, which might be induced by the northeasterly wind. During the fourth quarter of 16th and first quarter of 17th, an intensified ebb current resulted from the strong northwesterly wind during this period. Figure 2-16 shows the non-tidal current at Newport News. A large ebb surge current was found in the record. The magnitude of the current reaches 2.3. The time it occurred was right after the peak of surge in a relaxation phase. It should be noted that this is the time coincident with the shift of the wind direction from easterly to northwesterly. With the amplitude dramatically modified and the normal times for slack water, high water and low water shifted, the entire flood cycle was disrupted. When averaged over a tidal cycle, the non-tidal velocities ranged from 1.5 to 2.0 knots, which is a fairly large magnitude of current speed, considering regular tide is only 1-1.5 knots. It is also worthwhile to point out that the surge current (as differentiated from the astronomical tide) is much larger in the relaxation phase than in the developing phase of the storm surge.

At Craney Island, in Figure 2-15b, a very strong flood current was recorded during the third quarter of the 16th, and a strengthened ebb flow during the fourth quarter of the 16th was also generated. This might be related with the strong surface slope setup by the wind, as we discussed in Section 2-2-1. Also

shown in Figure 2-17 is the non-tidal current at Craney Island. The surge currents appeared at both ebb and flood, and their magnitudes are similar. These reached about 1.0 knot, which is twice the regular tidal current. Given that the Elizabeth River is a branch to the James River, one may expect that the dynamics should be very similar. However, we found that the responses of the James and the Elizabeth Rivers to the surge do have noticeable differences.

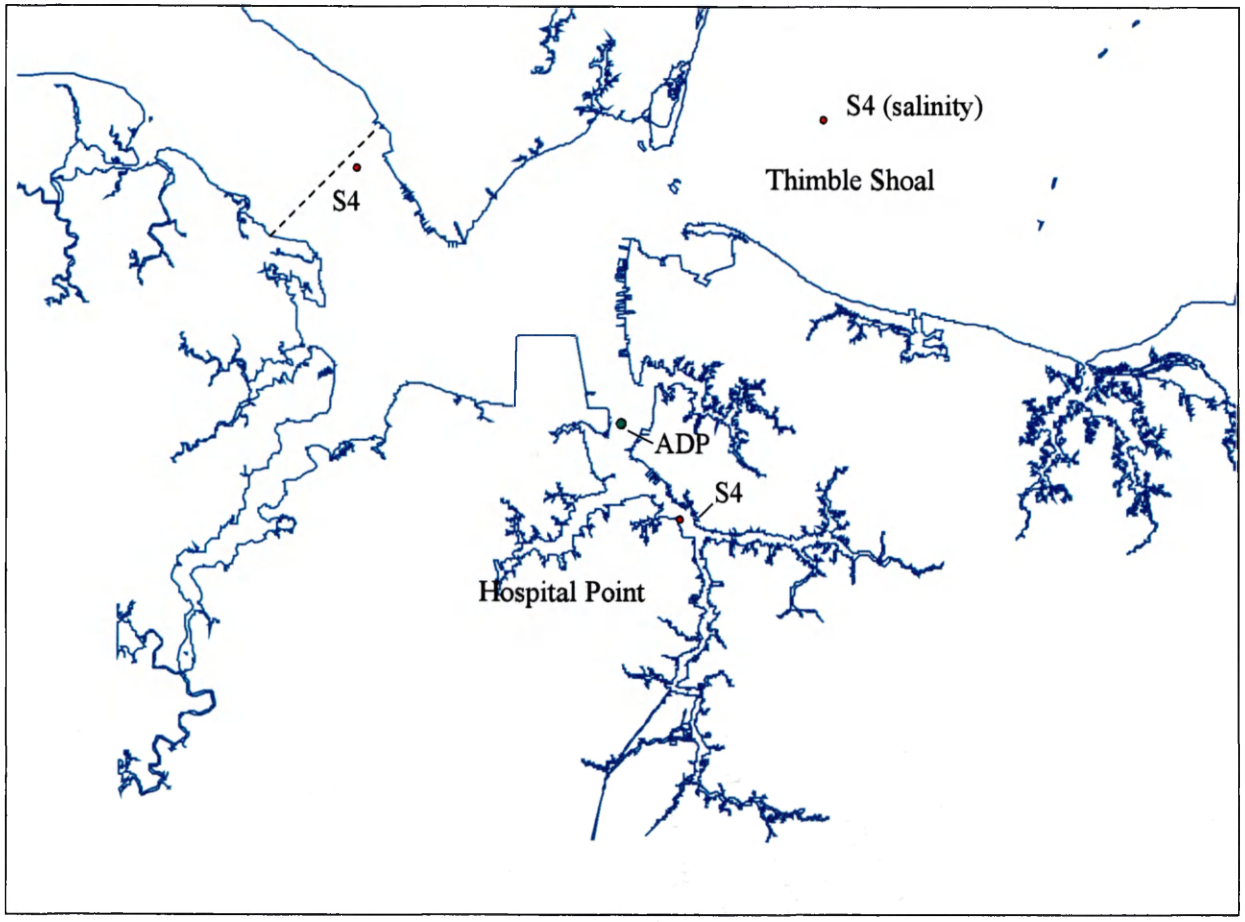

Figure 2-1a. Fixed measurement stations at Thimble Shoals and Hospital Point

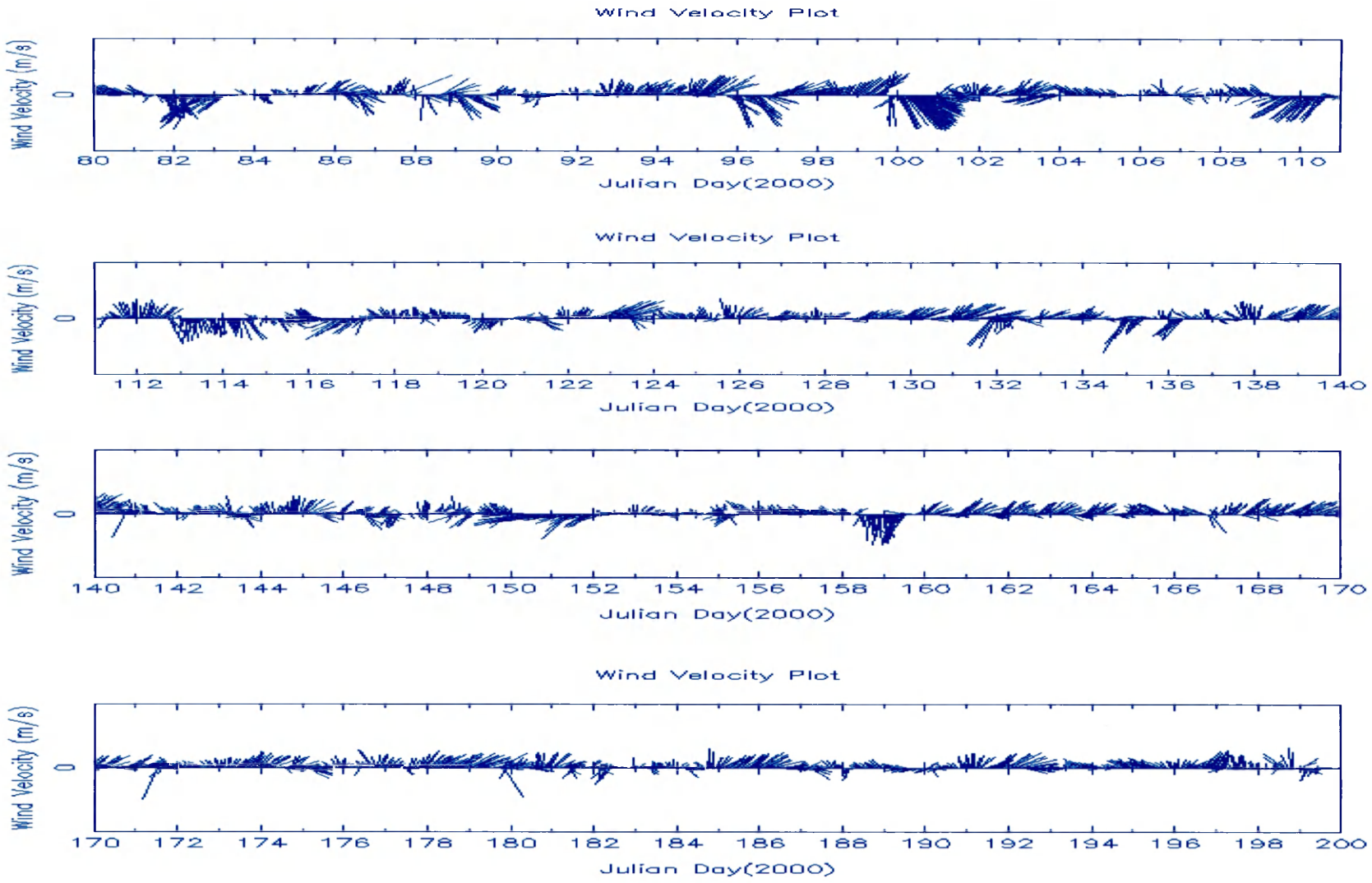

Figure 2-1. Observed wind velocity at Sewells Point

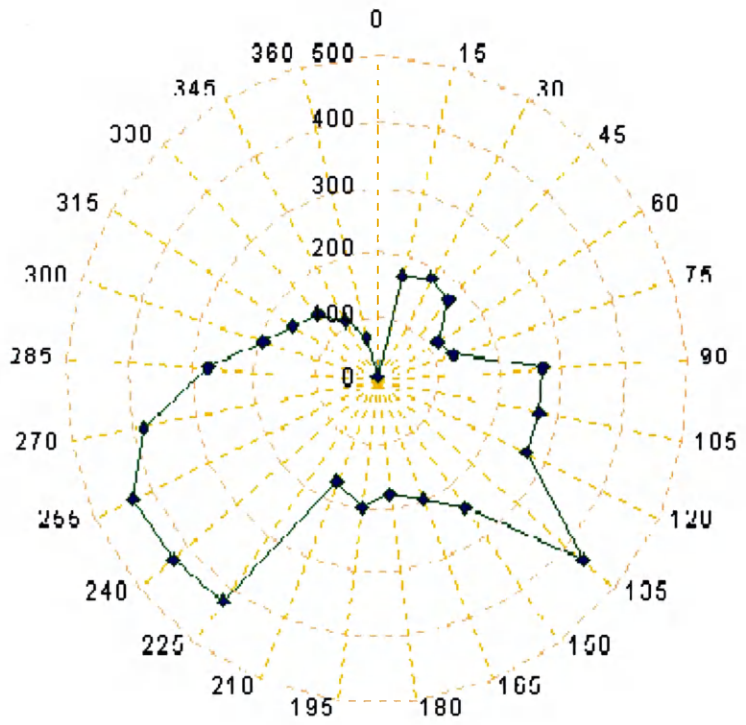

Wind direction frequency distribution

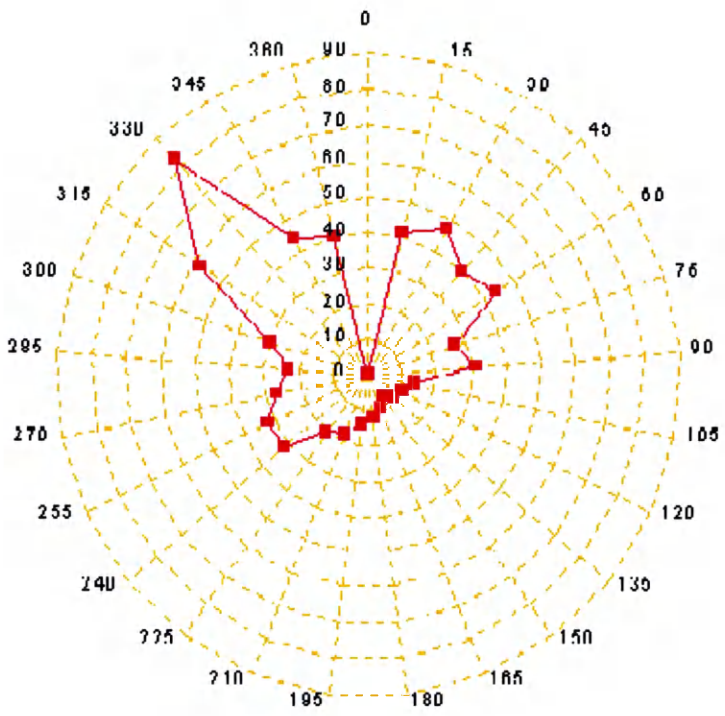

Wind energy distribution

Figure 2-2. Hourly wind frequency and direction distribution

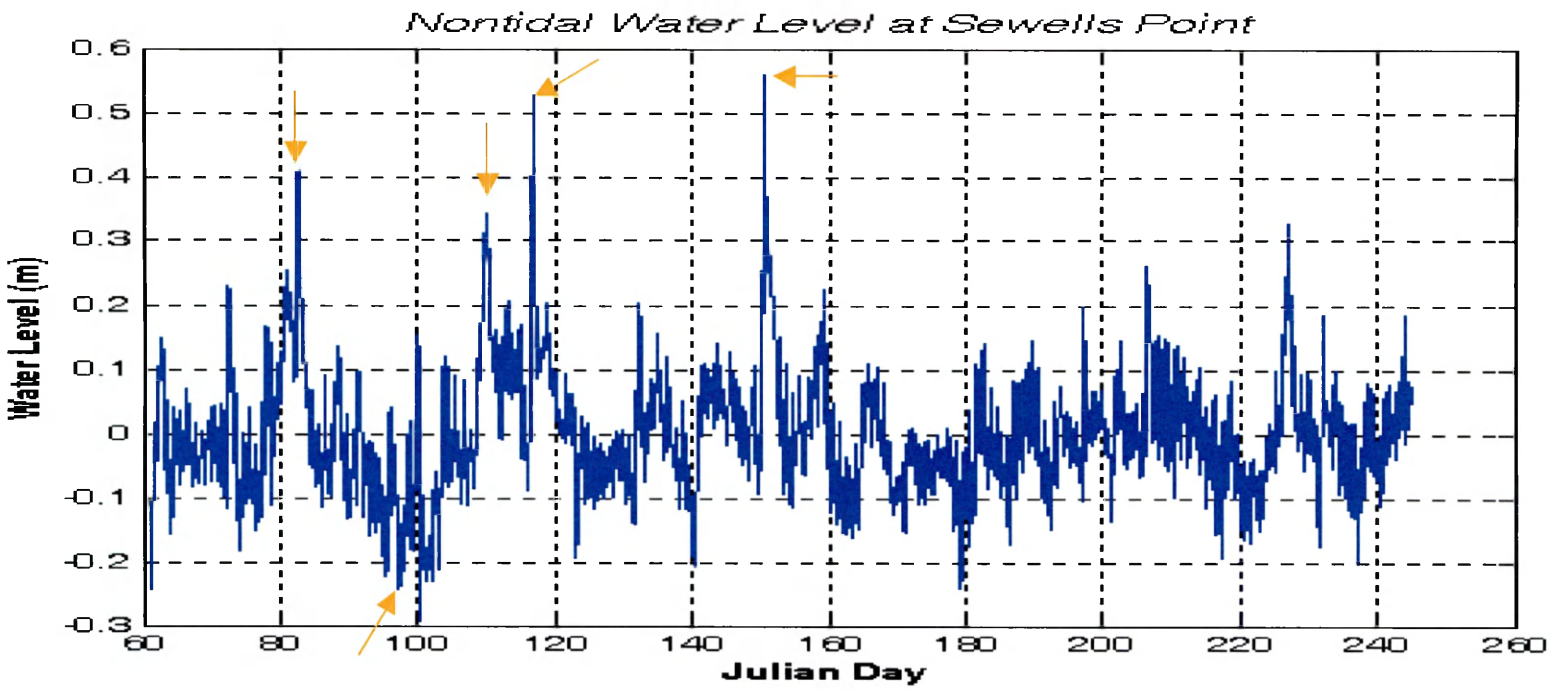

Figure 2-3. Low-pass filtered water level at Sewells Point

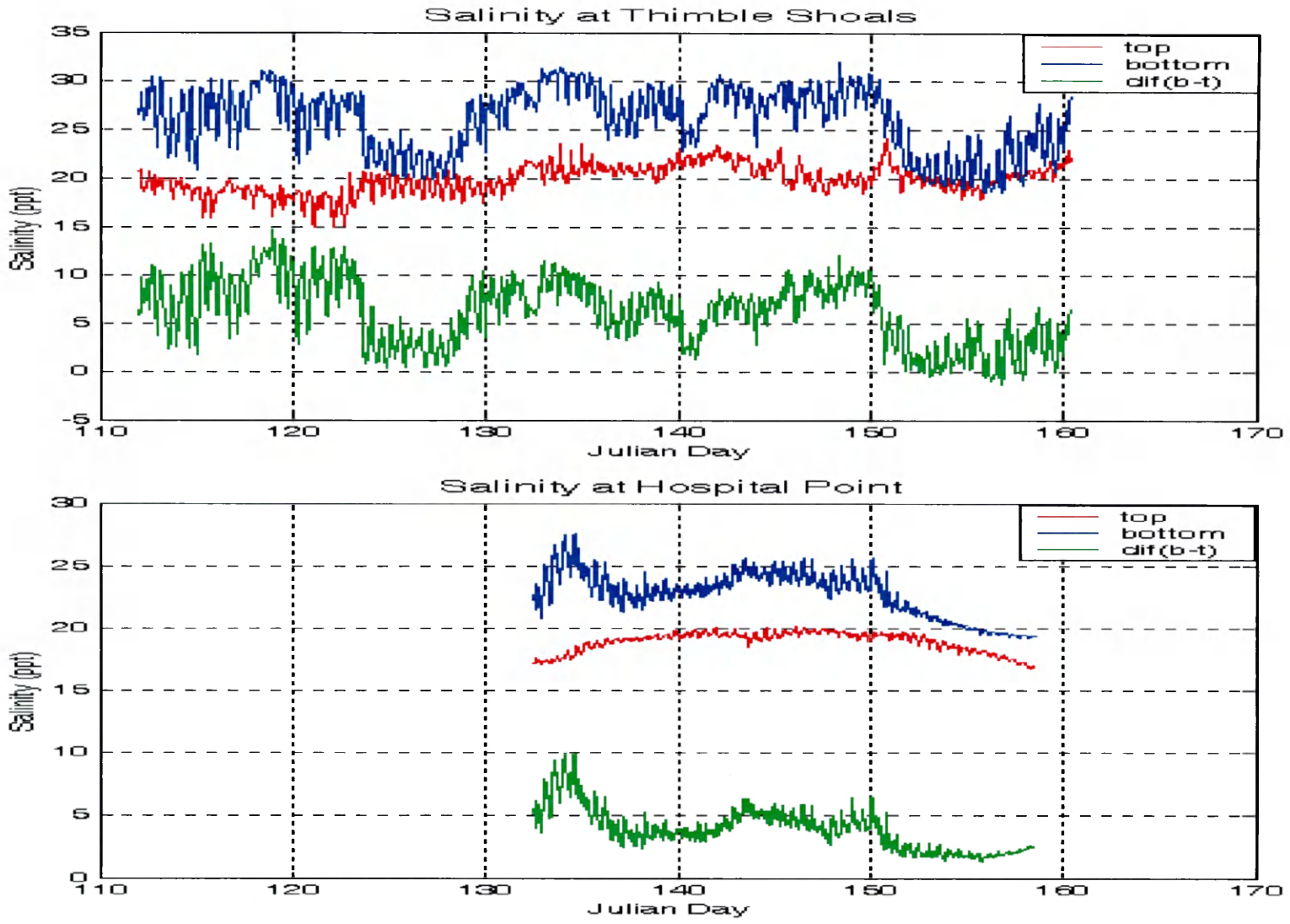

Figure 2-4. Measured surface and bottom salinity at TSCW (Thimble Shoals) and HSPT (Hospital Point) stations

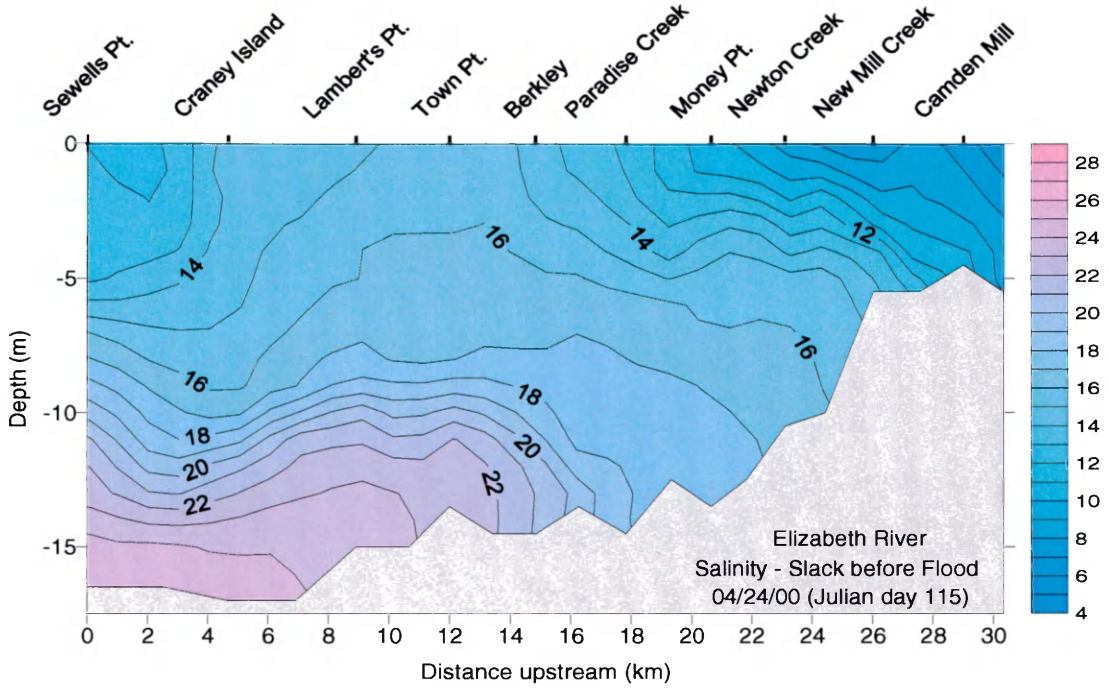

Figure 2-5a. Salinity distribution (ppt) in the Elizabeth River on April 24, 2000.

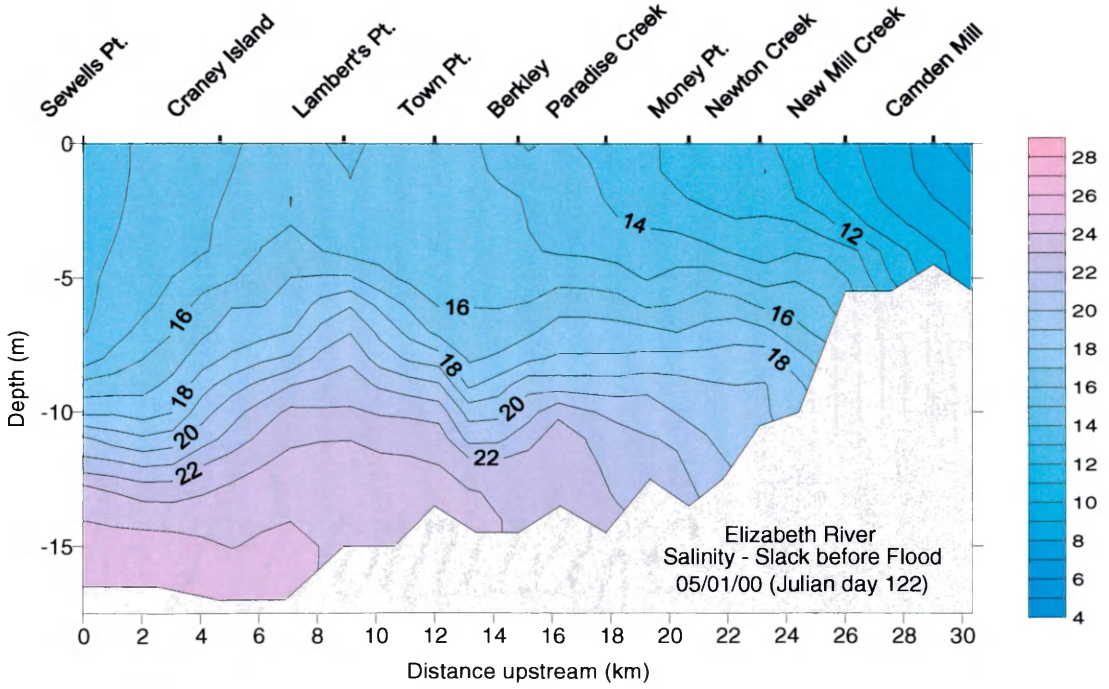

Figure 2-5b. Salinity distribution (ppt) in the Elizabeth River on May 1, 2000.

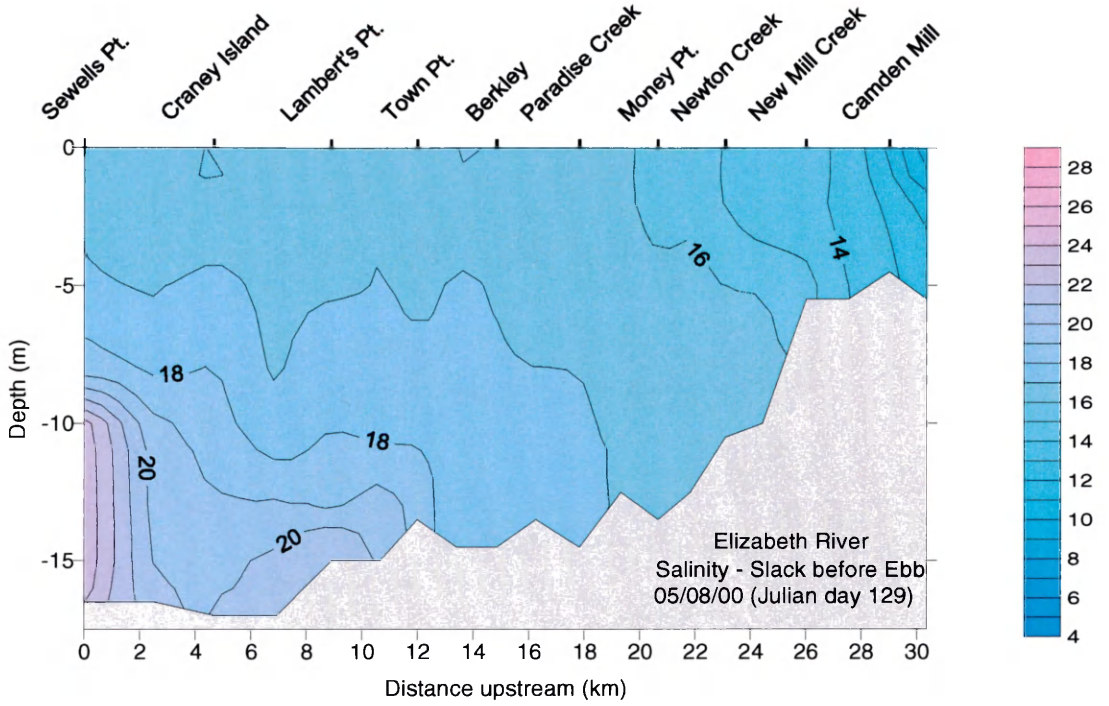

Figure 2-5c. Salinity distribution (ppt) in the Elizabeth River on May 8, 2000.

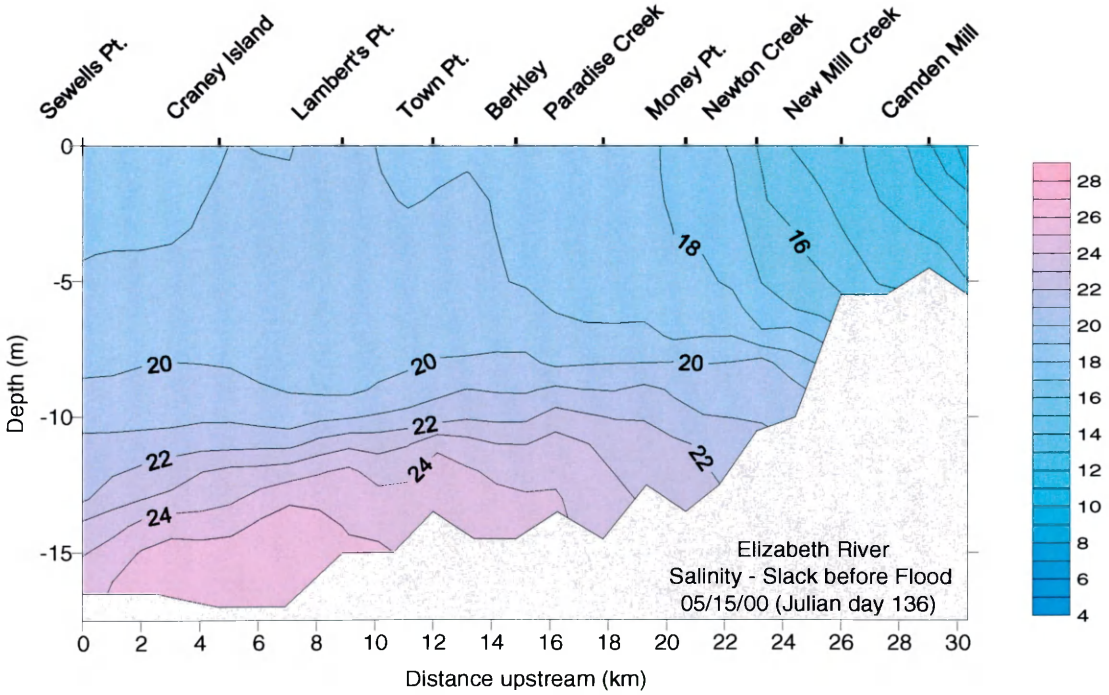

Figure 2-5d. Salinity distribution (ppt) in the Elizabeth River on May 15, 2000.

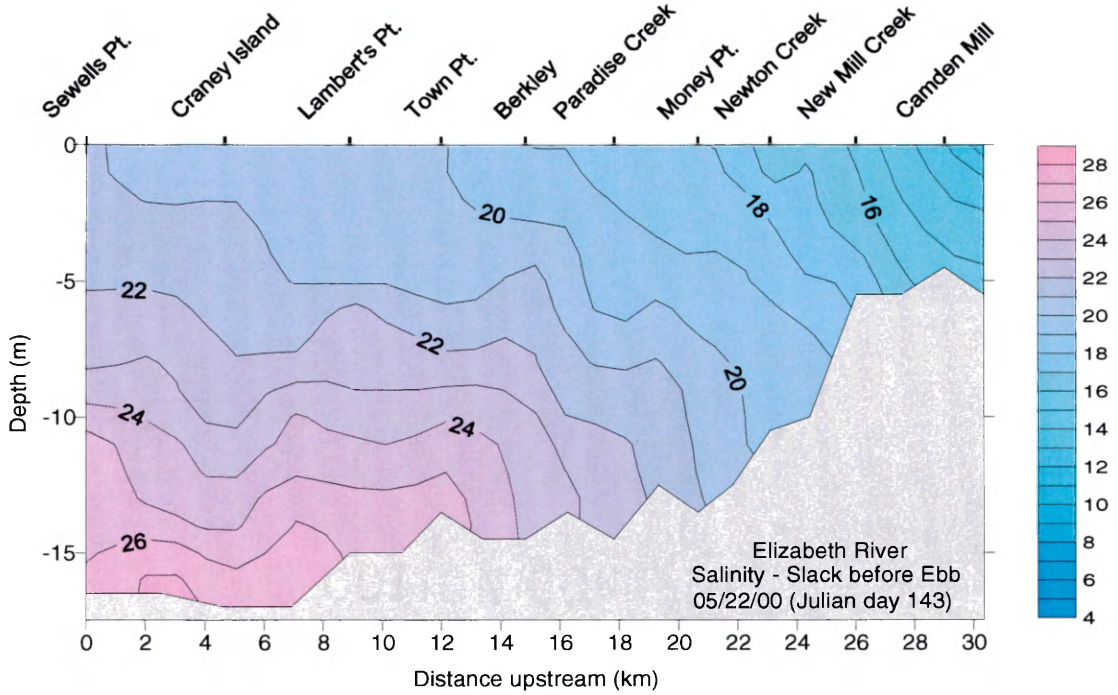

Figure 2-5e. Salinity distribution (ppt) in the Elizabeth River on May 22, 2000.

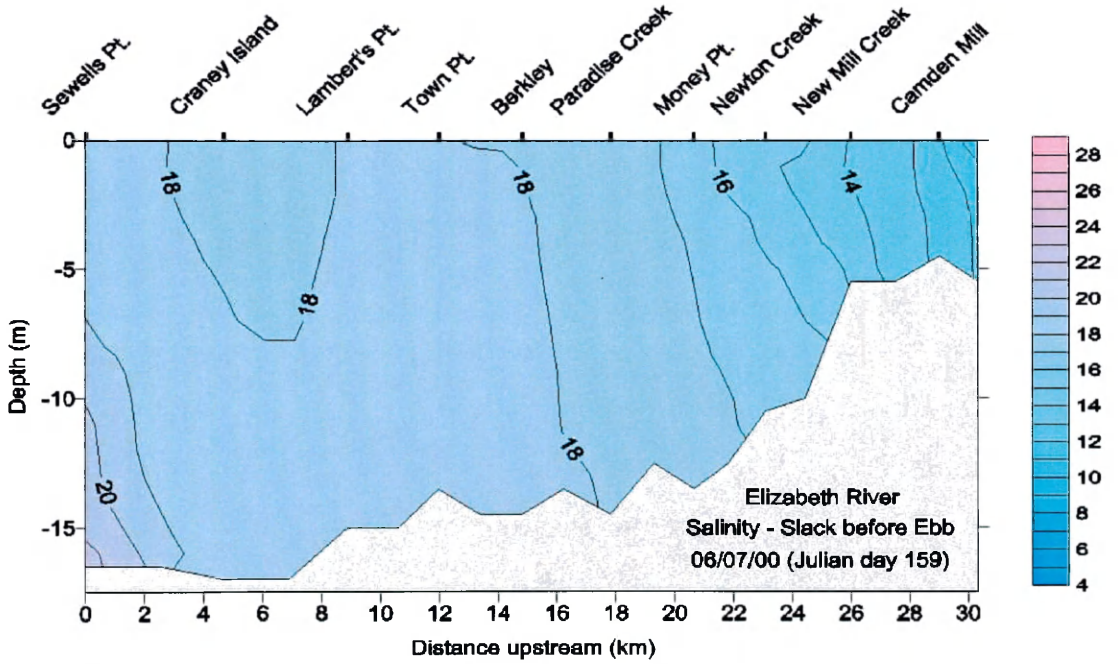

Figure 2-5f. Salinity distribution (ppt) in the Elizabeth River on June 7, 2000.

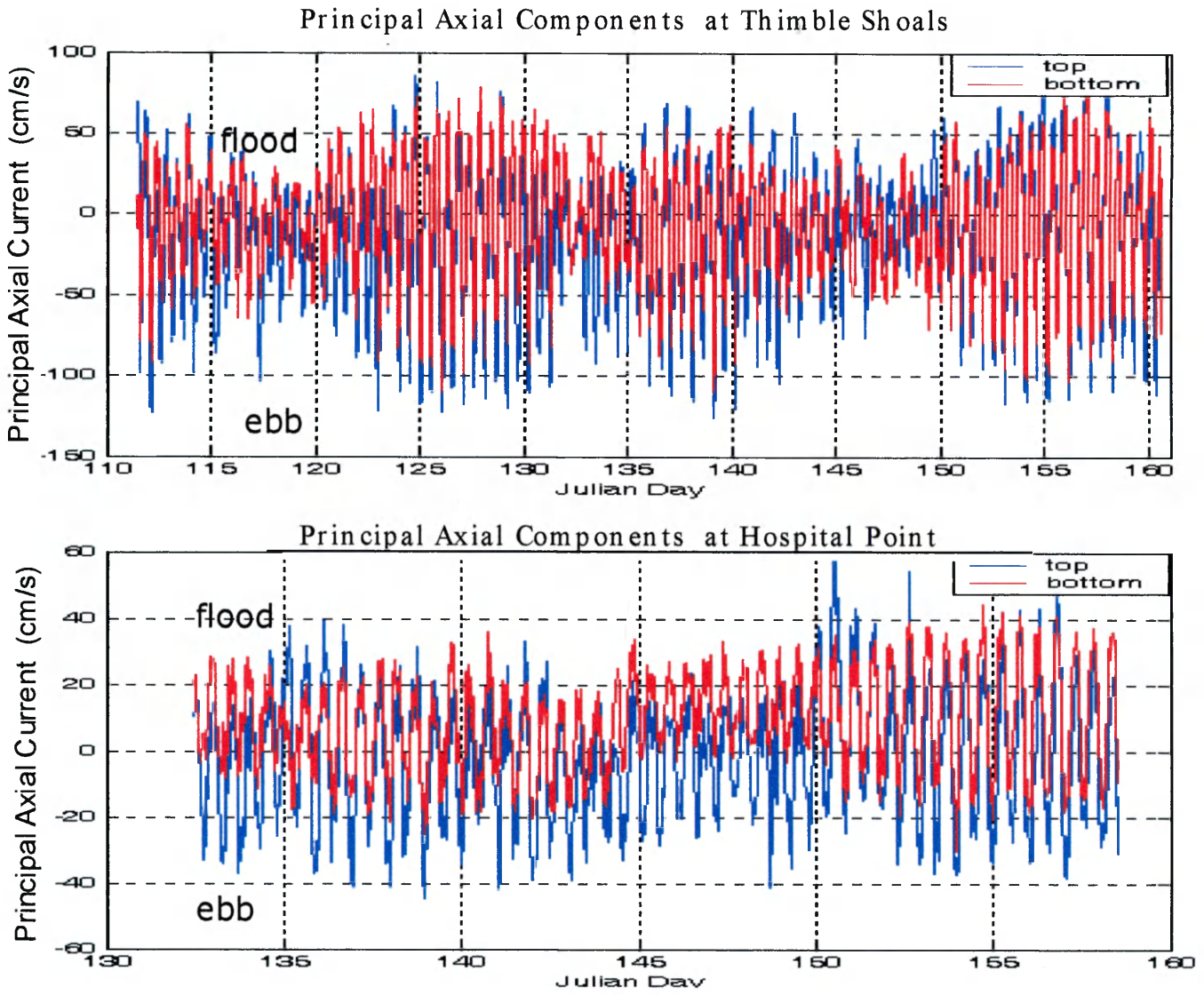

Figure 2-6. Principal axial current components at TSCW and HSPT stations

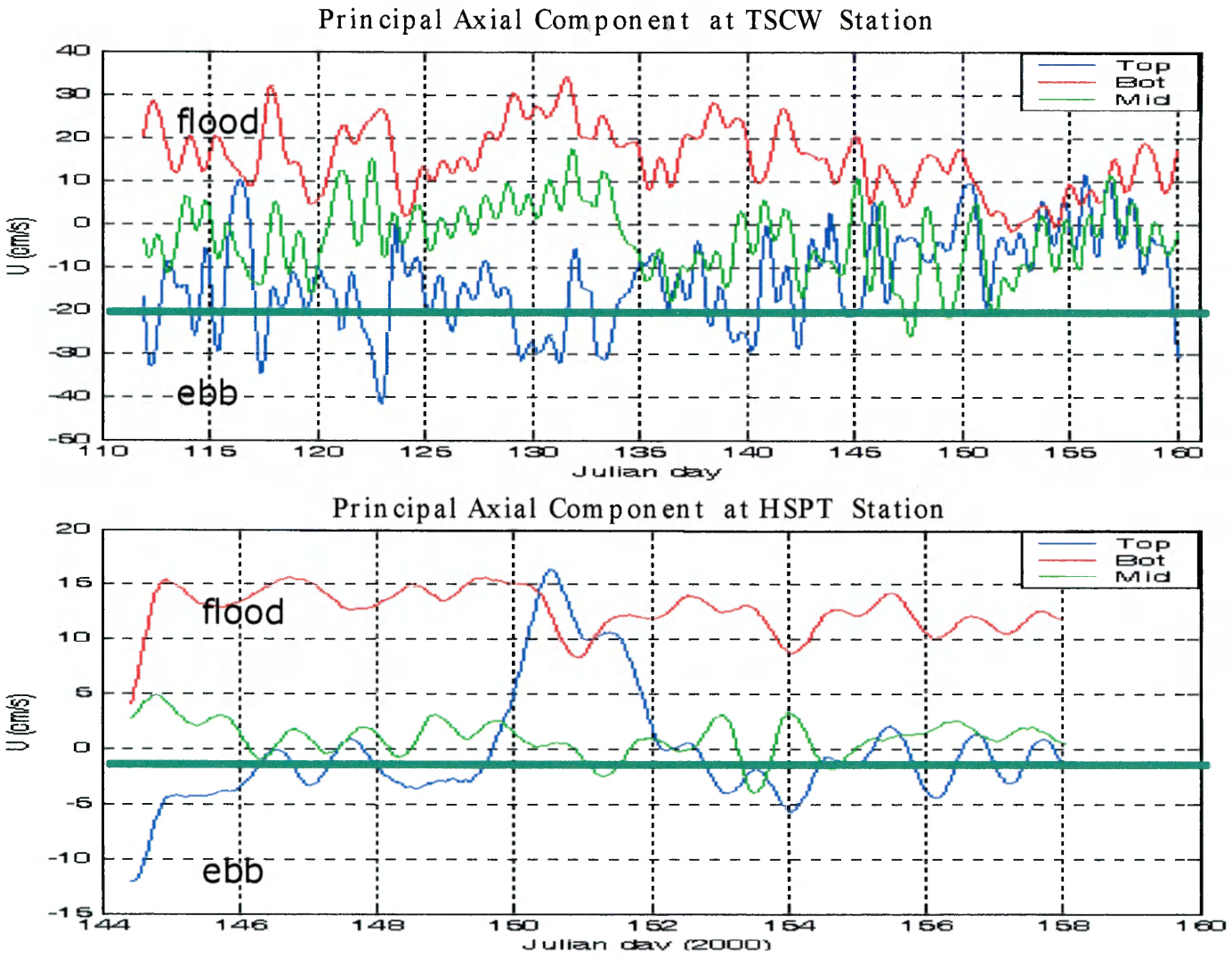

Figure 2-7. Low-pass filtered principal axial current components at TSCW and HSPT stations

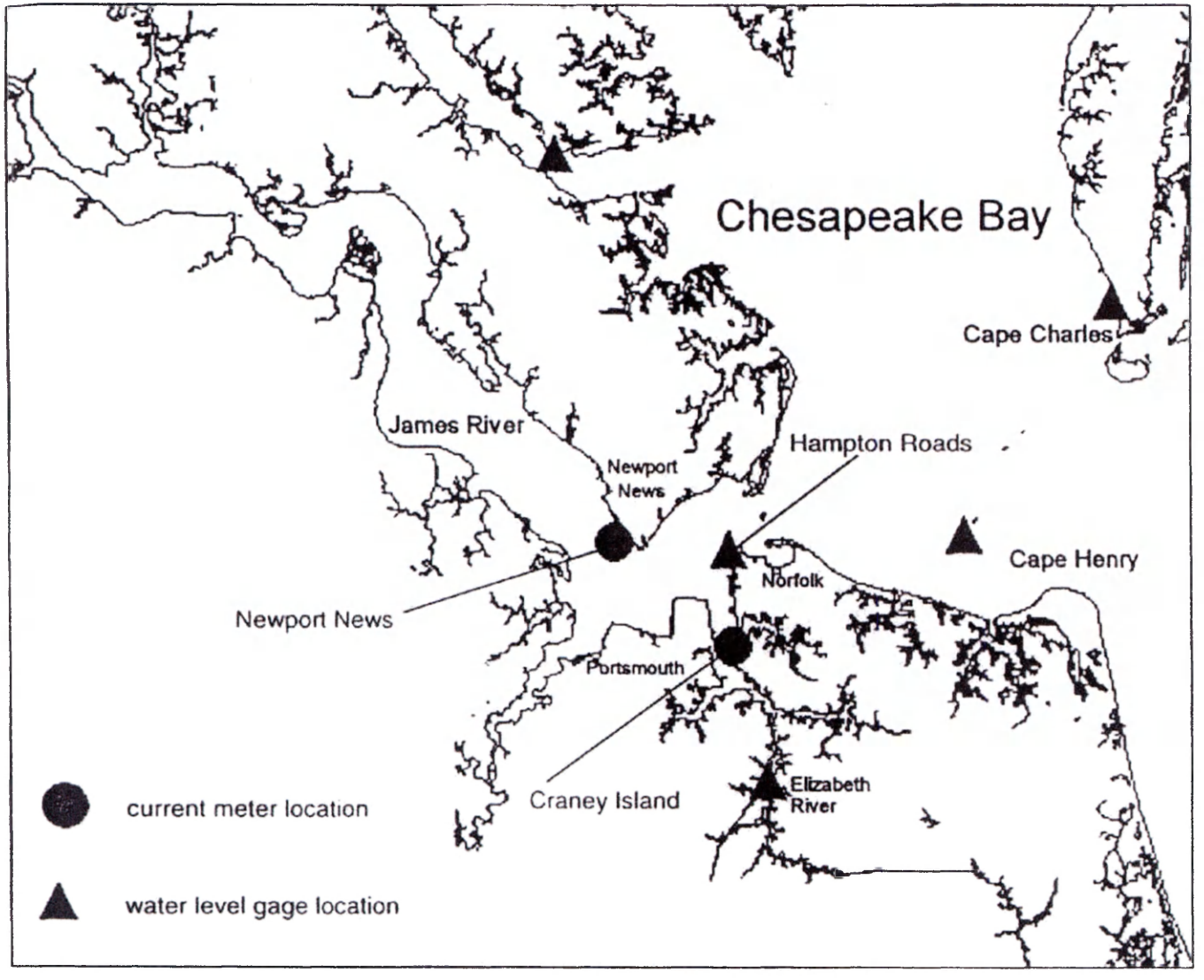

Figure 2-8. NOAA CO-OPS program measurement stations
(Zervas et al., 2000)

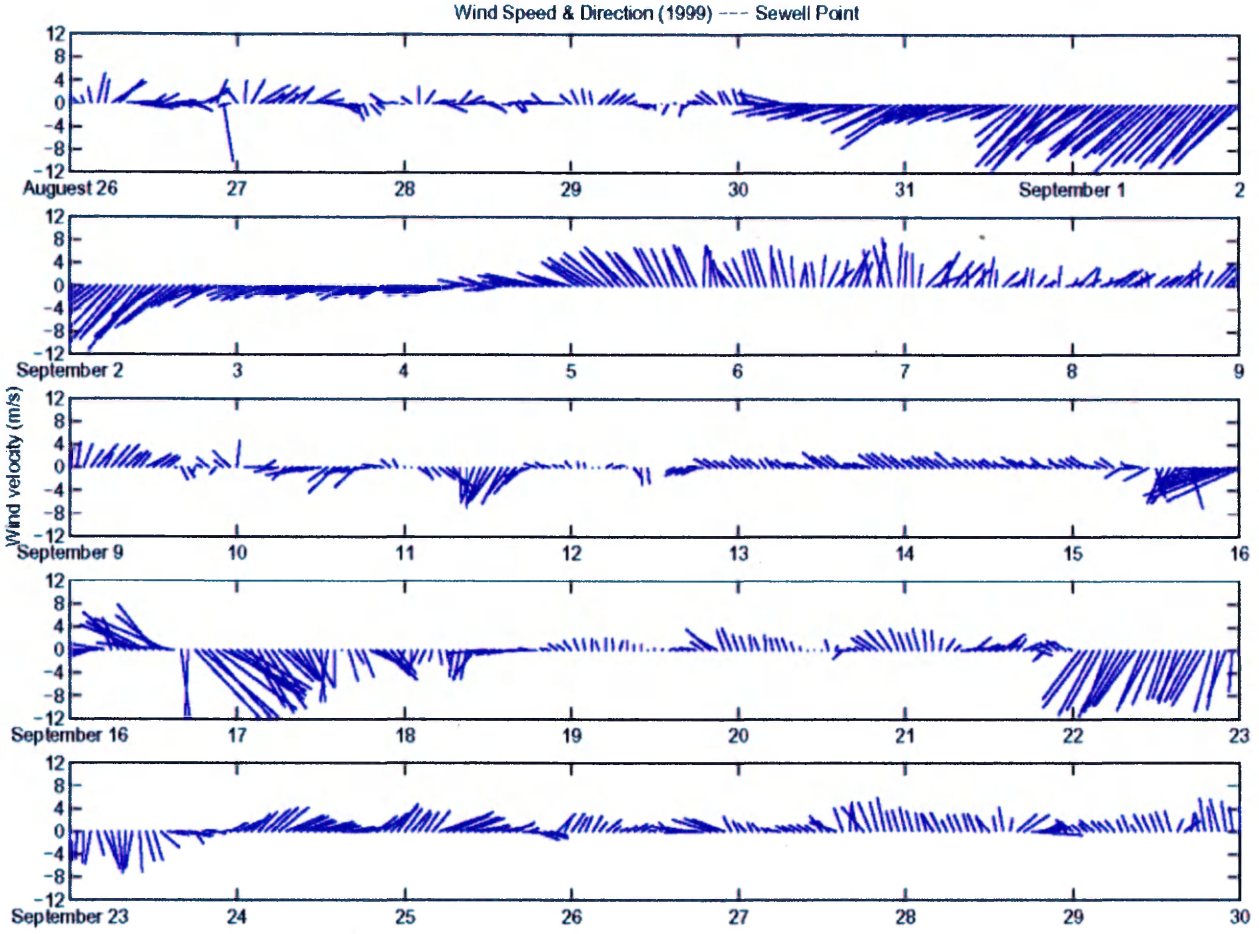

Figure 2-9a. Record of wind vectors at Sewells Point, from NOAA

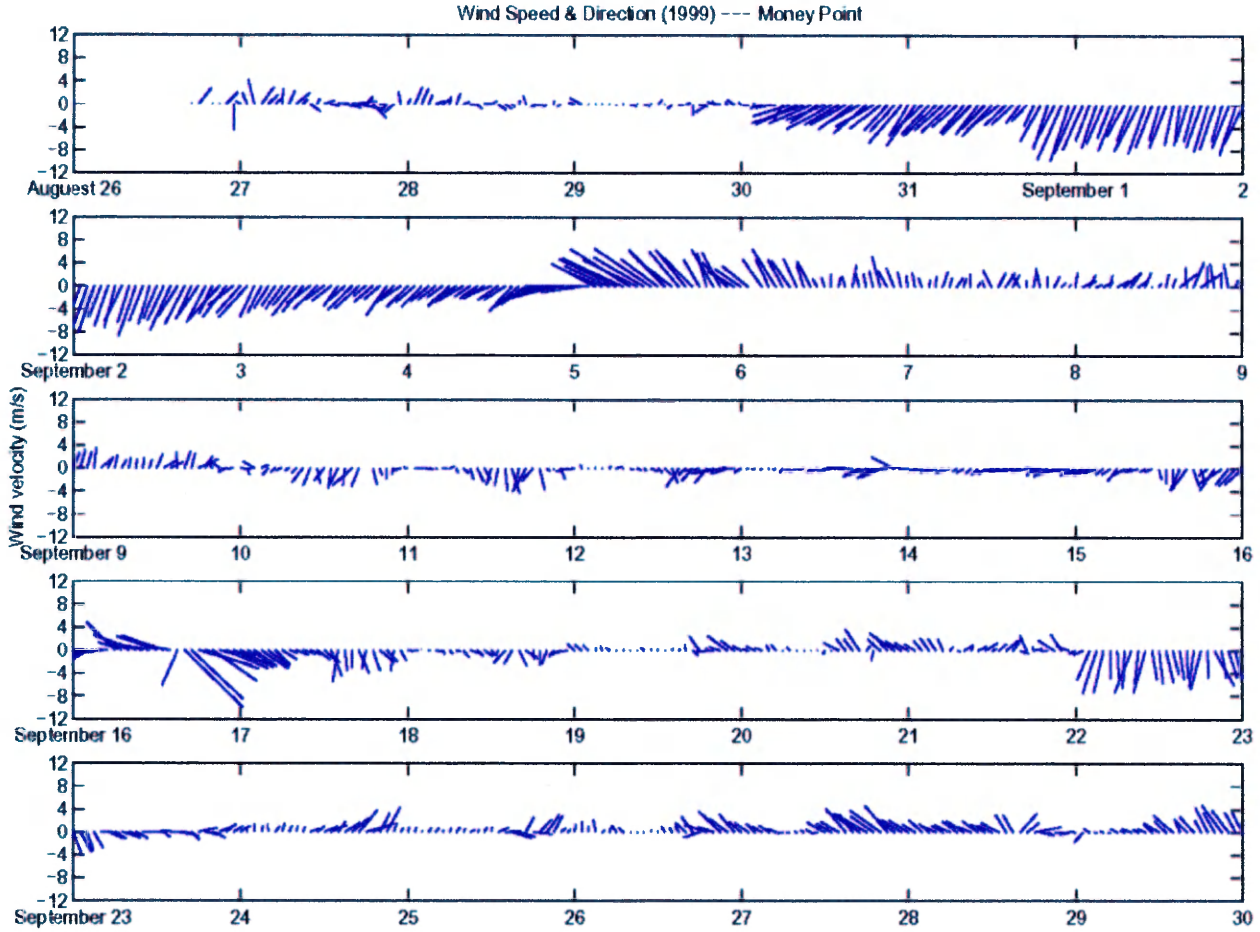

Figure 2-9b. Record of wind vectors at Money Point, from NOAA

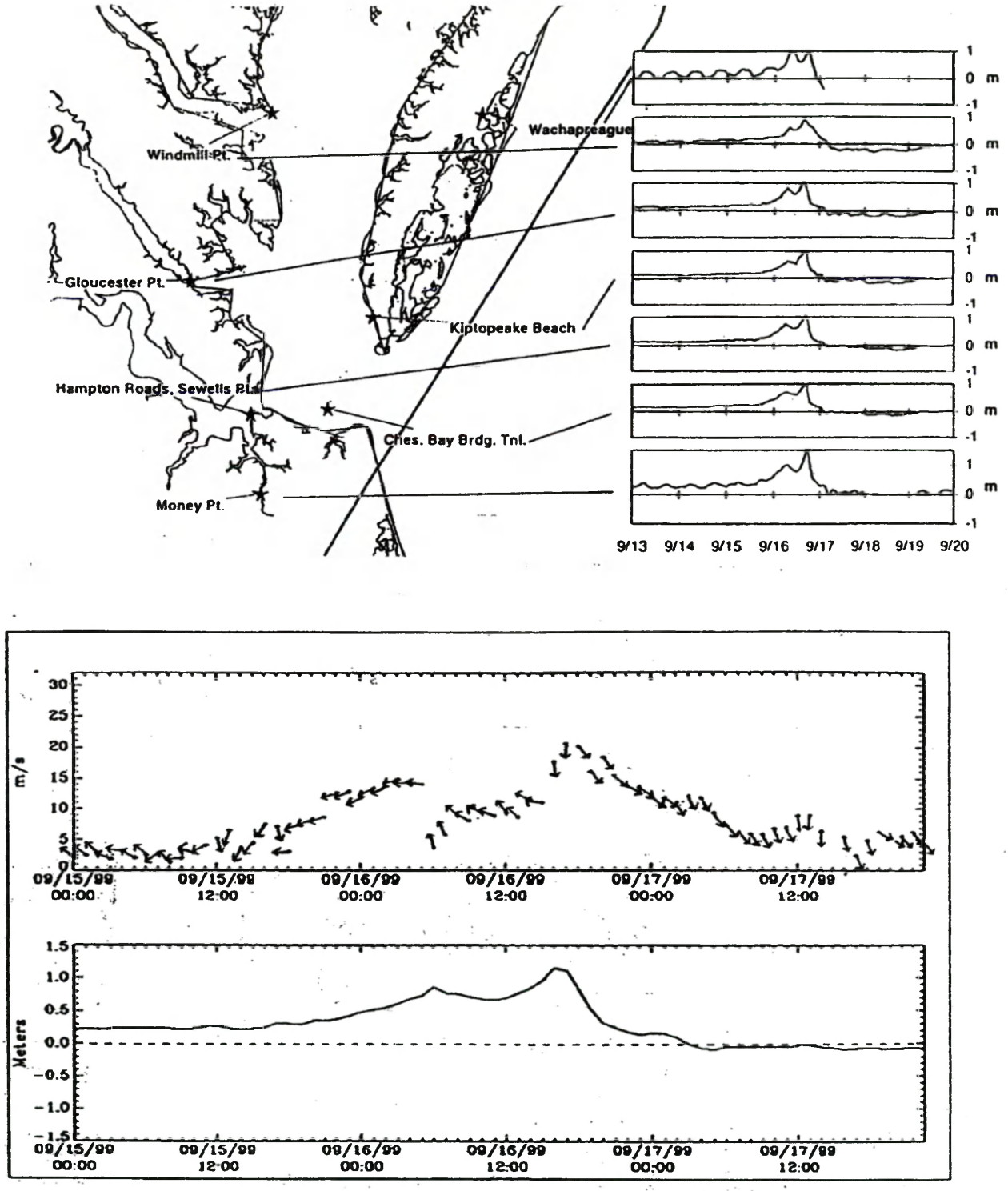

Figure 2-10. Hurricane route and the sea level recorded at 7 locations in the Lower Chesapeake Bay (upper panel);
Wind vector and sea level at Hampton Roads station (lower panel)
(Zervas et al., 2000)

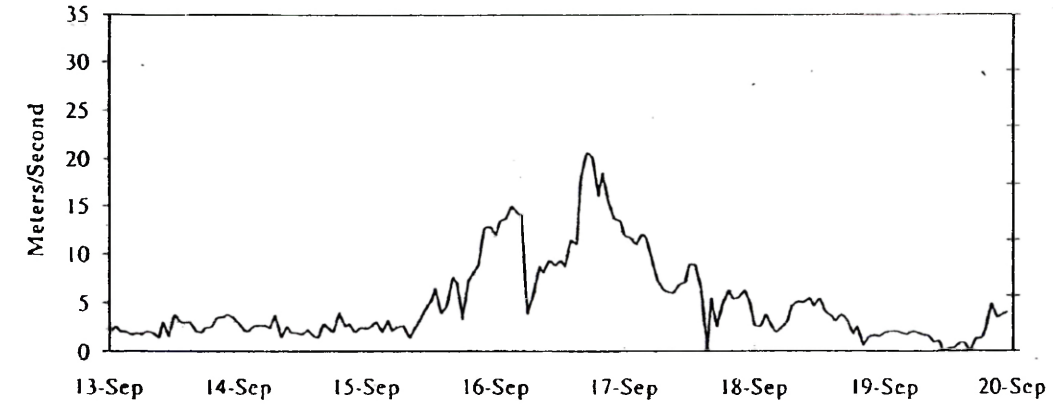

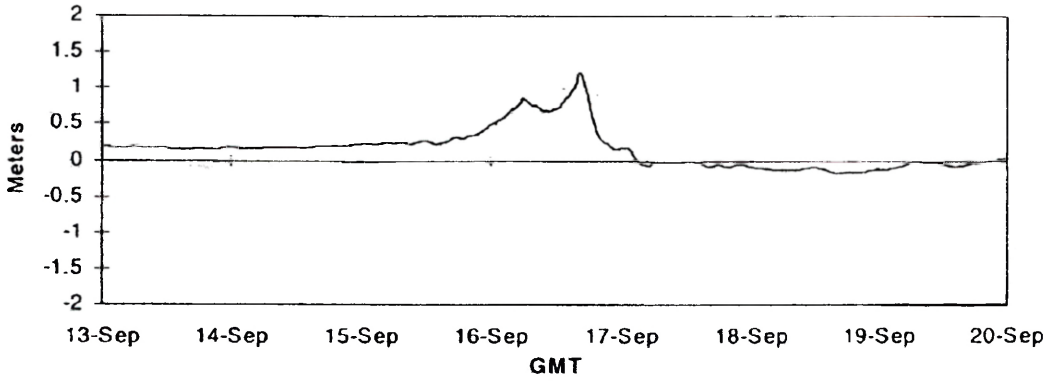

Hampton Roads, VA storm surge.

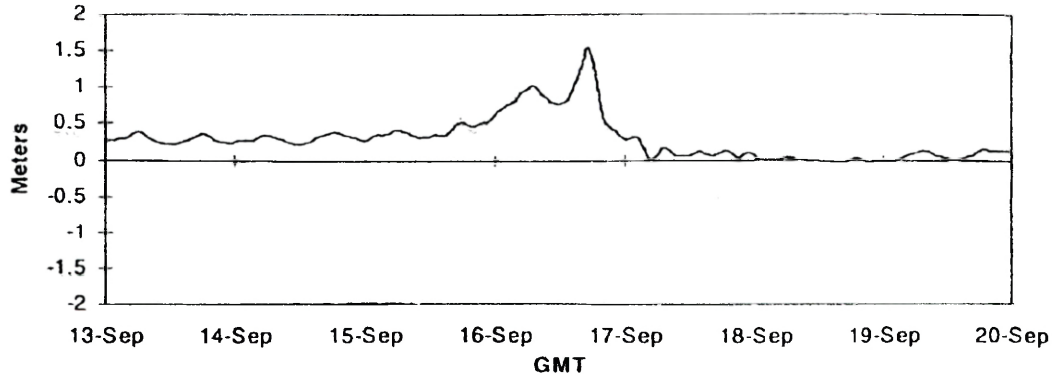

Money Point, VA storm surge.

Figure 2-11. Record of wind speed and storm surge at Hampton Roads and Money Point. (Zervas et al., 2000)

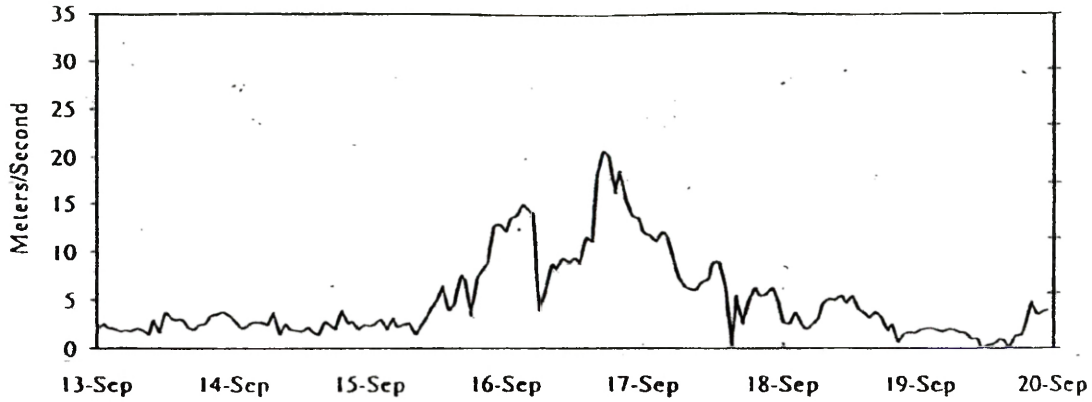

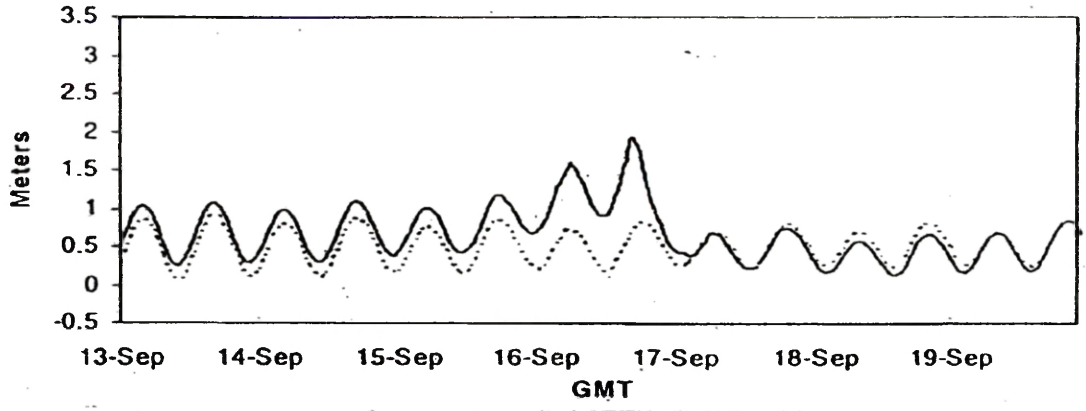

Hampton Roads, VA observed (solid) and predicted (dashed) water levels on MLLW.

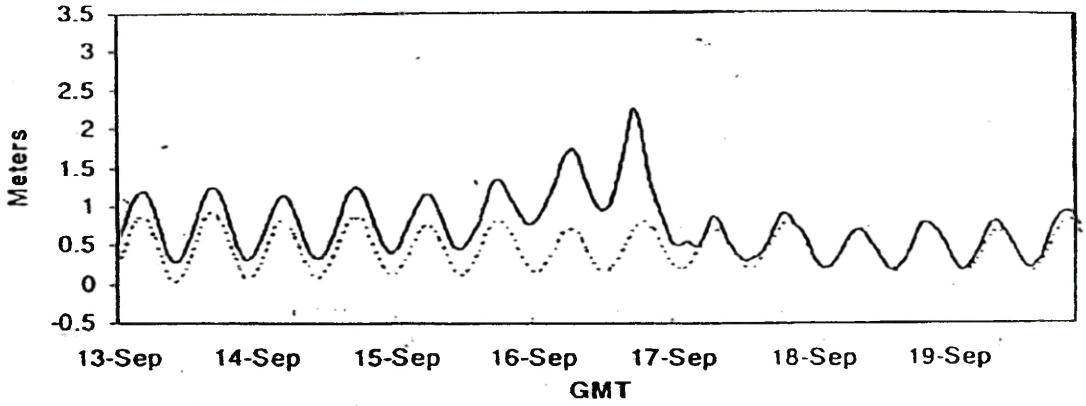

Money Point, VA observed (solid) and predicted (dashed) water levels on MLLW.

Figure 2-12. Predicted astronomical tide with real water level record at Hampton Roads and Money Point. (Zervas et al., 2000)

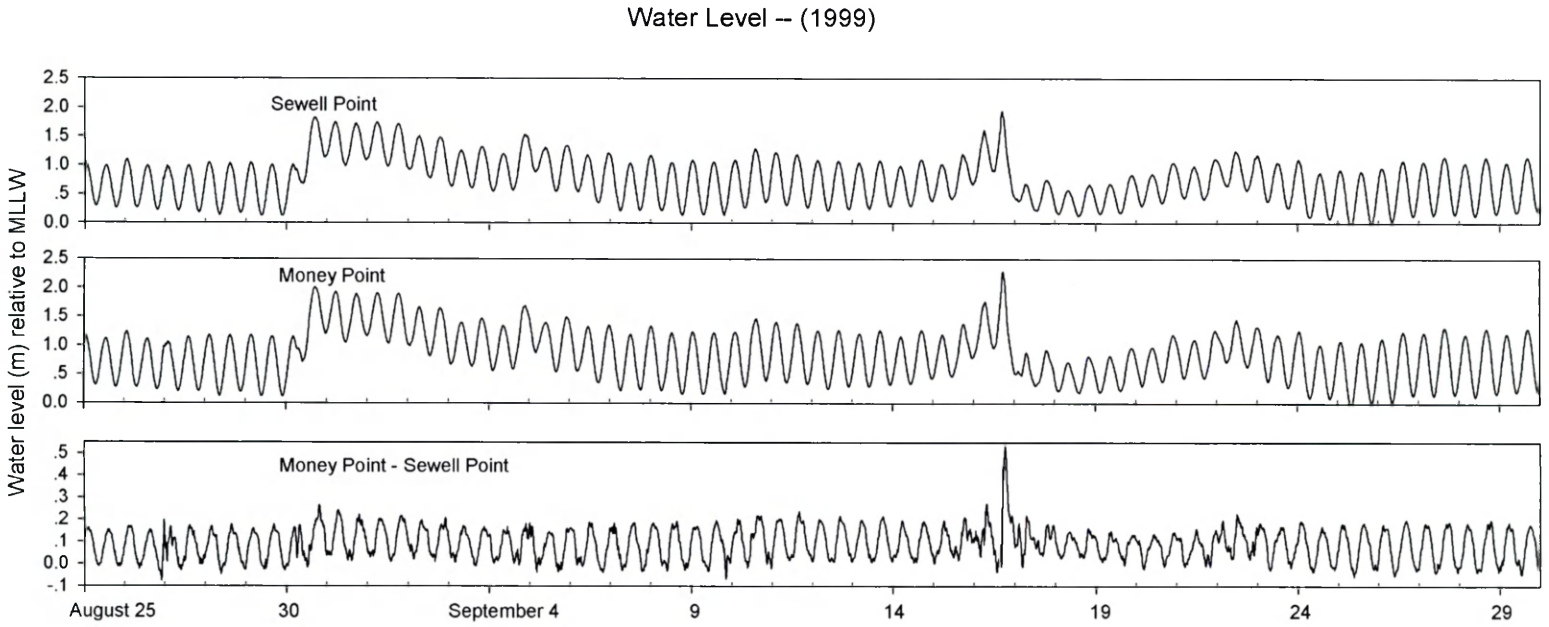

Figure 2-13. Water level relative to MLLW at Sewells Point and Money Point

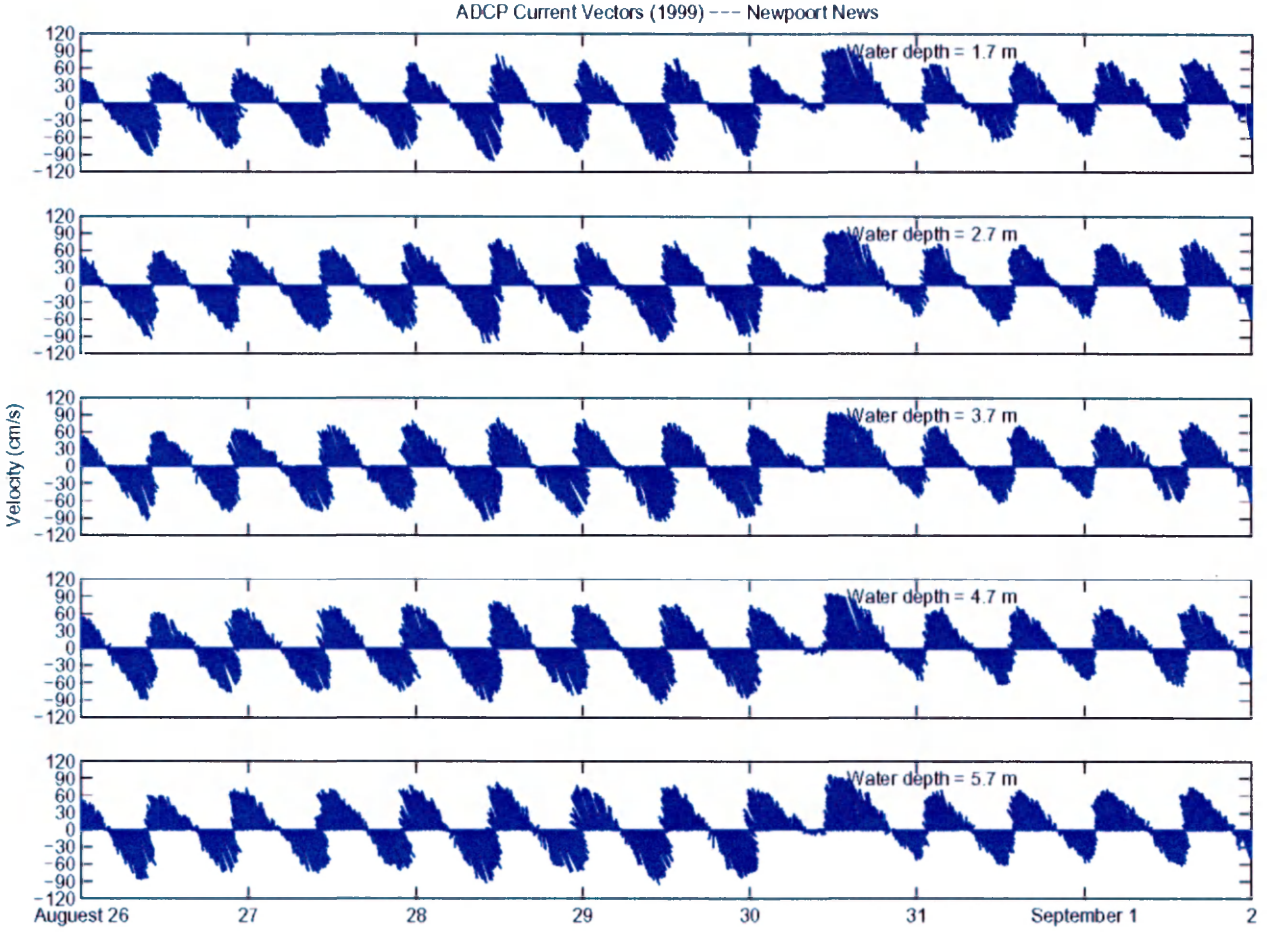

Figure 2-14a. Velocity vector plot during August 26 to September 2 at Newport News

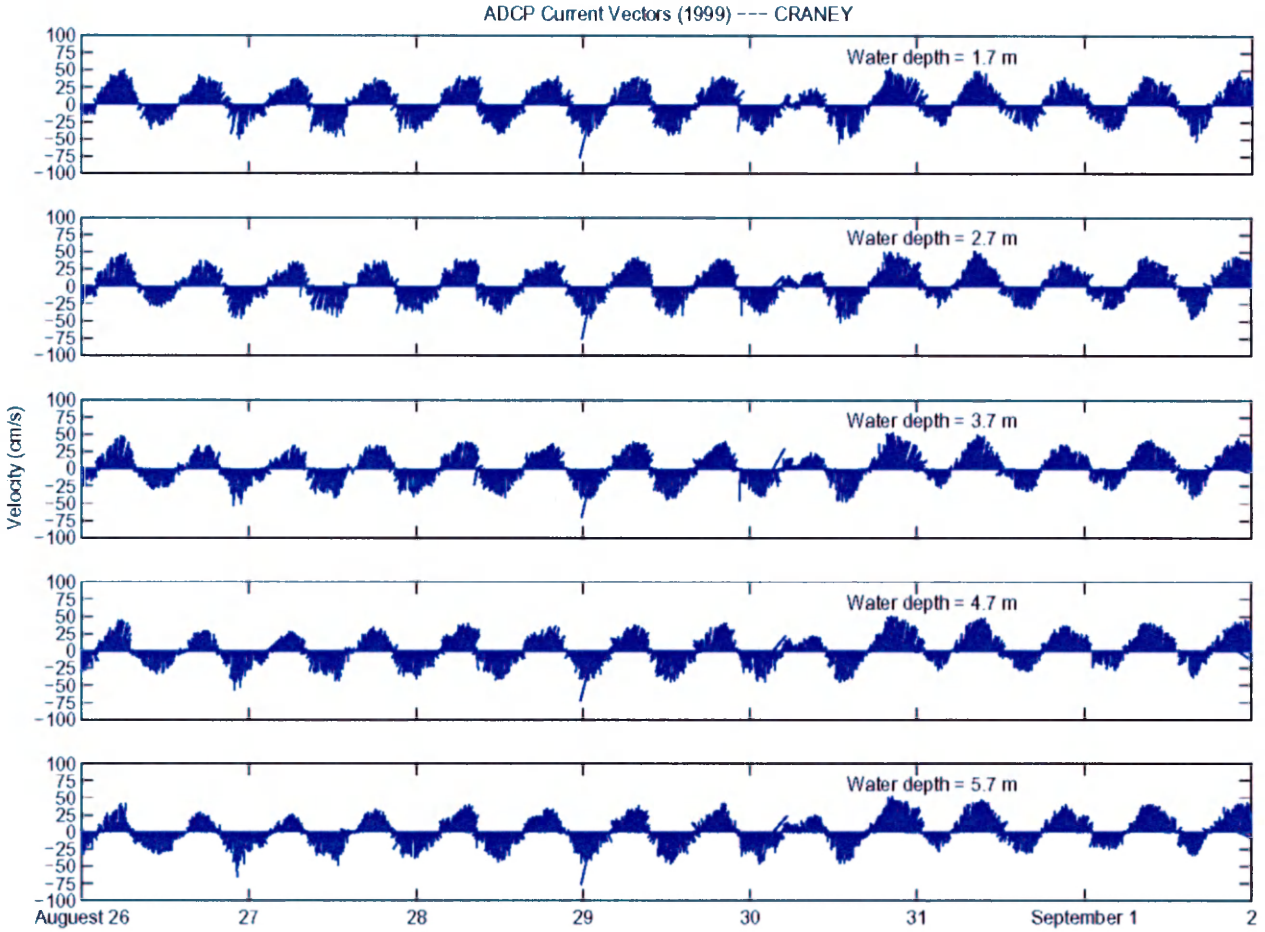

Figure 2-14b. Velocity vector plot during August 26 to September 2 at Craney Island

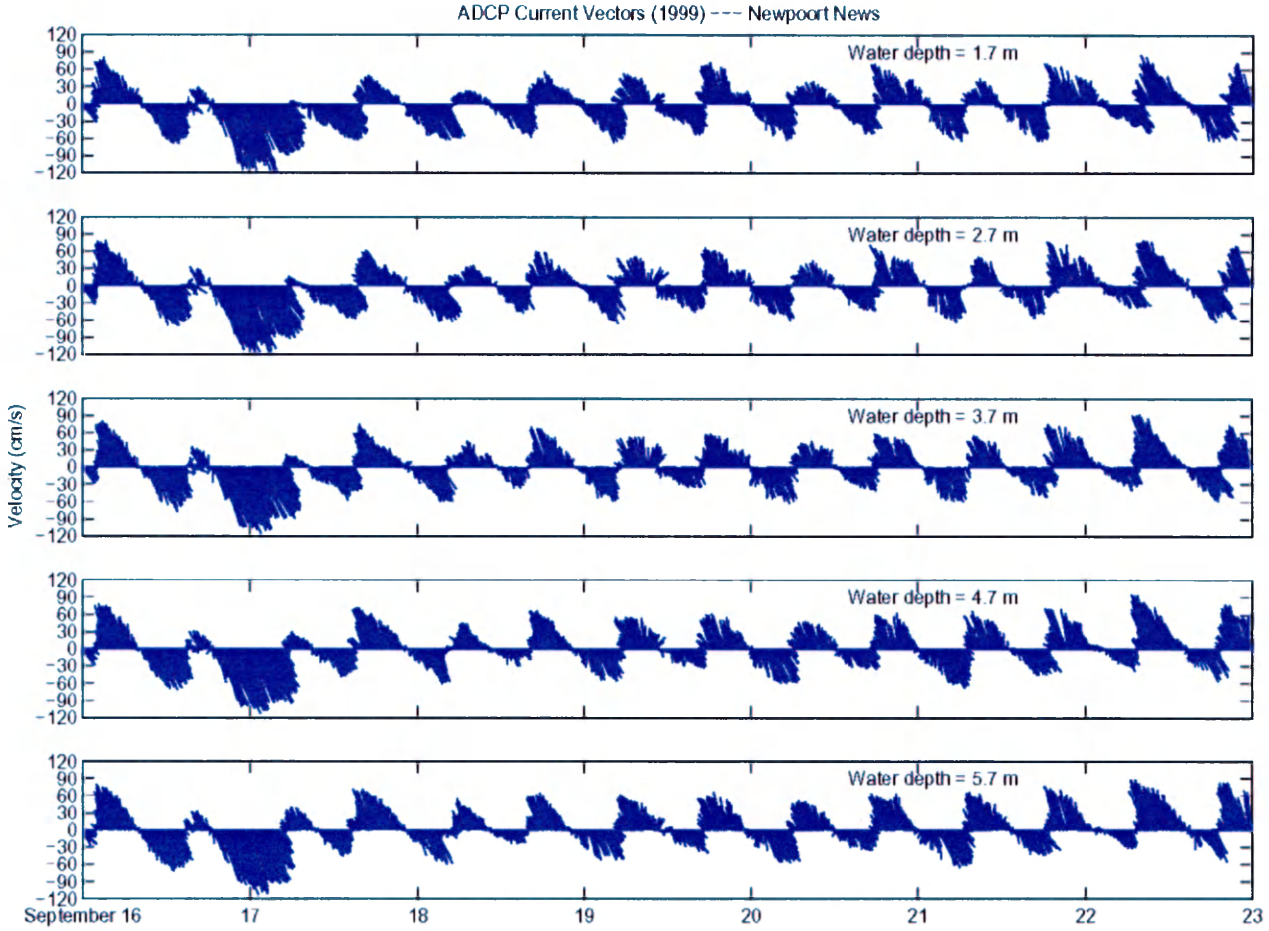

Figure 2-15a. Velocity vector plot during September 16 to September 23 at Newport News

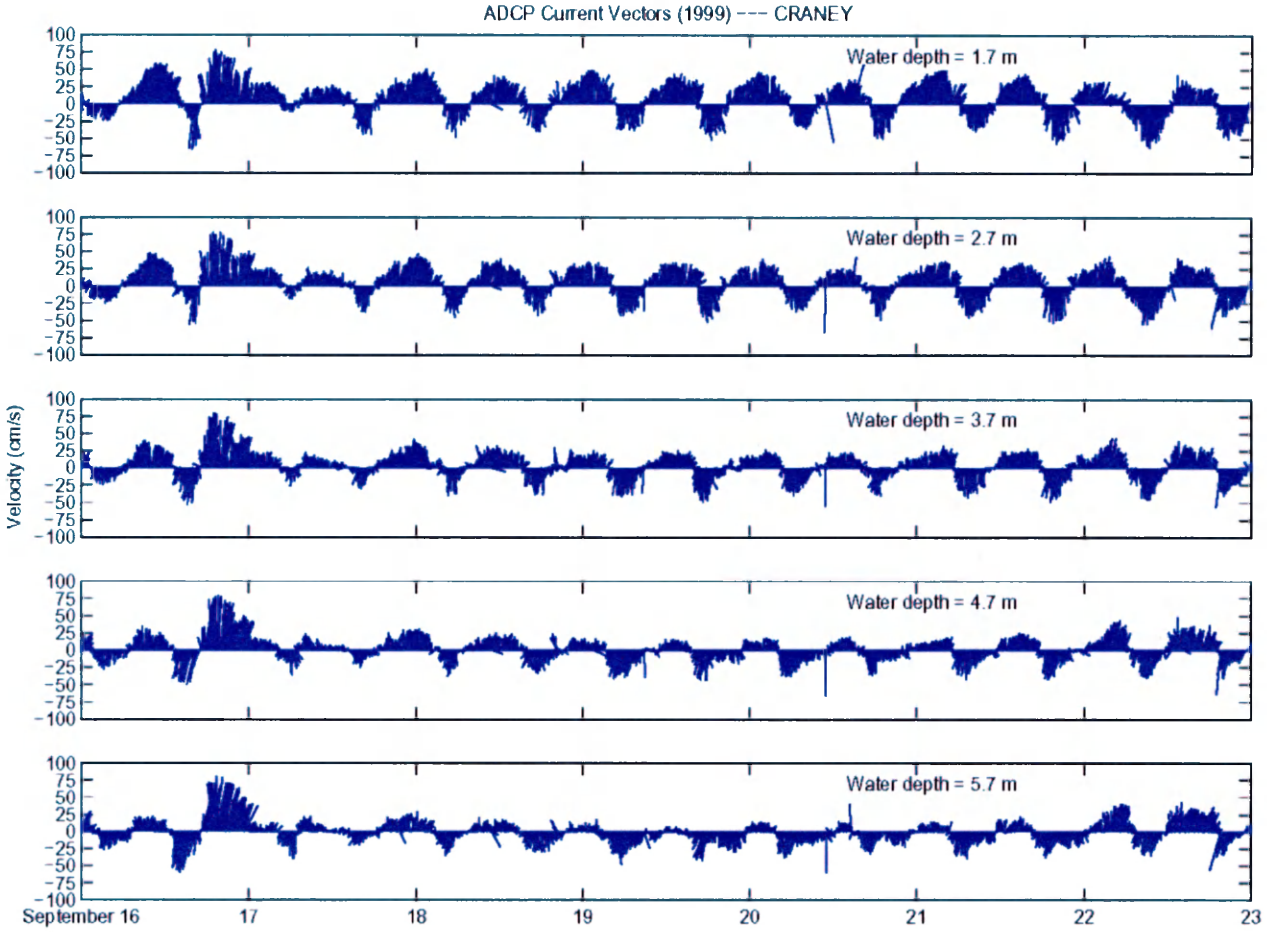

Figure 2-15b. Velocity vector plot during September 16 to September 23 at Craney Island

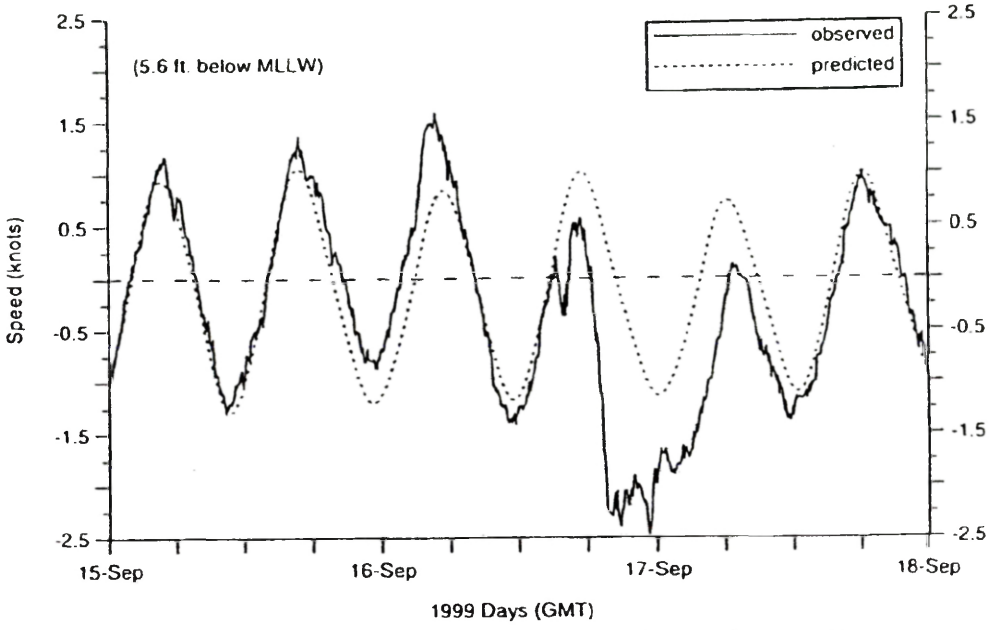

Observed current and tidal current prediction at Newport News during Hurricane Floyd. Positive current is flood along 183°.

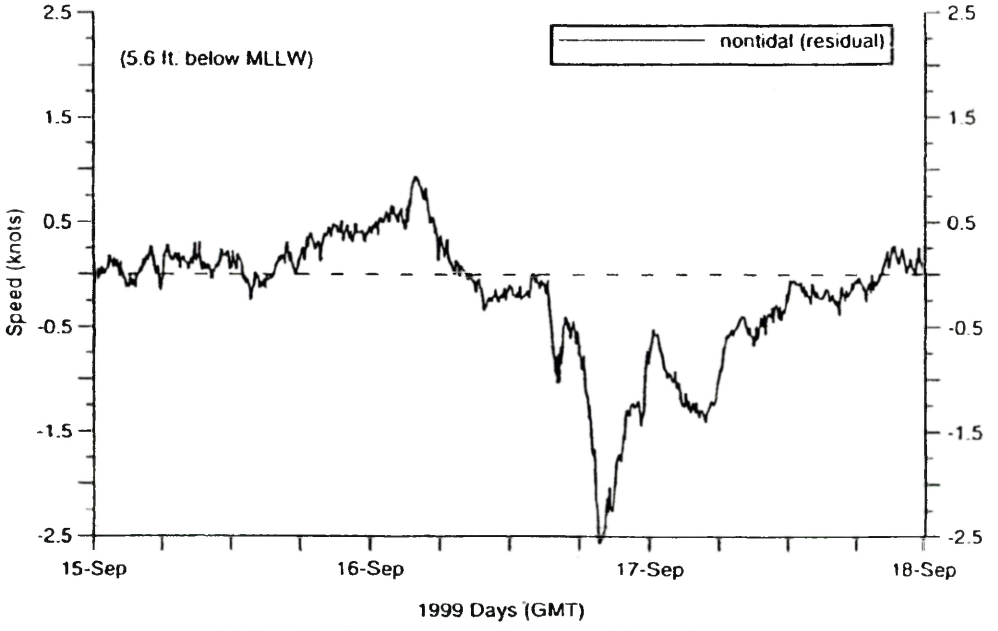

Nontidal (residual) current at Newport News during Hurricane Floyd. Positive current is flood along 183°.

Figure 2-16. Observed current and tidal current prediction at Newport News during Hurricane Floyd (upper panel); Nontidal (residual) current at Newport News during Hurricane Floyd. (Zervas et al., 2000)

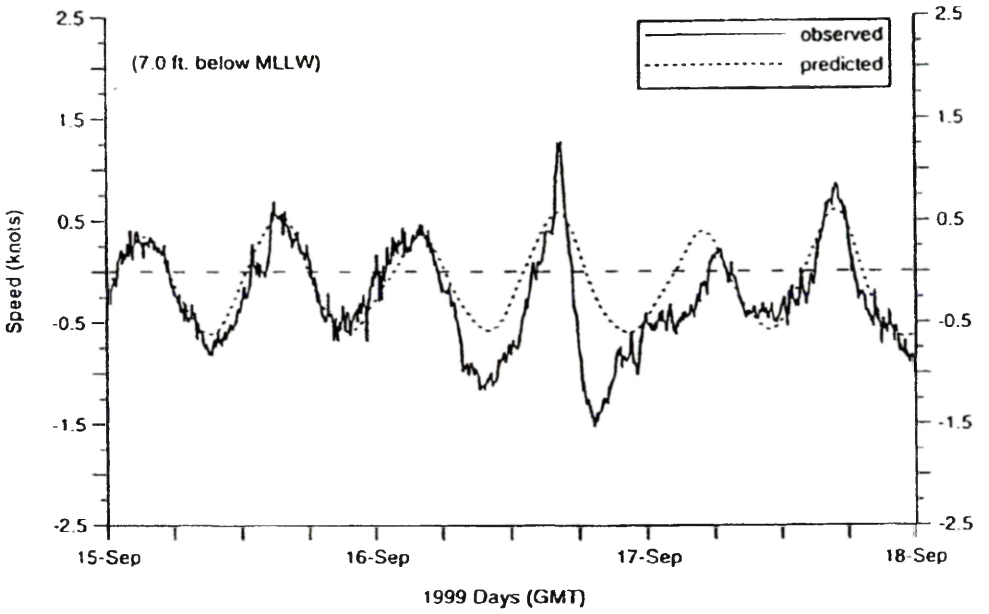

Observed current and tidal current prediction at Craney Island during Hurricane Floyd. Positive current is flood along 183°.

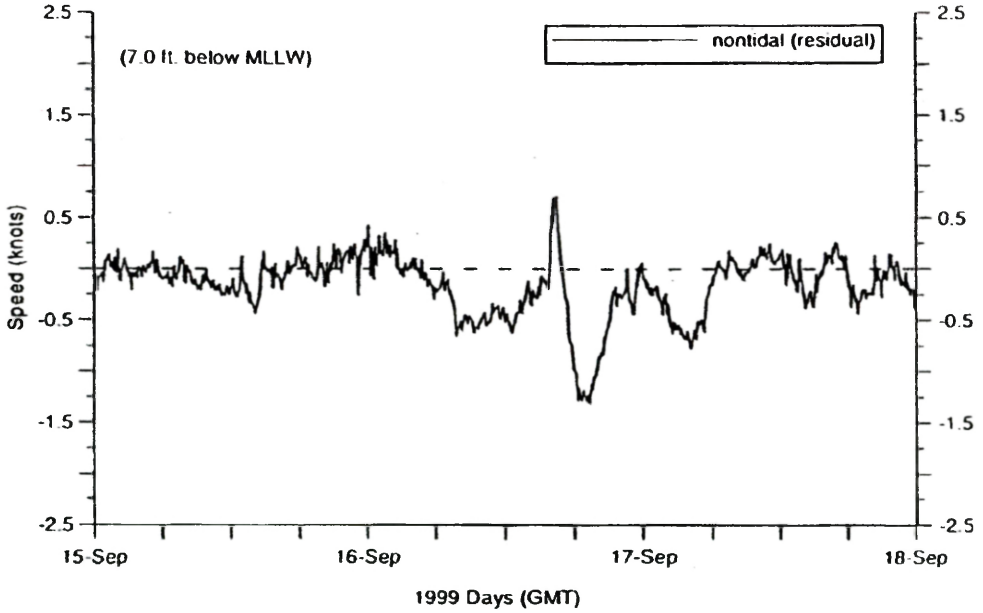

Nontidal (residual) current at Craney Island during Hurricane Floyd. Positive current is flood along 183°.

Figure 2-17. Observed current and tidal current prediction at Craney Island during Hurricane Floyd (upper panel); Nontidal (residual) current at Craney Island during Hurricane Floyd. (Zervas et al., 2000)

CHAPTER 3

Numerical Model Study

Winds generated by atmospheric circulation are random motions, which exert wind stress on the water surface. The water body moved by the winds depends on its direction, magnitude, and the characteristics of the adjacent landscape. The same wind can have very different effects on water level and the circulation pattern if the orientation of the estuary and coastline are different. For example, onshore wind tends to induce "setup", piling up water; offshore wind, on the other hand, tends to move water away and induce a "set down". Wind can also generate turbulence and waves, which in turn affect the velocity and density fields. It is obvious that winds could have significant effects on many physical aspects of the water in the estuary and coastal ocean. From the data analysis presented in the previous chapter, we see that wind can induce setup and set down and disturb salinity (or stratification) and velocity (current) profile in this lower James estuarine system. In an effort to assess a cause-and-effect relationship between different variables, it is warranted to examine the potential effect that the winds might have on this estuarine system. To further understand the dynamic processes, a numerical model study was conducted.

3-1. Model Framework

3-1-1. HEM-3D and Model Domain

In this study, a three-dimensional numerical model, the VIMS three-dimension hydrodynamic – eutrophication model (HEM-3D), was applied to simulate the hydrodynamic behavior of the lower James and Elizabeth River estuary system at various temporal and spatial scales. HEM-3D was developed at the Virginia Institute of Marine Science. This model has been applied to Virginia's James and York River estuaries as well as to several other prototypes. It solves the three-dimensional, vertically hydrostatic, free surface, turbulence averaged equations of motions for a variable density field. The model uses a stretched (or sigma) vertical coordinate system and operates on a Cartesian or curvilinear, orthogonal grid in the horizontal. In basic form, these models simulate the hydrodynamic behaviors of the estuary by predicting changes in surface elevation (including tides), horizontal and vertical water movement (including both tidal and non-tidal currents), and the three-dimensional distribution of conservative water properties such as the salinity. In addition, HEM-3D calculates the bottom shear stress, which is used to determine the sediment deposition potential. For the simulation of flow in vegetated environments, HEM-3D incorporates both two and three-dimensional vegetation resistance formulations (Hamrick and Moustafa, 1995).

To apply the HEM-3D model to our study, we first define the study domain for the model, which spans from the James River entrance to the limit of

tide at Richmond, including the major tributaries of the James River, and extends to the innermost reaches of the Norfolk Harbor and the Elizabeth River. The HEM-3D James and Elizabeth River model employs a dual-scale Cartesian horizontal grid, i. e., 123 × 123 m cell size inside the Elizabeth River and 370 × 370 m cell size for the James River (Figure 3-1), to get a higher resolution inside and around the Elizabeth River. To avoid a possibly negative impact of the sharp change between the dual grid scale (from 370 m to 123.33 m), a transition zone was also set up through four decreasing lengths in grid size with one sixth reduction of coarse grid spacing at each step. A combination of orthogonal curvilinear grids and rotated rectangular grids was used for locations such as the Lamberts Point, the entrance of the Southern Branch, Deep Creek, and the navigation channel. To model the effect caused by existing structures, a feature of the model known as 'masking' was implemented to block flow selectively in specified cells. For bridge pilings, flow impedance and resistance was parameterized for locations with pilings. Totally, there are 7,529 active horizontal cells, each with 6 vertical layers, in this study domain.

Model simulations of approximately six months duration (from March to August, 2000) were conducted using time-varying freshwater discharge and actual tides obtained from historical records. Appropriate surface and bottom salinity were used at the James River mouth (open boundary condition). Local winds recorded at Sewells Point are included through a surface stress parameter. The model will predict changes in surface elevation (including tides), horizontal and vertical water movement, and three-dimensional distribution of conservative

water properties such as the salinity. Results from these runs will permit event-specific or period-specific evaluation of simulation comparison results based on observed data. Based on the observation data and the base case model simulation results, the mechanisms and consequences of wind effects will be analyzed. To predict the possible estuarine response to wind events after the implementation of Craney Island Expansion designs, simulation results of water level, salinity distribution (or stratification), and velocity from each test case will be analyzed.

3-1-2. Input data and parameters

There are five groups of input files: horizontal grid specification files (for geometry, topography or bathymetry for the model domain); general data and run control files; initialization and restart files; physical process specification files; and time series forcing and boundary condition files (for salinity, surface elevation, river inflow, etc.). Among the input files, the topographic data and grid data are critical for model setup.

Several sources of bathymetry data were used for the model setup, which are the existing bathymetry data for the James River, USACE survey data and the NOAA bathymetry data. According to the resolution of the data source, the complete bathymetry data was composed of different weightings of the three sets of source data. Due to its high resolution, the USACE bathymetry data was given the highest weight to form the shoals around Craney Island and navigational channels to Lamberts Point, then the existing James River coarse model grid data was selected as baseline data, and the lowest weight was given to the NOAA data.

Wind stress (τ) was estimated using the quadratic relationship:

$$\tau_{sx} = \rho_a C_D W_x |W|$$

$$\tau_{sy} = \rho_a C_D W_y |W|$$

Where W_x, W_y are the east and north components of the wind velocity, respectively; $|W|$ is the wind speed in m/s; and ρ_a, the density of the air, is 1.2 kg/m^3. The drag coefficient, C_D, is (0.8+0.065*$|W|$)×10^{-3}. Wind speed and direction recorded at Sewells Point (Figure 3-2) were used to calculate wind shear stress.

3-1-3. Initial and Boundary Conditions

To develop the initial condition for the model domain, the model was first "spun up" for 30 days before the salinity calculation was initiated. During the spin-up period, the salinity field observed on March 23 was imposed as a time invariant condition. Concomitant with initialization, boundary conditions are imposed at the upstream and downstream ends of the model domain. For the downstream (open) boundary, these include bay salinity and the water surface elevation; for the upstream boundary, freshwater inflow is specified.

The water surface elevation for the open boundary condition was derived for data observed at Sewells Point. The boundary condition for salinity was constructed by interpolation of buoyed S4 current meter data measured near the model boundary.

Freshwater inputs were specified at 3 locations in the James River (Richmond, Appomattox, and Chickahominy) and 5 locations in the Elizabeth River (Deep Creek, Lafayette River, Eastern Branch, Western Branch, and

Southern Branch). Daily discharge were obtained at the 3 USGS gauge stations in the James, Appomattox, and Chickahominy Rivers, and at the US Army Corps of Engineer's flow station at the upstream end of Deep Creek (Figure 3-4).

3-2. Model Calibration

Some results from the numerical experiment are presented in this section. Besides being capable of reproducing the observed events, the numerical model study can provide insight into how the wind driven circulation interacts with water level, velocity, and salinity fields. A seven-day period (i.e., Julian days 149-155) was chosen. During this period, a northeasterly wind peaked at 14.1 m/s, the mean river discharge is 110 cms, which is below the annual average of 155 cms. Four locations in the Elizabeth River, shown in Figure 3-5, were selected for displaying salinity and water level. Two regions, one in the Hampton Roads area, and another near Lamberts Point within the Elizabeth River, were chosen to present the residual velocity vector distribution.

3-2-1. Water Level

As shown in Figure 3-6, the model-predicted water levels compared very well with the observed data. It is noted that the model not only predicts the astronomic tide but also reproduces the meteorological event accurately. For instance, as stated before for the observed data, the water level revealed a setup (i.e., on Julian days 110, 116, and 150) due to the northeasterly wind, and set down by southwesterly wind (i.e., on Julian days 100 and 140). It is noteworthy, for example, that the prediction not only caught the peak value, but also reflected the relaxation of the wind events.

3-2-2. Salinity

Salinity time series predicted by the numerical model for the base case with wind forcing are shown in Figure 3-7.

It can be seen that, generally, there is a stratification-destratification pattern that is regulated by the spring-neap tidal cycle. The tide forcing is much stronger in the lower James than that in the Elizabeth River, which is indicated by the ebb-flood signal at these stations. In addition to tides, river discharge and wind also play their roles in determining the salinity structure in this estuarine system.

In Figure 3-7, the salinity time series show that sometimes the regular stratification-destratificaiton pattern was disrupted by either river discharge or wind. For example, on Julian day 120, water columns were strongly stratified (the difference between surface and bottom salinity is up to 15 ppt at ER01, and 10 ppt at ER07) at both stations, which might be caused by the big pulse of river discharge on Julian day 110 measured at Richmond, in the upper James River. A large amount of freshwater flowing over saline water causes a surface salinity decrease. Immediately after passage of this freshwater pulse, the barotropic pressure gradient decreases, salt water intrudes upriver along the bottom, and these salinity increases at the bottom 'over-shoot ', resulting in a highly stratified condition. After that, vertical mixing between surface and bottom water begins to alter the salinity structure until it is similar to that expected during a 'normal' condition.

Also, it can be shown that the water column is extremely mixed during certain periods, which is probably caused by wind forcing. For example, the strong northeasterly wind on Julian day 150 causes both the surface and bottom salinities to decrease, which results in a well-mixed water column at all four locations. The destratification is possibly due to the advection of relatively fresh water into the lower James from the upper Chesapeake Bay by the strong northeasterly wind, and then mixed by wind. This is reflected in the boundary salinity profile of the Thimble Shoals station shown in Figure 2-4. A similar destratification phenomenon was reported in the York River (Hayward et al., 1982), where an estuary-subestuary interaction induces the advection of relatively fresh water into the river mouth from the Chesapeake Bay, and commences the destratified condition when spring tides exceed a critical height. In this case, in the lower James and Elizabeth River, instead of normal tidal motion, the strong northeasterly wind pushes the upper bay freshwater into the mouth region of the James, both surface and bottom salinity are decreased, strong wind mixing reduces the vertical salinity gradient, which, in turn, induces the destratification inside the James and Elizabeth.

Contour plots of salinity structures along the Elizabeth River are shown in Figures 3-8a to 3-8e. The upper panels show salinity data from 5 slackwater surveys whereas the lower panels show model predictions.

As can be seen from these plots, compared with the field data, the model did generate quite satisfactory results. The stratification-destratification pattern was reproduced at the right time, and those extreme conditions (i.e., a strongly

stratified water column on Julian day 122 or a well-mixed condition on Julian day 159) were also being displayed in these plots. Moreover, as observed in the slack surveys, a reverse surface salinity gradient was also captured on May 1 and May 15 by the model, revealing its capability to properly simulate dynamic mechanisms for the lower James and Elizabeth River system.

In summary, from the slackwater surveys and model results, it appears that the volume of fresh water inflow, tidal mixing, and suitable winds are the controlling variables determining the salinity structure in the Elizabeth. Accordingly, a model sensitivity experiment is conducted to determine how each individual forcing will affect the salinity structures in this system. This will be presented in Chapter 4 for a detailed description.

3-2-3. Currents

From an analysis of current records at fixed stations, it can be seen that the wind can greatly affect the velocities generated by tides and gravitational circulation. In this section, one more step is to examine the circulation pattern affected by the wind with the aid of the three-dimensional model.

In order to use the model results to assist in interpreting the wind effects, Hampton Roads in the lower James and Lamberts Point in the Elizabeth were selected to demonstrate the consequence of one strong northeaster wind (on Julian day 150).

The model was first used to simulate conditions without wind, using mean discharge, and a three-constituent (M_2+N_2+S_2) tide condition (i.e., single variable run, Wang et al., 2001). The results in the lower James show that the surface

residual currents are moving seaward with a speed on the order of 10-20 cm/sec. The strength of the surface residual current varies depending on neap, spring, and average tidal condition: the surface current being the strongest in the neap, followed by the average condition, and lastly the spring tide condition, when the current is weakest (Figure 3-8a). Inside the Elizabeth River at Lamberts Point, the surface residual current is less organized as compared to the lower James. In the neap, the surface circulation does show seaward movement with speeds on the order of 2-5 cm/sec. In the averaged spring tide condition, however, there is no clear indication of seaward surface flow. On the other hand, a circulation eddy current was obvious at Lamberts Point bend.

In order to examine the wind event effect on the two regions, model results from real time simulation (with recorded salinity, tidal elevation, and fresh water discharge as boundary conditions, and adding in the wind forcing) are plotted in Figure 3-8b. In the lower James region, the overall current magnitude has little change as compared with the single variable run. The current pattern on Julian day 149, before the wind event, is also similar: surface current flows downstream (ebbs) in the main channel, and very weakly floods on the shoal area. Part of the water in the Hampton Roads area was pumped into the Elizabeth. As wind is added, the current magnitude and pattern are strongly changed. Strong northeasterly wind pushes Bay water into the lower James, and reverses the direction of the surface flow in the main channel to that of the wind direction. It also enhances flooding on the shoal area. As the flood flow encounters the strong ebb current from the upper James below the sharp bend, the flood current still can

overcome the downstream current, but the magnitude is relatively small. Immediately after the wind event, on Julian day 151, its influence still exists with a strong flood flowing over the shoal area. On Julian day 152, the lower James almost completely returns to the pre-event condition. Inside the Elizabeth, a more obvious enhanced flood can be observed, with a magnitude several times larger than that of the single variable run. This could be a result of the strong northeaster wind pushing bay water into the Elizabeth, and strengthening the landward flow to the upper Elizabeth. It may also pile up the water level within this estuarine system, and will increase the total water volume (flushing) into the Elizabeth.

3-3. Model Sensitivity Test

3-3-1. Experiment Design

To have a basic understanding of the effect from different mechanisms (i.e. tide, river discharge, and wind) on the lower James system, three sets of model experiments were designed, as shown below.

Table 3-1. Model experiments

Model Experiment	Condition
1	Constant river inflow; $M_2+S_2+N_2$.
2	Real time river inflow ; $M_2+S_2+N_2$.
3	Wind; Constant river inflow; $M_2+S_2+N_2$.

1. The first model experiment has the same condition as the single variable simulation in the CIEE project (Wang et al., 2001), in which tidal range, as the only single input variable, varies between standard astronomical extremes

during the course of a run. A three-constituent harmonic model is used, composed of the M_2, S_2 and N_2 tidal constituents with phasing adjusted to produce tides of maximum, mean, and minimum range during a single run of 134 tidal cycles.

2. The second model experiment includes both the tidal forcing and river discharge as input variables. By comparing the results of model experiments 1 and 2, one can assess the effect of river discharge.

3. The third model experiment includes, instead of river discharge, wind forcing as the other input variable. By comparing the model results of model experiments 1 and 3, the wind effect on this system can be seen.

Time series of surface elevations and salinity at both surface and bottom from selected stations will be presented in order to compare the difference among these model simulations.

3-3-2 Model Results

1) Figures 3-10 and 3-11 show surface elevation variation at stations ER01, ER03, ER05 and ER07. From these plots, we can see that, not only in the lower James but in the Elizabeth River, both surface elevations display a strong tidal signal. Also, flood-ebb and spring-neap alternation is obvious. As water travels upstream, the magnitude of surface elevation increases, given the standing wave characteristic of the Elizabeth. Figures 3-12 and 3-13 show the salinity variation. Through these plots, we see that after JD 100, the model reaches its equilibrium, both surface and bottom salinity vary regularly in response to the tidal forcing. Oscillations in salinity reflect the flood-ebb changes. There is a very strong spring-neap tidal variation that results in a periodic stratification-

destratification in the estuary. Bottom salinity varies obviously as a result of spring-neap alternation: bottom salinity reaches its maximum during neap, while it reaches its minimum during spring. Compared with bottom salinity, surface salinity varies less, but still the alternation phenomenon is observed, with surface salinity rising to a maximum during the spring tide period and dropping to a minimum during the neap tide period. In an attempt to quantify the surface and bottom variation patterns, the salinity difference between the two is used here as a relative measure of stratification. Generally, this difference is bigger during spring than during neap. Thus, it causes a stronger stratified water body during the neap tide period. This may be explained by the estuarine circulation pattern. In a classical partially stratified estuarine system, the surface layer water flows outside and the bottom water intrudes. During the spring tide period, a stronger tidal current induces a better mixed water column. Conversely, during the neap tide period, the water column is relatively steady. As expected, salinity at slack before ebb tide would be higher at spring tides than at neap tides, and salinity at slack before ebb tide would be lower at spring tide than at neap tide.

2) Figure 3-4 shows the real time recorded river discharge, which is used as river inflow boundary condition for the model simulation. There is a peak river inflow around Julian day 110, reaching a maximum of 1000 cms. This large volume of river inflow has little impact on water level as shown in Figures 3-14 and 3-15. However, it affects the salinity distribution (Figures 3-16 and 3-17). This time, surface salinity has a big drop four days after the peak river inflow (around Julian day 119). After the pulse of huge river inflow, surface salinity

gradually increases, overcoming the tidal forcing influence, while salinity just changes slightly. This causes the water column to become strongly stratified on Julian day 119, and then continue to mix. The result is a better mixed water body than one resulting from tidal mixing alone. In Figure 3-4, this big pulse of fresh water inflow enhances the surface outflow in the Lower James area. As a result, stronger bottom flows from the Bay area, brings much saltier water into the lower James and reaches further upstream, which causes a strongly stratified water column. While in the Elizabeth, part of the fresh water brought down from the Hampton Roads region was pumped into the Elizabeth, reversing its surface flow. To compensate for the reversed surface flow, the direction of bottom current changes from intrusion into to extrusion from the Elizabeth, which drives fresher water from the upper Elizabeth into the lower James. This pushes salt water, brought into Elizabeth before this pulse, to the downstream.

3) Wind data recorded at Sewells Point was input to the model. As shown in Figures 3-18 to 3-19, the salinity variation still reflects the tidal signals. However, superimposed on this tidal signal are more irregular mixing events associated with peaks in the surface wind stress. Indeed, these wind-mixing events appear at least as important as strong tides in mixing the predominantly stratified water column. Both surface and bottom salinities display larger oscillations, especially surface salinity. Instead of a gradual change, this variation is obviously in response to wind forcing, wind-induced mixing exceeds tidal mixing, and the water column is better mixed compared with that only forced by tides. An extreme mixing event appears around JD 150. A stronger stratification

stage is observed from these plots around Julian day 120, which coincides with a strong northeasterly, as shown in Figure 2-1. Several northeasterly wind events occurred during this simulation period (on Julian days 82, 110, 116, 150, and 226). Associated with these strong wind events, the water column is well mixed, except during one event on Julian day 116. The weakening of the winds coincides with neap tidal currents, which were not energetic enough to maintain vertical homogeneity and must have allowed the self-adjustment of the density gradient and the seaward advection of relatively buoyant waters near the surface. This results in the extremely stratified water column on JD 120. The findings of this model experiment indicate that, in general, enhanced stratification in the lower James follows a northeasterly wind event, provided that this relaxation period coincides with a weak regime (i.e., neap tide). Wind is composed of different magnitudes and directions, and both of them have different effects on this estuarine system, as shown in chapter two. Therefore, to get a better understanding of the impacts of different wind directions and magnitudes on the lower James system, another set of numerical model experiments was designed, as described in the next chapter.

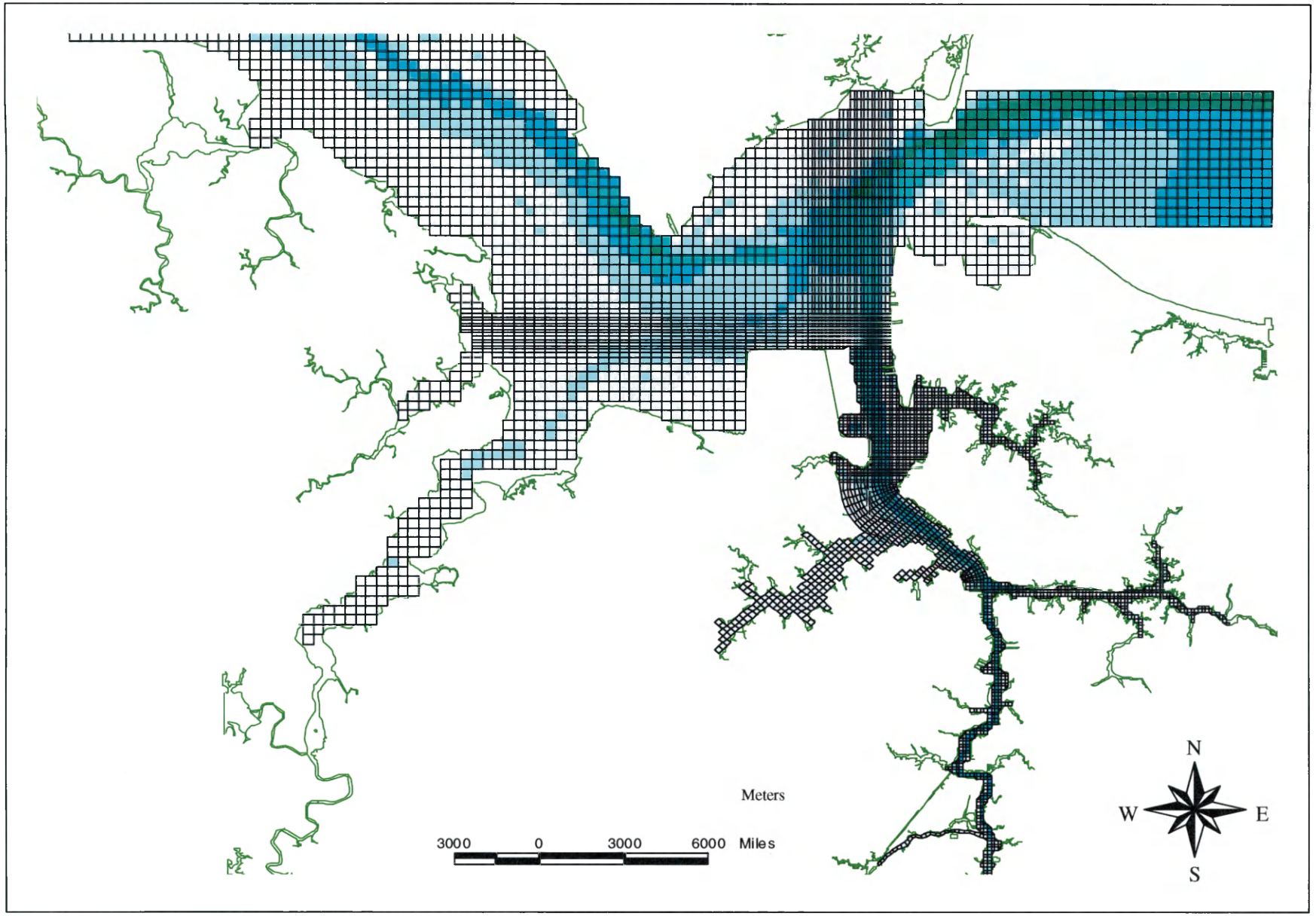

Figure 3-1. Dual-Scale Model Grids of study domain

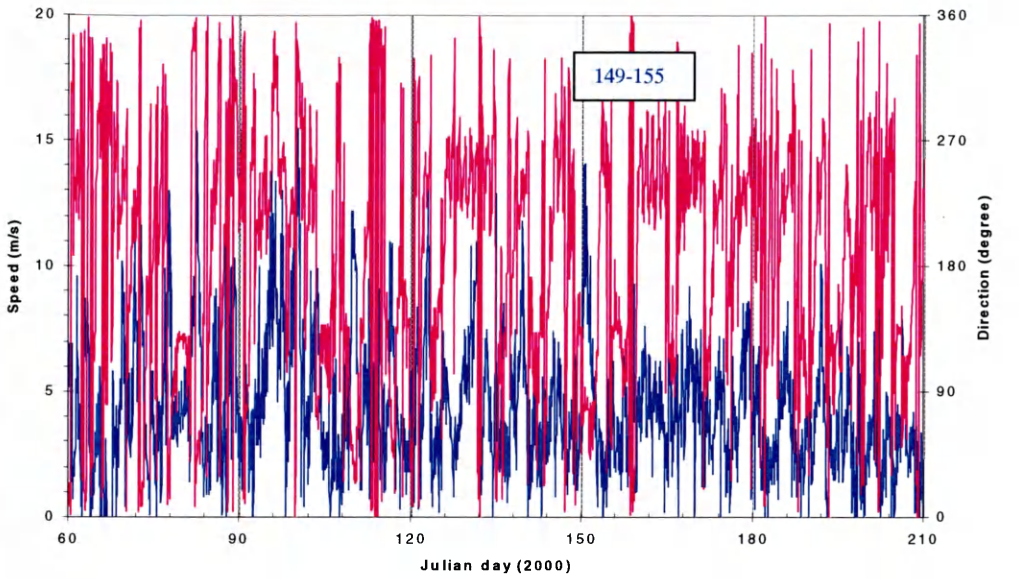

Figure 3-2. Wind Speed and Direction – Sewells Point, VA

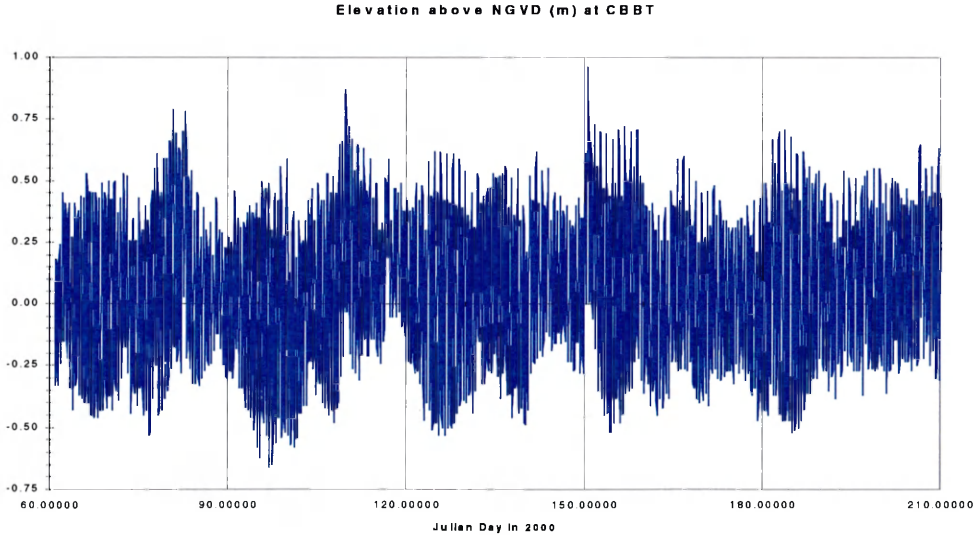

Figure 3-3. Historical records of water Level in meters above NGVD
Chesapeake Bay Bridge Tunnel

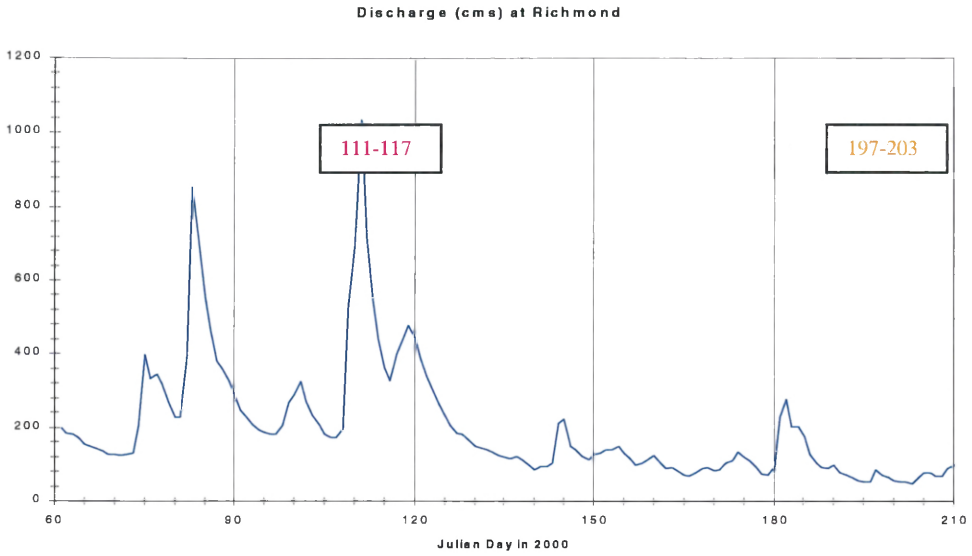

Figure 3-4. Mean daily river discharge measured at Richmond

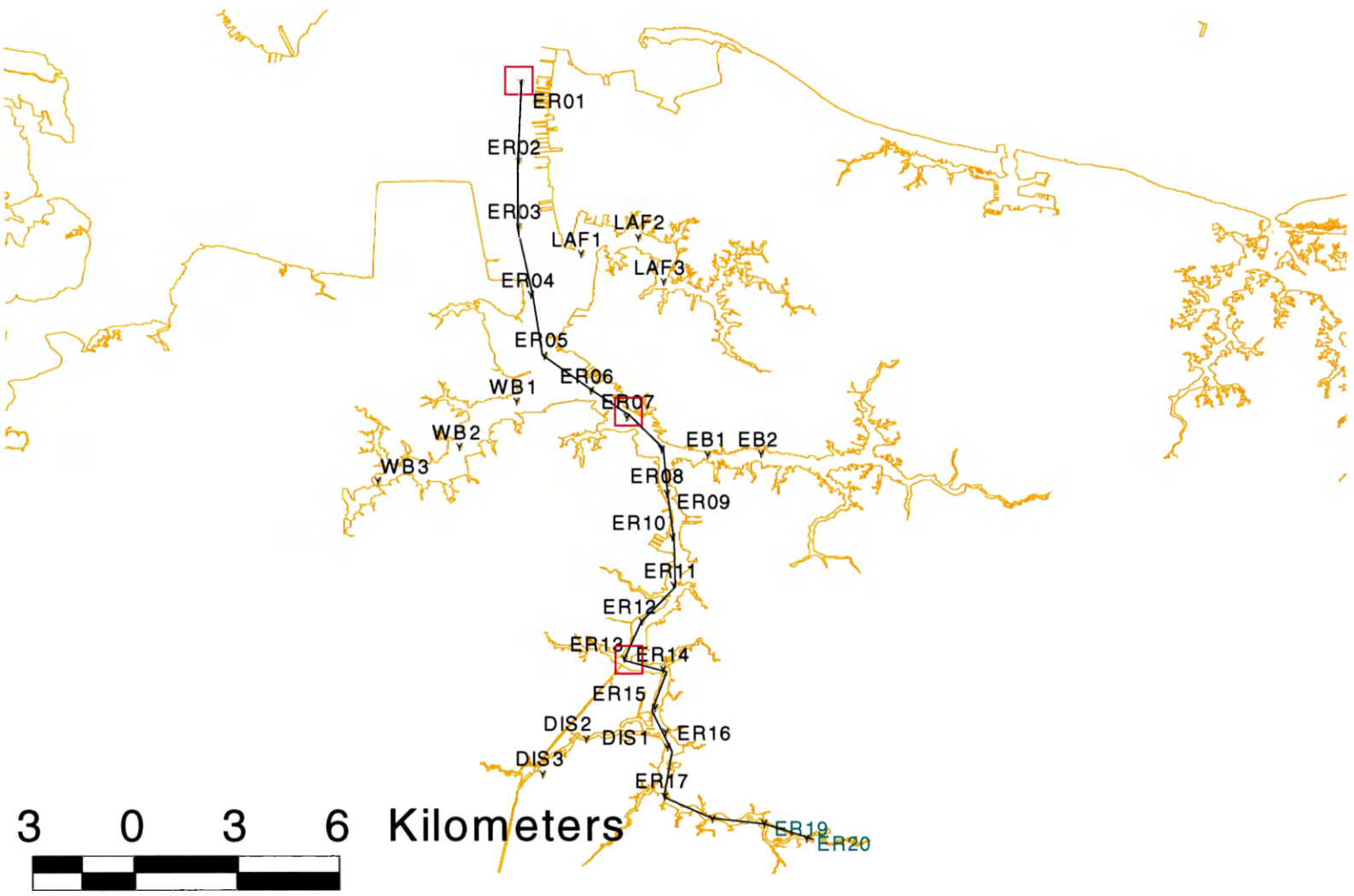

Figure 3-5. Selected locations for model results

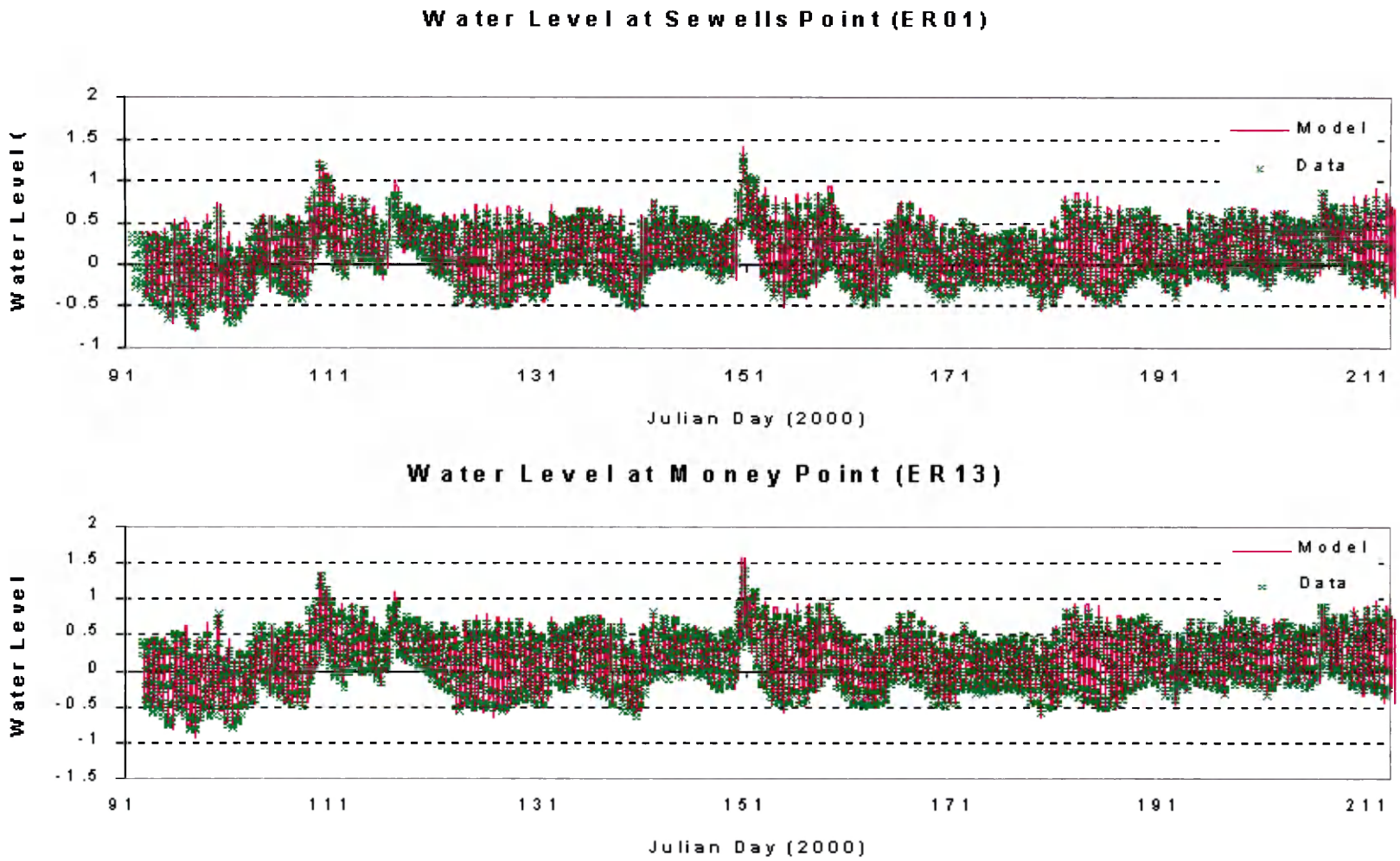

Figure 3-6. Water Level comparison between model results and data at Sewells Point and Money Point

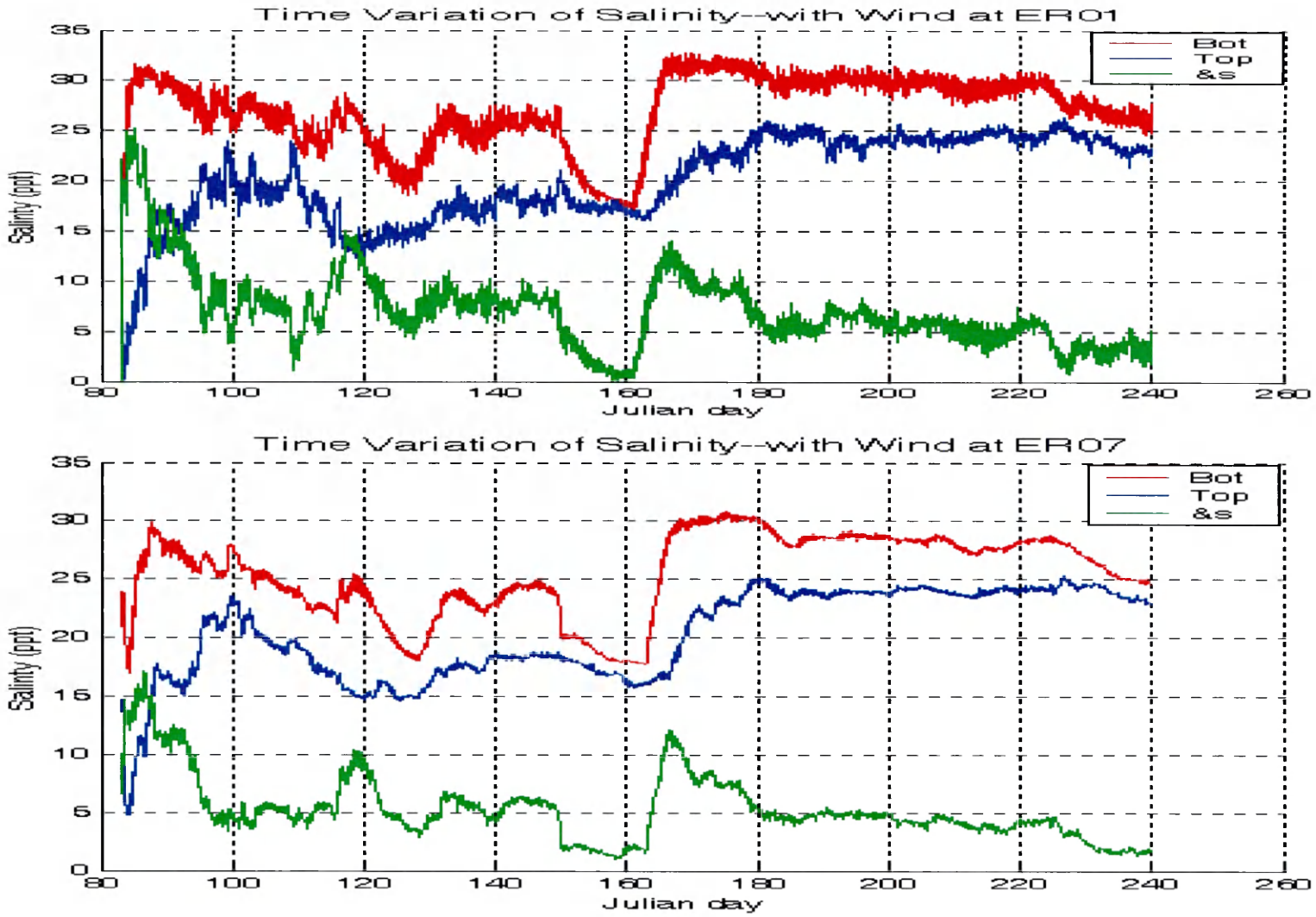

Figure 3-7. Predicted salinity time series at location ER01 and ER07

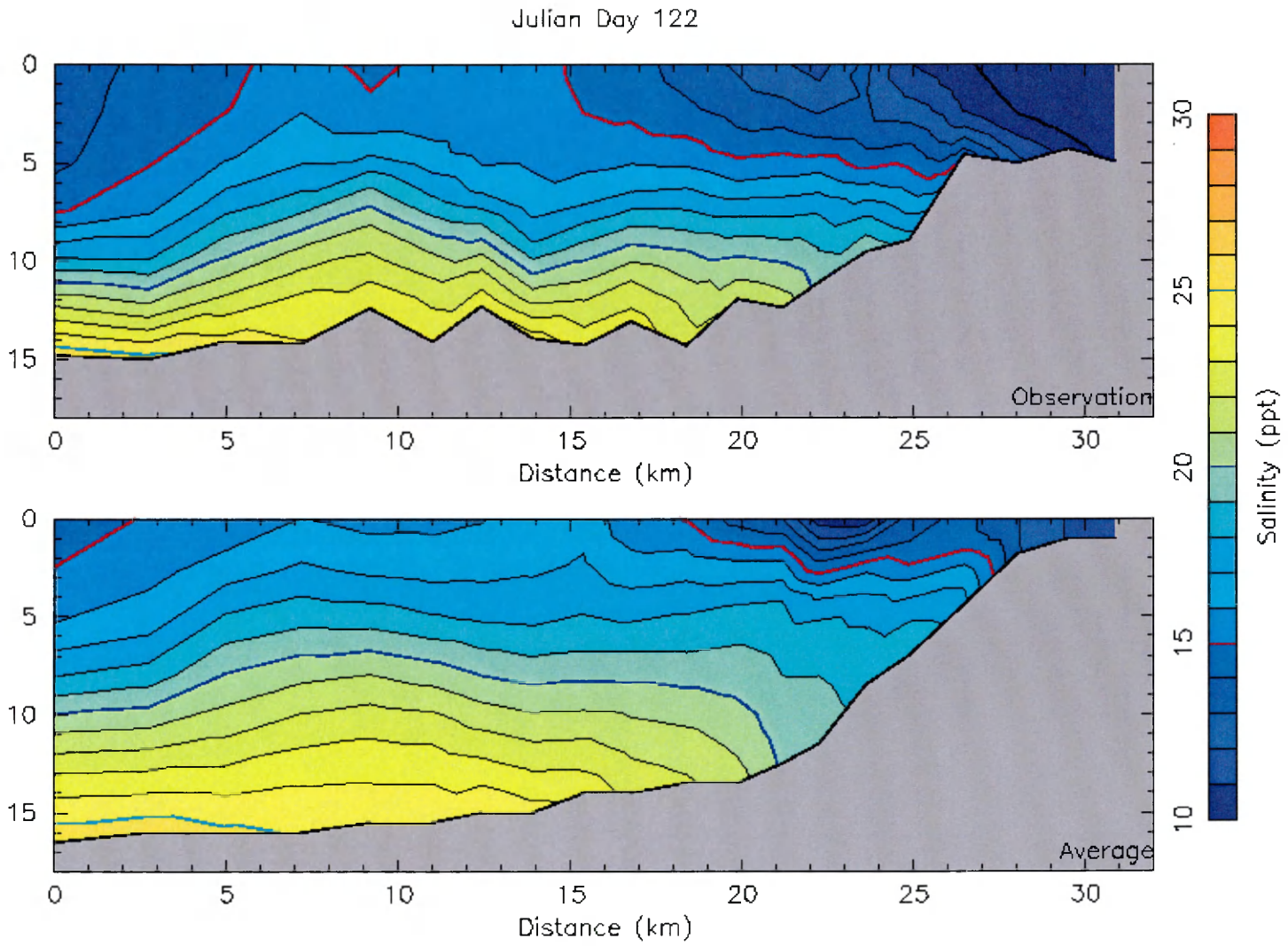

Figure 3-8a. Salinity contour plots on May 1, 2000; observed (top), modeled (bottom).

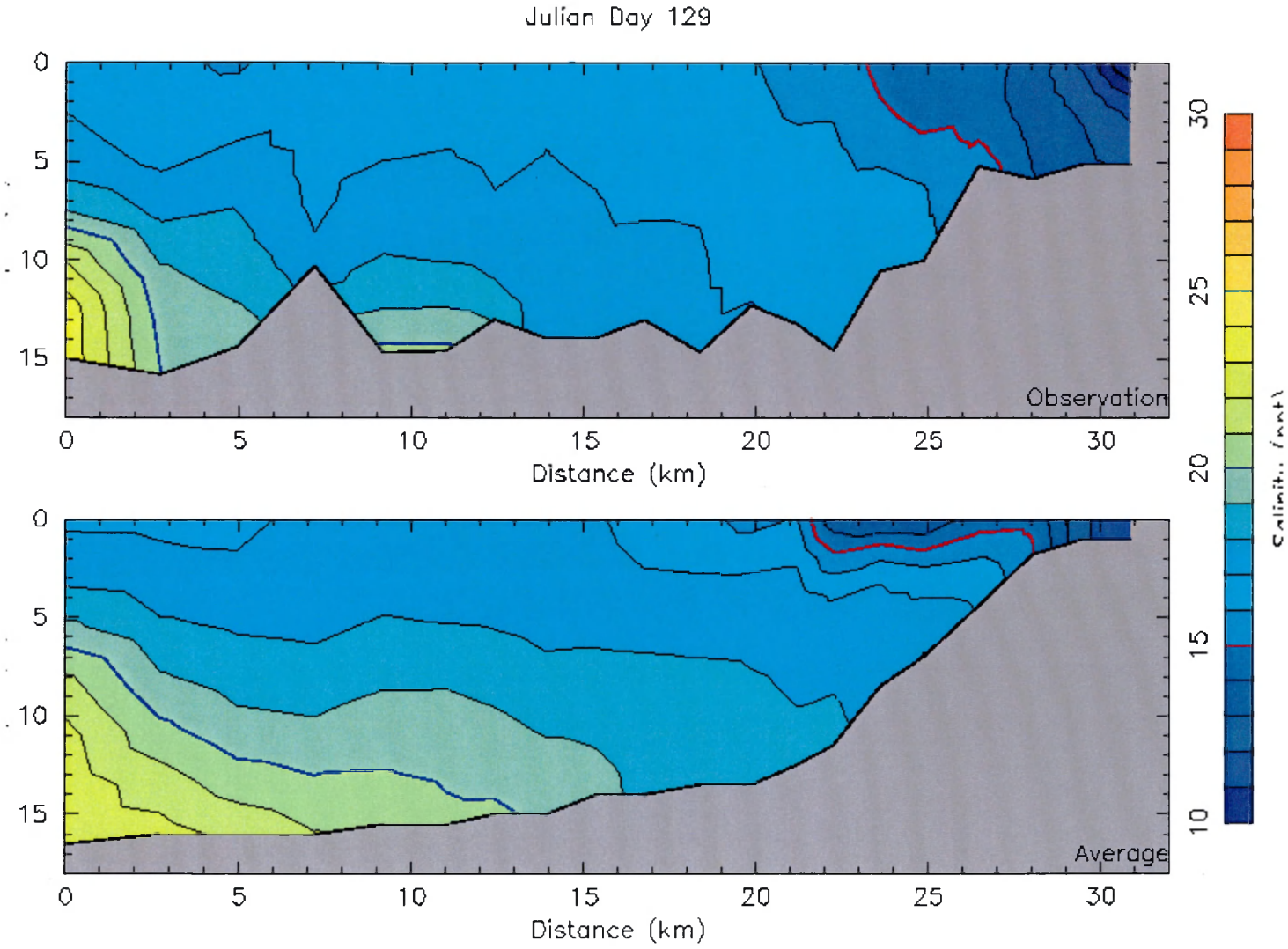

Figure 3-8b. Salinity contour plots on May 8, 2000; observed (top), modeled (bottom).

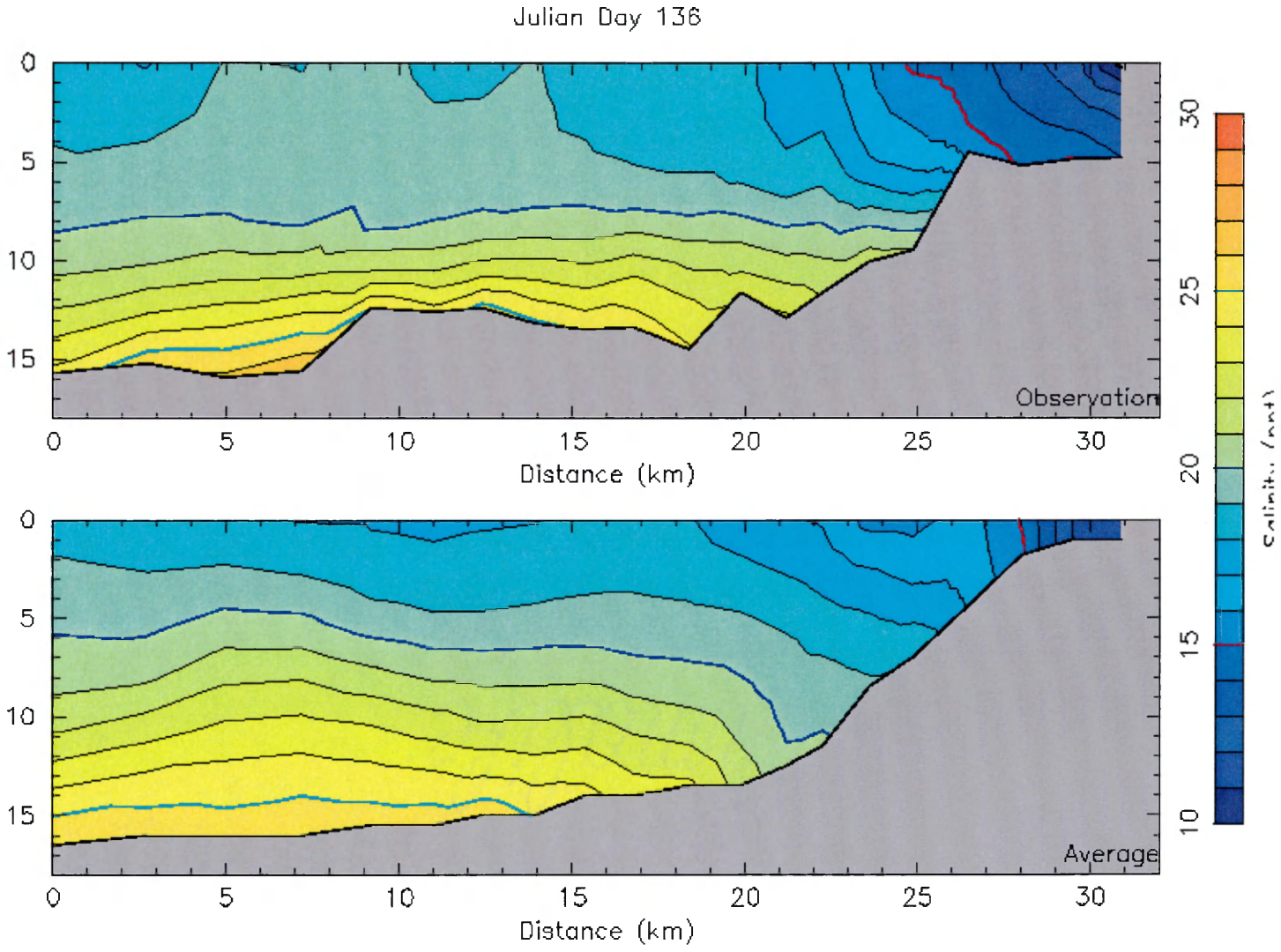

Figure 3-8c. Salinity contour plots on May 15, 2000; observed (top), modeled (bottom).

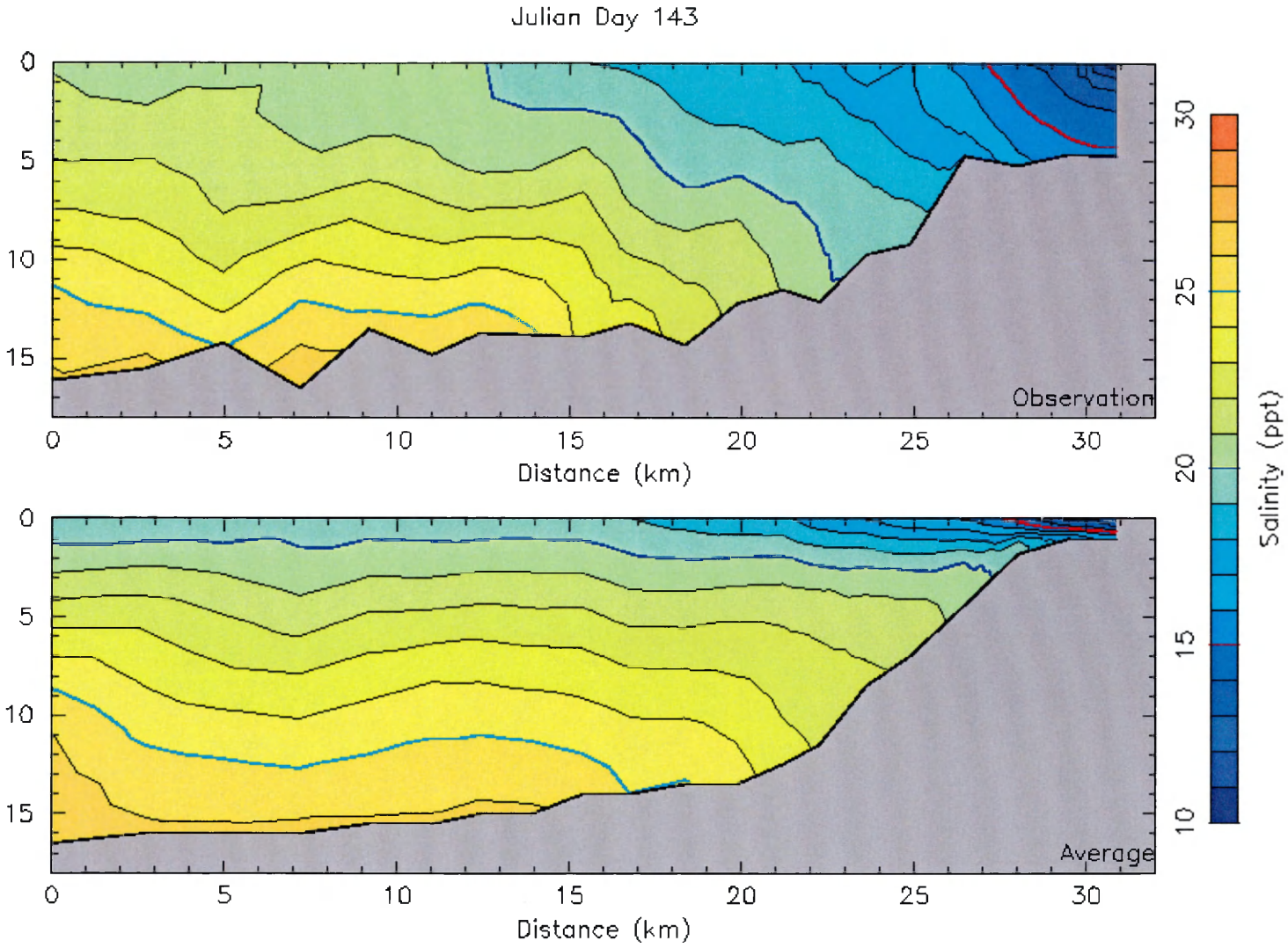

Figure 3-8d. Salinity contour plots on May 22, 2000; observed (top), modeled (bottom).

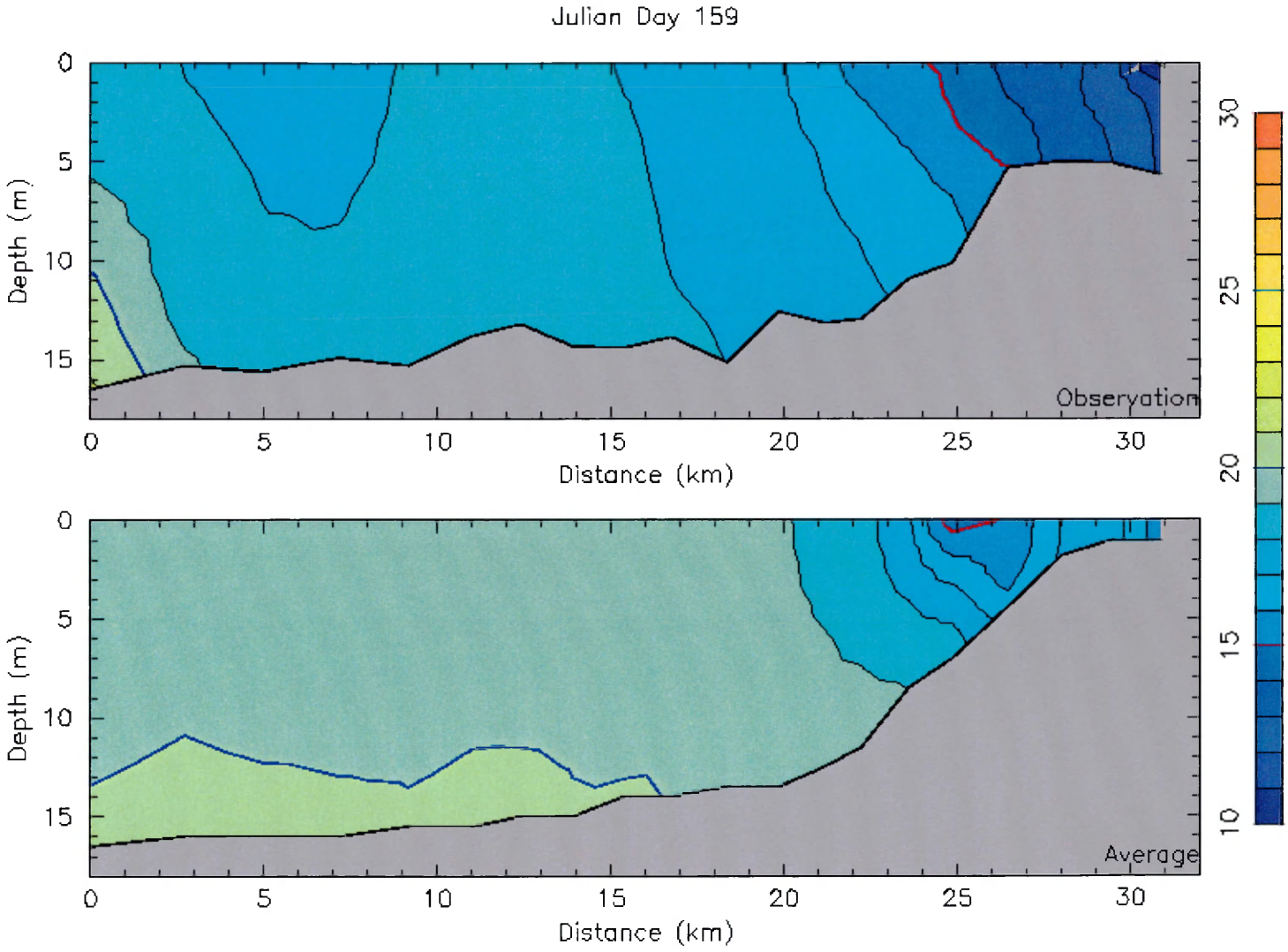

Figure 3-8e. Salinity contour plots on June 7, 2000; observed (top), modeled (bottom).

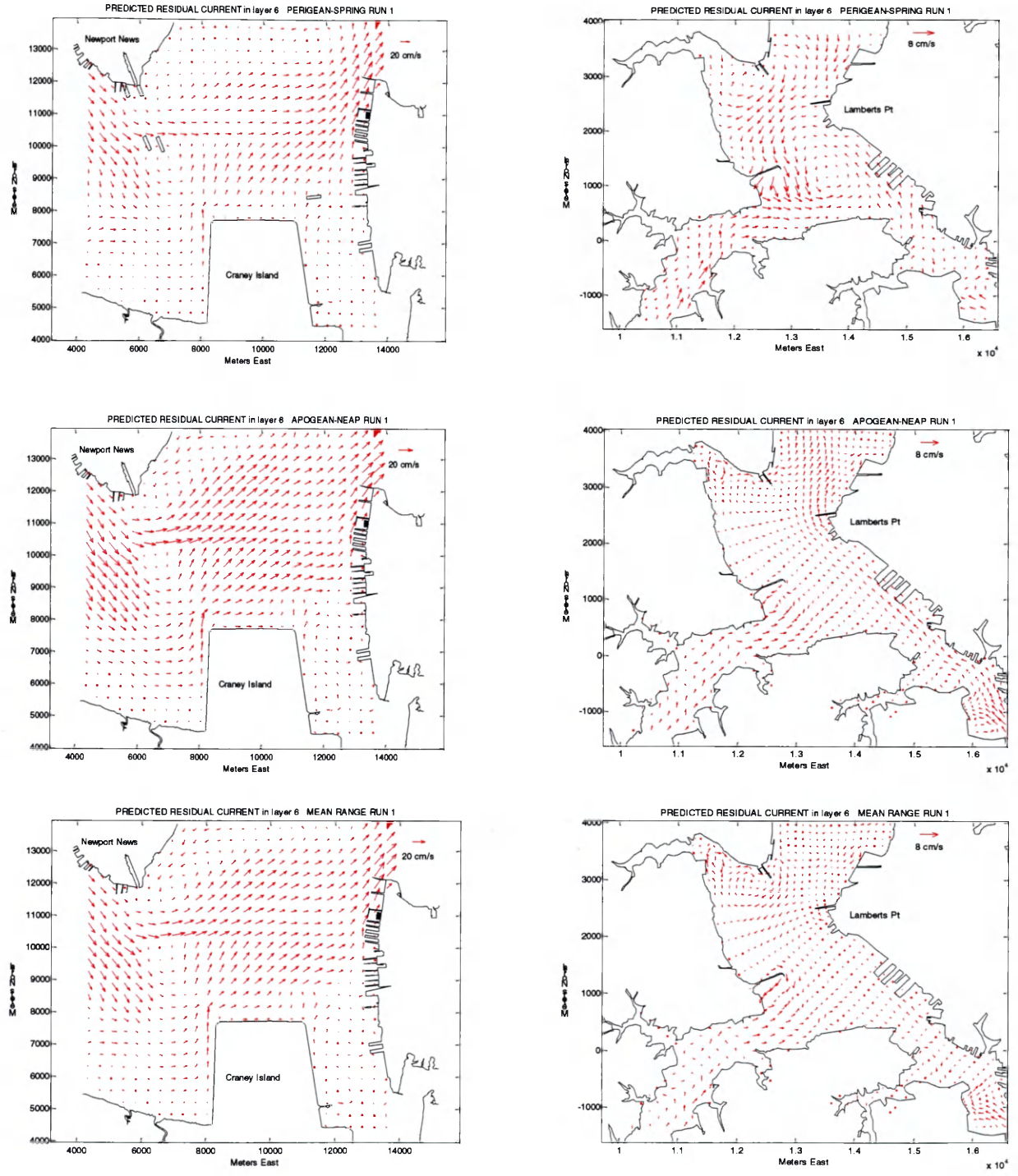

Figure3-9a. Predicted surface residual flow for the lower James and Elizabeth River (from single variable run, with no wind)

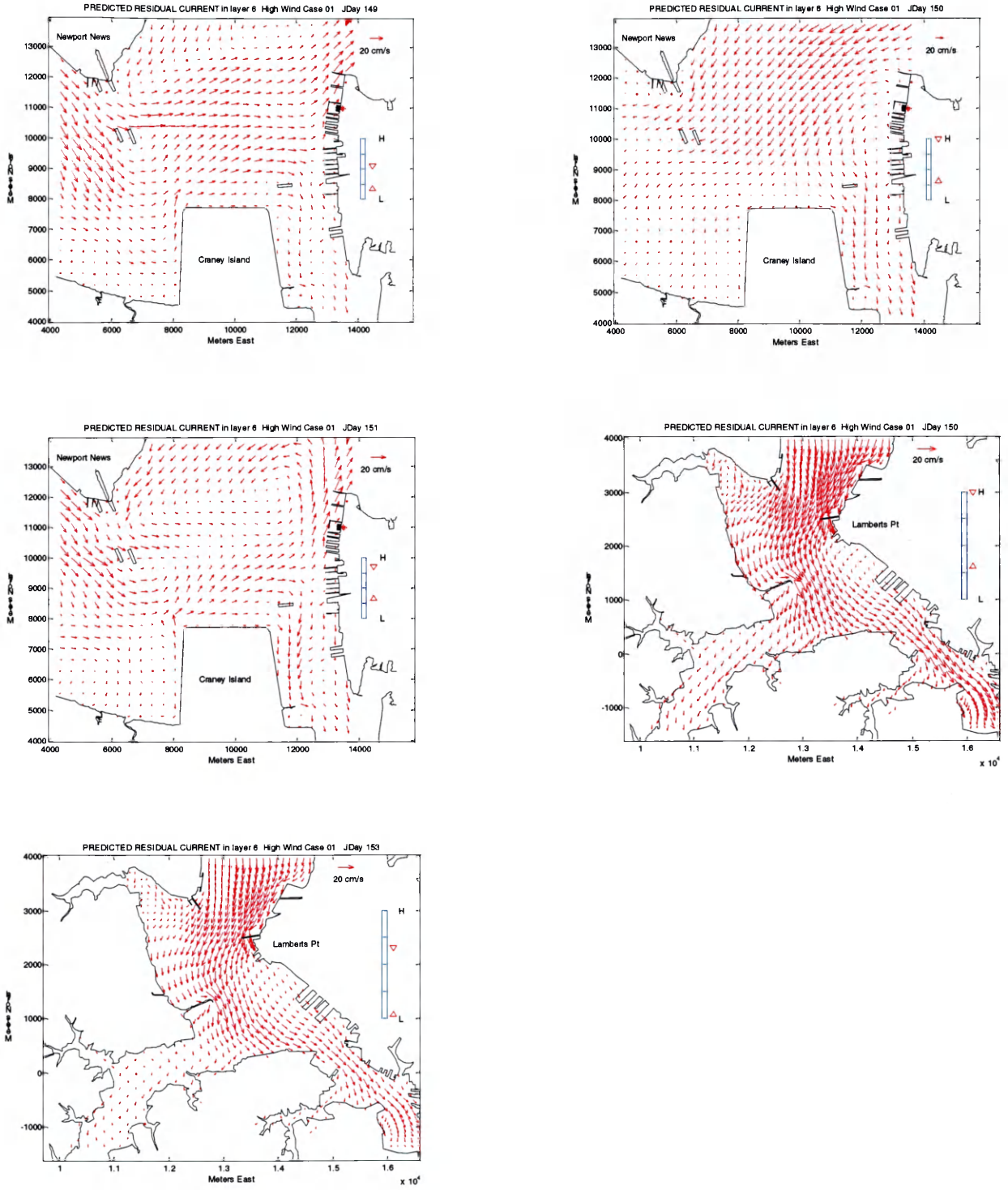

Figure 3-9b. Predicted surface residual flow for the lower James and Elizabeth River (from real time simulation, with wind forcing)

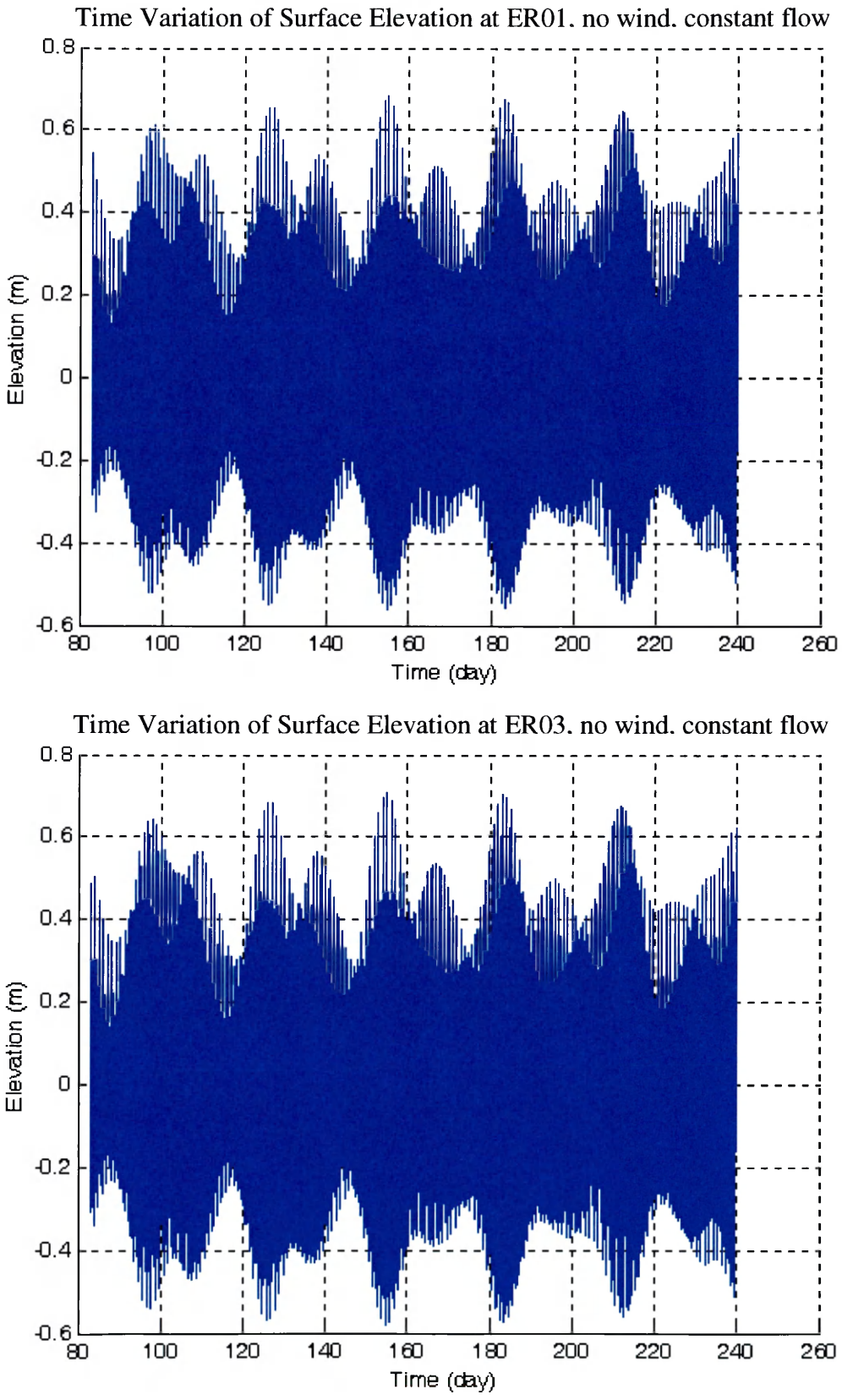

Figure 3-10. Surface elevation variation at station ER01 & ER03, under no wind constant flow condition

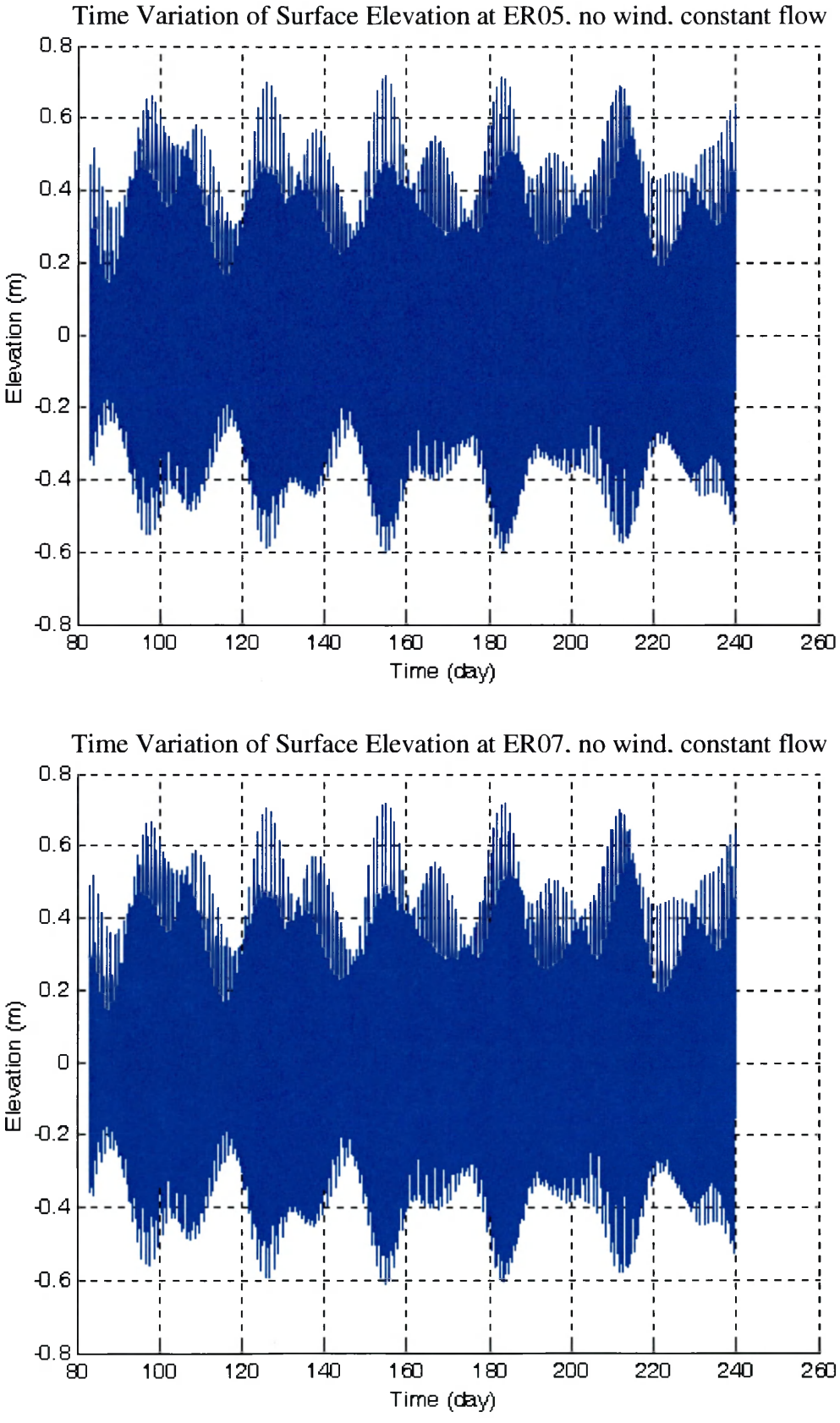

Figure 3-11. Surface elevation variation at station ER05 & ER07, under no wind constant flow condition

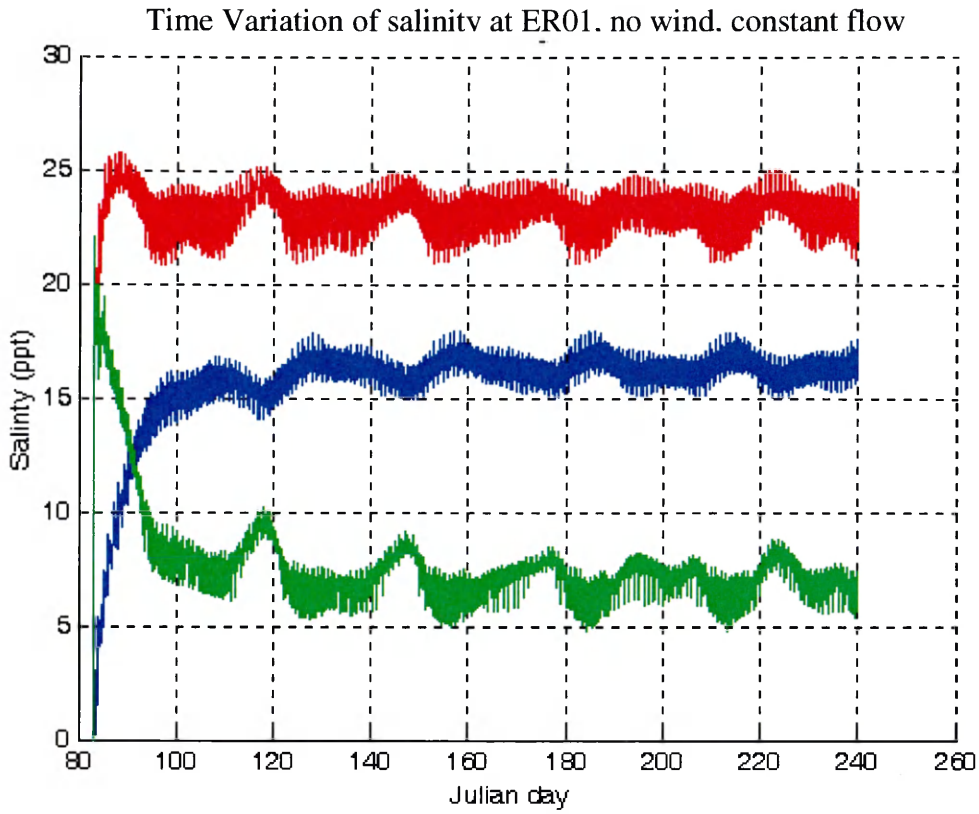

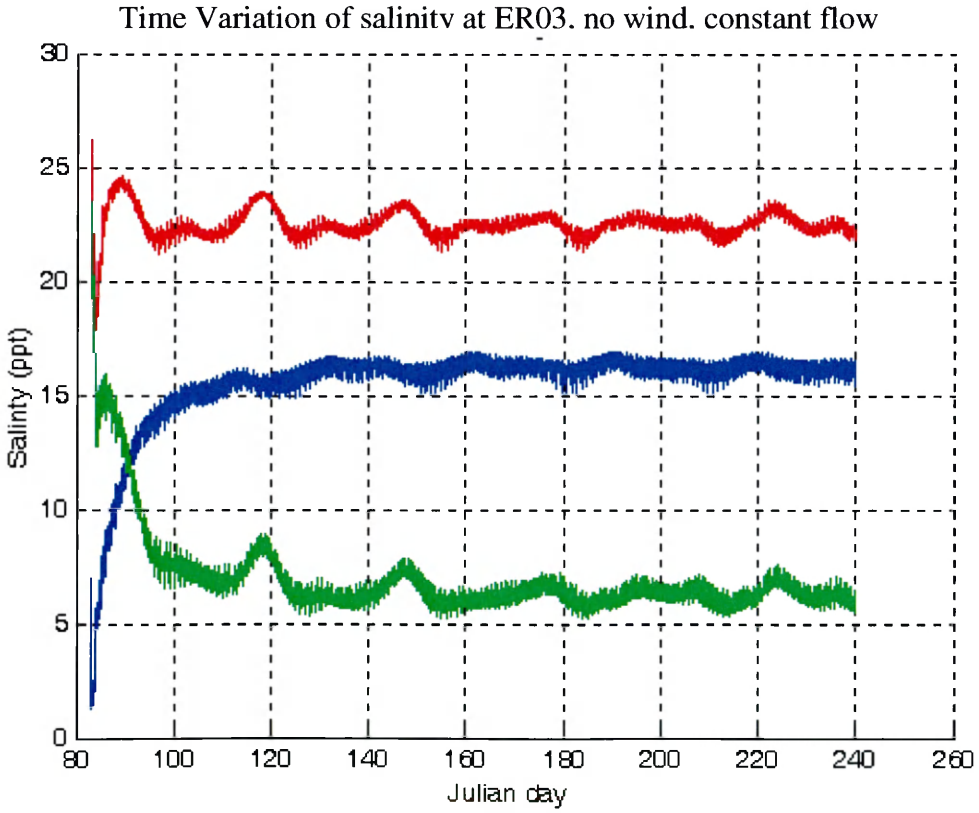

Figure 3-12. Salinity variation at station ER01 & ER03, under no wind constant flow condition. (blue: surface salinity; red: bottom salinity; green: difference)

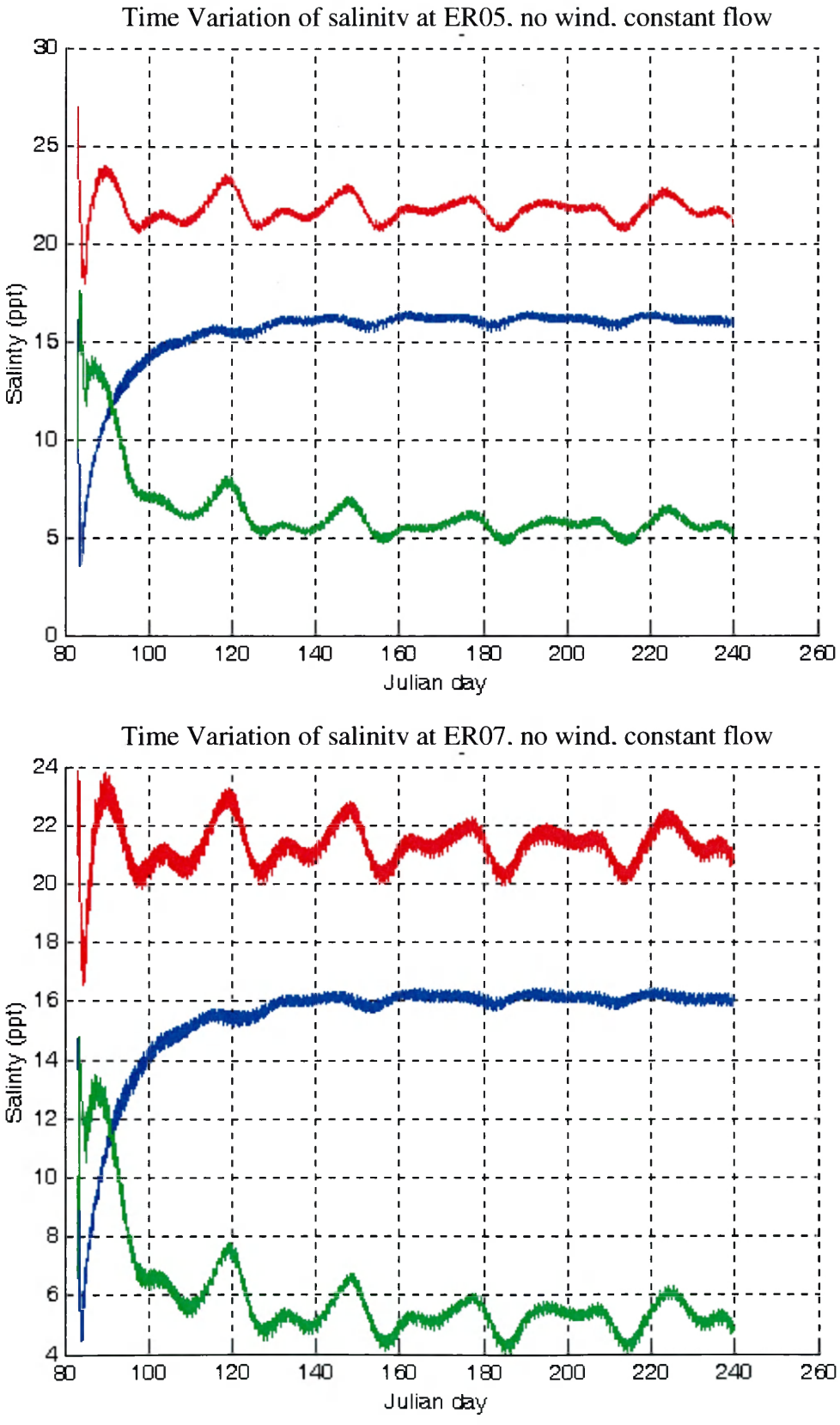

Figure 3-13. Salinity variation at station ER05 & ER07, under no wind constant flow condition. (blue: surface salinity; red: bottom salinity; green: difference)

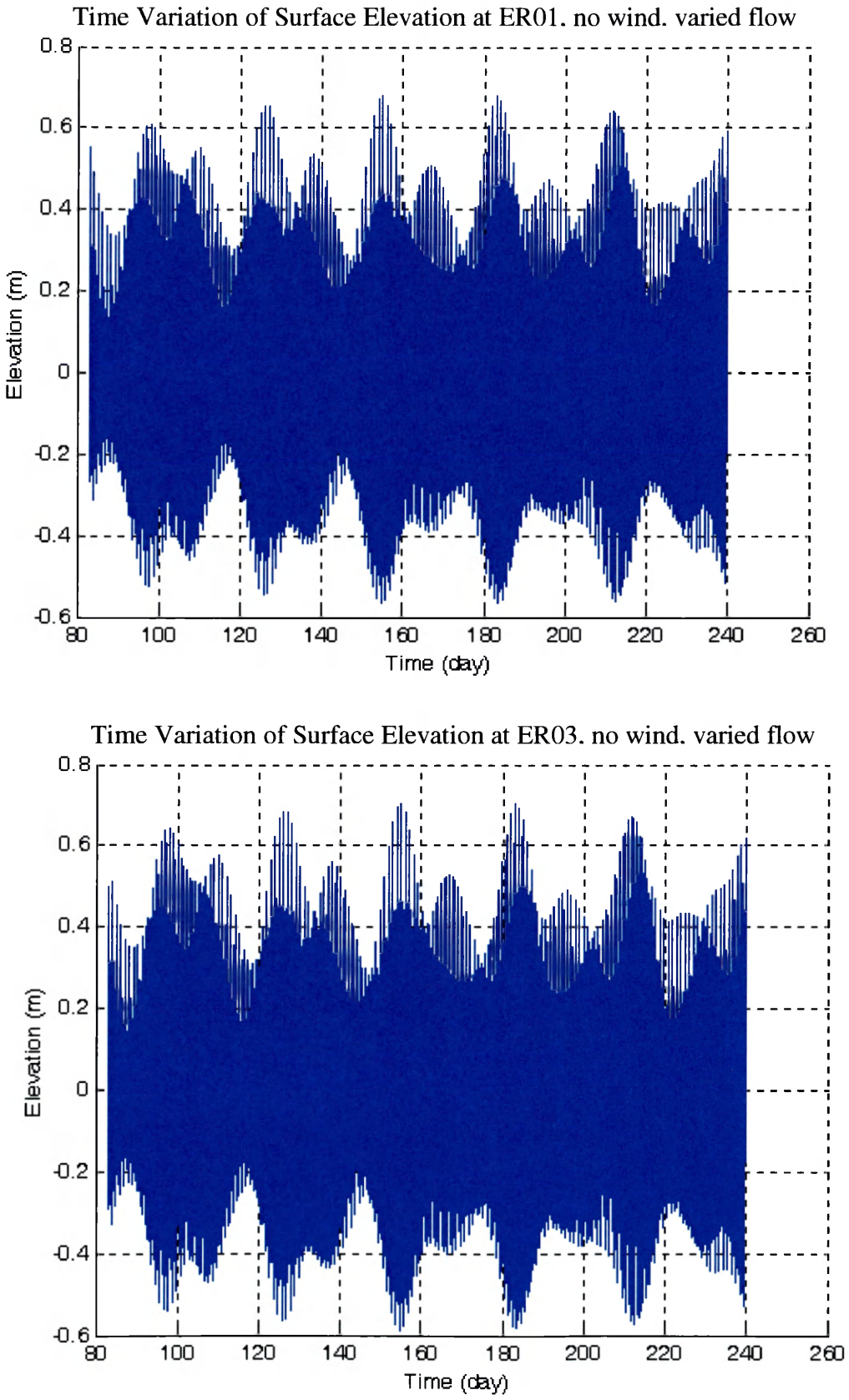

Figure 3-14. Surface elevation variation at station ER01 & ER03, under no wind, varied flow condition

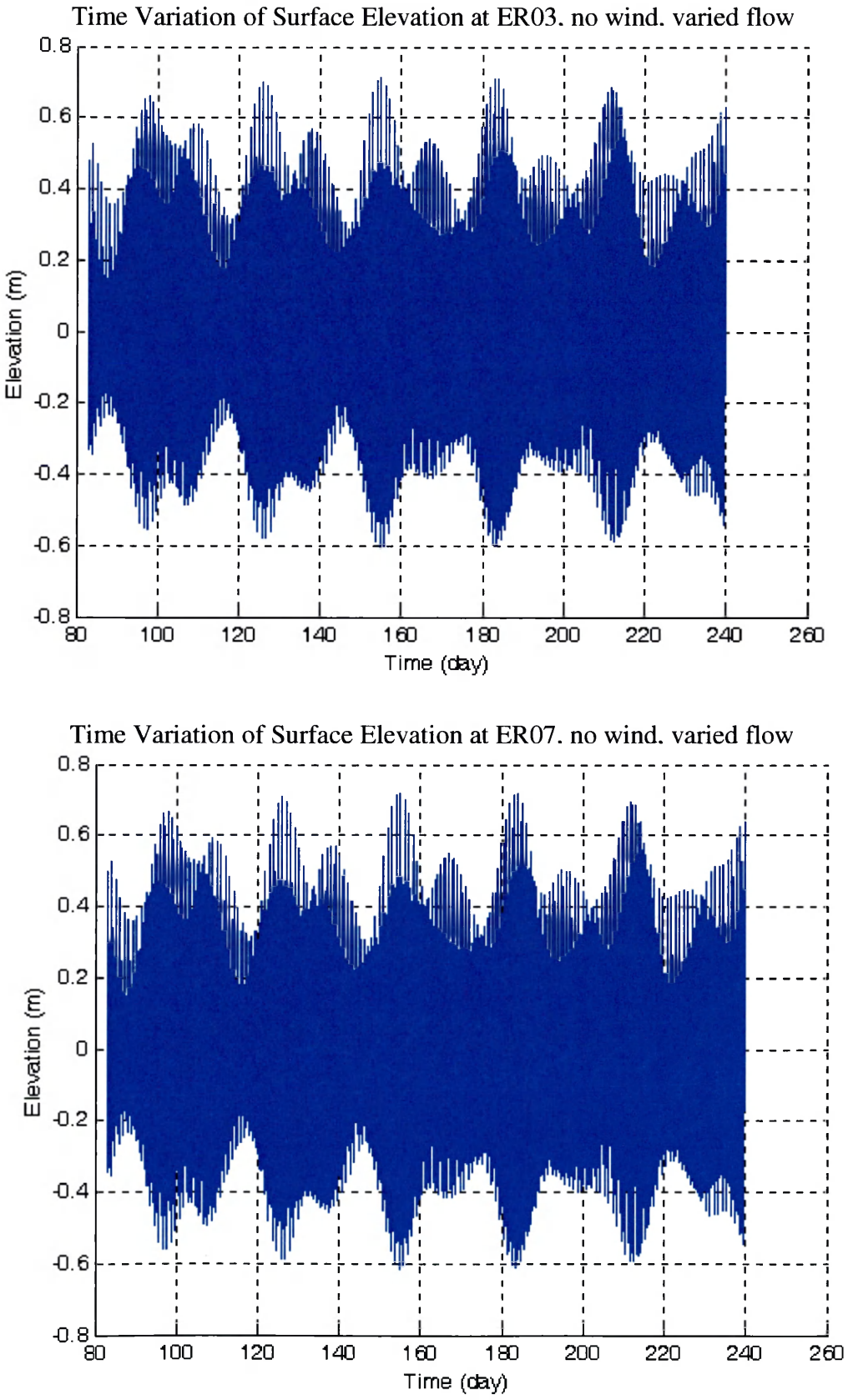

Figure 3-15. Surface elevation variation at station ER05 & ER07, under no wind, varied flow condition

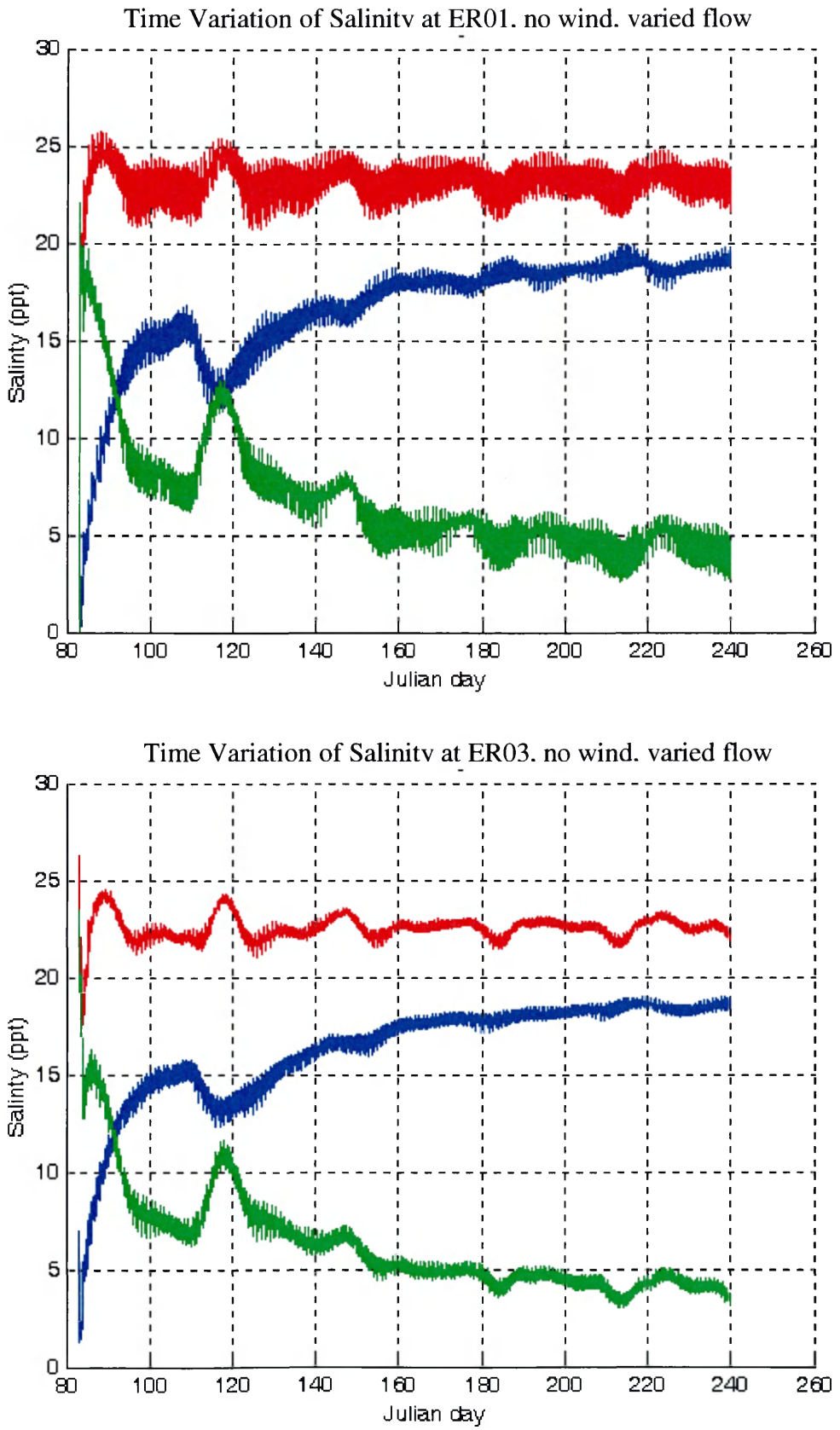

Figure 3-16. Salinity variation at station ER01 & ER03, under no wind, varied flow condition. (blue: surface salinity; red: bottom salinity; green: difference)

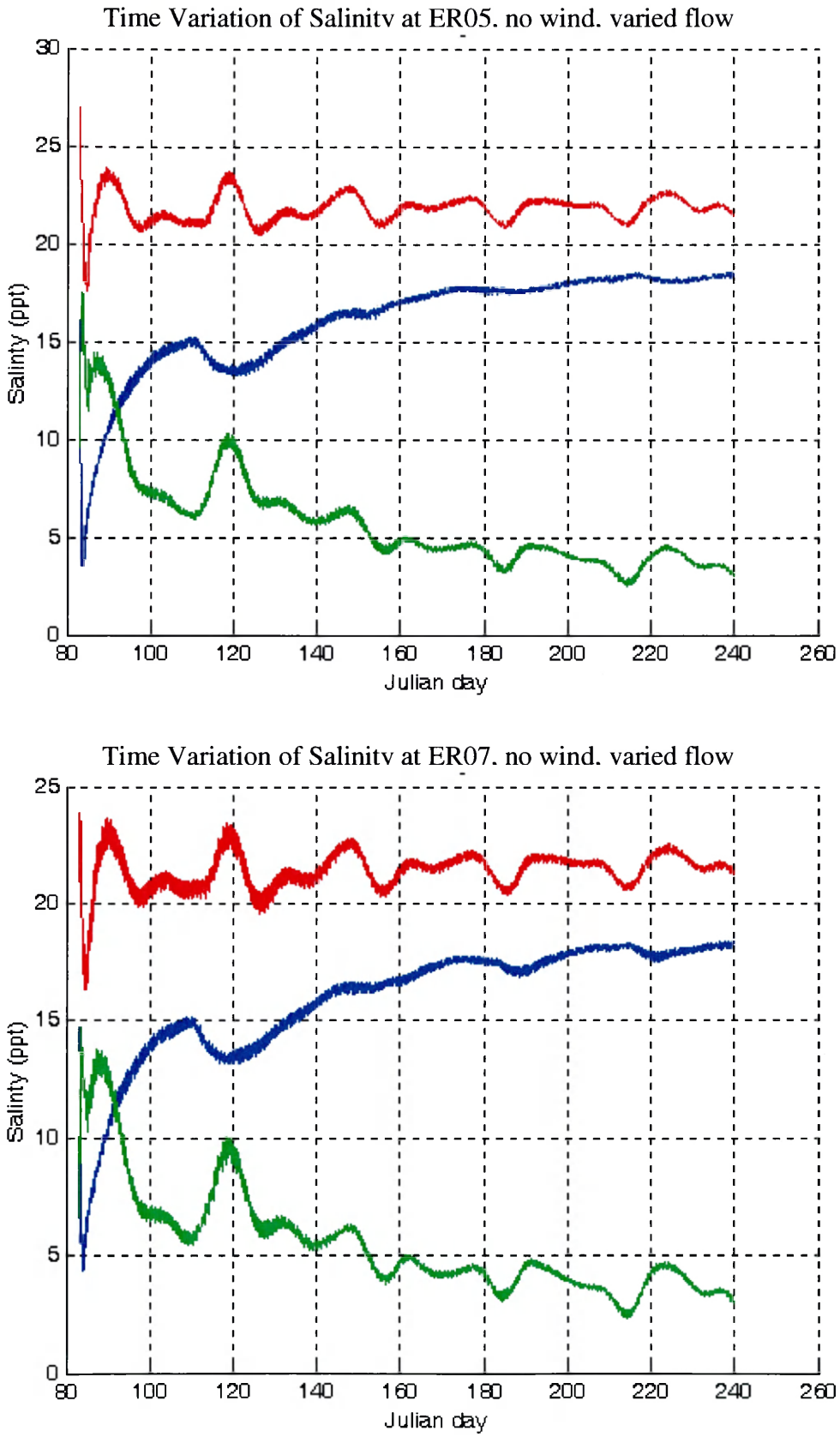

Figure 3-17. Salinity variation at station ER05 & ER07, under no wind, varied flow condition. (blue: surface salinity; red: bottom salinity; green: difference)

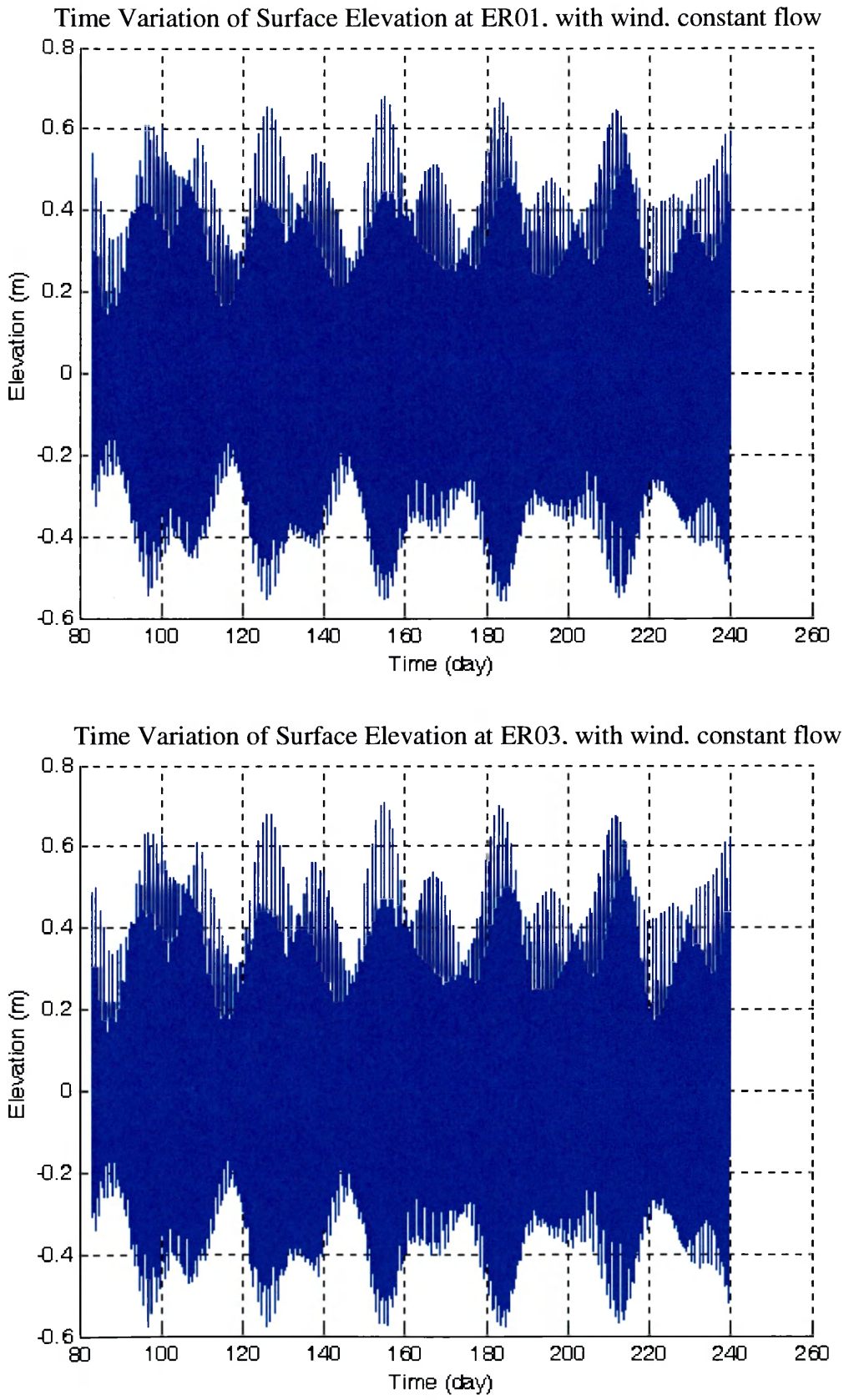

Figure 3-18. Surface elevation variation at station ER01 & ER03, under wind, constant flow condition

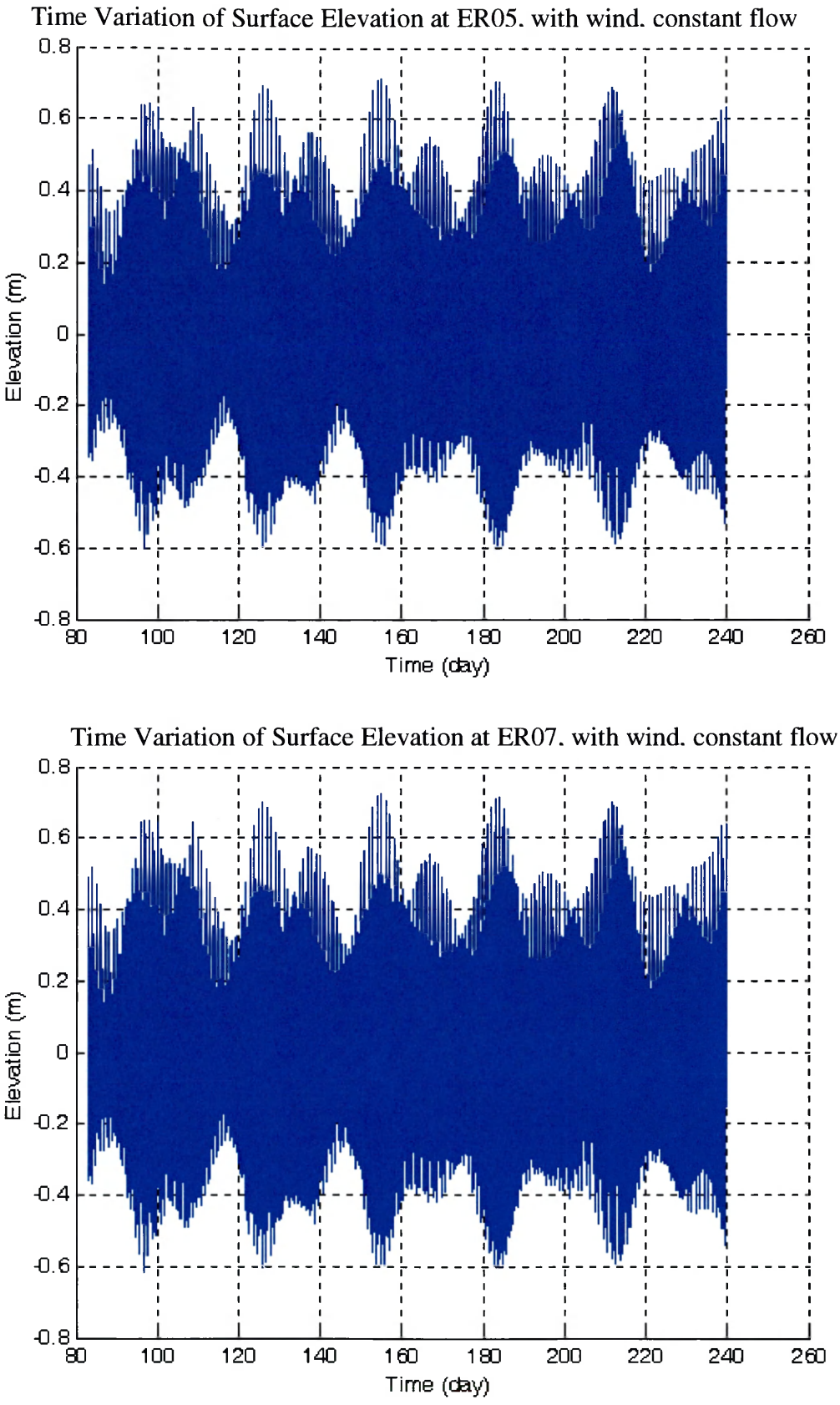

Figure 3-19. Surface elevation variation at station ER05 & ER07, under wind, constant flow condition

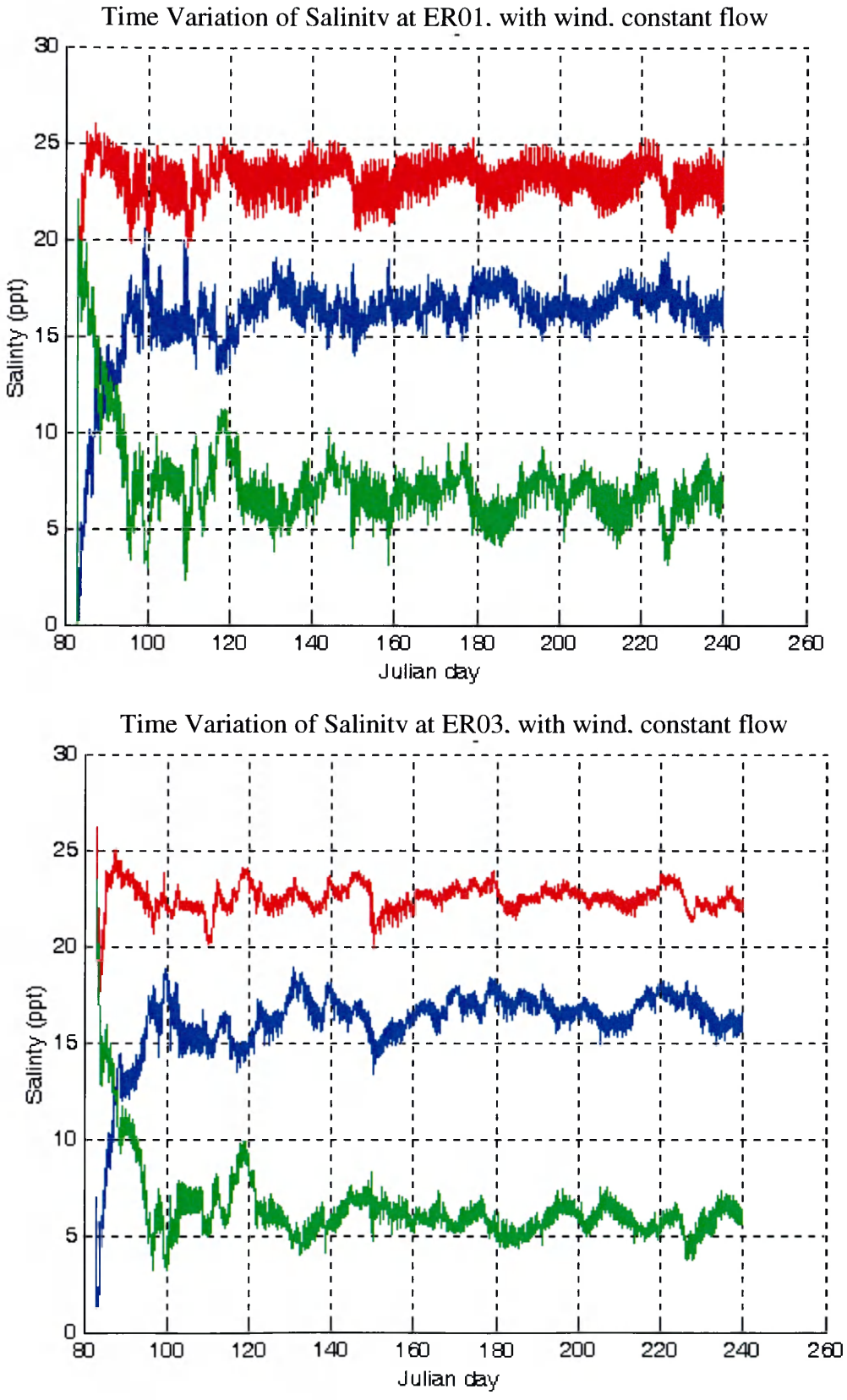

Figure 3-20. Salinity variation at station ER01 & ER03, under wind, constant flow condition. (blue: surface salinity; red: bottom salinity; green: difference)

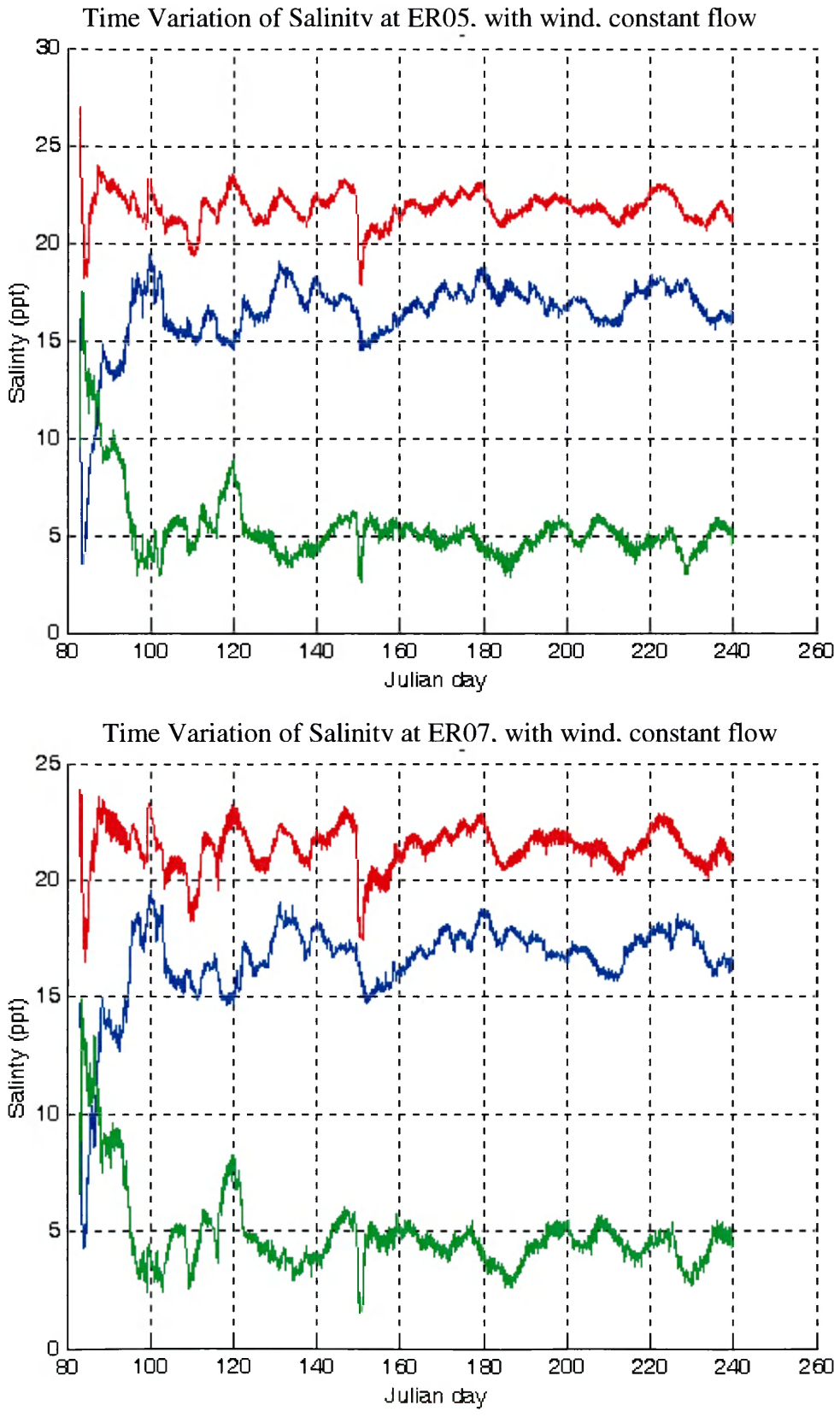

Figure 3-21. Salinity variation at station ER05 & ER07, under wind, constant flow condition. (blue: surface salinity; red: bottom salinity; green: difference)

Chapter 4

Model Experiments for Episodic Wind Events

4-1. CIEE Episodic Wind Events

Currents in the James and Elizabeth River are tidally dominated; they are primarily driven by astronomical tides. The tidal currents are semidiurnal, consisting of two flood and two ebb periods each day. They are rectilinear and reversing in that the water flows alternately in approximately opposite directions with a slack water at each reversal of direction. Maximum tidal current velocities generally range 20 - 50 cm/s in the lower James and 15 –30 cm/s in the Elizabeth. In order to study the events in detail, we divide the events into two periods: (1) the April wind event, ranging from Julian days 111-117, and (2) the May wind event, from Julian days 149-154.

4-1-1. April Wind Event

Hourly wind directions and magnitudes obtained from Sewells Point are plotted in the wind rose diagrams for Julian days 111-117 (see Figure 4-1). Wind speed during this period is mostly +/- 5 m/sec before and after the surge. The pattern of wind direction is quite variable until Julian days 116 and 117, when a strong persistent easterly wind blows for 12 – 24 hours. The surge was observed starting to grow when the easterly wind persisted for a duration of more than 6 hours and the magnitude exceeded 10 m/sec. The effectiveness of the easterly

wind in generating surge is consistent with the orientation of the James River Channel, which is aligned along an axis of 342 degrees upstream of Newport News Point and one of 70 degrees downstream of Newport News. The similar criterion was also observed in the case of tropical storm Floyd. Taking the customary estimate of current velocity as 3% of the wind speed, the 10 m/sec wind speed translates to 30 cm/sec of current velocity, which is enough to overcome the tidal velocity that usually exists in the Lower James.

A corresponding time series of simulated water level (see Figure 3-6) shows that the surge actually occurred in the second half of Julian day 116. When it happened, the water level rose, did not return to the slack water, the ebb disappeared, and the regular tidal cycle was disrupted. A simulated time series for current velocity (rotated to its principal axis) also shows the similar disruption of the regular tidal cycle at JR01 (near the Newport News station) and at ER01 (Elizabeth River station near Craney Island), as shown in Figure 4-2. When comparing between ER01 and JR01, it is interesting to observe that the surge has a larger effect on ER01 than on JR01. The velocity variation associated with surge at JR01 is 40 cm/s, while at ER01, a huge flood surge reaches 50 cm/s. Given the background tidal velocity amplitude 40 cm/s at JR01 and 20 cm/s at ER01, the percentage change is 100% at JR01 versus 250% at ER01. The root mean square deviation from the astronomical tide during the entire period is also higher for ER01 than for JR01. It was also noticed that the mean sea level at ER01 was significantly shifted upward during the event. This is due presumably

to the fact that a large volume of surge water actually altered the mean water level in the Elizabeth River.

The disruption of the regular tidal cycle described above is also reflected in the simulated circulation pattern. Figures 4-3 and 4-4 show the non-tidal surface circulation for Julian days 115 and 116, respectively. During JD 115, the surface non-tidal circulation was obtained by averaging over 0.5 hour of the 25 hours of predictions. The result shows a typical non-tidal circulation with surface outflow at about 15 -20 cm/sec. A similar procedure was conducted for JD 116 and obtained a very different pattern. The surface outflow completely disappears and is replaced by a surface inflow with magnitudes of 15-20 cm/s. This surface inflow is particularly strong in the northern shore of the lower James; a very strong inflow into Elizabeth River near Craney Island was also evident. This may explain why there is very strong flood current recorded in the Elizabeth River time series plot described earlier. The non-tidal circulation patterns were also present inside the Elizabeth River near Lamberts Point. During Julian day 115, the surface non-tidal circulation has a surface outflow of about 5-7 cm/s near the center of the channel. One day later, the flow pattern is completely changed. A strong non-tidal current at about 30 cm/s was observed near Lamberts Point. The flow continues downstream and then splits into two tributaries: the Western Branch and the Southern Branch.

4-1-2. May Wind Event

Hourly wind directions and magnitudes for Julian days 149-155 are shown in Figure 4-5. The easterly wind persisted from JD 150-152 with the strongest

wind speed being over 14 m/sec on JD 150 and gradually diminished the rest of the two days. During JD 153–154, the wind was modest and mostly from the southwest. It was observed that the surge started to grow at the beginning of JD 150, which coincided with neap tide and the low tide was at midnight. The strong easterly wind had persisted and its magnitude was over 10 m/sec during JD 150. The effectiveness of the easterly wind beyond 10 m/s in generating the surge is again demonstrated in the Lower James River. With this interesting pattern of a persistent easterly wind with its speed gradually diminished over the course of 3 days, it is a good case to examine how the water level and velocity respond to the subsidence of a major wind event. During JD 153-154, southwest winds persisted for two days; the model results could be useful for comparing with the constant wind scenarios studied in the previous section.

Figure 4-6 presents the long-term tidal records at three stations: Hampton Roads at Sewells Point, Fort Norfolk (intermediate in the Elizabeth), and Money Point (upstream part of the Elizabeth). The surge amplitude during the May event is by far larger than that of the April event at all these three stations. The reason could be that the May event had greater forcing than the April event in terms of magnitude and duration of its easterly direction. Among the three stations, the surge amplitude is larger inside the Elizabeth than in Hampton Roads. We attributed this to the fact that the width of the Elizabeth River is more constricted than in Hampton Roads and thus a given volume of water can induce a larger surge. Both events occurred during the tidal phase of neap tide with the amplitude almost at the minimum around 0.9 m. The surges during both events

started from near the low water stage. For example, the April event started at 9:00 a.m. and the May event started at midnight. Both were at the low waters. This is consistent with Proudman's (1955) finding that surge amplitude is greater at low water than at high water for a progressive wave.

We have attempted to show in Section 2-2 that extremely large tidal or residual currents (with speed exceeding 2 knots) can be generated in the relaxation phase of a wind event (see Figure 2-11). Since from JD 150 - 152, easterly winds were steadily diminished, it provides a natural setting to test the velocity response to the retraction of wind forcing. Figures 4-7a, 4-7b and 4-7c display the surface residual currents for each day from JD 149 - 154. It is obvious that a large reversal circulation pattern occurred during JD 150 that disrupted the normal outflow pattern. During JD 150, a slightly larger flow appeared at the northern bank of Hampton Roads. During JD 152, the pattern is back to normal and persisted through JD 154. Inside the Elizabeth River, Figure 4-8 shows that, instead of an outflow on the surface, a strong surface flood current was generated at JD 150 during the surge. In response, a strong bottom outflow was generated with residual flow reaching 20 cm/s in the Elizabeth River. Boon et al. (2002) demonstrated that the circulation of the Lower James is driven by a progressive wave while that of the Elizabeth River is driven by a standing wave. Because of this, the surge characteristic modulated by the astronomical tide could be different (Proudman, 1955, 1957). As a result, it is conceivable that an above normal current can be triggered due to the imbalance of the pressure gradient force

between the Lower James and the Elizabeth River. The subject is interesting and worth further investigation but beyond the scope of this thesis.

4-2. Model Experiment II

It has been demonstrated that the physical characteristics of the Lower James and Elizabeth responded differently from different wind conditions (magnitude and direction). In this section, a set of model experiments was conducted to examine how different wind conditions will affect the current and salinity in this estuarine system.

4-2-1. Experiment Design

Surface and bottom current and salinity within the lower James were simulated in response to wind from eight different directions (N, NE, E, SE, S, SW, W, and NW). Except for the wind, other conditions were kept the same as the single variable run in the CIEE study (Wang, 2001). In all model simulations, a normally distributed wind speed with a maximum of 10 m/s was assumed in order to make the model reach a stable state. To isolate the wind effect, no heat flux was considered. Each simulation began with a cold start, with constant salinity and temperature specified at the open boundary near the James River mouth. Each model simulation ran continuously for 40 days (including 60 tidal cycles as spin-up time). The resultant circulation patterns over days 35 and 36 of each simulation were very similar, suggesting that the system has reached a quasi-steady state condition. In the following discussion, only the results on day 36 were presented.

4-2-2. Results

No wind

Figures 4-9 and 4-10 show the surface and bottom residual current and salinity distribution. They illustrate the dominant seaward surface flow and bottom landward flow. With no wind, the circulation pattern within the lower James and Elizabeth display the classical estuarine circulation in a partially stratified estuary system.

Freshwater from the upper James follows the geometry of the V-shaped headland, which is formed where the James River Channel and the northern shoreline make a 90^{o} bend around Newport News Point. This special geometry forces the flow to turn to the left just before it reaches the river mouth. In making what might otherwise be a smooth left turn, part of the eastward flow encounters a barrier, Craney Island, forcing it to accelerate and setting up a strong northward residual current near the northwest corner of the island. Above this point, the residual flow resumes eastward movement across the northern edge of Craney Island until it reaches the entrance to the Elizabeth River. There it joins an eddy, or eddy-like feature, turning in a clockwise direction. Above Craney Island, the surface current flows primarily northeastward. Part of this flow reaches the shoreline, where it is forced to go northward and join the dominant seaward flow into the Chesapeake Bay. This seaward dominant surface flow maintains fresher water in the surface water column. In the bottom layer, to compensate for the loss of surface flow, bottom landward flow advects saltier water from the river mouth into the lower James region. This mass of water is carried to the upper James and

into the Elizabeth. Tidal mixing causes a slightly mixed water column throughout the Hampton Road region and in the Elizabeth.

Northerly (N) winds

As shown in Figures 4-11 and 4-12, under north wind, the circulation pattern remains the same in the lower James, but is reversed in the Elizabeth. Due to the orientation of the lower James and Elizabeth, northerly wind drives saltier water from the James River mouth at the open boundary into this region, reversing the surface flow. Over the Hampton Roads region, the surface flow is southwardly dominant, which causes the eastward flow from the upper James to only exist on the left and above the Craney Island region. This keeps much of the fresher water on the west side of Craney Island. When these two flows encounter, the eastward flow is forced to join the main southward flow from outside of this region, which drives a large volume of the existing freshwater, in addition to the new relatively saltier flow, into the Elizabeth. A strong surface landward flow is formed in the Elizabeth River, which results in a strong seaward bottom flow from the upper Elizabeth. This strong bottom flow pushes saltier water down to the Elizabeth River mouth. There is a similar pattern in the lower James. Due to the reduced strength of the eastward flow, bottom landward water cannot carry saltier water upstream as had occurred under the no-wind condition. The water column is better mixed as the result of this wind mixing.

Northeasterly (NE) winds

When wind blows from the northeast, the classical estuarine circulation pattern in the lower James and Elizabeth is reversed, with a surface landward flow

and bottom seaward flow (Figures 4-13 and 4-14). Most of the northeastward surface current flow above Craney Island is totally reversed, both on the Hampton Roads Flat and in the main channel. This wind-induced landward surface flow even drives the strong southeastward flow from the upper James southward, and piles up on the left side of Craney Island. When part of this flow reaches the shoreline, it turns westward. Around the Elizabeth River mouth, part of this new surface water is driven into the Elizabeth. In the lower James River main channel (and the Elizabeth), reverse bottom seaward flow pushes saltier water further downstream, reducing the difference between surface and bottom salinity, and resulting in a less stratified water body.

Easterly (E) winds

Under an easterly wind condition, the estuarine circulation in the lower James is reversed, while it is enhanced in the Elizabeth (Figures 4-15 and 4-16). This easterly wind drives saltier water into the lower James, when this wind-driven flow reaches the sharp bend. Because of this special geometry, this westward flow turns southwestward, near Norfolk. The seaward flow is changed to northward first, then turns westward, finally joins the southwestward flow over the Hampton Roads Flat area. In the main channel, the surface eastward flow is totally reversed to become westward. This wind-induced dominant westward flow drives most of the existing fresher water to the upper James. As a result of the reversed circulation, bottom seaward flow pushes saltier water further downstream, reducing the difference between surface and bottom salinity. This results in a less stratified water body in the lower James. Correspondingly, the

bottom salinity level in the Elizabeth River is also reduced. Across the upper Elizabeth River, the east wind blows the surface water out of the river, and saltier water is advected into the estuary by a compensating return flow. Wind mixing (generated internal shear) significantly increases the vertical exchange of momentum, thereby increasing surface salinity.

Southeasterly (SE) winds

Under a southeasterly wind, the estuarine circulation pattern is almost the same as that under an Easterly wind. However, in the lower James, the classical circulation resumes, but with diminished strength (Figures 4-17 and 4-18). Above Craney Island, wind blows the surface water southward. On the left side of Craney, the water is driven westward. In the main channel, there is still a small branch of freshwater from the upper James flowing eastward, and then joining the dominant northward flow to seaward. As a result, in the bottom layer, there is a landward inflow that carries saltier water into the lower James and Elizabeth.

Southerly (S) winds

Under a southerly wind, the estuarine circulation pattern is enhanced in both the lower James and Elizabeth. This south wind diverts eastward flow to become northward over the lower James. It also blows surface water out of the Elizabeth, joining this northward flow and resulting in a dominant northeastward surface flow as shown in Figures 4-19 and 4-20. To balance this enhanced seaward surface flow, a stronger bottom current is formed. This brings much saltier water into both the lower James and the Elizabeth, and reaches upstream.

Southwesterly (SW) winds

Under a southwesterly wind, the estuarine circulation pattern is pretty much the same as that under the southerly wind, except for the diminished strength of the surface outflow in the Elizabeth. This southwesterly wind causes the surface water above Craney Island to flow northeastward over the lower James. It also blows surface water out of the Elizabeth, joining this northward flow and resulting in a dominant northeastward surface flow as shown in Figures 4-21 and 4-22. To balance this enhanced seaward surface flow, a stronger bottom current is formed, bringing much saltier water into both the lower James and the Elizabeth, and reaching upstream.

Westerly (W) winds

Under a westerly wind, the estuarine circulation pattern in the lower James is enhanced, while in the Elizabeth, a three-layer circulation is formed (inflow in surface and bottom layers, outflow at mid-depth) (Figures 4-23 and 4-24). Westerly wind blows surface water above Craney into the Elizabeth, reversing the surface seaward flow, but is not strong enough to overcome the gravitational circulation. In the bottom layer, bottom landward inflow still exists, while at mid-depth, water extrudes. Over the lower James, in the main channel, a stronger bottom current is formed, bringing much saltier water into the lower James, and reaching upstream.

Northwesterly (NW) winds

Under a northwesterly wind, the estuarine circulation pattern in the lower James is the same, while it is reversed in the Elizabeth (Figures 4-25 and 4-26). A

northwesterly wind drives fresher water from the upper James into the lower James, above Craney Island. The surface water flows eastward, and in passing the Elizabeth River mouth, a huge amount of this fresher water is driven into the Elizabeth. Another part of this water is also reflected into the Elizabeth when it reaches the shoreline. The left part continues to go all the way towards the James River mouth. In the Elizabeth (Figures 4-27 and 4-28), this surface inflow is strong enough to overcome the gravitational circulation. The bottom layer flow is also reversed to seaward outflow, which pushes saltier water further downstream.

4-2-3. Summary

Winds axial to the lower James estuarine system have the strongest effects on physical characteristics (i.e., water level, salinity distribution, and current). A downstream wind will enhance estuarine circulation, and strengthen stratification in the water column; Conversely, an upstream wind might be able to reverse the classical estuarine circulation. For example, in the lower James, since its orientation is in the east-west direction, winds from the east, blowing upstream, drive saltier water from outside into this lower James in the upper water column. To compensate, bottom water will flow to the outside, which results in a reversed circulation pattern. While, when a downstream wind blows, it will drive more freshwater out of the lower James, causing more salt water to intrude into this system, which will enhance the gravitational circulation. Also, the wind serves as a strong mixing factor.

For the Elizabeth River system, since its orientation is in the south-north direction, wind from either the south or north will have a stronger effect on it.

Also, since it is a tributary to the lower James, there is an interaction between this 'estuary and sub-estuary system'. As an example, when the west wind blows, it will push some freshwater, driven from the upper James to the lower James, into the Elizabeth. Then, a reverse circulation pattern, even a reverse three-layer circulation, may be formed under special wind conditions.

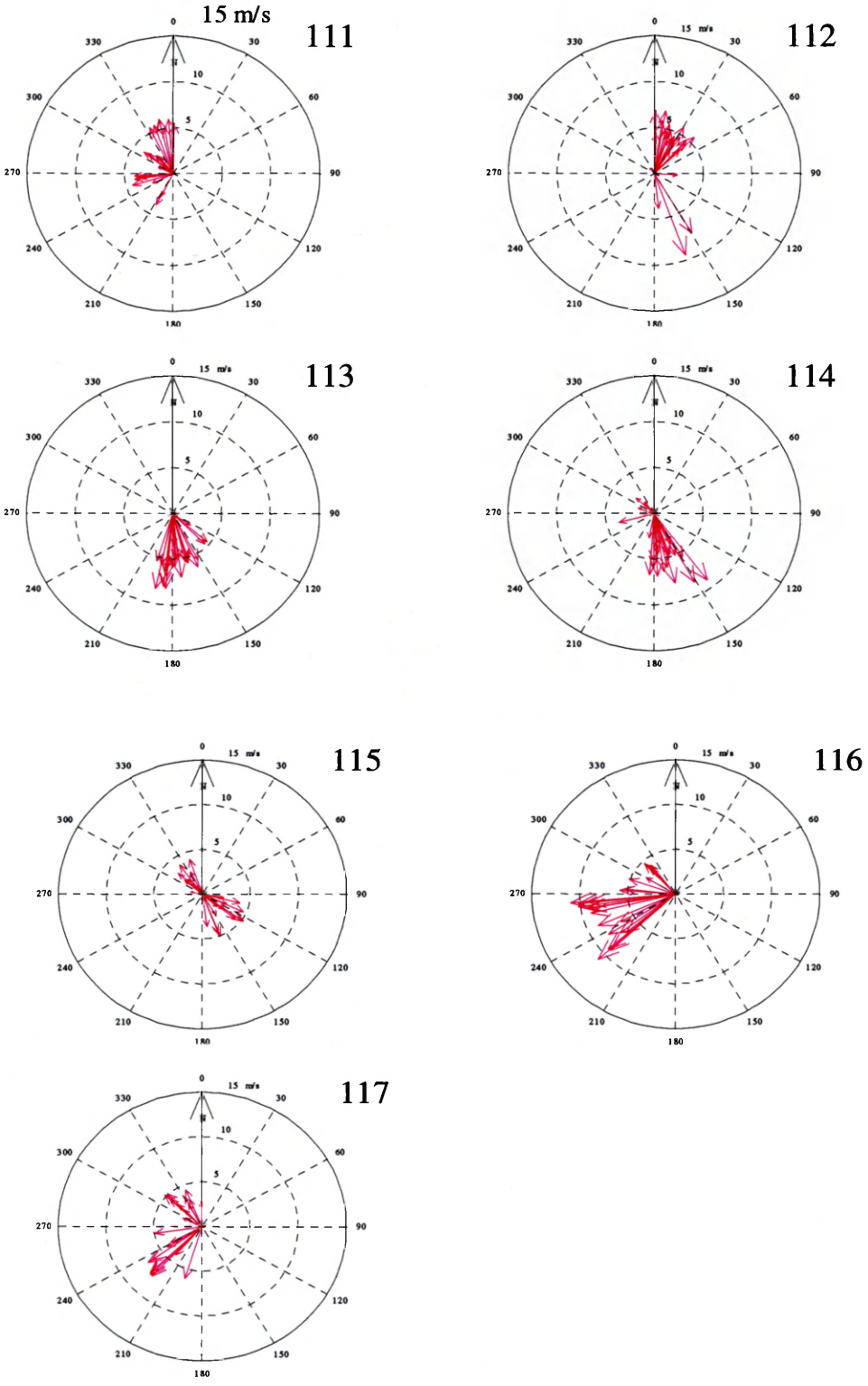

Figure 4-1. Hourly wind directions and magnitudes at Sewells Point

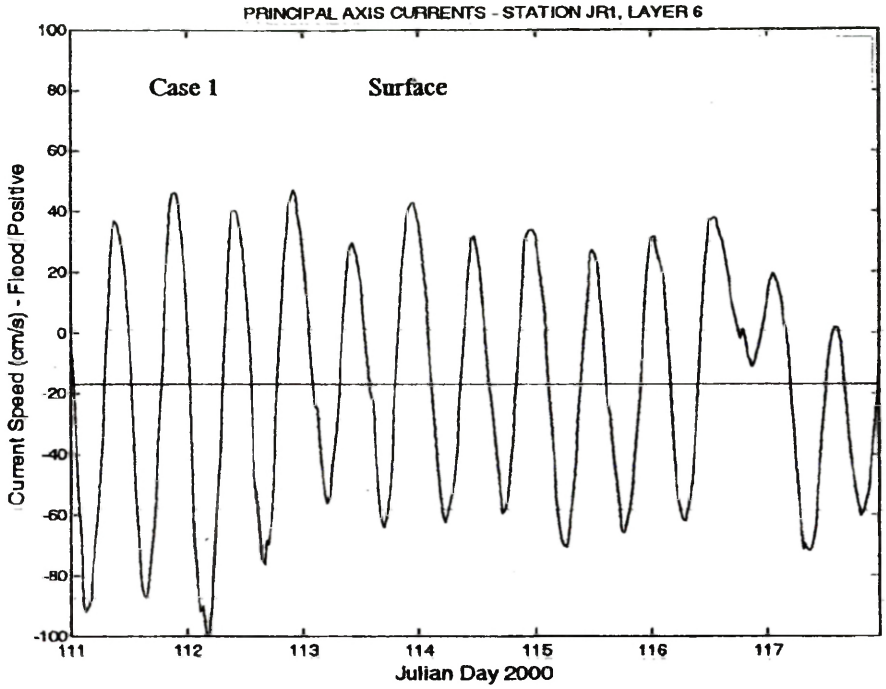

Principal axis current at Station JR1

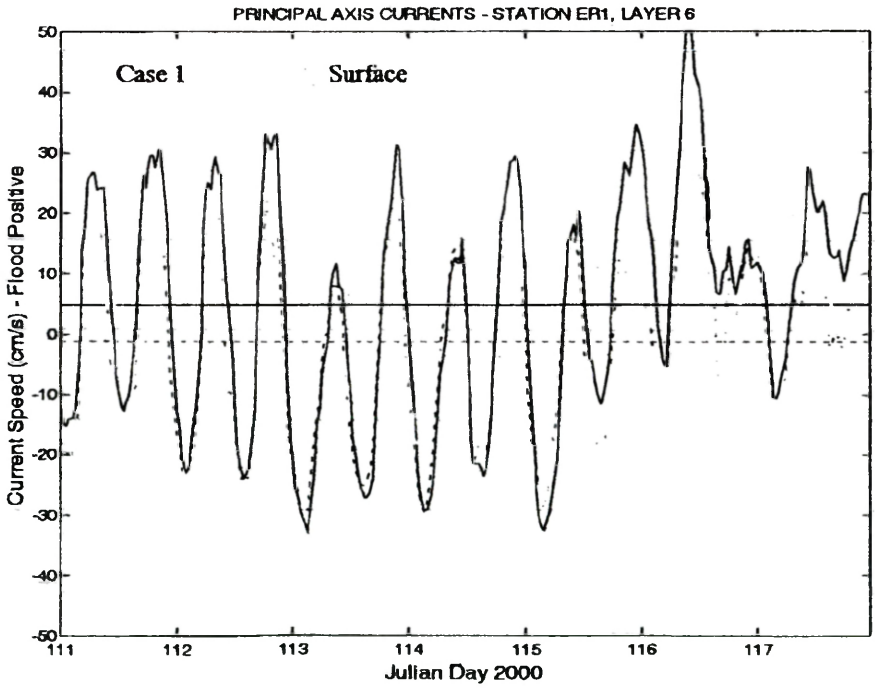

Principal axis currents at Station ER1

Figure 4-2. Time series of simulated current velocity (rotated to its principal axis)

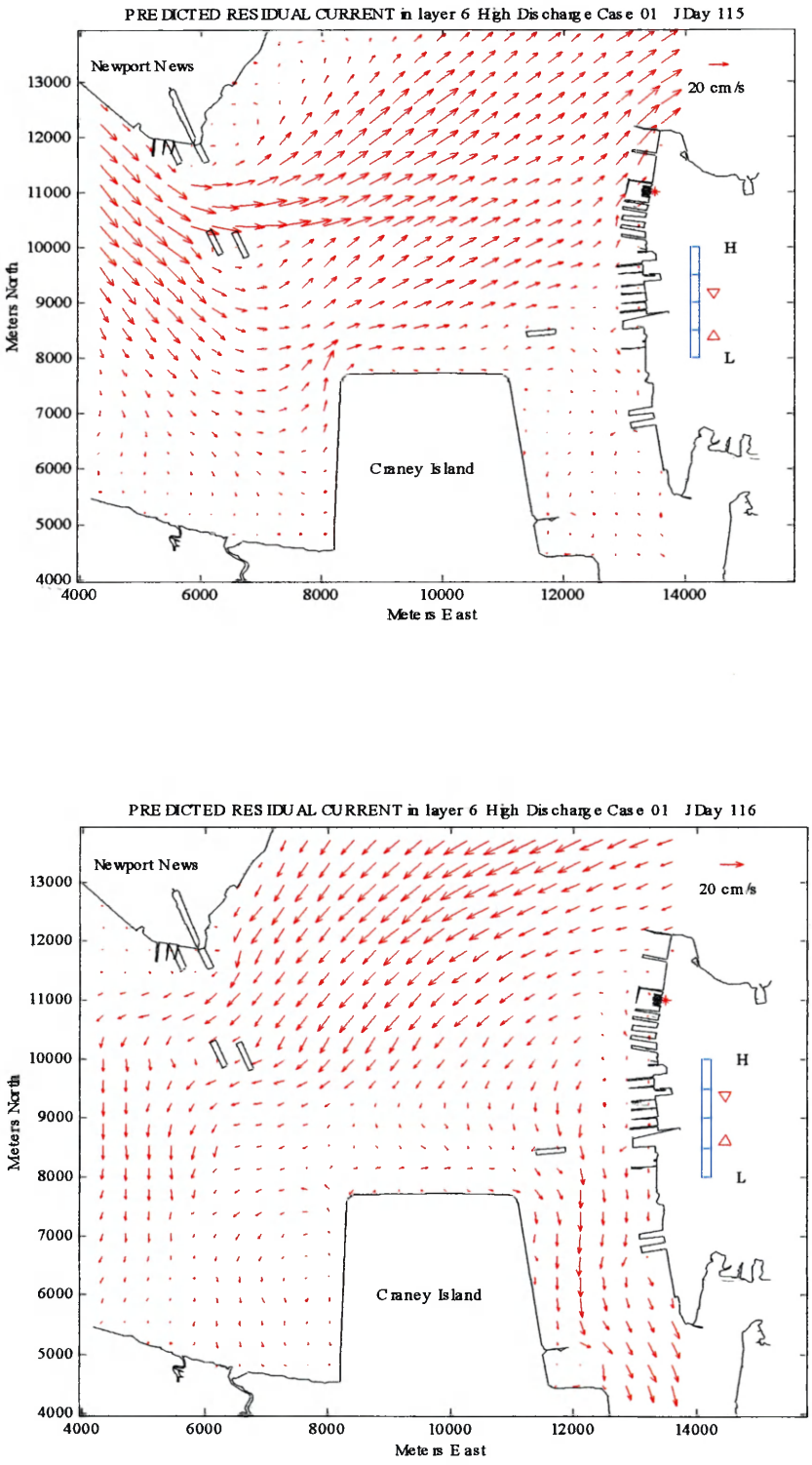

Figure 4-3. Non-tidal surface circulation in the lower James region on Julian days 115 & 116, 2000

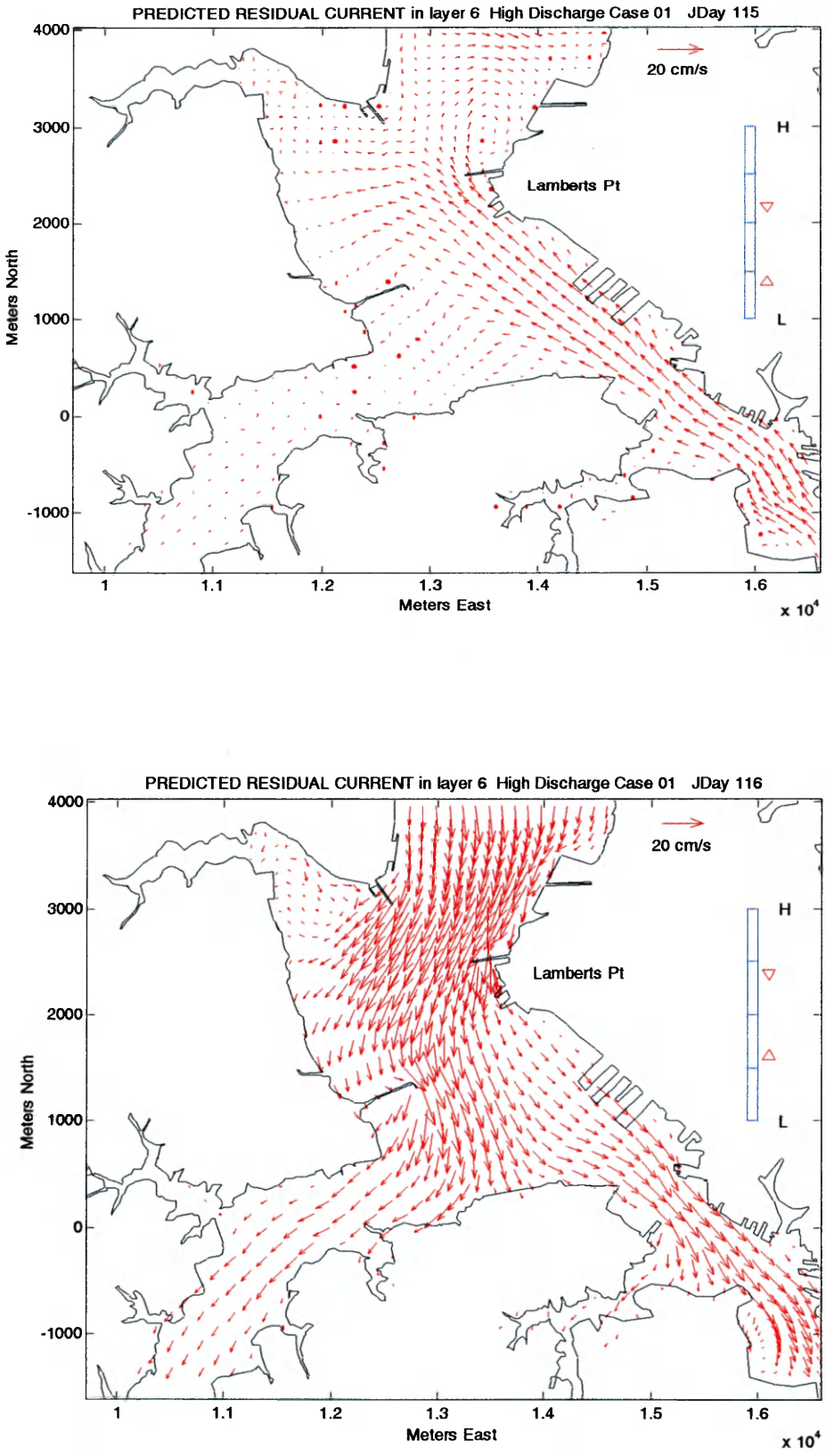

Figure 4-4. Non-tidal surface circulation in the Elizabeth River region on Julian days 115 & 116, 2000

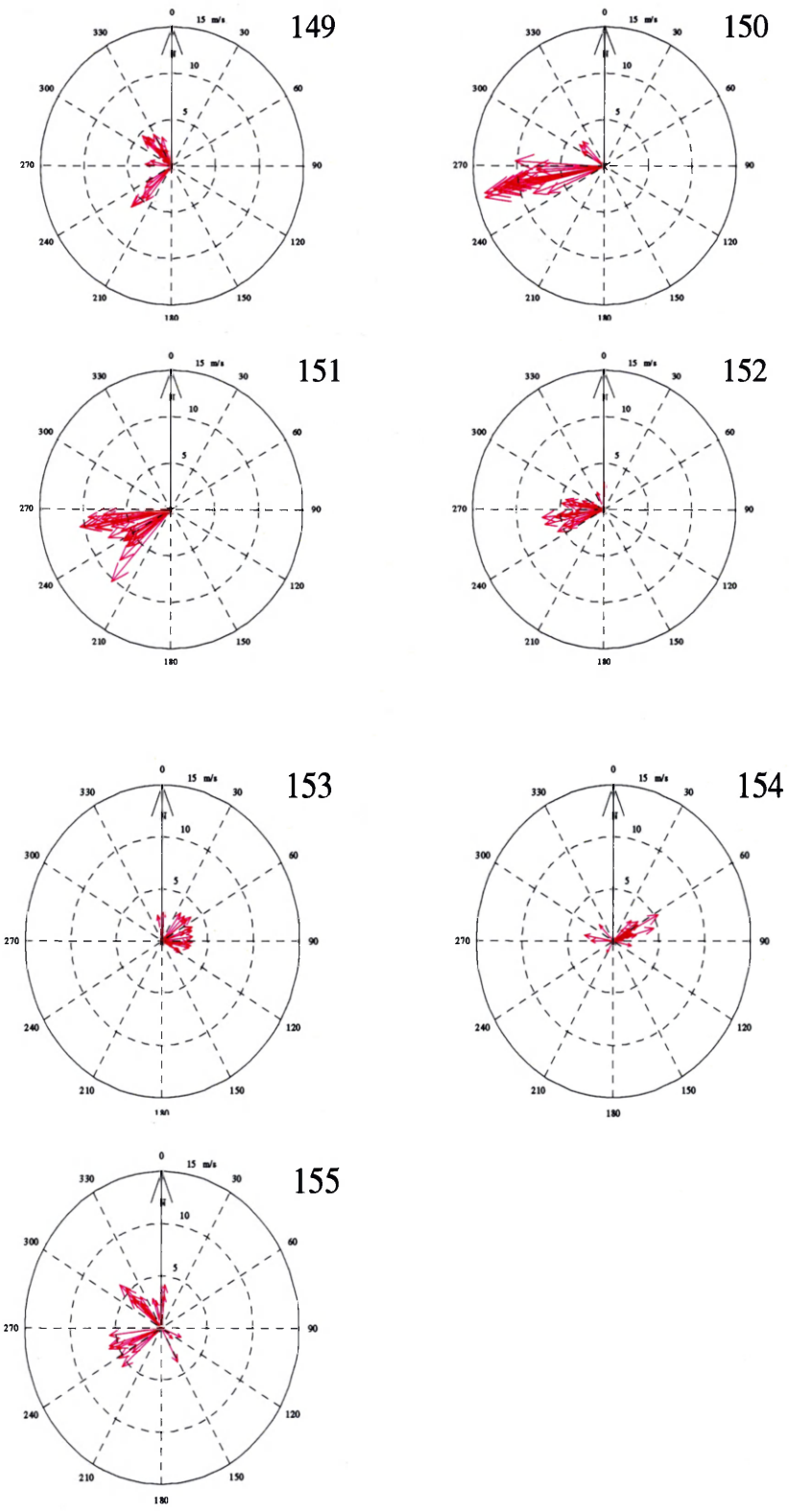

Figure 4-5. Hourly wind directions and magnitudes at Sewells Point

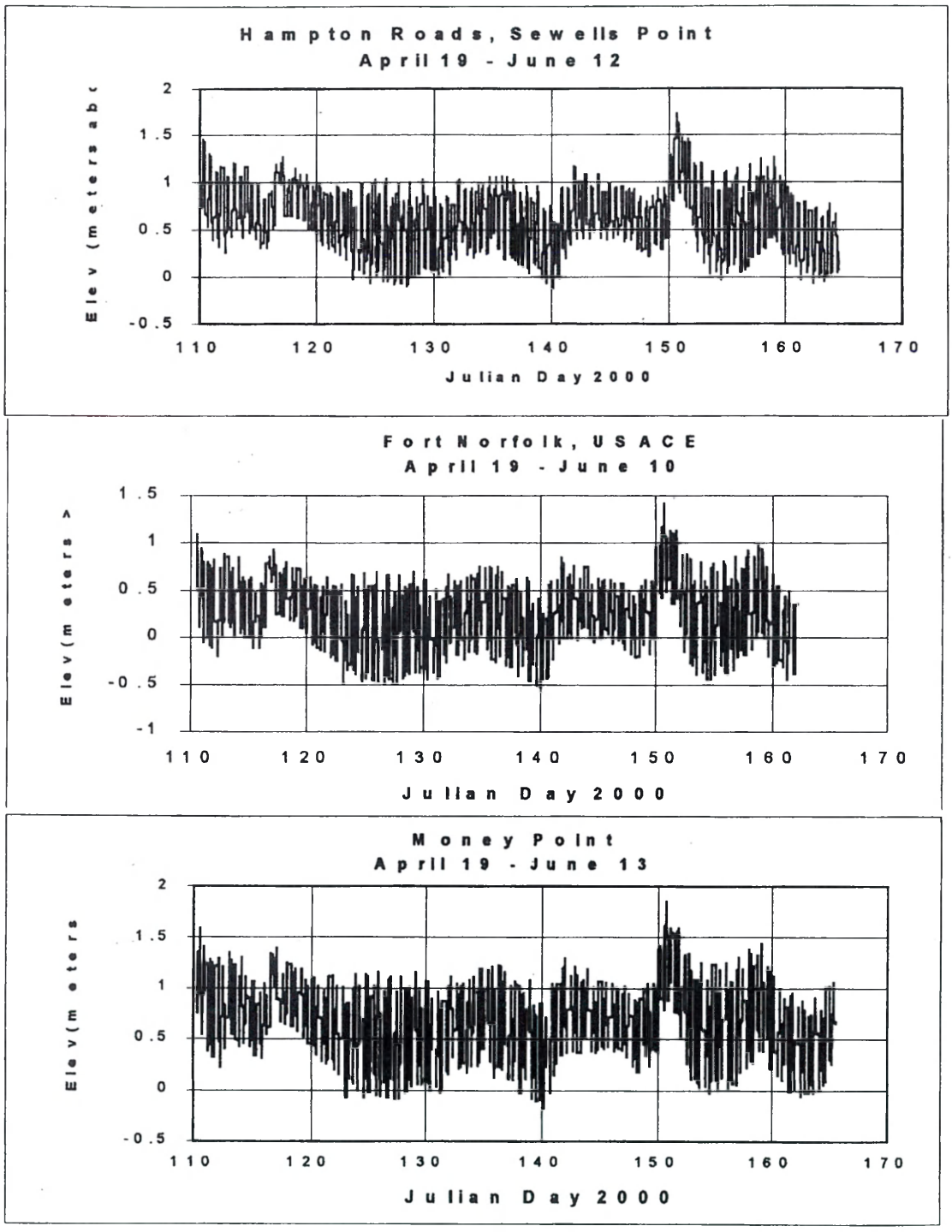

Figure 4-6. Long term tidal record at three stations: Hampton Roads, Fort Norfolk, and Money Point

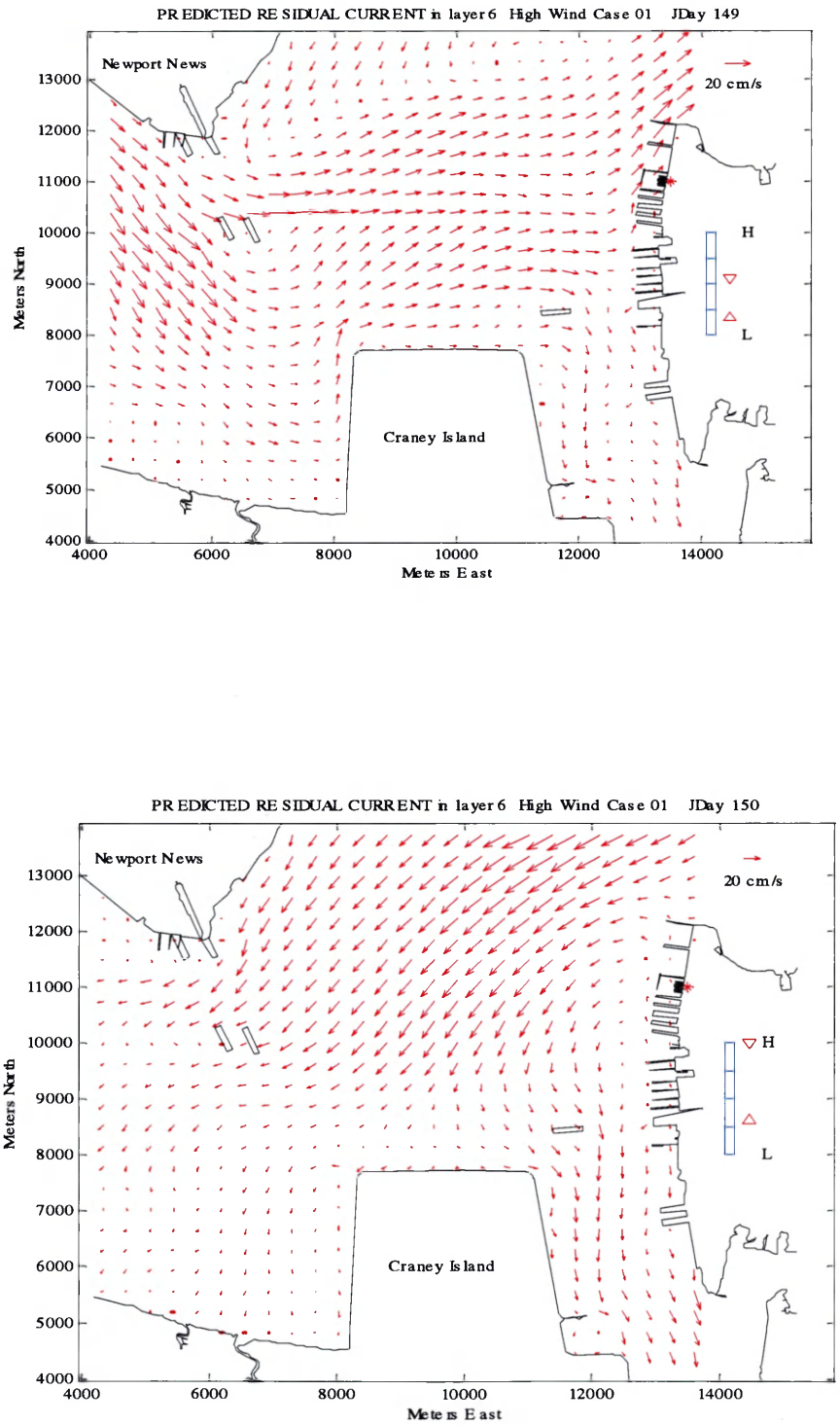

Figure 4-7 (a). Surface residual current for each day from Julian day 149 through 154, 2000, lower James region

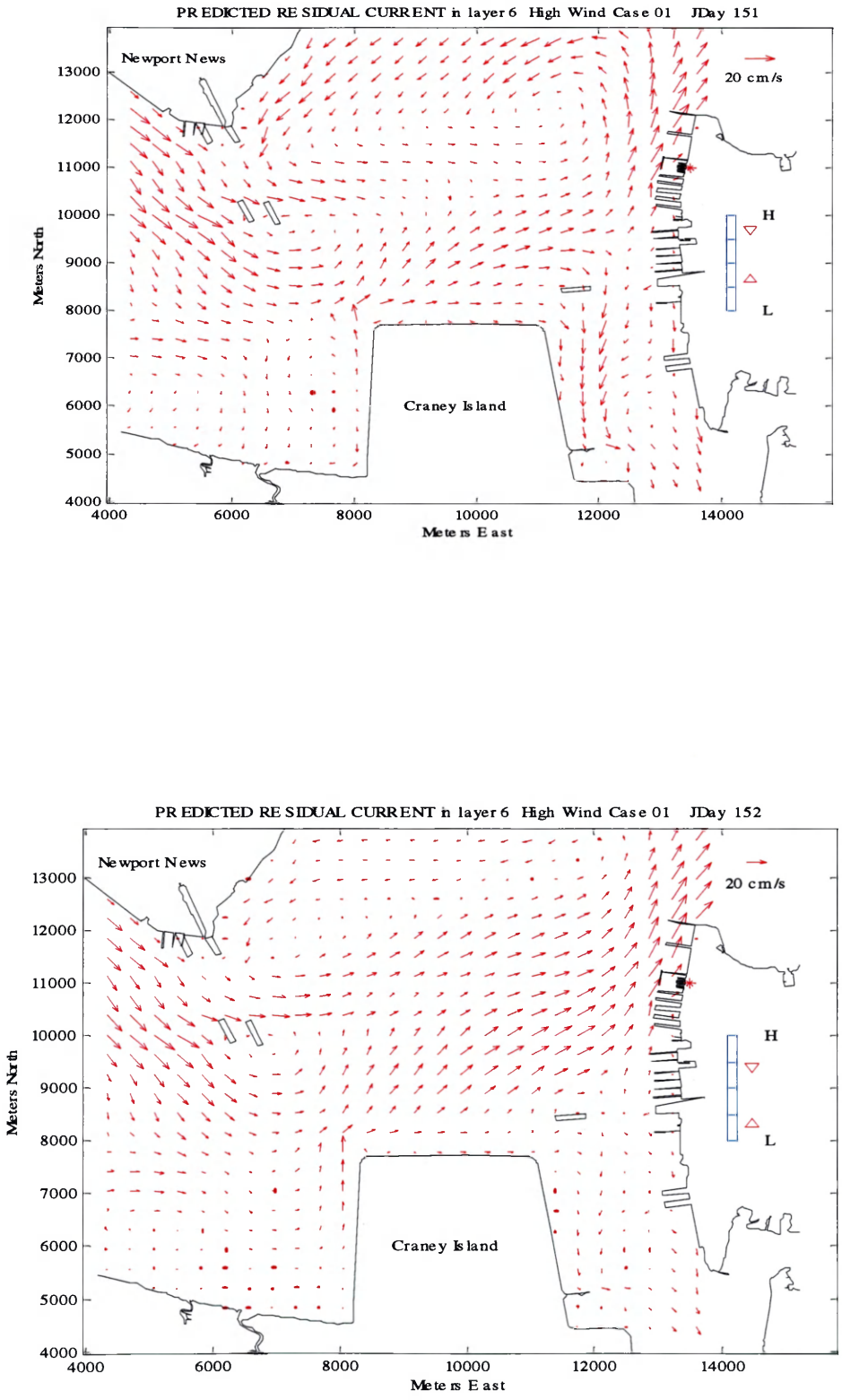

Figure 4-7 (b). Surface residual current for each day from Julian day 149 through 154, 2000, lower James region

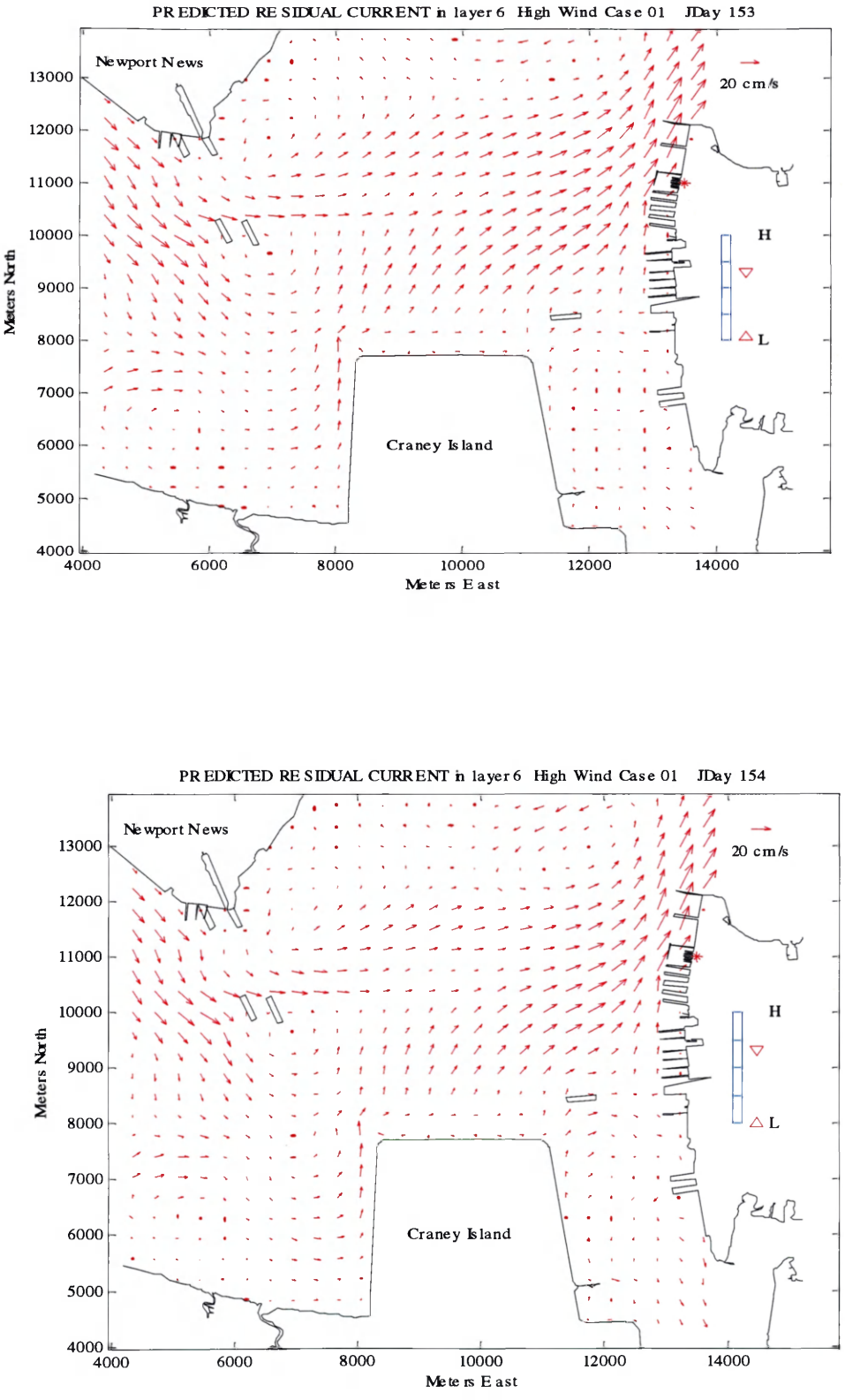

Figure 4-7 (c). Surface residual current for each day from Julian day 149 through 154, 2000, lower James region

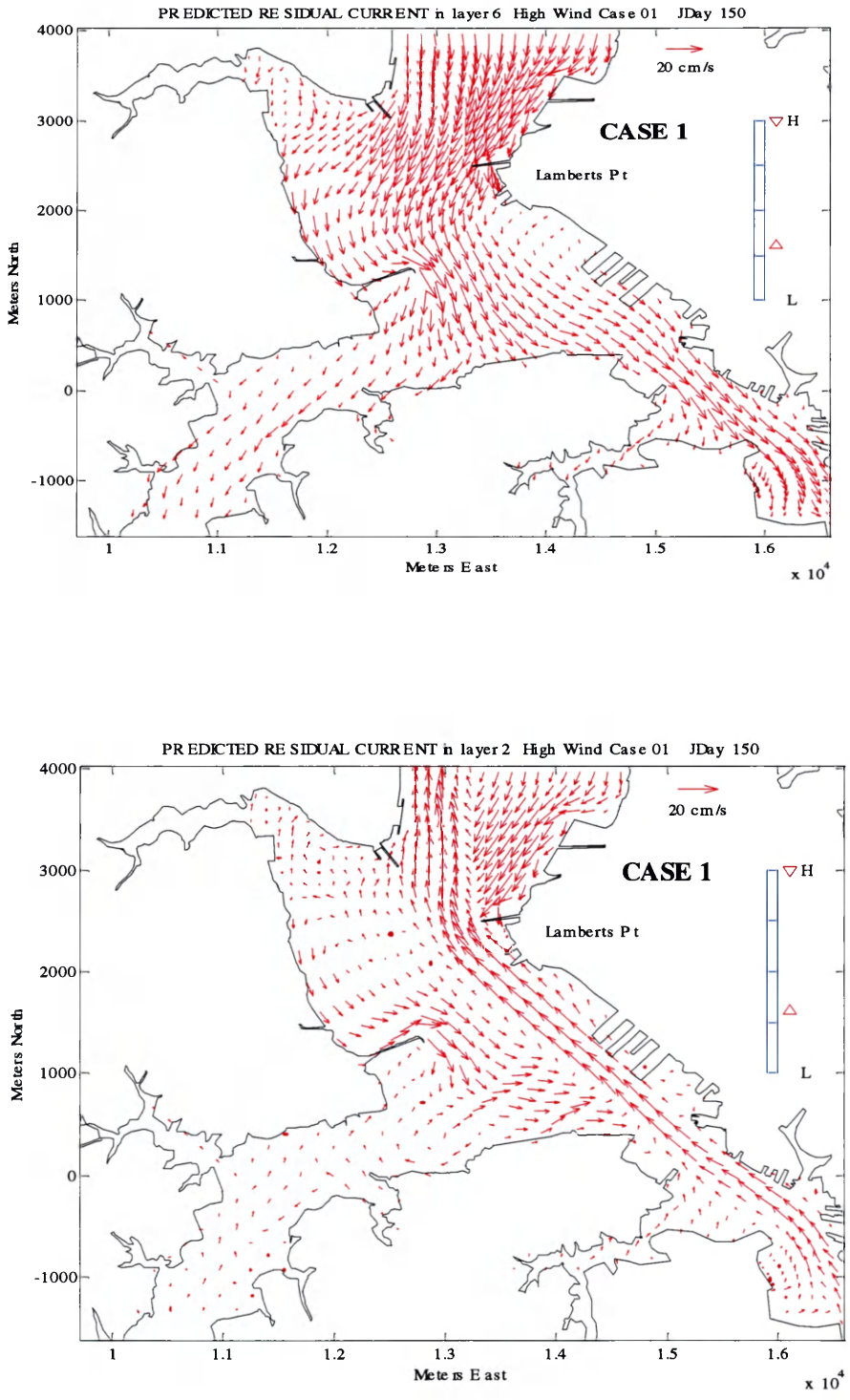

Figure 4-8. Surface and bottom residual current on Julian day 150, 2000, inside Elizabeth

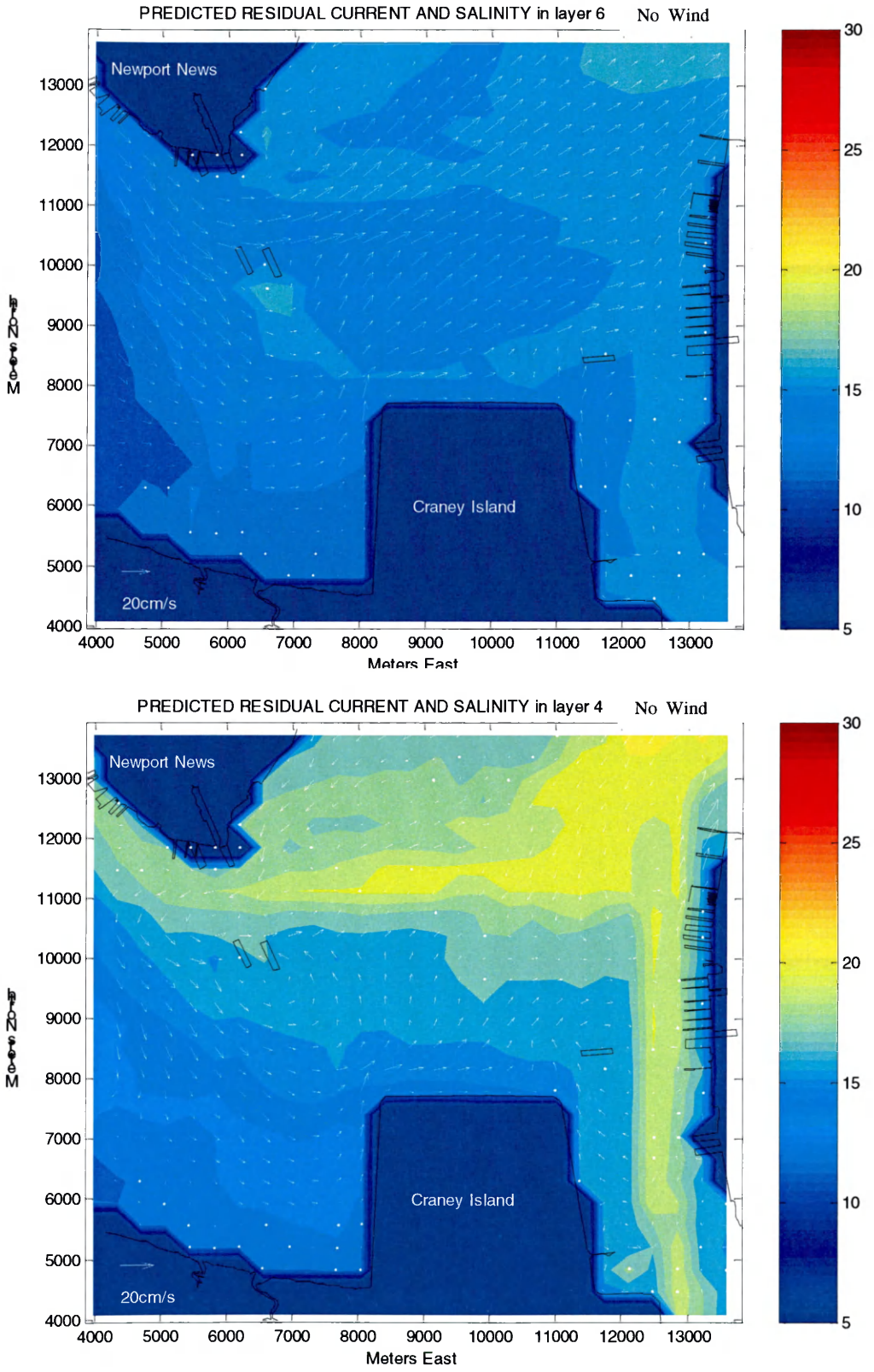

Figure 4-9. Model predicted surface and middle layer residual current and salinity under no wind condition

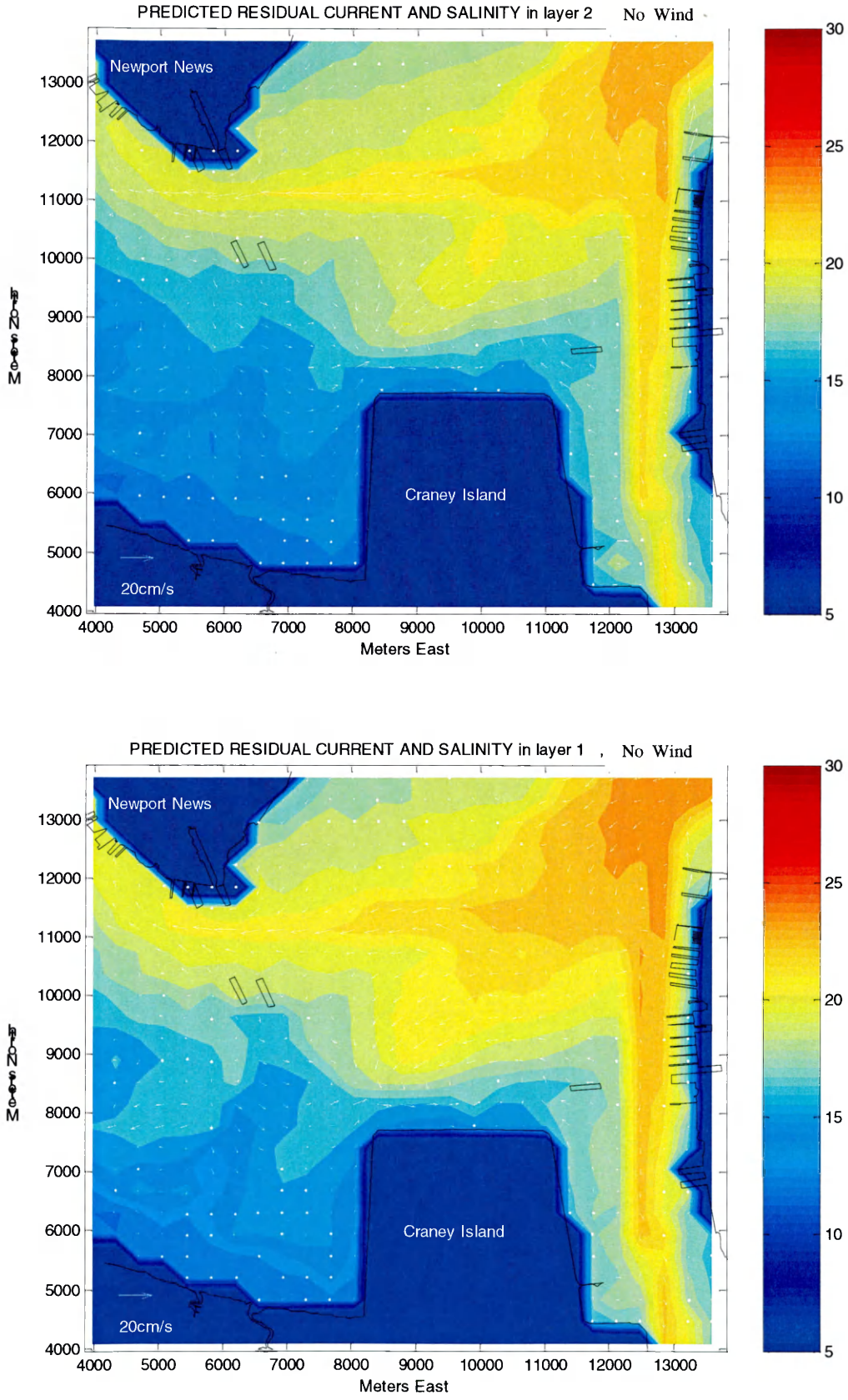

Figure 4-10. Model predicted bottom layer residual current and salinity under no wind condition

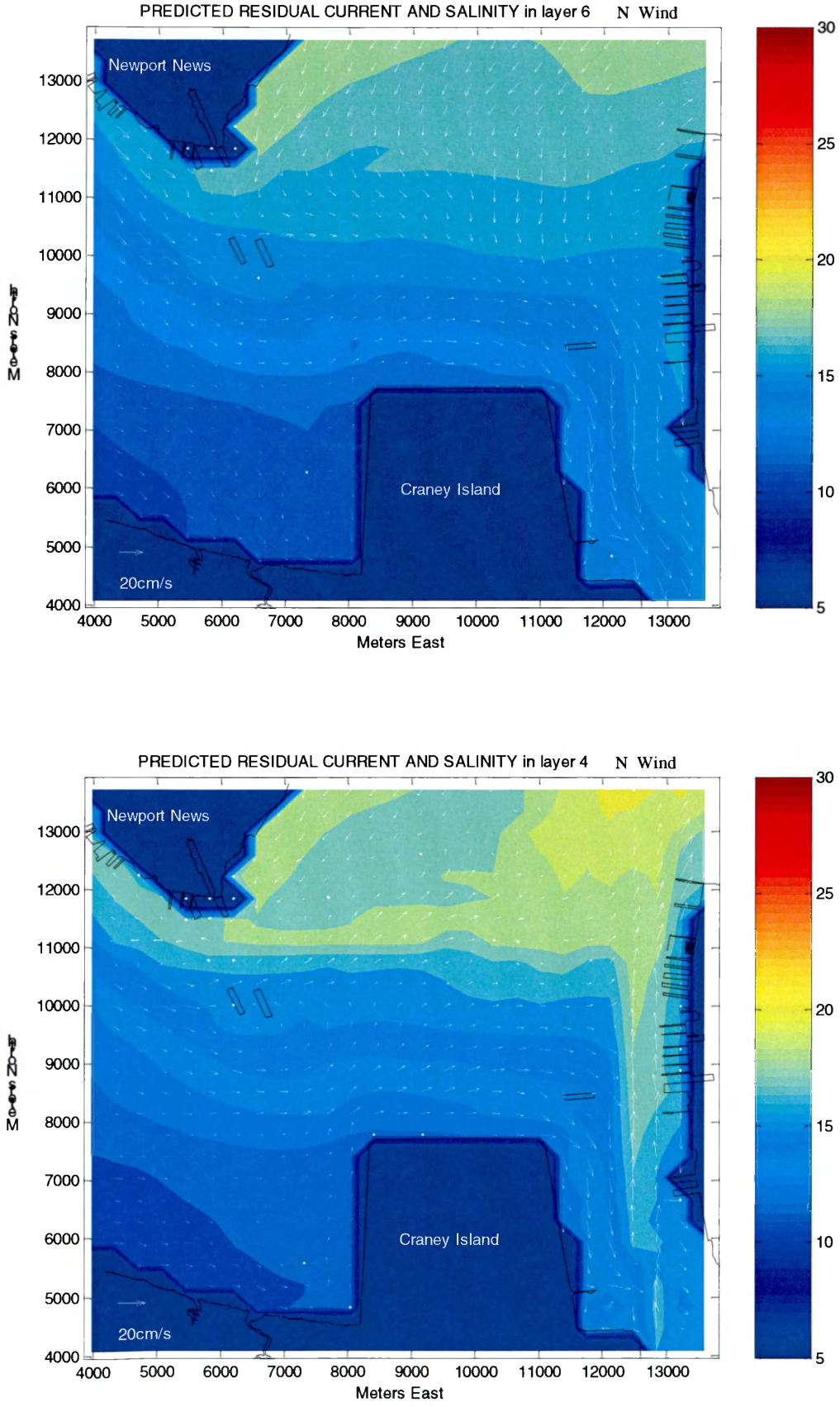

Figure 4-11. Model predicted surface and middle layer residual current and salinity under N wind condition

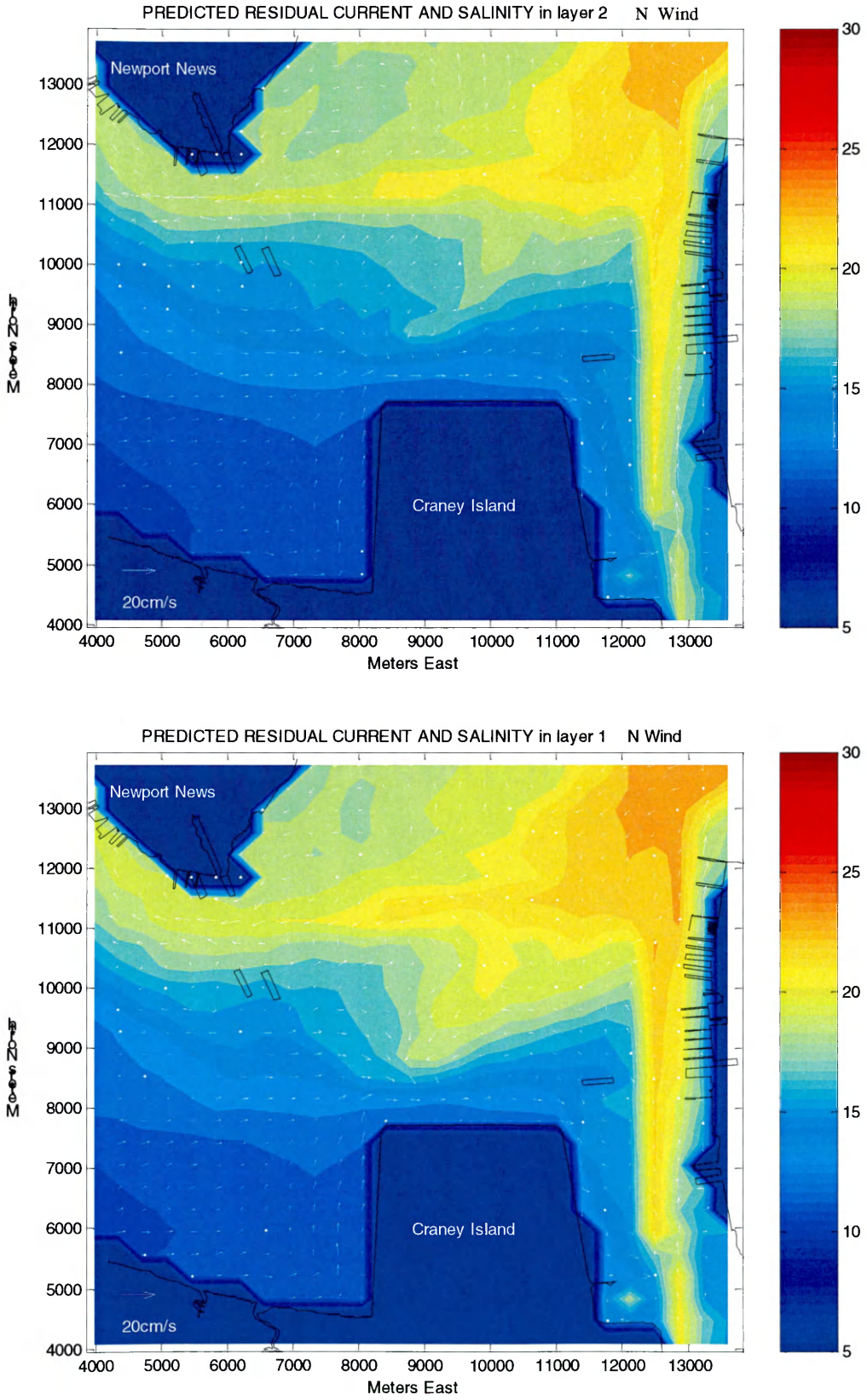

Figure 4-12. Model predicted bottom layer residual current and salinity under N wind condition

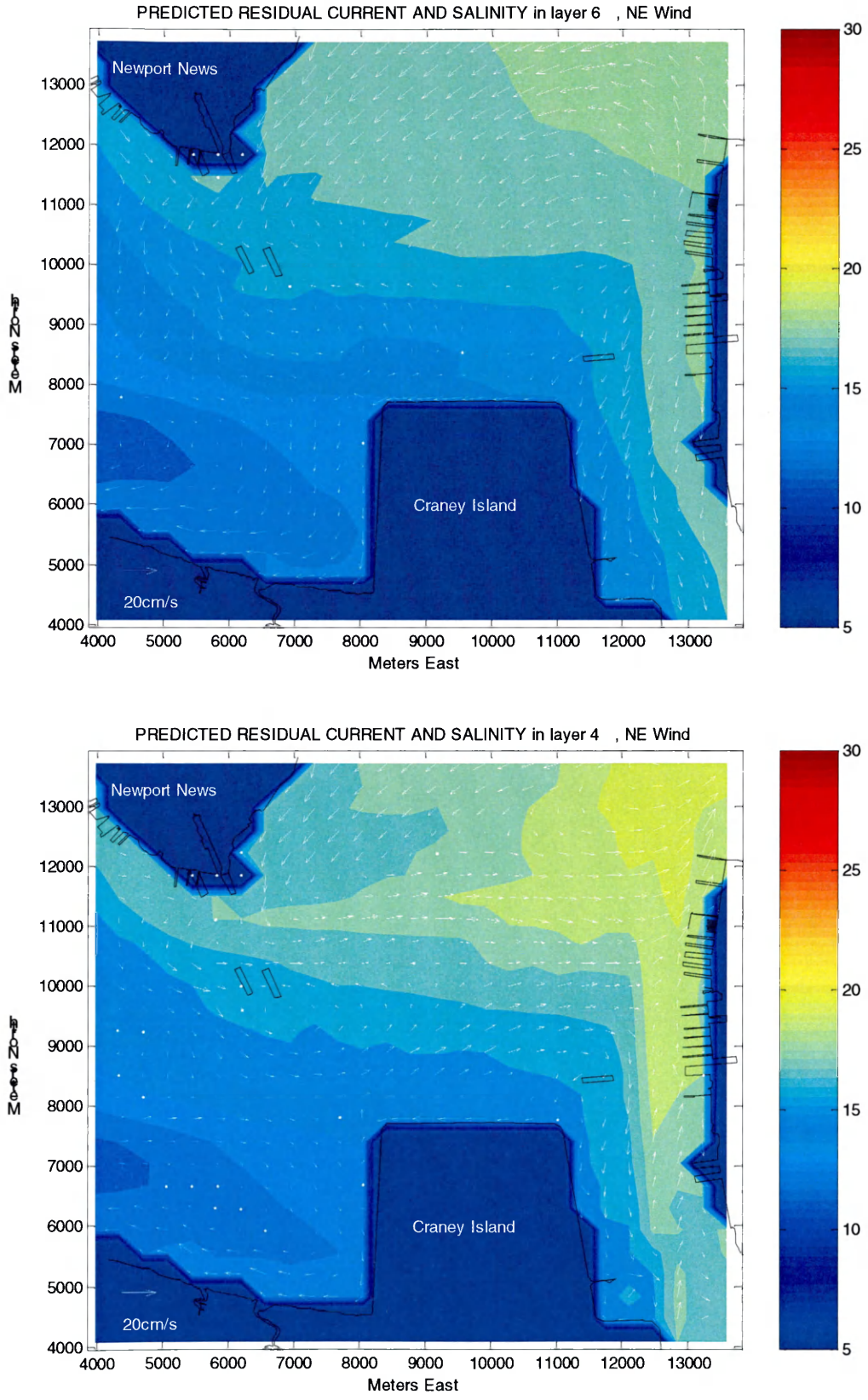

Figure 4-13. Model predicted surface and middle layer residual current and salinity under NE wind condition

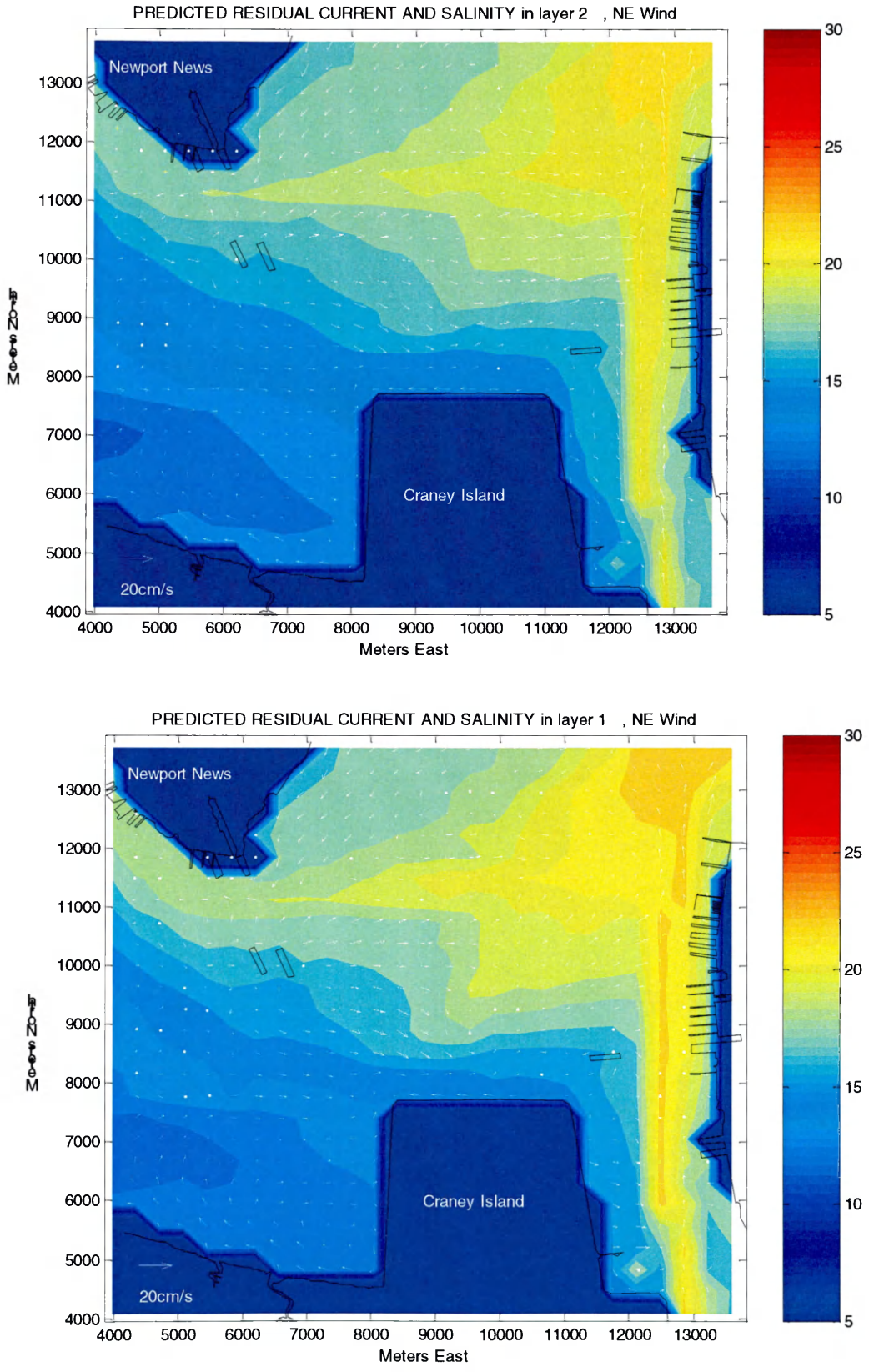

Figure 4-14. Model predicted bottom layer residual current and salinity under NE wind condition

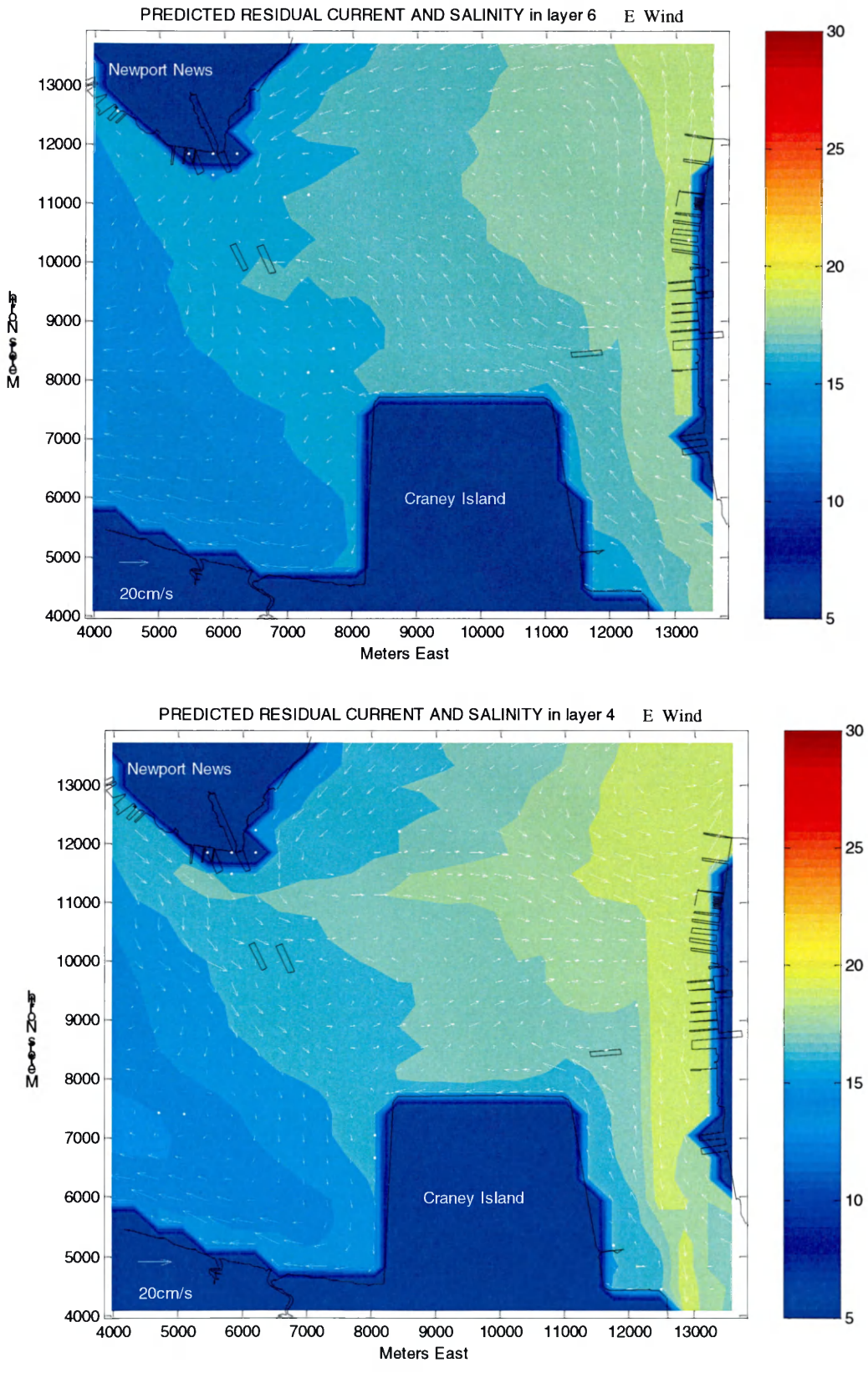

Figure 4-15. Model predicted surface and middle layer residual current and salinity under E wind condition

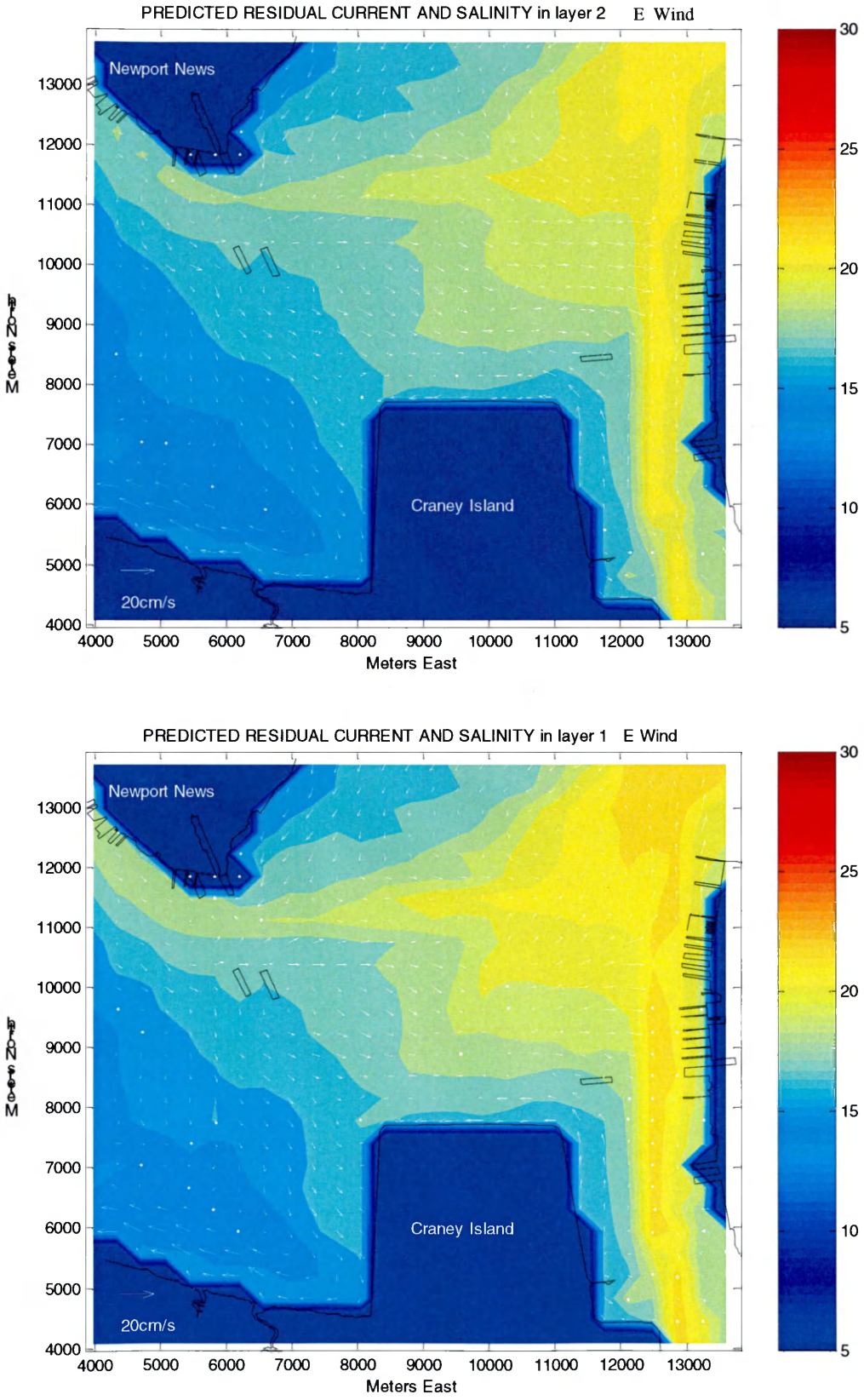

Figure 4-16. Model predicted bottom layer residual current and salinity under E wind condition

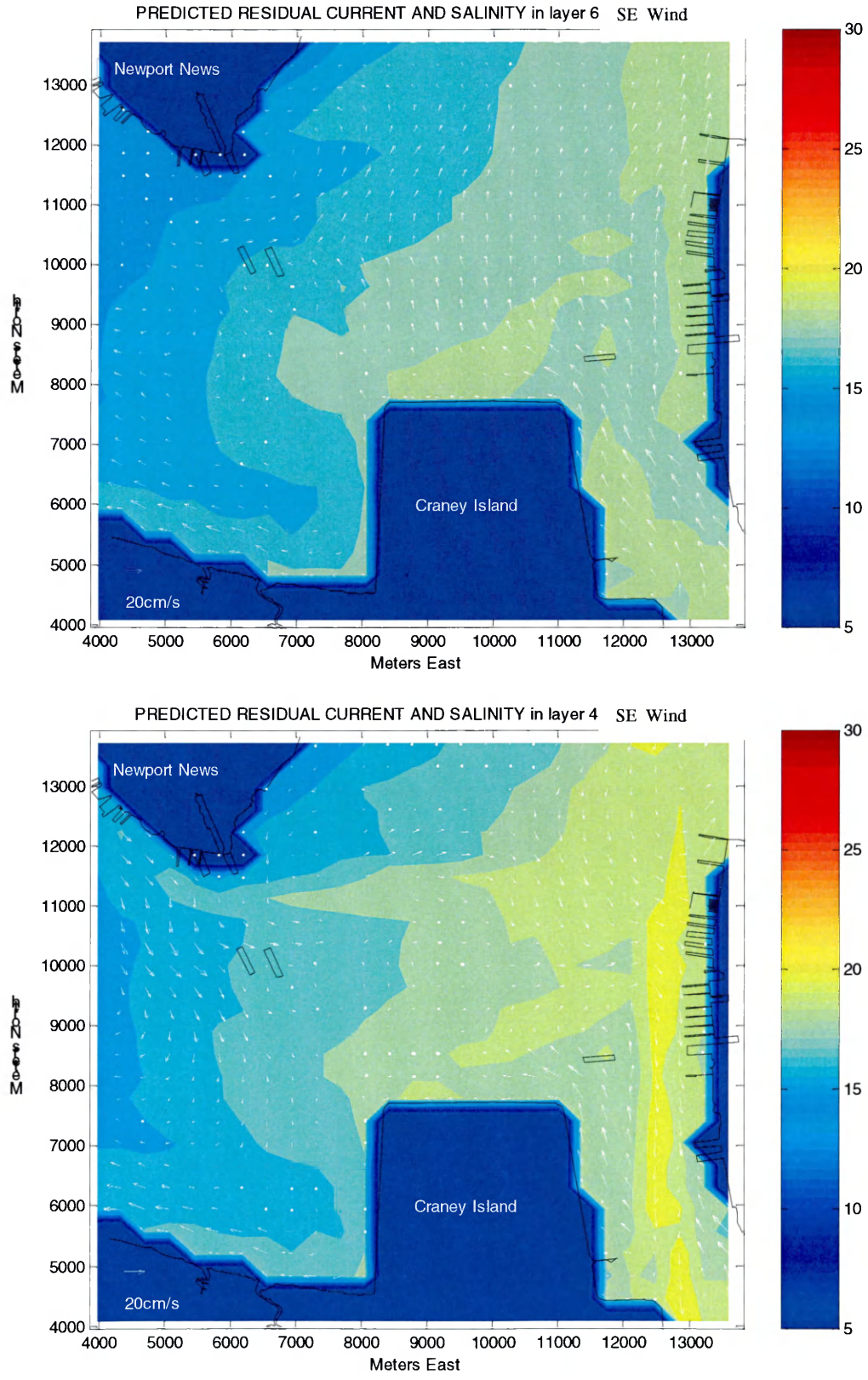

Figure 4-17. Model predicted surface and middle layer residual current and salinity under SE wind condition

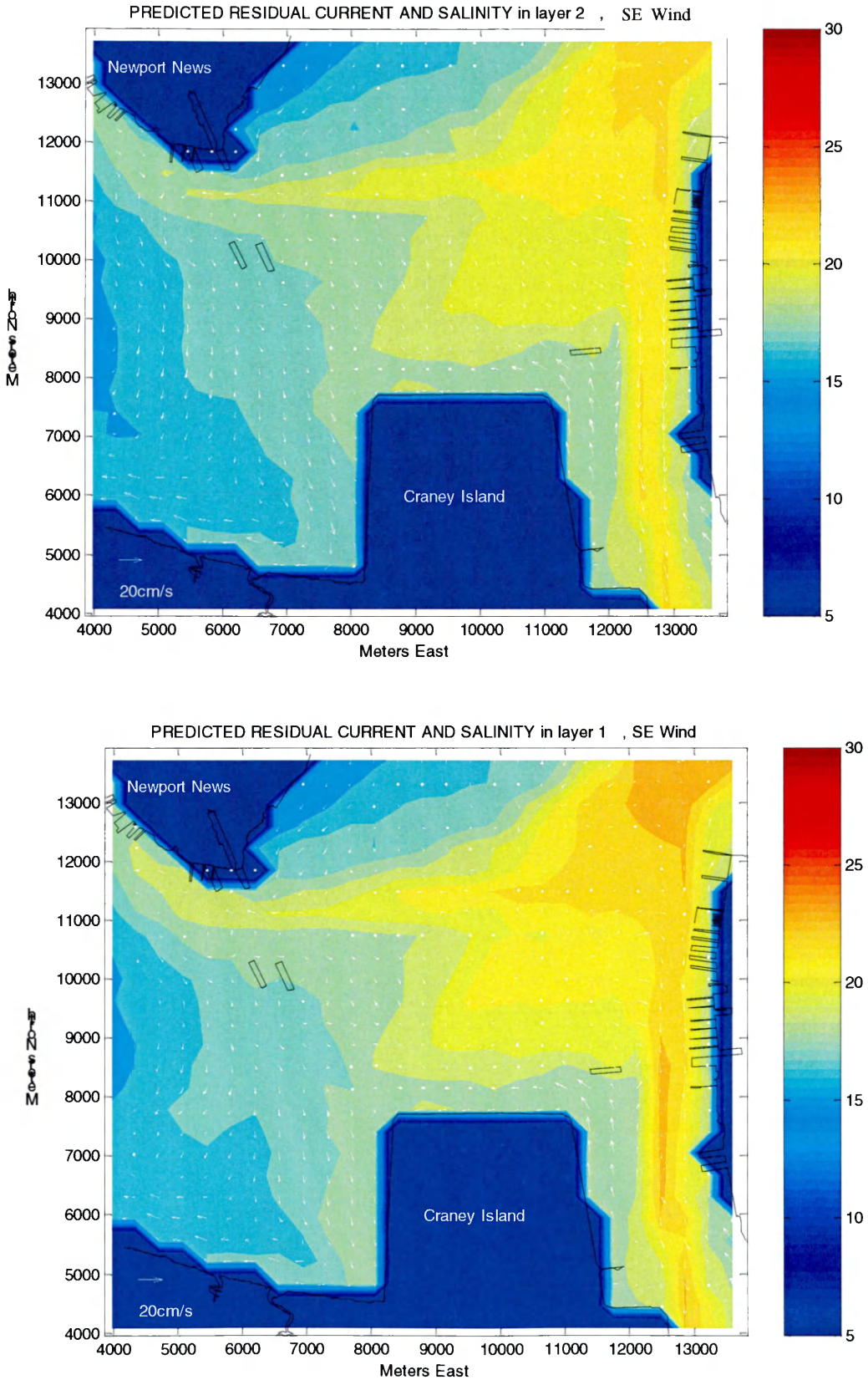

Figure 4-18. Model predicted bottom layer residual current and salinity under SE wind condition

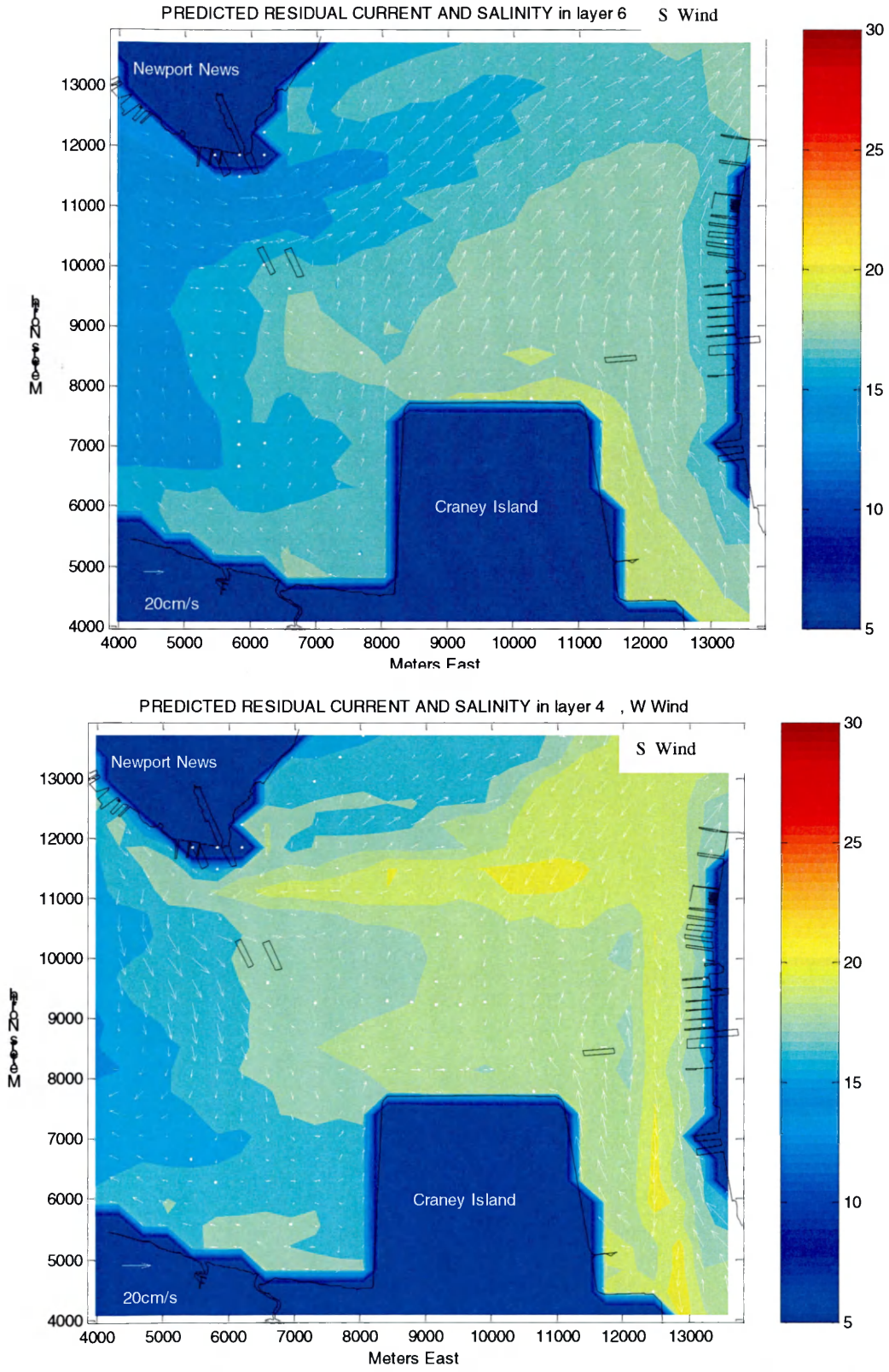

Figure 4-19. Model predicted surface and middle layer residual current and salinity under S wind condition

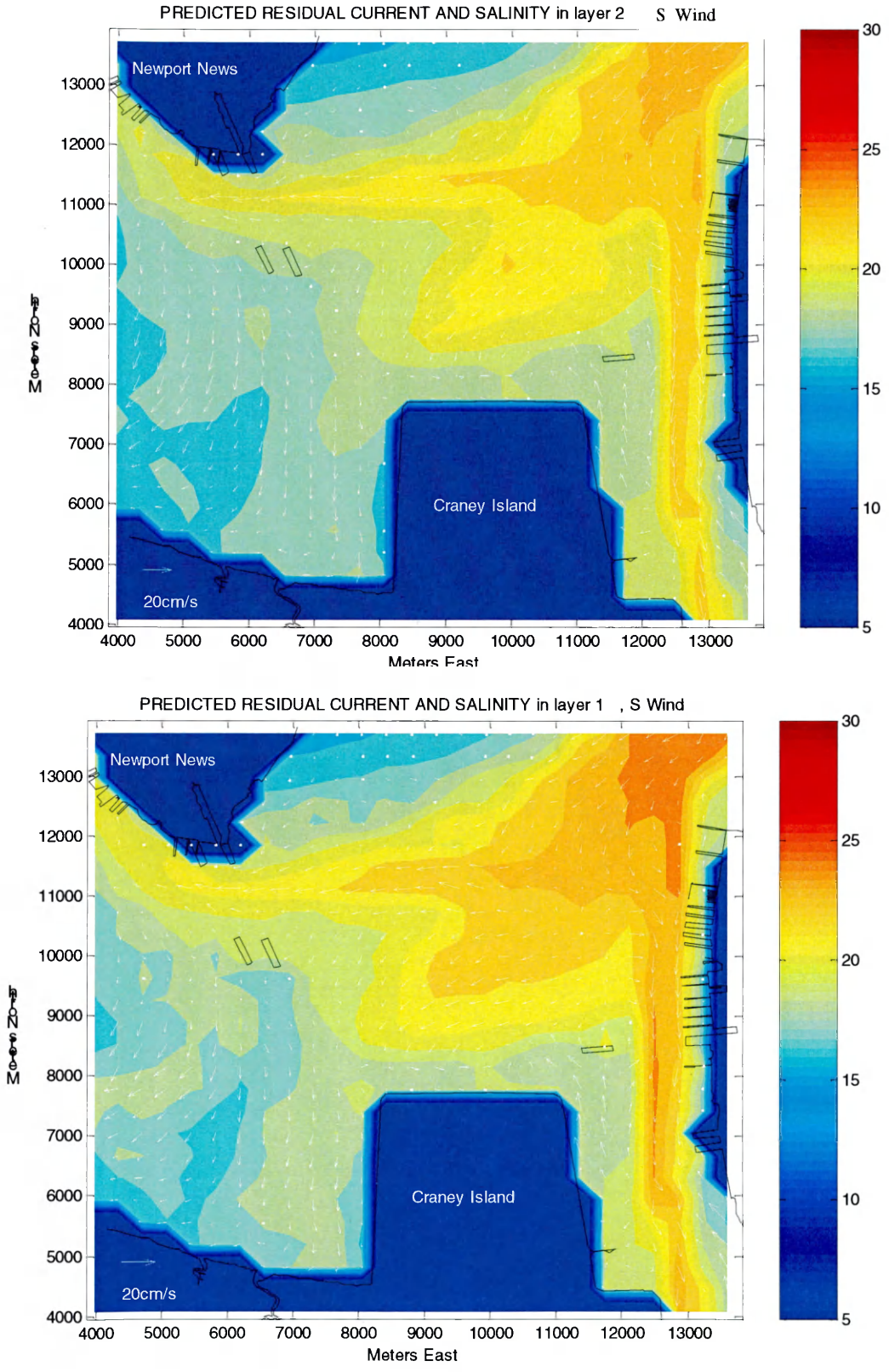

Figure 4-20. Model predicted bottom layer residual current and salinity under S wind condition

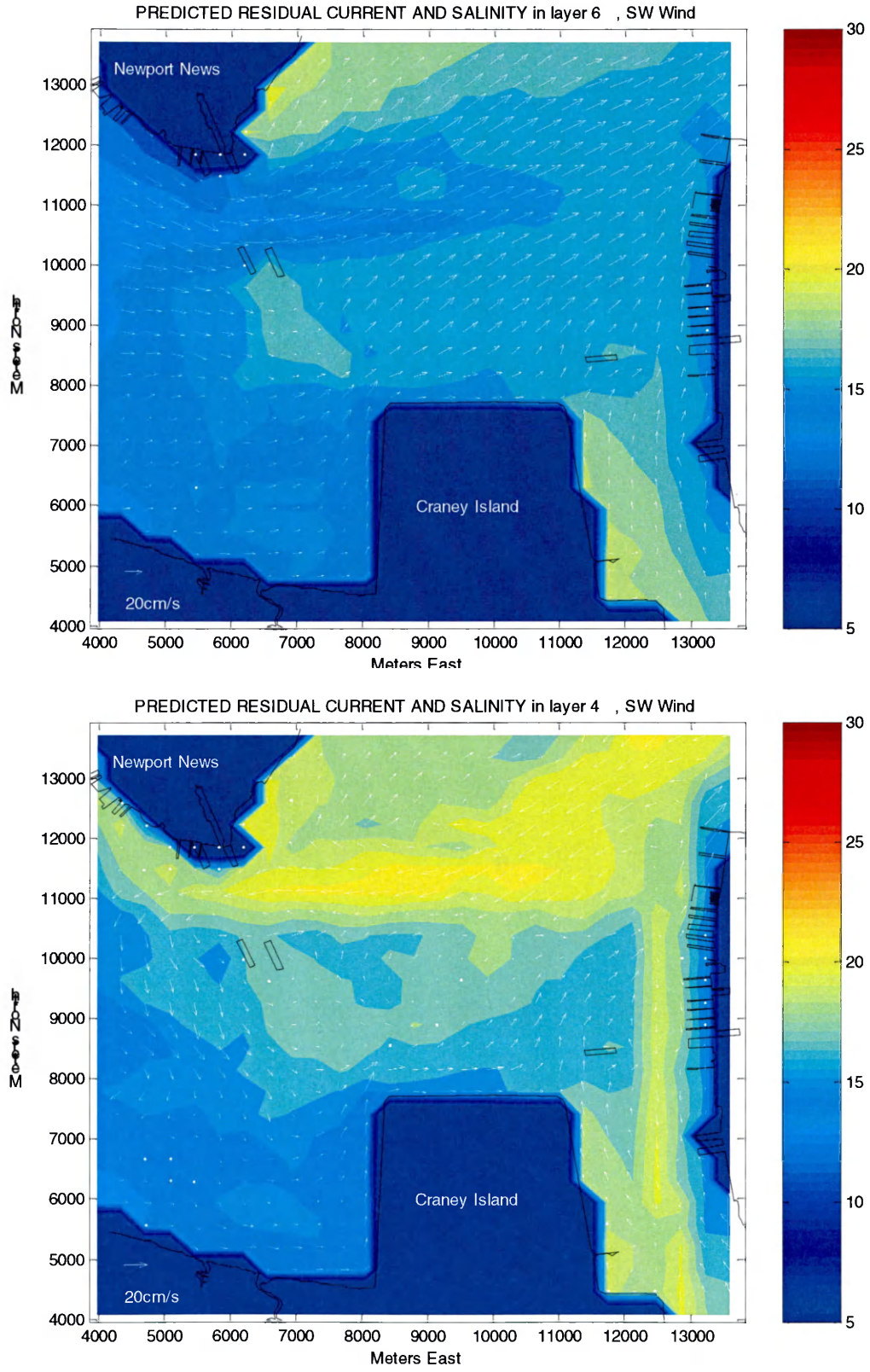

Figure 4-21. Model predicted surface and middle layer residual current and salinity under SW wind condition

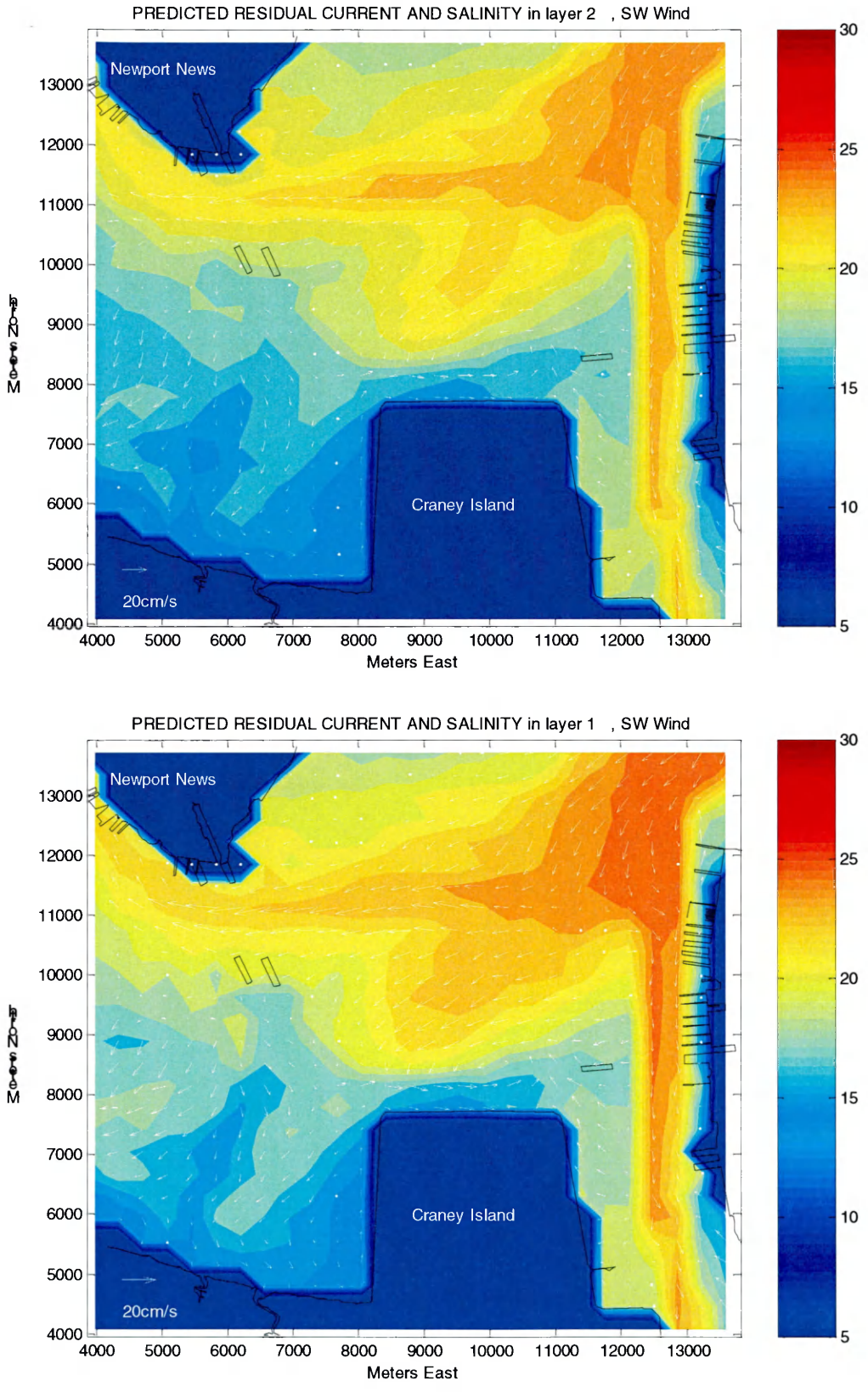

Figure 4-22. Model predicted bottom layer residual current and salinity under SW wind condition

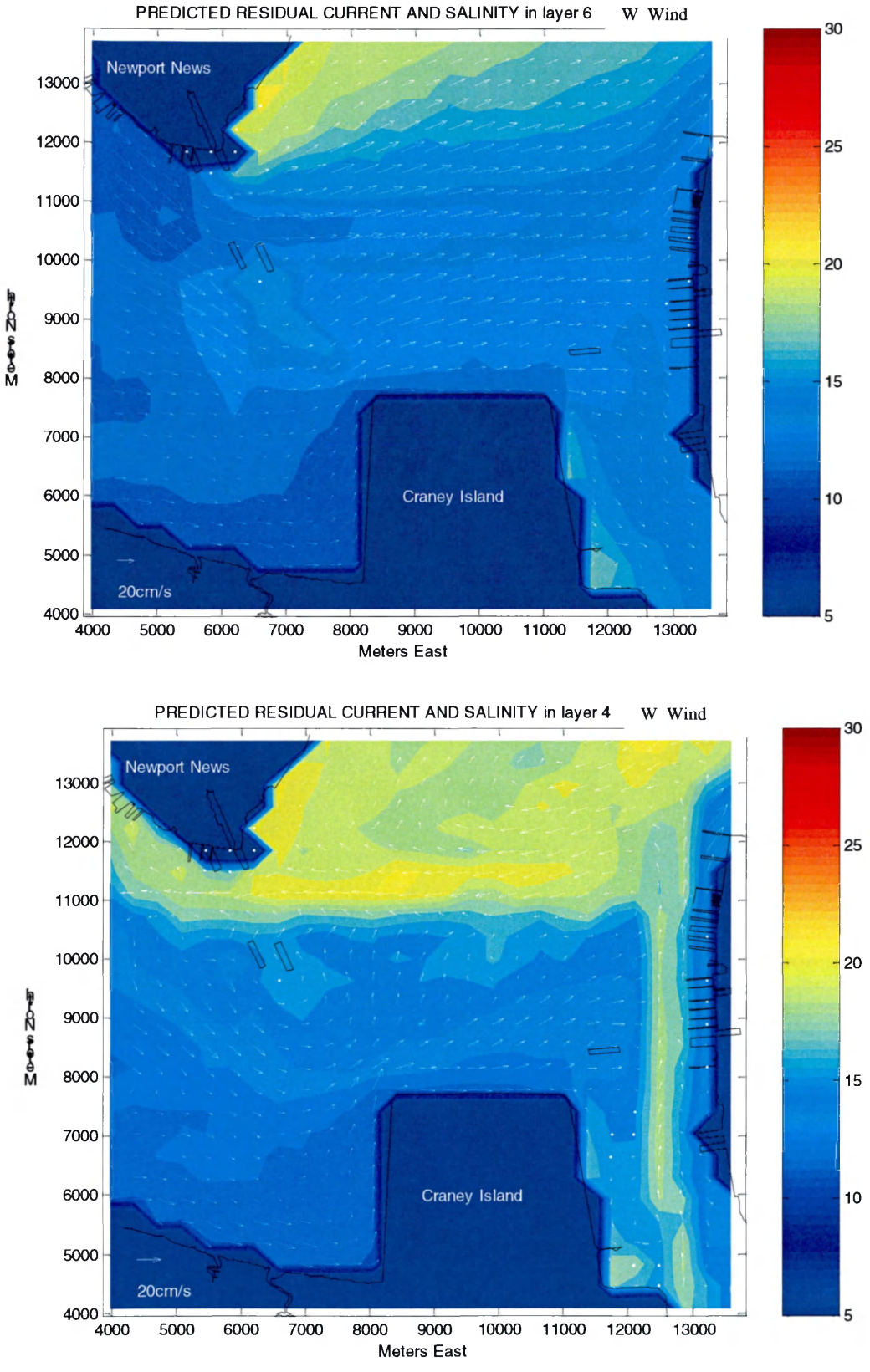

Figure 4-23. Model predicted surface and middle layer residual current and salinity under W wind condition

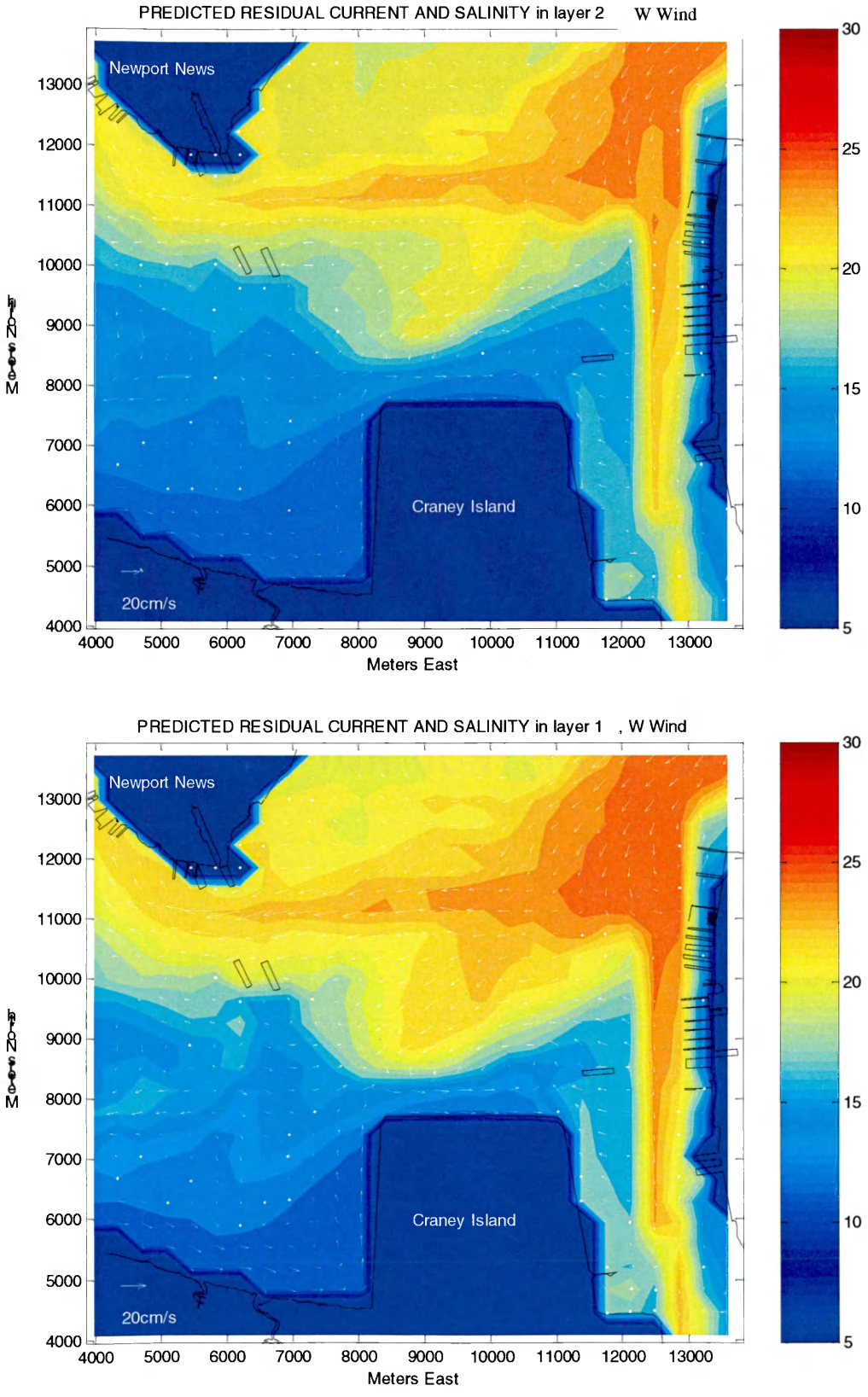

Figure 4-24. Model predicted bottom layer residual current and salinity under W wind condition

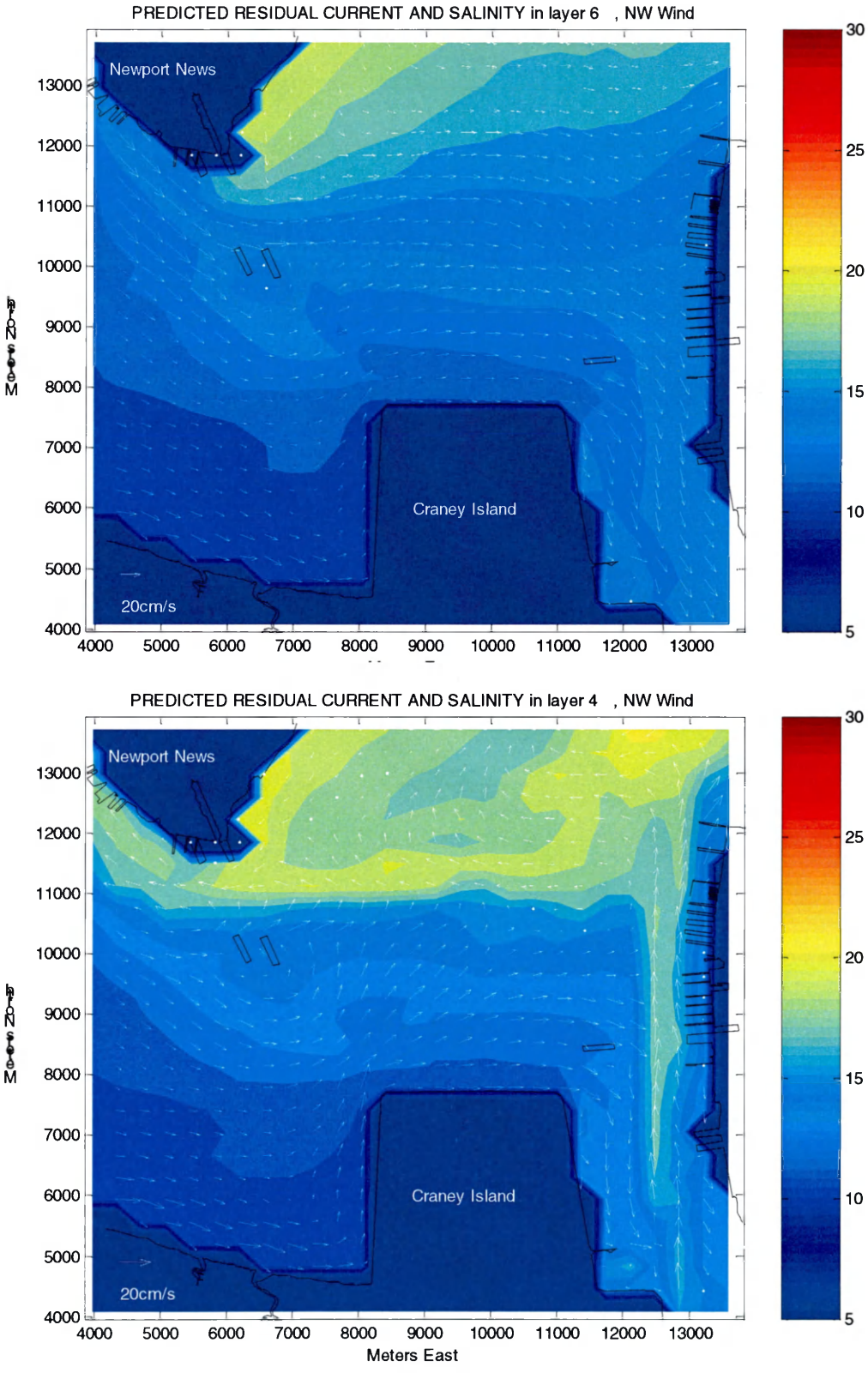

Figure 4-25. Model predicted surface and middle layer residual current and salinity under NW wind condition

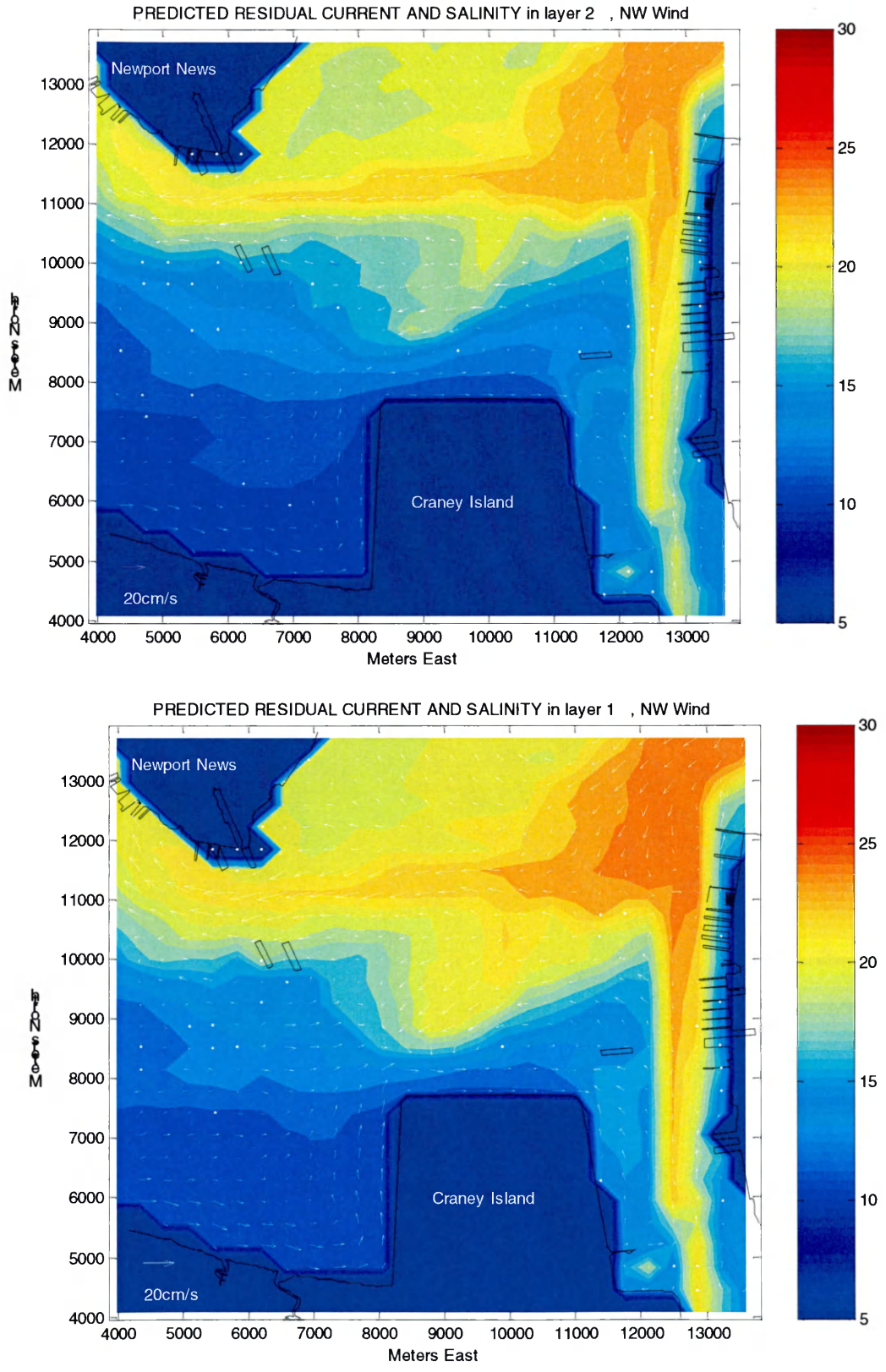

Figure 4-26. Model predicted bottom layer residual current and salinity under NW wind condition

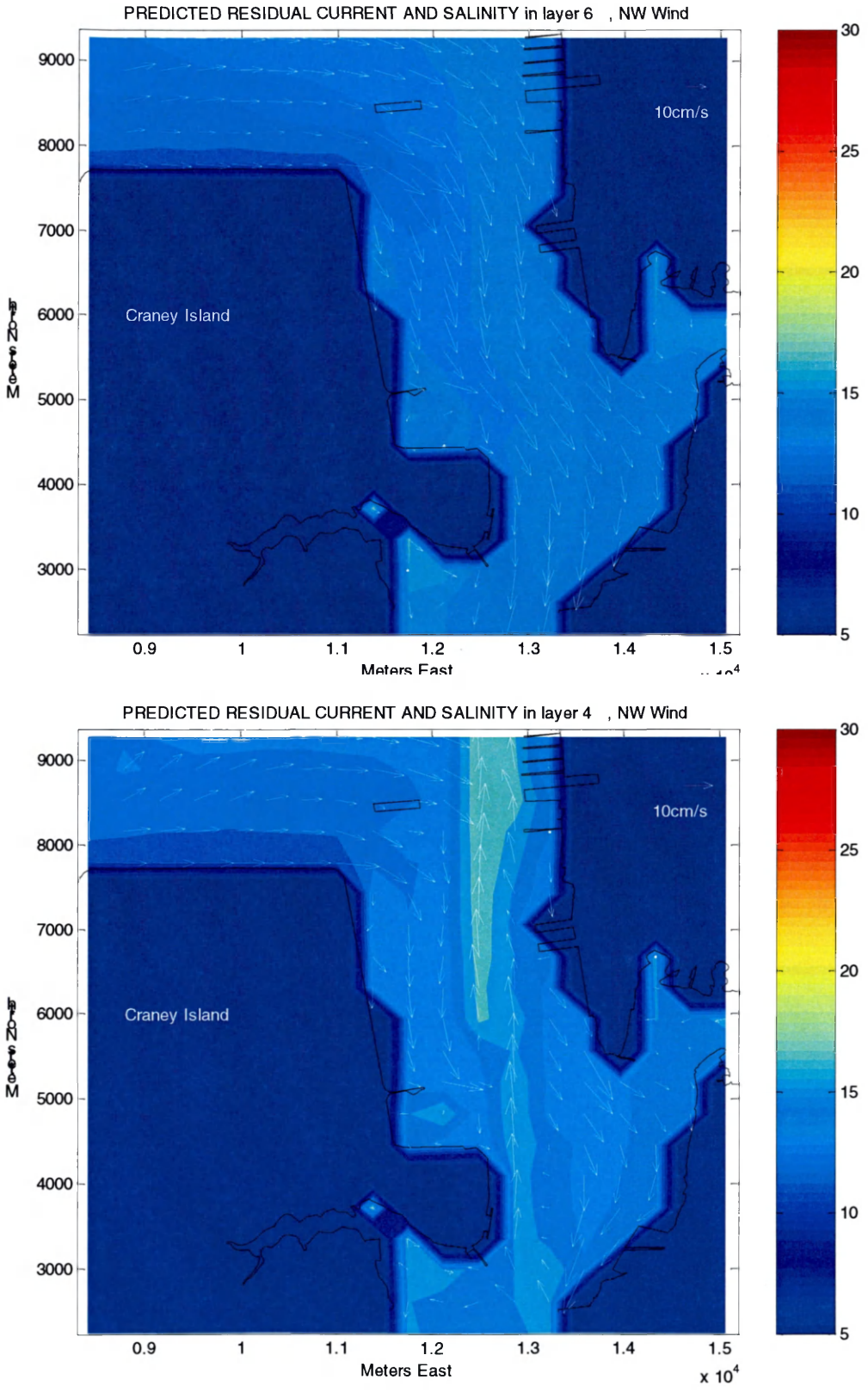

Figure 4-27. Model predicted surface and middle layer residual current and salinity under NW wind condition, in Elizabeth

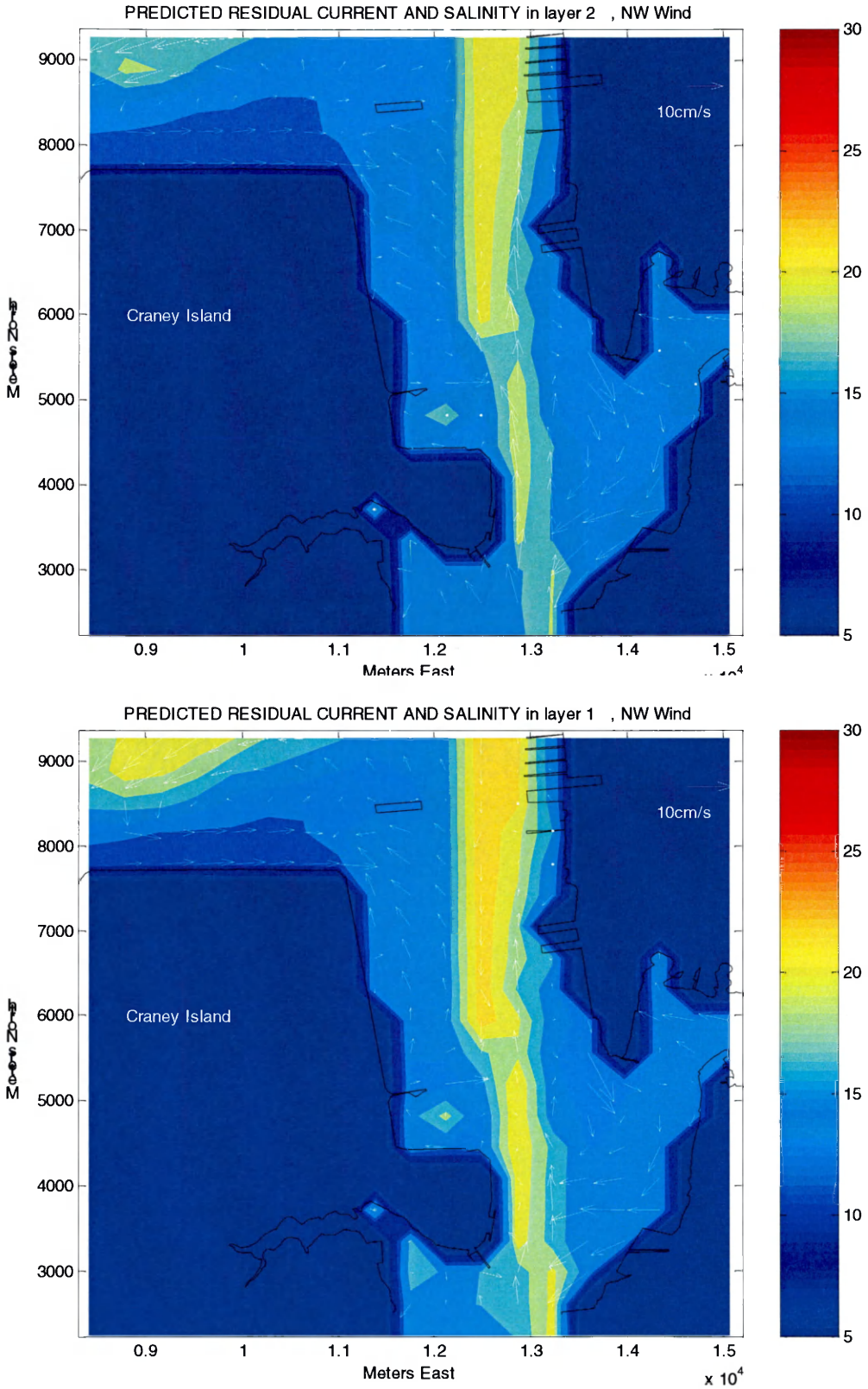

Figure 4-28. Model predicted bottom layer residual current and salinity under NW wind condition, in Elizabeth

Chapter 5

Evaluation of Proposed Craney Island Expansions under Wind Events

For the two expansion designs (Option 7 and Option7/5a), 3 scenario runs/test cases in addition to the base case are summarized in Table 5-1. For each scenario run, the same time step, 30 seconds, was specified with a duration time of six months (March 1 to August 27, 2000, Julian days 60-240). Freshwater discharges inputs used the actual measurements of daily discharges at the 4 stations to generate 8 time series input files for input to the same 8 upstream model cells (main stem of James, Appomattox, Chickahominy, Deep Creek, Lafayette River, and the Eastern, Western, and Southern Branches of the Elizabeth River). Appropriate surface and bottom salinities and observed water levels were used at the James River mouth (open boundary condition). Local winds recorded at Sewells Point were included through a surface stress parameter.

Since extreme conditions (i.e. strong wind event, high/low freshwater inflow) can cause significant impacts to characteristics (i.e., water level, salinity, current) of the estuarine system, these events are always of much concern. In this study, to assess the impacts from these two designs, a method of event-specific evaluation of simulation comparison is used based on results from each run. From within this simulation period, two 7-day event periods were selected to represent

the relatively extreme wind conditions of 'May high wind event' [Julian days 149-155] and 'April high wind event' [Julian days 111-117] .

In order to evaluate the impacts exerted on the James/Elizabeth River system due to each expansion design during this high wind event, a global analysis was conducted for changes in selected parameters (i.e., surface elevation, current velocity, salinity) changes between the base case and variable test case by area. Through an analysis of area-based distribution curves and cumulative curves using the GIS tool, a ranking of the impacts is possible. A local analysis in the critical, so-called "hot spots", areas was then performed for an investigation of the local processes, including currents and circulation features at various sections of the modeling domain. By combining the global and local analyses, a balanced view of assessment from both large scale as well as local scale can be achieved in a more objective manner.

5-1. Global Analysis

The essential idea of Global Analysis is to determine the area-based percentage change of a variable due to the implementation of each expansion design. For each location in the model domain, predicted time series of the base case versus each test case is compared, and changes in each parameter are characterized either as an RMS (root mean square) difference or as a simple average difference:

$$\mathrm{RMS\_DIFFERENCE} = \sqrt{\sum_{i=1}^{n} (MP_{test,i} - MP_{base,i})^2 / n}$$

for tidal elevation, velocity magnitude;

$$AVERAGE\_DIFFERENCE = \sum_{i=1}^{n} (MP_{test,i} - MP_{base,i}) / n$$

for salinity, sedimentation potential and residual velocity.

where: n is number of data points, (1776 for 74 tidal cycles)
MP_{test} is model prediction for the test case
MP_{base} is model prediction for the Base Case

In this manner, changes in each parameter can be evaluated in the form of a simple difference between the predicted value of each test case and that of the base case for each cell and layer of within the entire study domain. Since each Expansion Option grid contains fewer cells than the Base Case grid, locations for comparison are restricted to those common to both.

5-1-1. Spatial Distribution

In order to get an overall view of the difference distribution within the study domain, Spatial Distribution Plots of difference are used to visualize the changes/difference distribution in the study area, hence, range/magnitude of changes and regions with maximum changes can be identified.

For each run comparison, 8 spatial distribution plots were generated by using the ArcView Avenue scripts tool, as described below:

1) RMS difference of tidal elevation
2) average difference of surface salinity
3) average difference of bottom salinity
4) RMS difference of surface velocity magnitude
5) RMS difference of bottom velocity magnitude
6) average difference of surface residual velocity magnitude
7) average difference of bottom residual velocity magnitude
8) sedimentation potential for test case
9) sedimentation potential difference between test case and Base Case

Findings from these RMS difference spatial distribution plots are summarized as follows:

Eastward Expansion (Option 7, Case 2 vs. Base Case, May High Wind Event) – Plots contrasting Case 1 against the Base Case for the high wind event are shown in Figures 5-1 to 5-7. For surface elevation (Figure 5-1), all RMS average differences fall below 0.25 cm except for a small area northeast the expansion option and the southern portion of the Southern Branch, where differences above 0.25 cm are shown in pink. Average differences in surface salinity (Figure 5-2) fall below ±0.2 ppt everywhere except directly adjacent to the expansion option. Bottom salinity average differences (Figure 5-3) are everywhere under ±0.2 ppt except in small areas around the option where differences range to ±1.0 ppt. Surface velocity magnitude differences (Figure 5-4) and bottom velocity magnitude differences (Figure 5-5) reach 12 cm/sec and 8 cm/sec, respectively, near the eastward expansion but are limited to 4 cm/sec in the far field. Surface and bottom residual velocity magnitude differences (Figures 5-6 and 5-7) show, respectively, limits of ±10 cm/sec and ± 3 cm/sec in areas immediately adjacent to the structure.

East/West Expansion (Option 7/5A, Case 10 vs. Base Case, May High Wind Event) – Plots contrasting Case 10 against the Base Case for the high wind event are shown in Figures 5-8 to 5-14. For surface elevation (Figure 5-8), RMS average differences fall between 0.25 cm and 0.50 cm for most of Hampton Roads, except for small areas near the expansion options and the upriver portions of the Western, Southern, and Eastern Branches, where differences above 0.50 cm are shown in gold. Average differences in surface salinity (Figure 5-9) fall below ±0.2 ppt everywhere except north of the expansion option, where they range to

±1.0 ppt. Bottom salinity average differences (Figure 5-10) are everywhere under ±0.2 ppt except in small areas around the option where differences range to ±2.0 ppt. Surface velocity magnitude differences (Figure 5-11) and bottom velocity magnitude differences (Figure 5-12) reach 25 cm/sec and 16 cm/sec, respectively, near the eastward expansion but are limited to 4 cm/sec in the far field. Surface and bottom residual velocity magnitude differences (Figures 5-13 and 5-14) show, respectively, limits of ±10 cm/sec and ± 3 cm/sec in areas immediately adjacent to the structure.

The spatial distributions of the case comparison differences are useful in delineating areas of maximum impact and yet, they are qualitative in nature. An attempt to quantify this analysis is described in the next section.

5-1-2. Percentile Analysis

Based on spatial distribution plots, to quantify these differences, a technique using percentile analysis was incorporated. Spatial accumulation curves, over the entire model surface area of Hampton Roads, as shown in Figures 5-15 to 5-28, was employed for all the run comparison.

The cumulative percent or percentile value indicates that how many percent of the modeled surface area will contain changes in a variable that are less than or equal to the corresponding RMS difference value. In this study, a 95^{th} percentile value was specified. By comparing the RMS difference value, for each run comparison, corresponding to the 95 cumulative percent values, the impacts from each design expansion option is able to be ranked. The 95^{th} percentile values derived from those cumulative curves, for comparing the impacts from different

option designs under high wind condition, were summarized as shown in Table 5-2.

Global analysis suggest that notable changes in those physical characteristics (water level, current magnitude, salinity and sedimentation potential) are predicted to occur in certain locations due to the effects of the expansion designs. Since local hydrodynamic features are directly affected by those physical changes, i.e., the circulation patterns depend on the speed and direction of current, and the flushing characteristics in a estuarine system is directed by both tidal as well as non-tidal current and also water levels. One known circulation feature in the estuarine system is the tidal front and its associated eddy system near Newport News Point, both of which are critical to the movement of shellfish larvae (Shen, Boon, and Kuo, 1999; Shen and Kuo, 1999). Also, since the Elizabeth River has been identified as one of the most polluted bodies of water in the entire Chesapeake watershed, flushing of pollutants in the river is always of great concern. Thus, a local analysis is used to investigate possible impacts on these local hydrodynamic features.

5-2. Local Analysis

Local analysis was conducted here through time series of model results comparisons at selected locations. A seven-day period from model outputs was analyzed for the April storm event.

Due to diurnal inequalities in the strength of flood and ebb, it is therefore necessary to develop the residual (tidally averaged) current field by averaging model-predicted u (positive east) and v (positive north) velocity components over

a lunar day. Examples of the residual surface current vector fields for the April wind condition in the Hampton Roads and inside the Elizabeth regions are shown in Figures 5-29 and 5-30. Three stations, as indicated in these two figures, were selected for local time series analysis.

Comparisons of principal axes of surface, middle, and bottom residual currents between Case 2 and Base Case are shown in Figures 5-31 to 5-39. Surface, middle layer, and bottom residual current comparisons between Case 10 and Base Case are shown in Figures 5-40 to 5-48. Because of the similarity with Case 2 vs. Base Case, here, only the results for Case 2 vs. Base Case will be discussed.

Surface Residual Current—Case 2 vs. Base Case

Principal axis surface residual currents comparison between Case 2 and Base Case at stations JR1, ER1 and ER2 are shown in Figures 5-31, 5-32 and 5-33, respectively. As shown in these three figures, the ebb flood alternation pattern of surface currents is disrupted. All the surface residuals are positive, which means that the surface currents flow upstream. This might be caused by the strong northeasterly wind occurred during JD 116.

At station JR1, located in the main channel near Newport News, current are identical for Case 2 and the Base Case. The RMSD (root mean square difference) value for this pair of curves is 0.5 cm/s. At station ER3, which is below Lamberts Point in the Elizabeth River, only a slight difference between the two is observed as shown in Figure 5-33. While at station ER1, close to the east of Craney Island, there is a clear difference between Case 2 and the Base Case as

shown in Figure 5-32. RMSD between the two cases is 9.1 cm/s. These are consistent with what have been shown in the aforementioned spatial distribution plot. Difference of surface residual current between Case 2 and the Base Case appears mainly around the vicinity of the Eastward Expansion of Craney Island.

Middle Layer Residual Current—Case 2 vs. Base Case

Principal axis middle layer residual currents comparison between Case 2 and the Base Case at stations JR1, ER1 and ER2 are shown in Figures 5-34, 5-35 and 5-36, respectively.

At station JR1, the middle layer currents are almost identical for Case 2 and Base Case. At station ER3, only slight difference between the two is observed as shown in Figure 5-36. While at station ER1, both magnitude and phase differences between the two cases are observed as shown in Figure 5-34.

Bottom Residual Current—Case 2 vs. Base Case

Principal axis bottom residual currents comparison between Case 2 and the Base Case at stations JR1, ER1 and ER2 are shown in Figures 5-37, 5-38 and 5-39, respectively.

At station JR1, the bottom residual currents are almost identical for Case 2 and Base case. At station ER3, only slight difference between the two is observed as shown in Figure 5-39. While at station ER1, both magnitude and phase differences between the two cases are observed as shown in Figure 5-38.

As a summary, the mean, amplitude and phase differences of surface, middle layer and bottom residual currents between Case 2 vs. the Base Case and Case 10 vs. the Base Case are presented in Tables 5-3 and 5-4.

At station JR1, differences in mean current, current amplitude and current phase between Case 2 and the Base Case are small at all three depths. Differences in these three current parameters are slightly larger for Case 10 vs. the Base Case. This is not out of expectation due to the new placement nearby the west of Craney Island. The changes, however, remain small as compared to conservative estimates of model accuracy and support the conclusion that the current field north and west of Craney Island is essentially unchanged by either Expansion Option 7 or 7/5a.

At Station ER1, things are quite different. The differences in these three current parameters exhibit significant change in both Case 2 and Case 10 comparisons with Case 1 (Base Case). Current phase for Case 2 leads that for Case 1 by approximately 30 minutes at the surface and 52 minutes near the bottom. Similar differences are indicated for Case 10. Current amplitudes decrease about 6 cm/s at the surface and 5 cm/s near bottom for both cases as compared with the Base Case. Changes in magnitude are not unexpected at ER1, given its location in an area of maximum change in channel dimensions immediately east of the Eastward Expansion (Option 7).

At station ER2, slight differences of less than 1 cm/s are indicated in current mean and current amplitude comparisons for both cases. Current phase leads varying from 17 minutes at the surface to 12-13 minutes in the middle and near the bottom layers are predicted for both cases.

Summary

Findings from the model simulation comparisons based on Global and Local Analysis are summarized as follows:

East Expansion (Option 7) produced less change among global analysis variables than East/West Expansion (Option7/5a). Neither produced change comparable to North (Option 6) or North/East Expansion (Option 9) and very minor changes occurred due to channel deepening.

Local changes in the residual current field are not significant except in the vicinity of Craney Island. In the region immediately north of Craney Island, East/West Expansion (Option 7/5a) redirects northward surface and bottom residual current to the east. This might cause changes over a relatively larger region around Craney Island.

Case	Design	Channel Depth (ft)	Event
			High wind
1	Base Case	50	Case 1 results
2	Option 7	50	Case 2 results
10	Option 7/5A	50	Case 10 results

Table 5-1. Historical Model Cases, Event Categories.

Global Change – 95th Percentile (5% of area contains change greater than value listed)		
Historical – High Wind Event		
Change in:	**Case 2 East 50' channel**	**Case 10 East/West 50' channel**
Surface Elevation	0.21 cm	0.46 cm
Surface Current	2.2 cm/s	**5.0 cm/s**
Bottom Current	1.5 cm/s	3.0 cm/s
Surface Salinity	0.00 ppt	0.00 ppt
Bottom Salinity	0.00 ppt	0.02 ppt
Sedimentation Potential	0.8 %	1.7 %

Table 5-2. Summary of 95th percentile values for cumulative curves of differences of selected state variables for each historical case versus the base case. For each state variable, the maximum value within each event is displayed as **bold**.

a. Surface layer

Station	Case 1	Case 2	Difference
JR1 Mean (cm/s)	-17.36	-17.33	0.03
Amp (cm/s)	53.99	54.05	0.05
Phase (min)	0	1.58	1.58
ER1 Mean (cm/s)	4.77	-1.34	-6.11
Amp (cm/s)	27.14	21.37	-5.77
Phase (min)	0	30.12	30.12
ER2 Mean (cm/s)	-0.25	-0.42	-0.17
Amp (cm/s)	14.52	14.41	-0.11
Phase (min)	0	16.51	16.51

b. Middle layer

Station	Case 1	Case 2	Difference
JR1 Mean (cm/s)	-9.55	-9.60	-0.05
Amp (cm/s)	45.62	45.81	0.19
Phase (min)	0	2.44	2.44
ER1 Mean (cm/s)	0.02	-2.91	-2.93
Amp (cm/s)	20.00	14.53	-5.47
Phase (min)	0	45.15	45.15
ER2 Mean (cm/s)	-0.31	-0.23	0.08
Amp (cm/s)	10.33	9.86	-0.47
Phase (min)	0	12.62	12.62

c. Near-bottom layer

Station	Case 1	Case 2	Difference
JR1 Mean (cm/s)	-3.31	-3.29	0.02
Amp (cm/s)	36.23	36.38	0.15
Phase (min)	0	2.75	2.75
ER1 Mean (cm/s)	-2.06	-0.39	1.67
Amp (cm/s)	13.81	9.16	-4.64
Phase (min)	0	52.37	52.37
ER2 Mean (cm/s)	-0.39	-0.32	0.07
Amp (cm/s)	13.15	13.34	0.19
Phase (min)	0	13.27	13.27

Table 5-3. Principal axis current comparisons, Base Case and Case 2, High wind event (days 111-117): a. surface layer, b. middle layer, c. near-bottom layer of water column.

a. Surface Layer

Station	Case 1	Case 10	Difference
JR1 Mean (cm/s)	-17.36	-16.44	0.92
Amp (cm/s)	53.99	54.55	0.56
Phase (min)	0	5.20	5.20
ER1 Mean (cm/s)	4.77	-1.29	-6.06
Amp (cm/s)	27.14	21.28	-5.87
Phase (min)	0	32.31	32.31
ER2 Mean (cm/s)	-0.25	-0.29	-0.04
Amp (cm/s)	14.52	14.43	-0.09
Phase (min)	0	17.35	17.35

b. Middle layer

Station	Case 1	Case 10	Difference
JR1 Mean (cm/s)	-9.55	-9.19	0.36
Amp (cm/s)	45.62	46.77	1.14
Phase (min)	0	6.22	6.22
ER1 Mean (cm/s)	0.02	-2.98	-3.00
Amp (cm/s)	20.00	14.20	-5.80
Phase (min)	0	45.52	45.52
ER2 Mean (cm/s)	-0.31	-0.44	-0.13
Amp (cm/s)	10.33	9.79	-0.54
Phase (min)	0	13.76	13.76

c. Near-bottom layer

Station	Case 1	Case 10	Difference
JR1 Mean (cm/s)	-3.31	-3.56	-0.25
Amp (cm/s)	36.23	37.60	1.37
Phase (min)	0	7.35	7.35
ER1 Mean (cm/s)	-2.06	-0.40	1.66
Amp (cm/s)	13.81	9.07	-4.73
Phase (min)	0	51.10	51.10
ER2 Mean (cm/s)	-0.39	-0.32	0.07
Amp (cm/s)	13.15	13.39	0.24
Phase (min)	0	11.70	11.70

Table 5-4. Principal axis current comparisons, Base Case and Case 10, high wind event (days 111-117): a. surface layer, b. middle layer, c. near-bottom layer of water column.

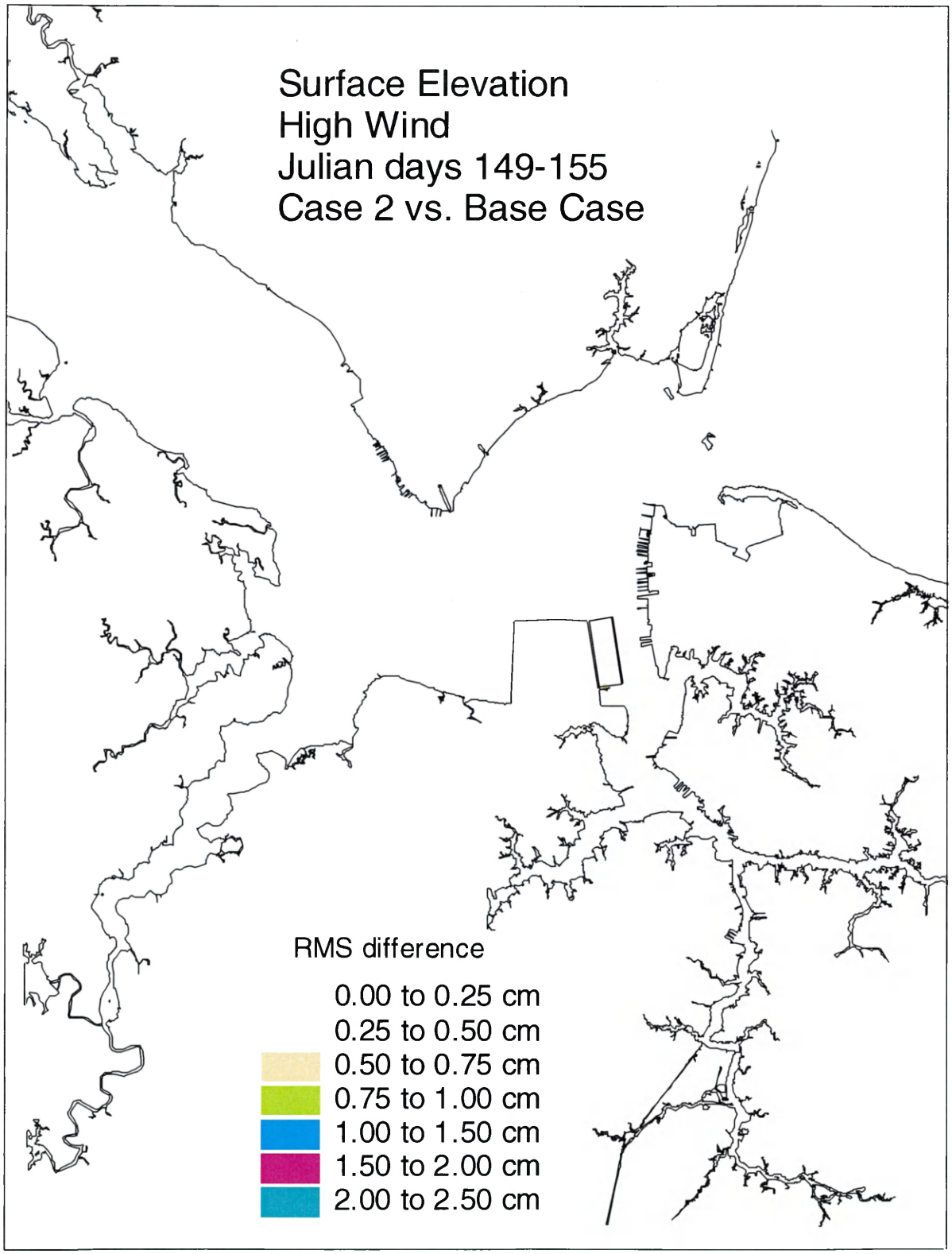

Figure 5-1. Historical simulation comparison (high wind) of the surface elevation RMS difference for the Eastward Expansion (Option 7, 50-foot channel) versus the Base Case.

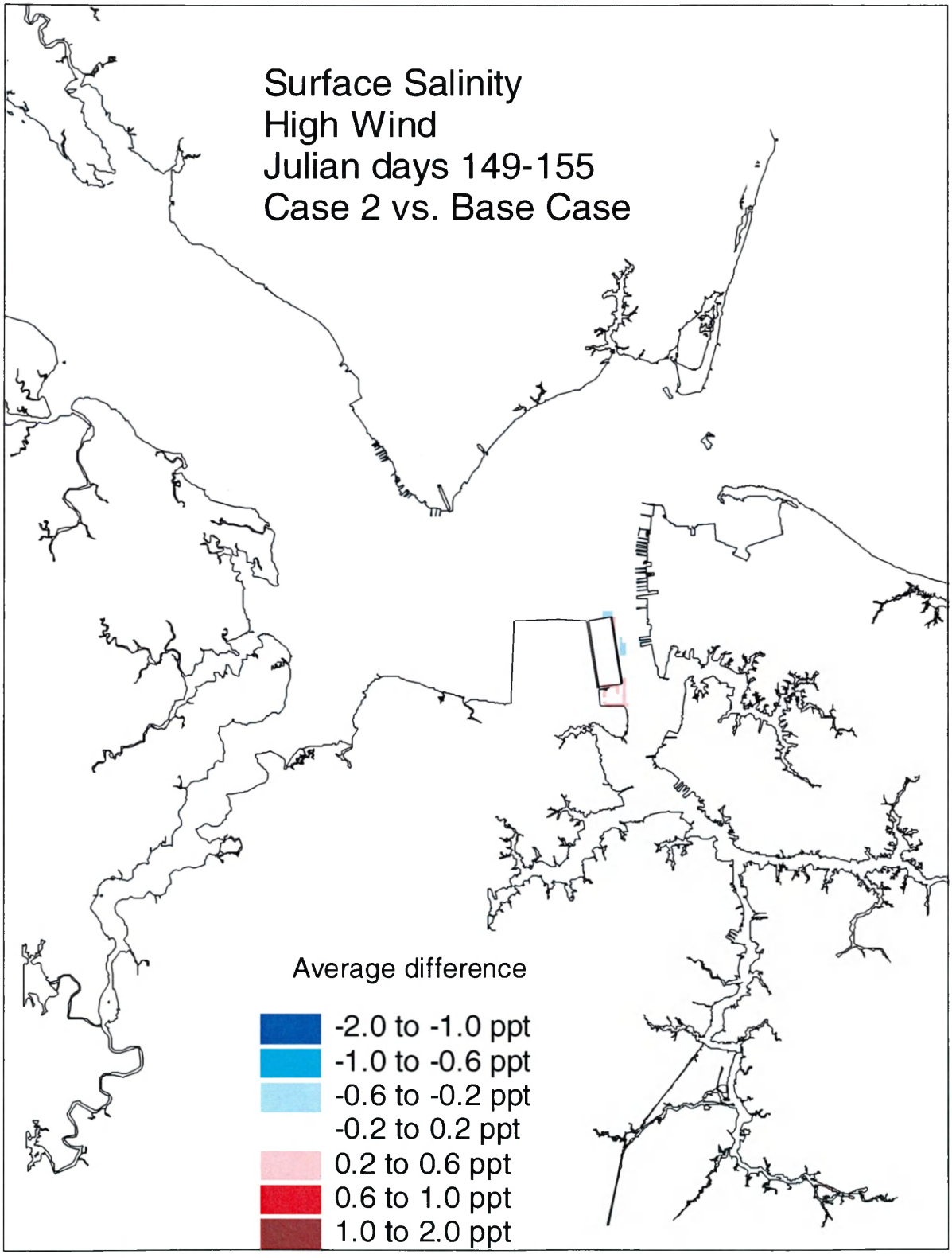

Figure 5-2. Historical simulation comparison (high wind) of the surface salinity average difference for the Eastward Expansion (Option 7, 50-foot channel) versus the Base Case.

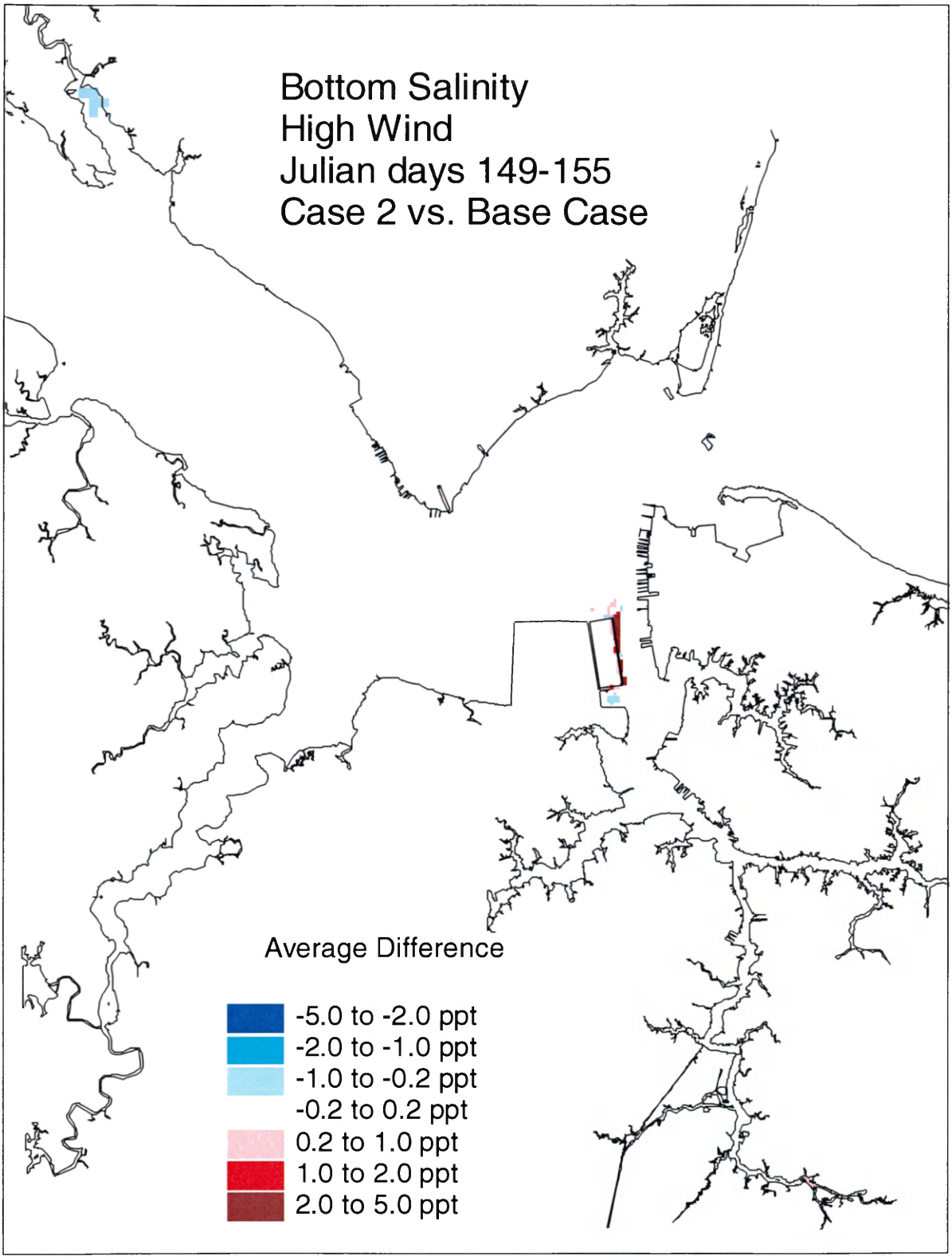

Figure 5-3. Historical simulation comparison (high wind) of the bottom salinity average difference for the Eastward Expansion (Option 7, 50-foot channel) versus the Base Case.

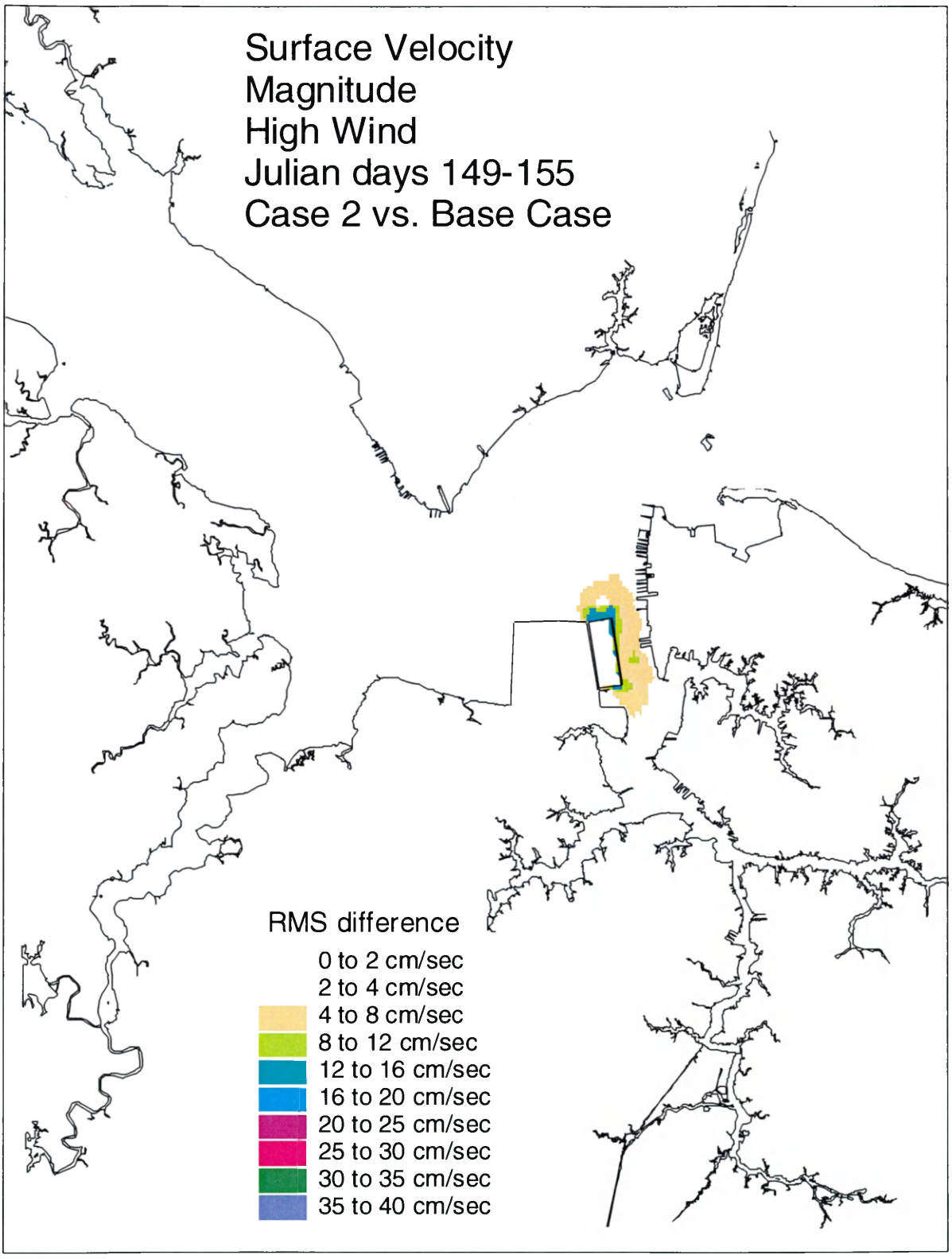

Figure 5-4. Historical simulation comparison (high wind) of the surface velocity RMS difference for the Eastward Expansion (Option 7, 50-foot channel) versus the Base Case.

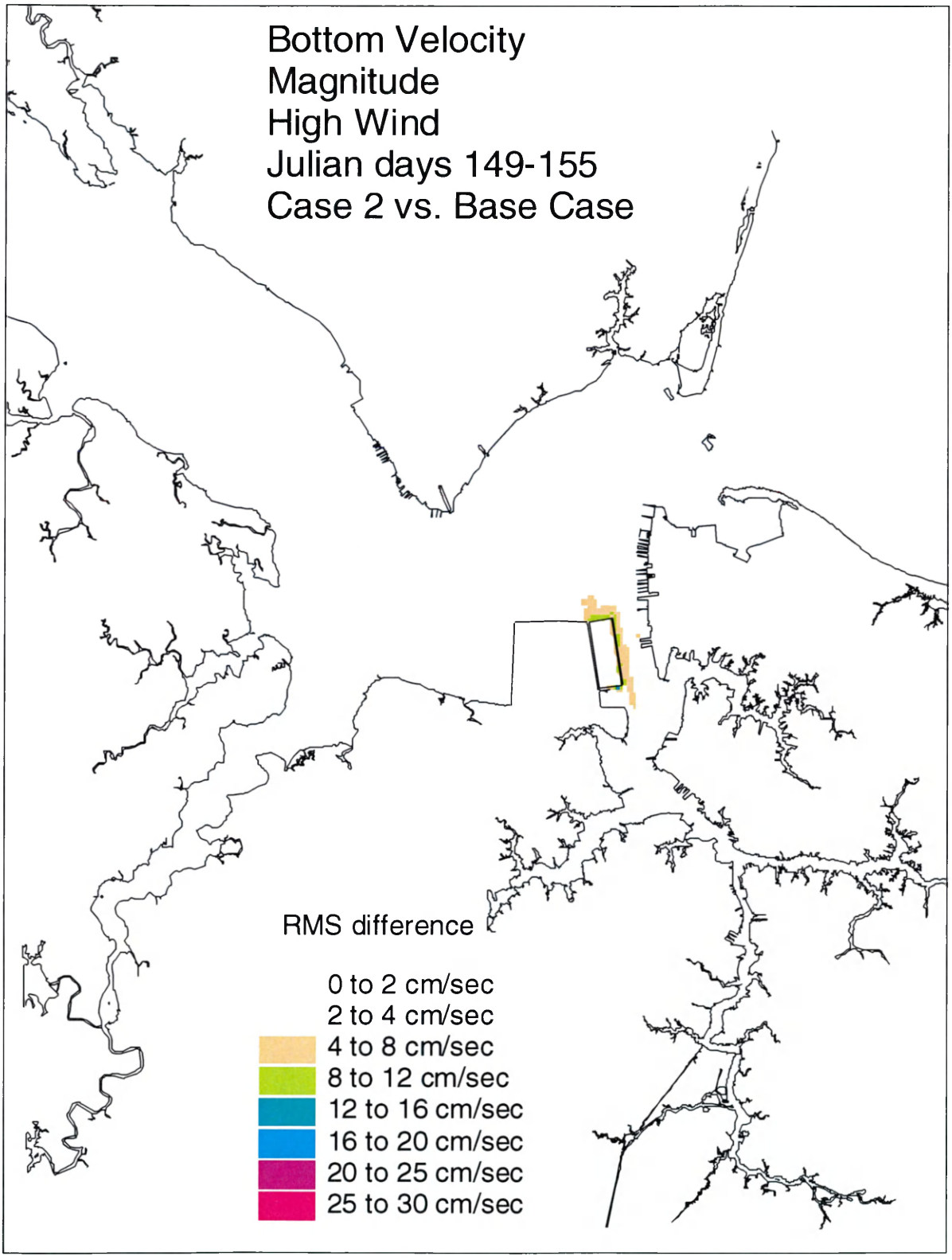

Figure 5-5. Historical simulation comparison (high wind) of the bottom velocity RMS difference for the Eastward Expansion (Option 7, 50-foot channel) versus the Base Case.

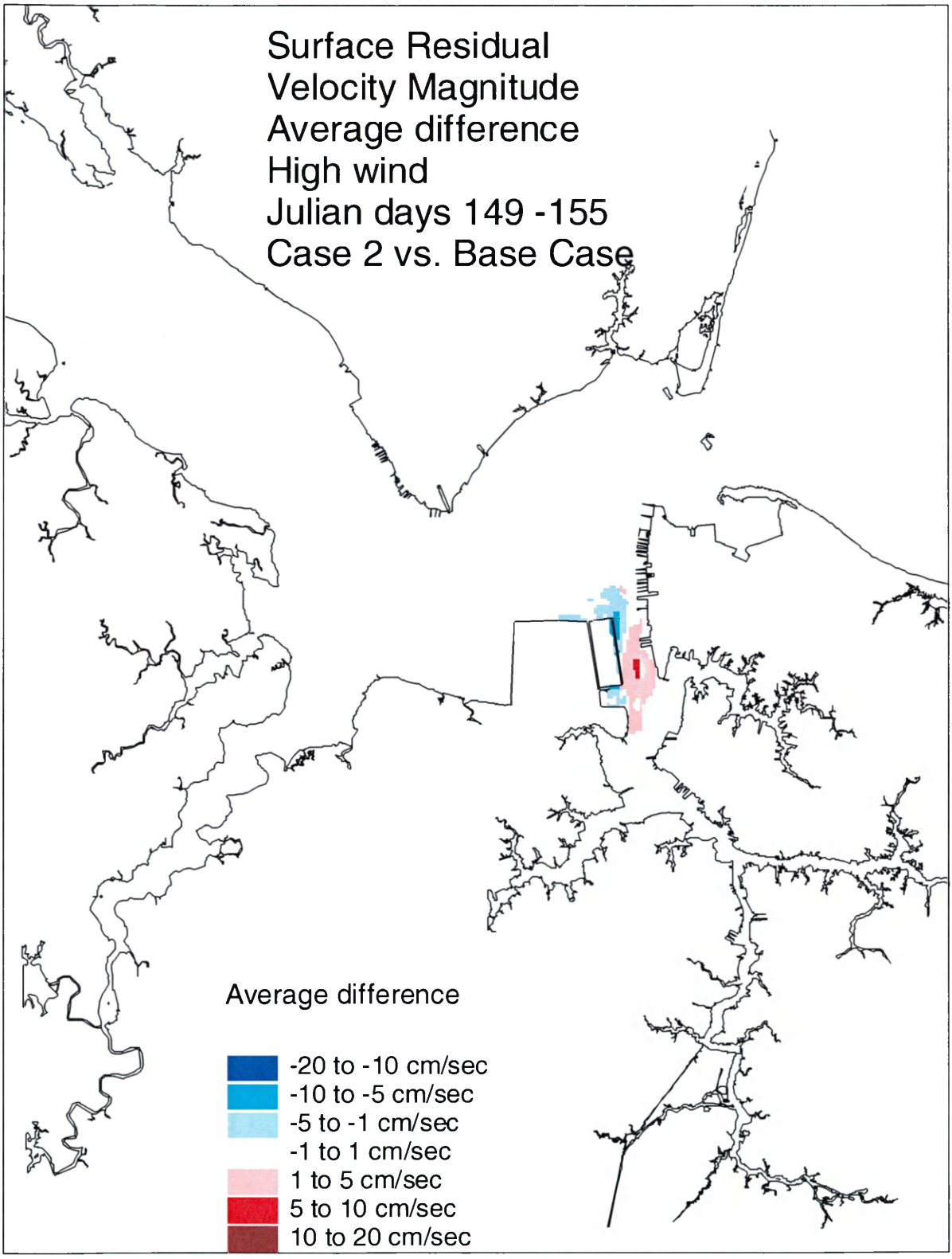

Figure 5-6. Historical simulation comparison (high wind) of the surface residual velocity average difference for the Eastward Expansion (Option 7, 50-foot channel) versus the Base Case.

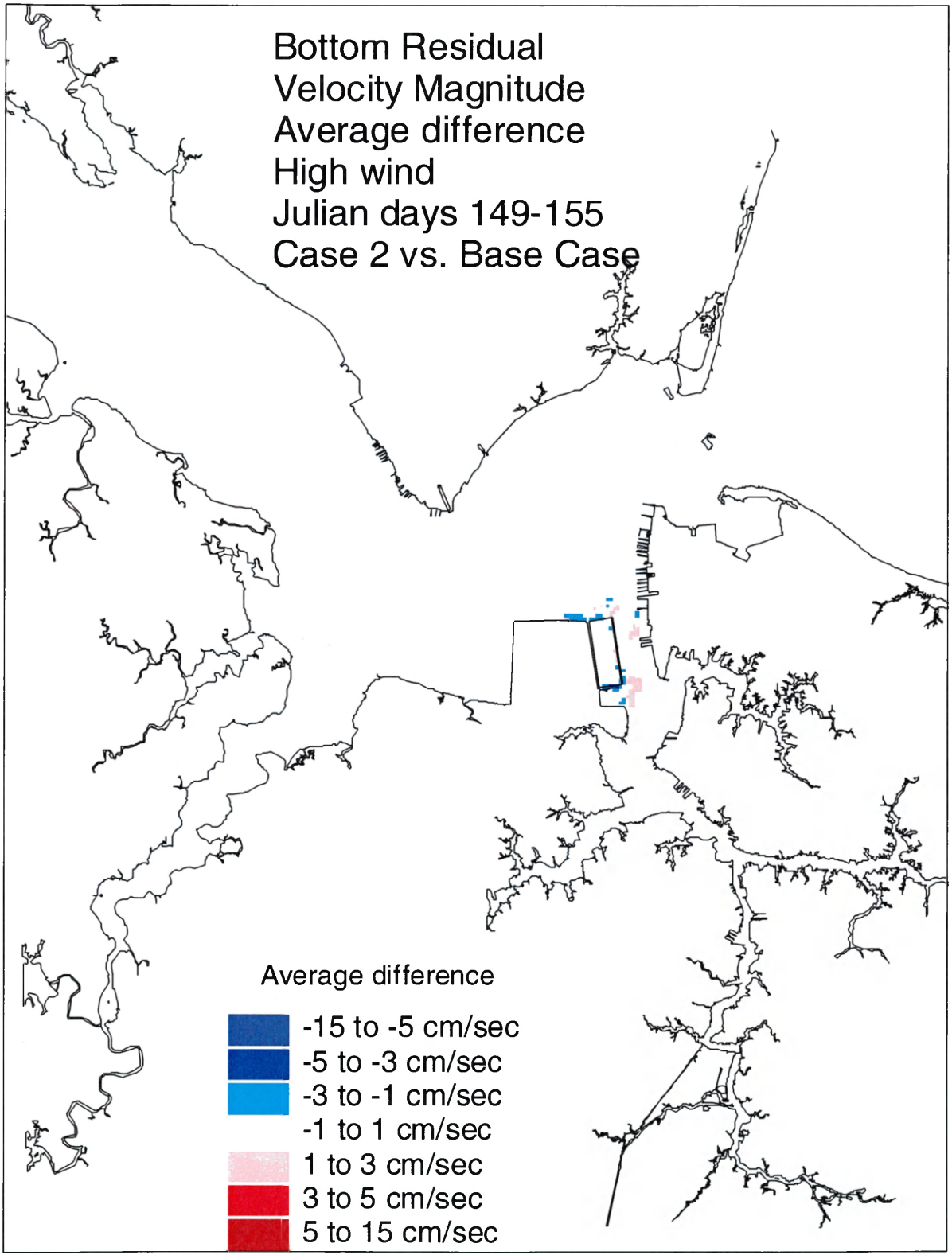

Figure 5-7. Historical simulation comparison (high wind) of the bottom residual velocity average difference for the Eastward Expansion (Option 7, 50-foot channel) versus the Base Case.

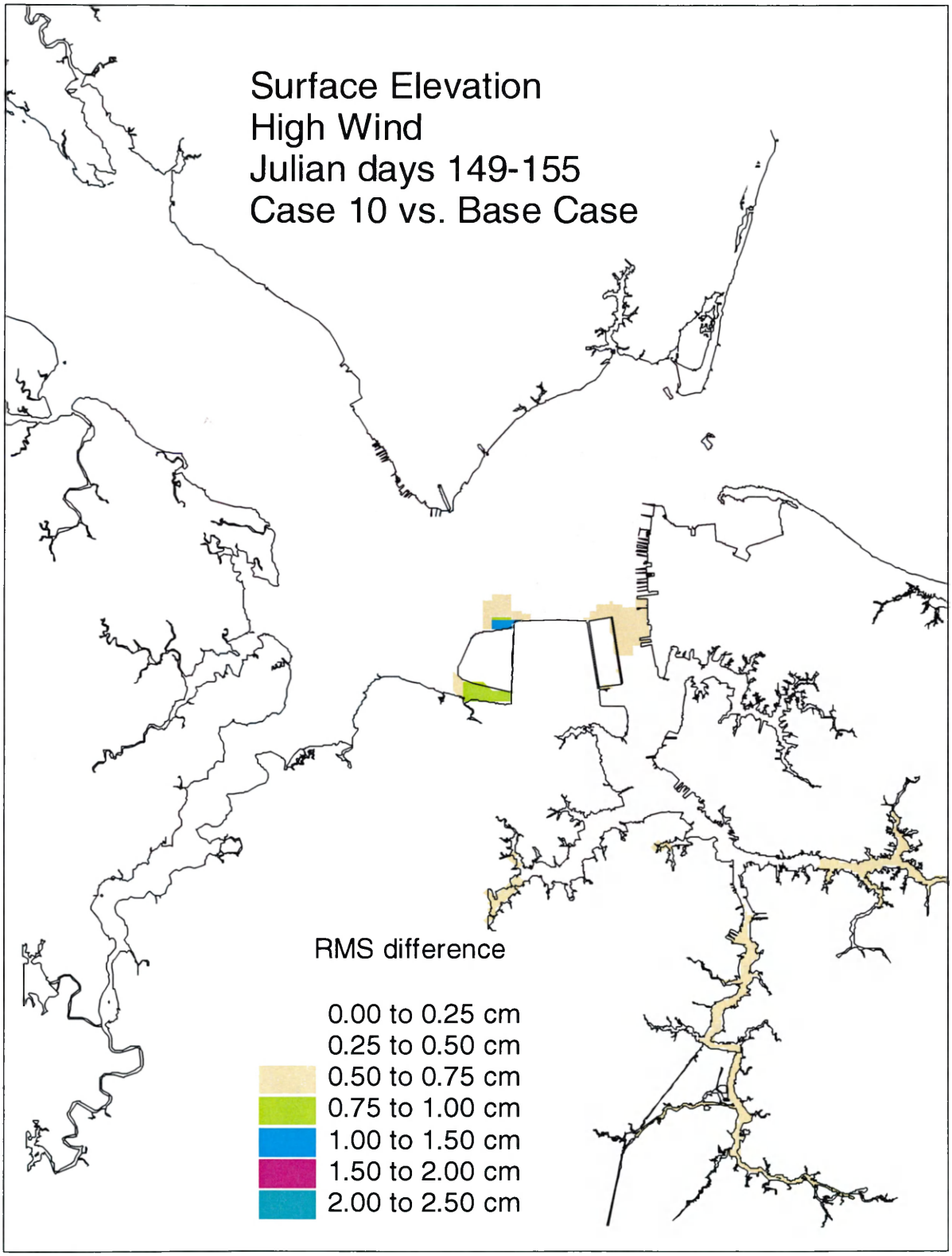

Figure 5-8. Historical simulation comparison (high wind) of the surface elevation RMS difference for the Eastward and Westward Expansion (Option 7/5a, 50-foot channel) versus the Base Case.

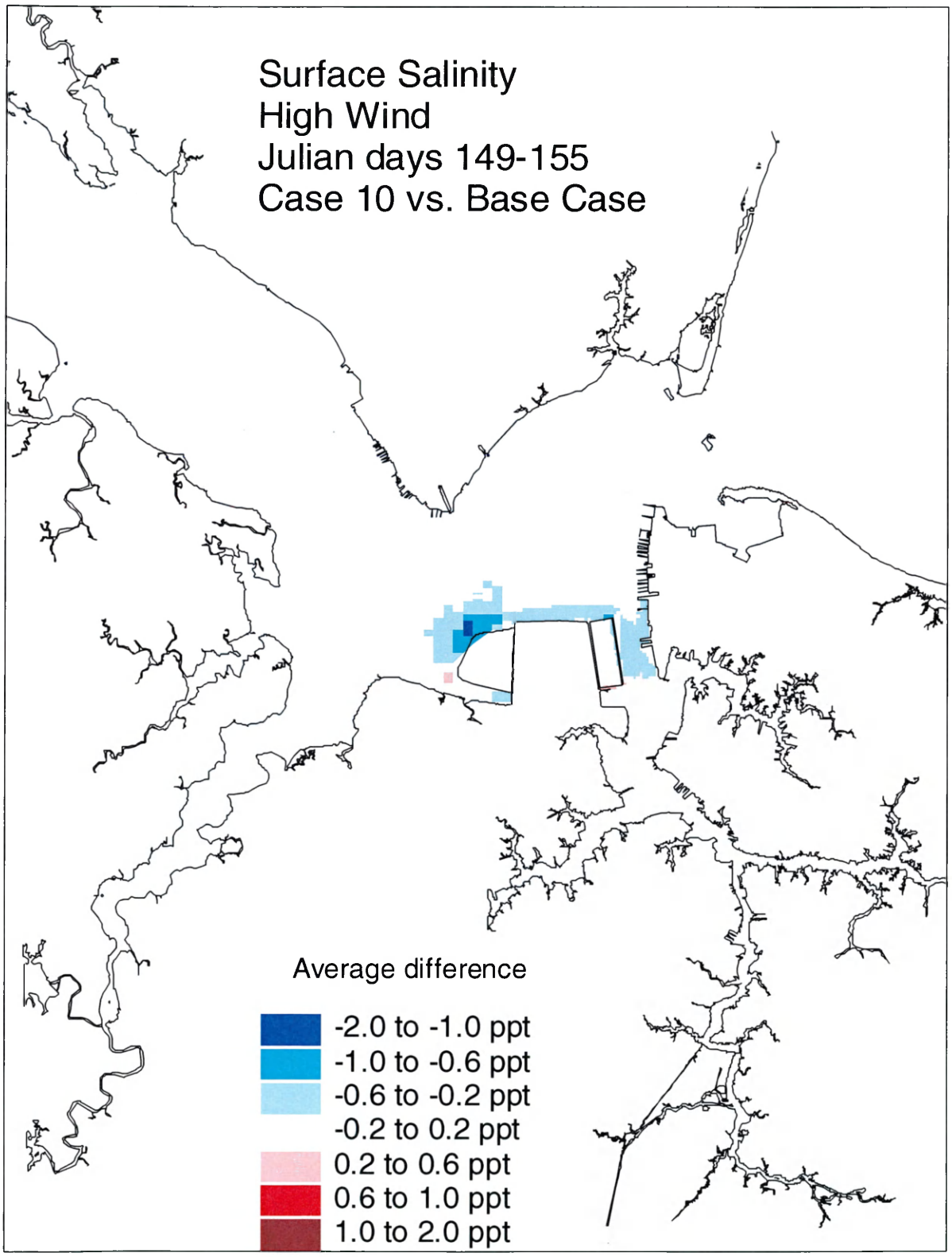

Figure 5-9. Historical simulation comparison (high wind) of the surface salinity average difference for the Eastward and Westward Expansion (Option 7/5a, 50-foot channel) versus the Base Case.

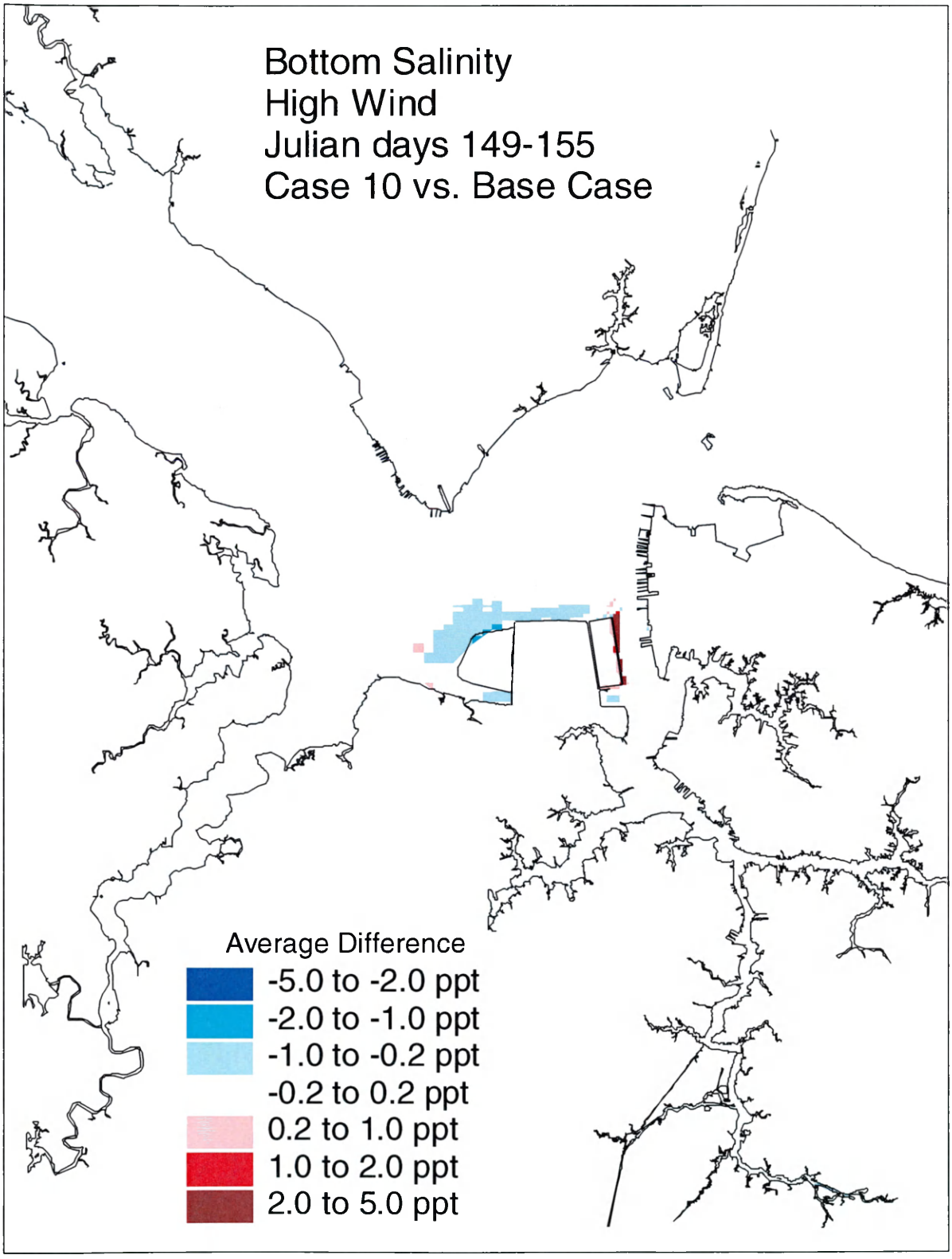

Figure 5-10. Historical simulation comparison (high wind) of the bottom salinity average difference for the Eastward and Westward Expansion (Option 7/5a, 50-foot channel) versus the Base Case.

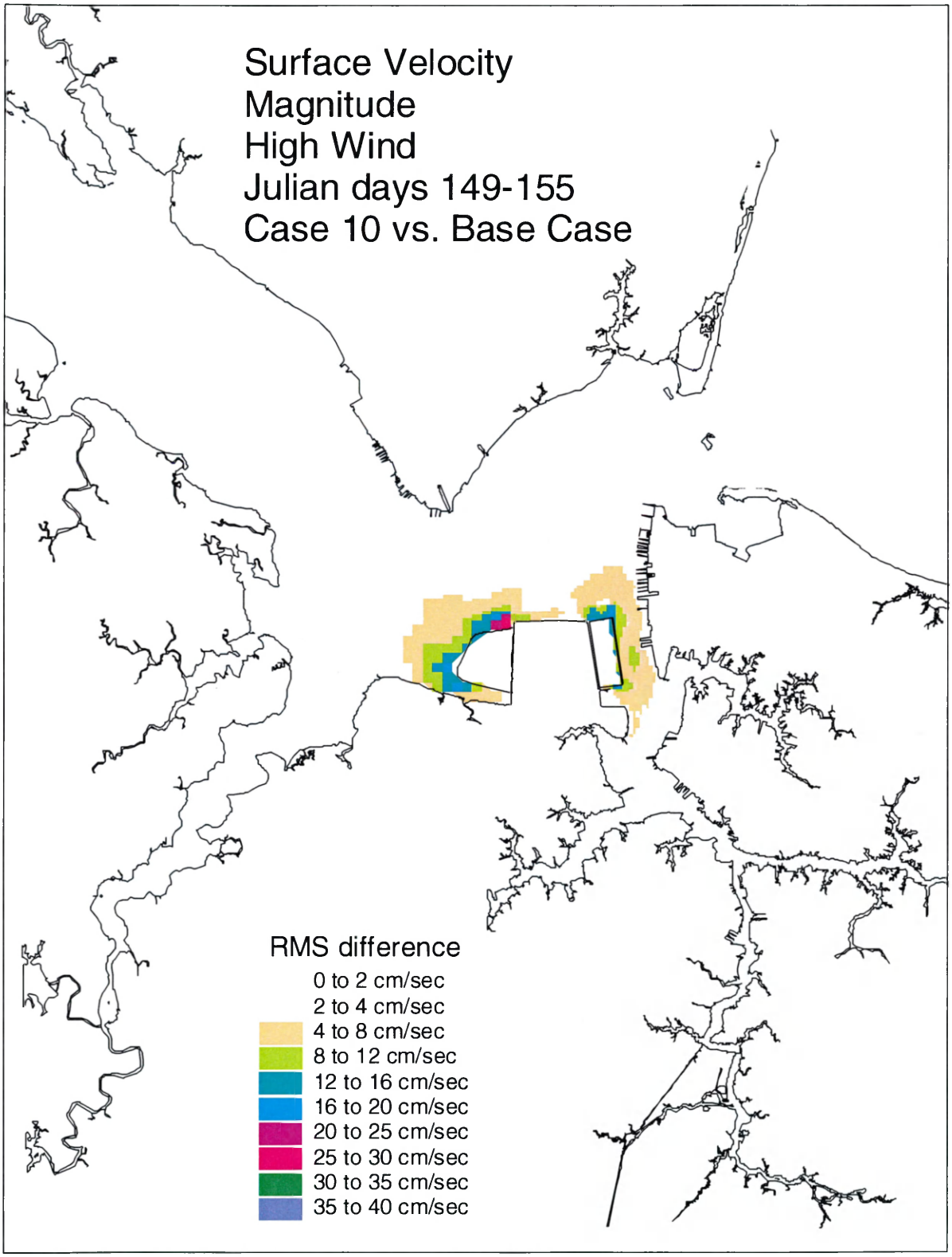

Figure 5-11. Historical simulation comparison (high wind) of the surface velocity RMS difference for the Eastward and Westward Expansion (Option 7/5a, 50-foot channel) versus the Base Case.

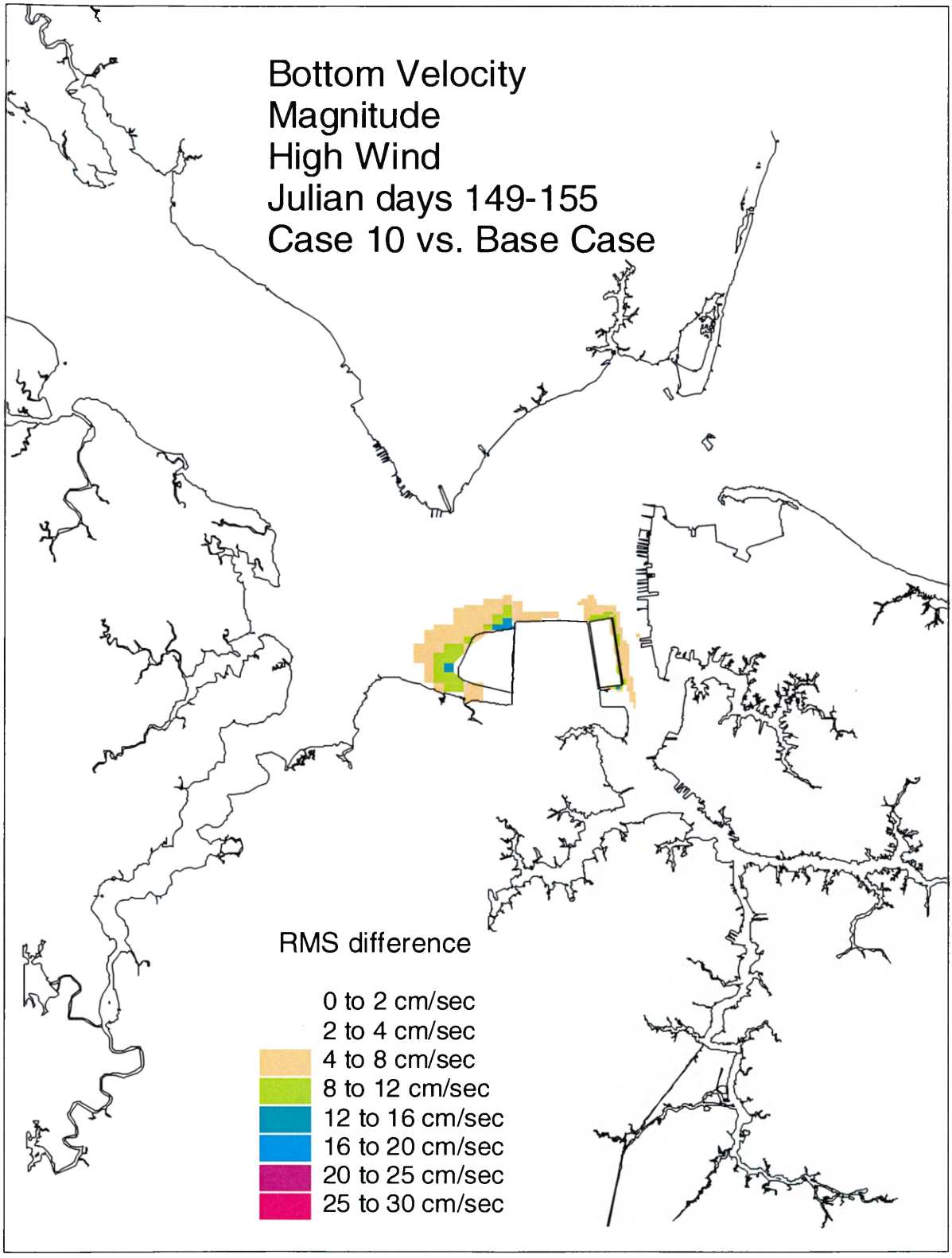

Figure 5-12. Historical simulation comparison (high wind) of the bottom velocity RMS difference for the Eastward and Westward Expansion (Option 7/5a, 50-foot channel) versus the Base Case.

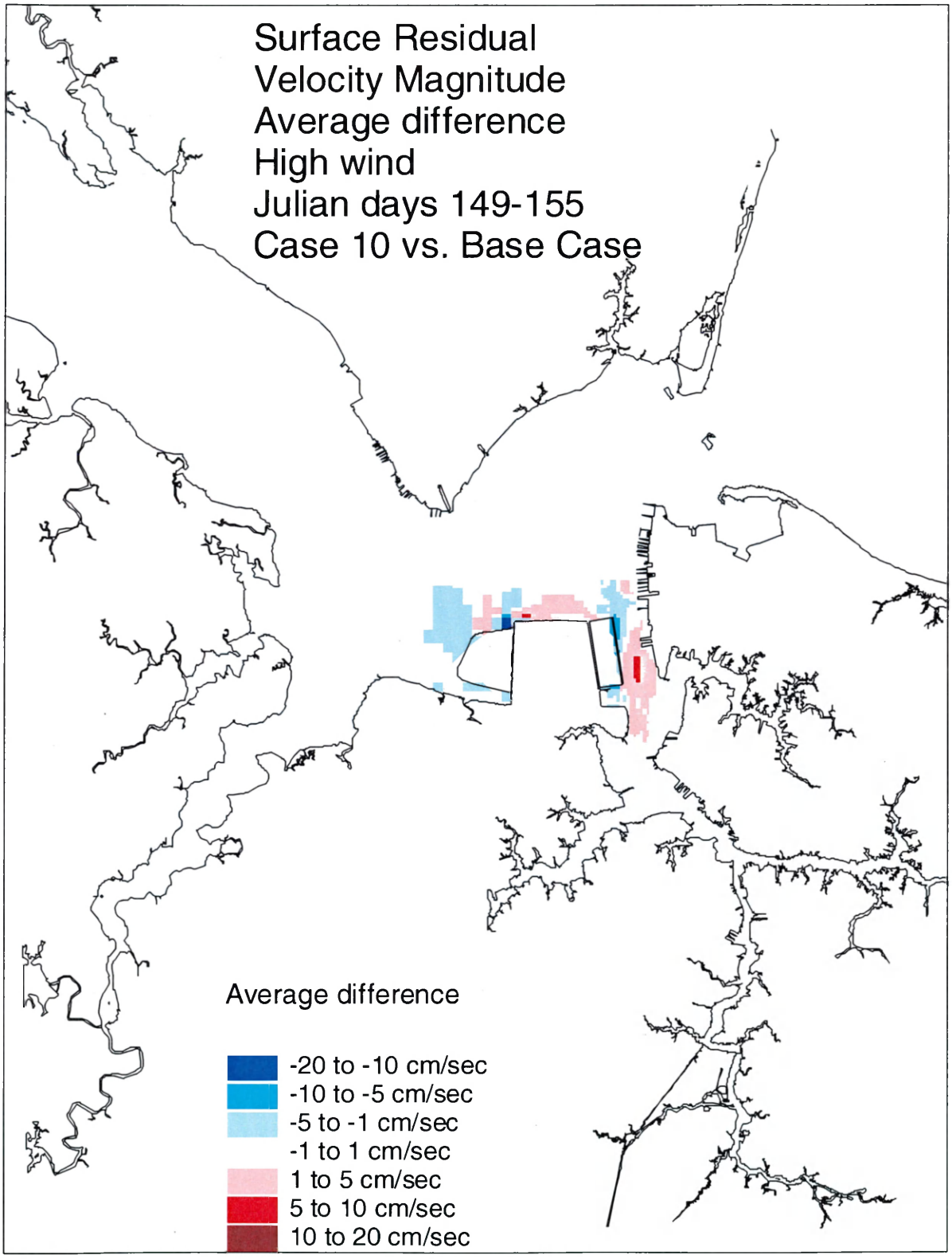

Figure 5-13. Historical simulation comparison (high wind) of the surface residual velocity average difference for the Eastward and Westward Expansion (Option 7/5a, 50-foot channel) versus the Base Case.

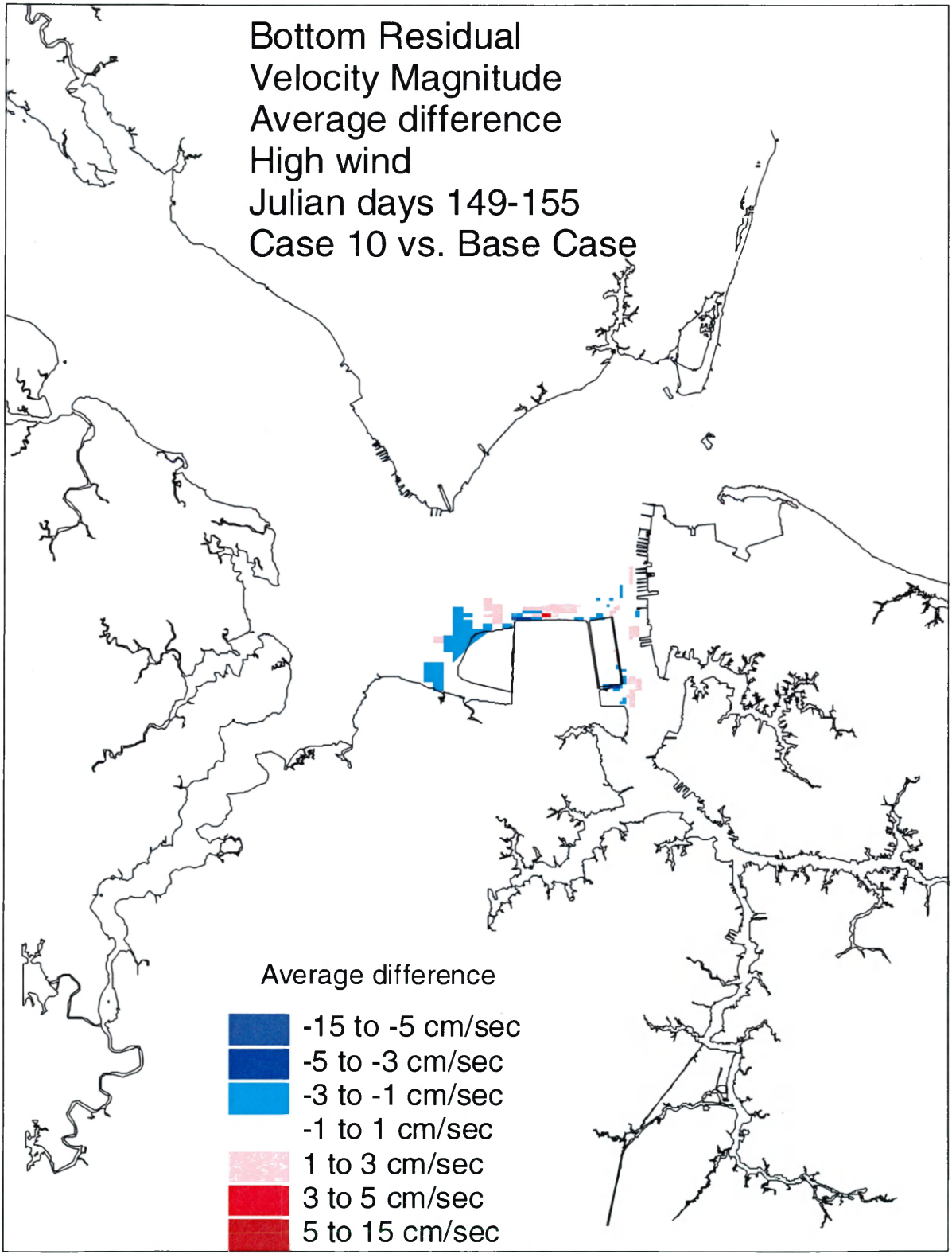

Figure 5-14. Historical simulation comparison (high wind) of the bottom residual velocity average difference for the Eastward and Westward Expansion (Option 7/5a, 50-foot channel) versus the Base Case.

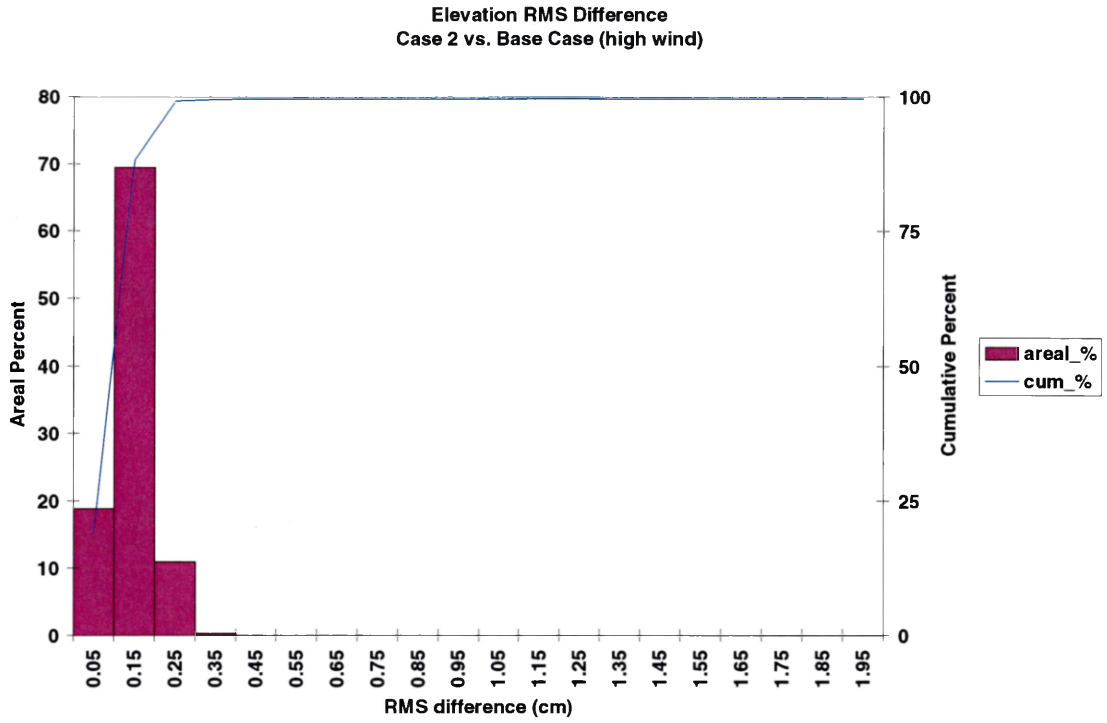

Figure 5-15. Frequency distribution of elevation RMS difference for the Eastward Expansion (Option 7, 50–foot channel) versus the Base Case during the high wind event of historical simulation.

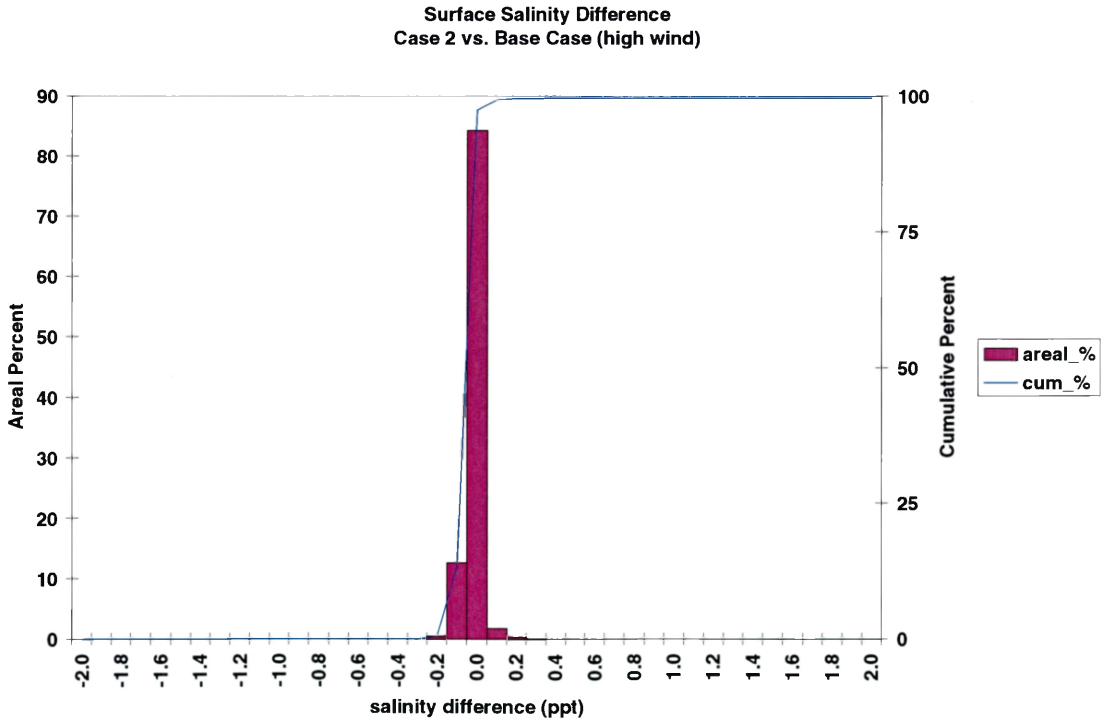

Figure 5-16. Frequency distribution of surface salinity average difference for the Eastward Expansion (Option 7, 50–foot channel) versus the Base Case during the high wind event of historical simulation.

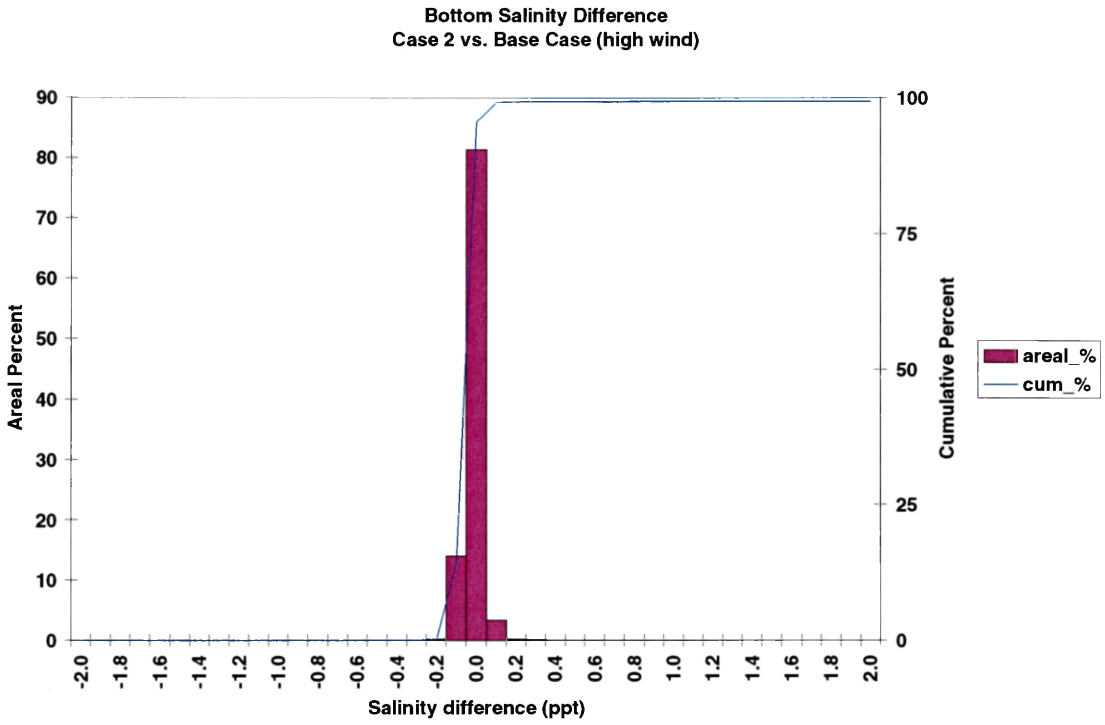

Figure 5-17. Frequency distribution of bottom salinity average difference for the Eastward Expansion (Option 7, 50–foot channel) versus the Base Case during the high wind event of historical simulation.

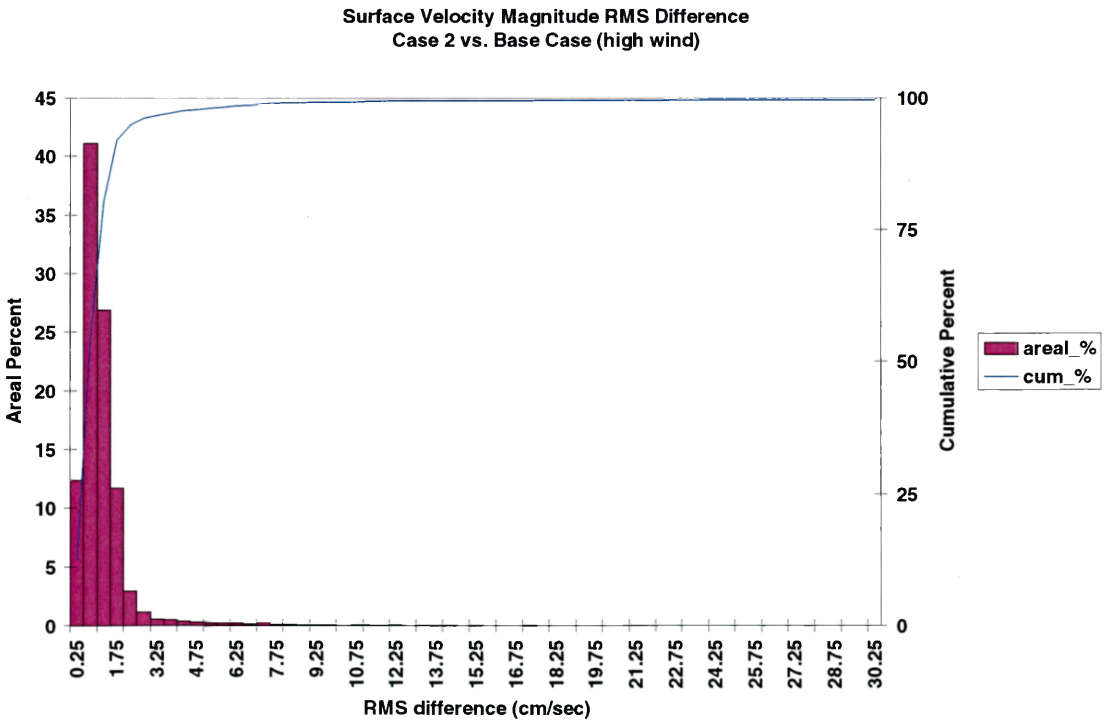

Figure 5-18. Frequency distribution of surface velocity RMS difference for the Eastward Expansion (Option 7, 50–foot channel) versus the Base Case during the high wind event of historical simulation.

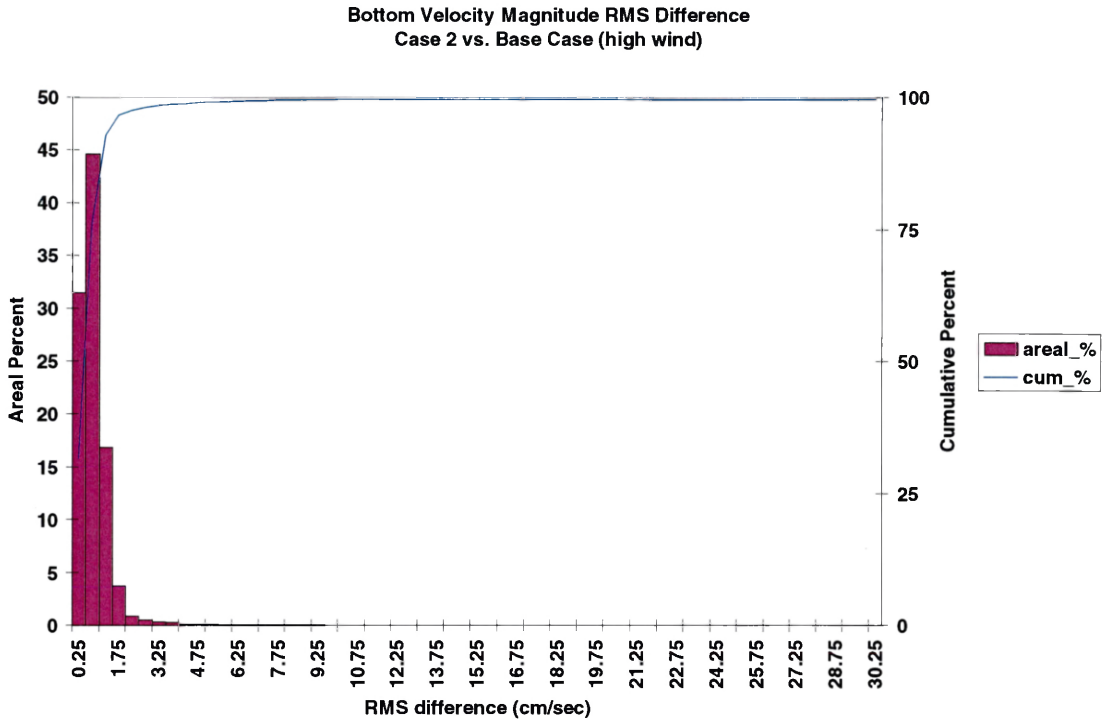

Figure 5-19. Frequency distribution of bottom velocity RMS difference for the Eastward Expansion (Option 7, 50–foot channel) versus the Base Case during the high wind event of historical simulation.

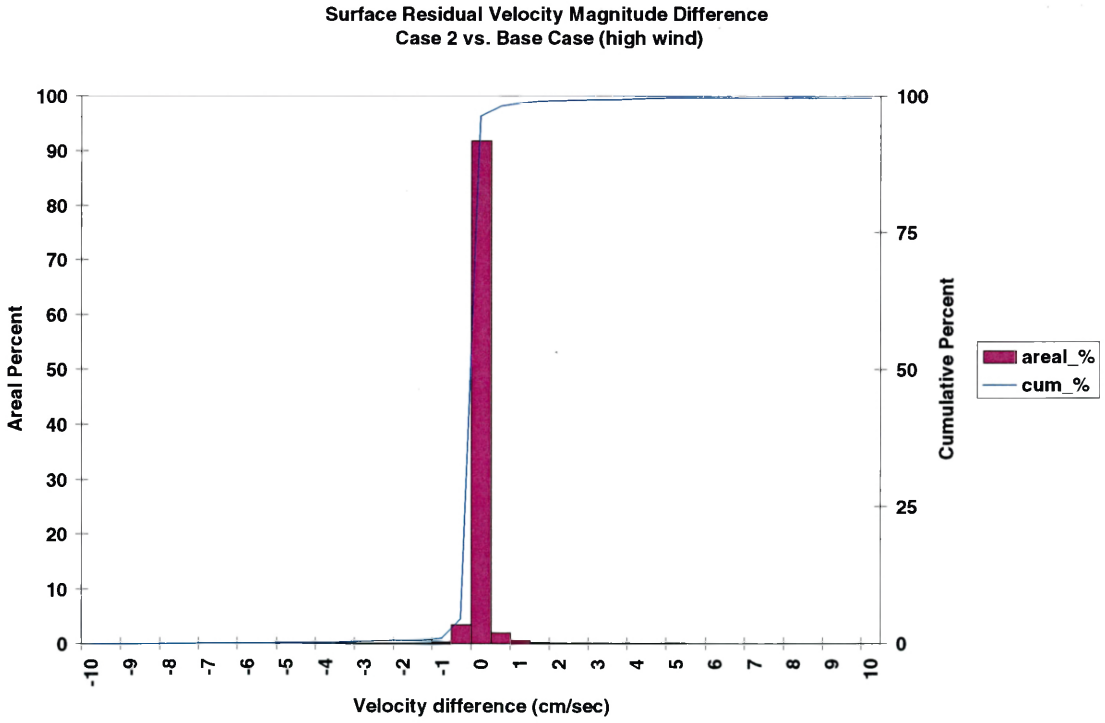

Figure 5-20. Frequency distribution of surface residual velocity magnitude average difference for the Eastward Expansion (Option 7, 50–foot channel) versus the Base Case during the high wind event of historical simulation.

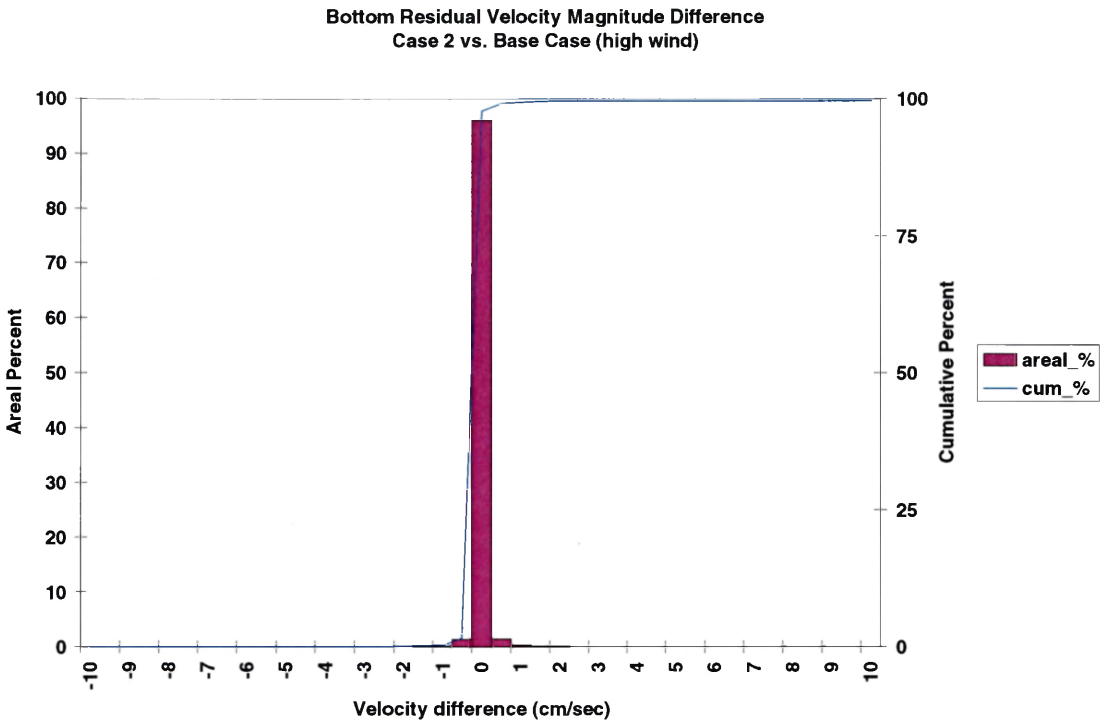

Figure 5-21. Frequency distribution of bottom residual velocity magnitude average difference for the Eastward Expansion (Option 7, 50–foot channel) versus the Base Case during the high wind event of historical simulation.

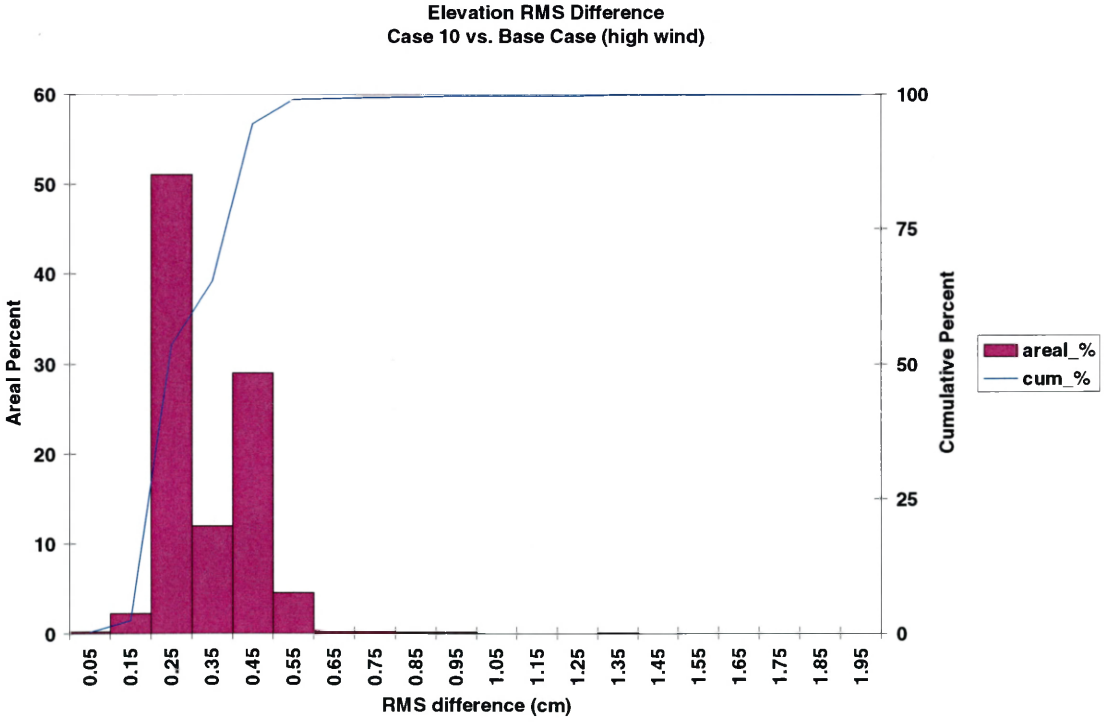

Figure 5-22. Frequency distribution of elevation RMS difference for the Eastward and Westward Expansion (Option 7/5a, 50–foot channel) versus the Base Case during the high wind event of historical simulation.

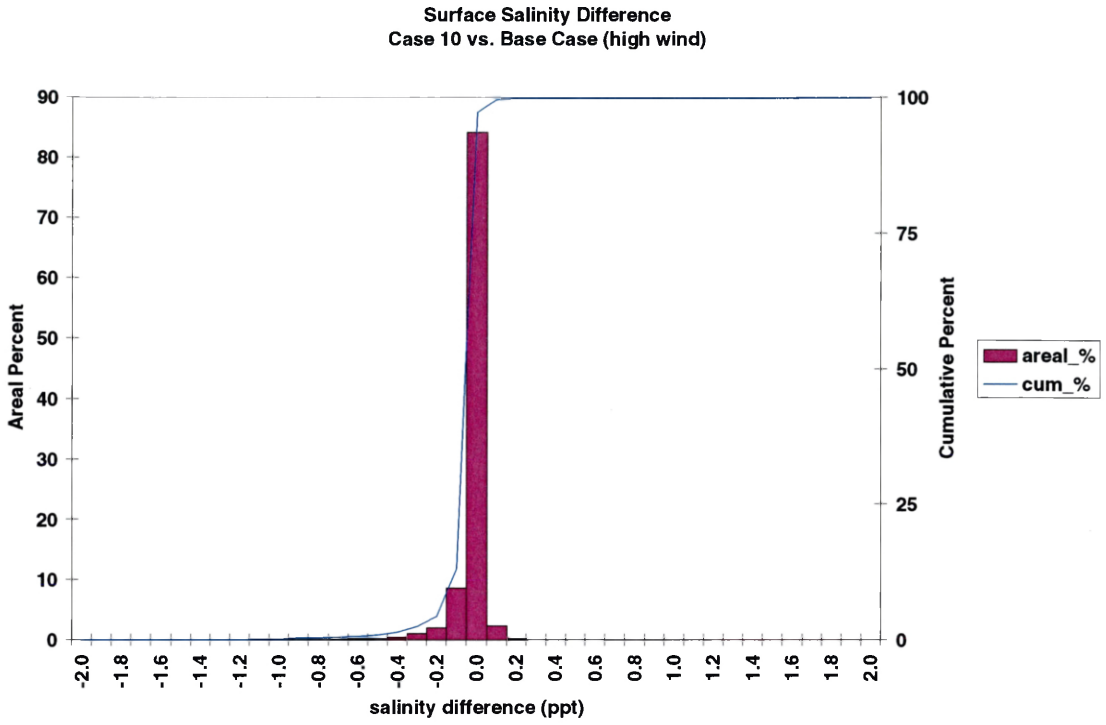

Figure 5-23. Frequency distribution of surface salinity average difference for the Eastward and Westward Expansion (Option 7/5a, 50–foot channel) versus the Base Case during the high wind event of historical simulation.

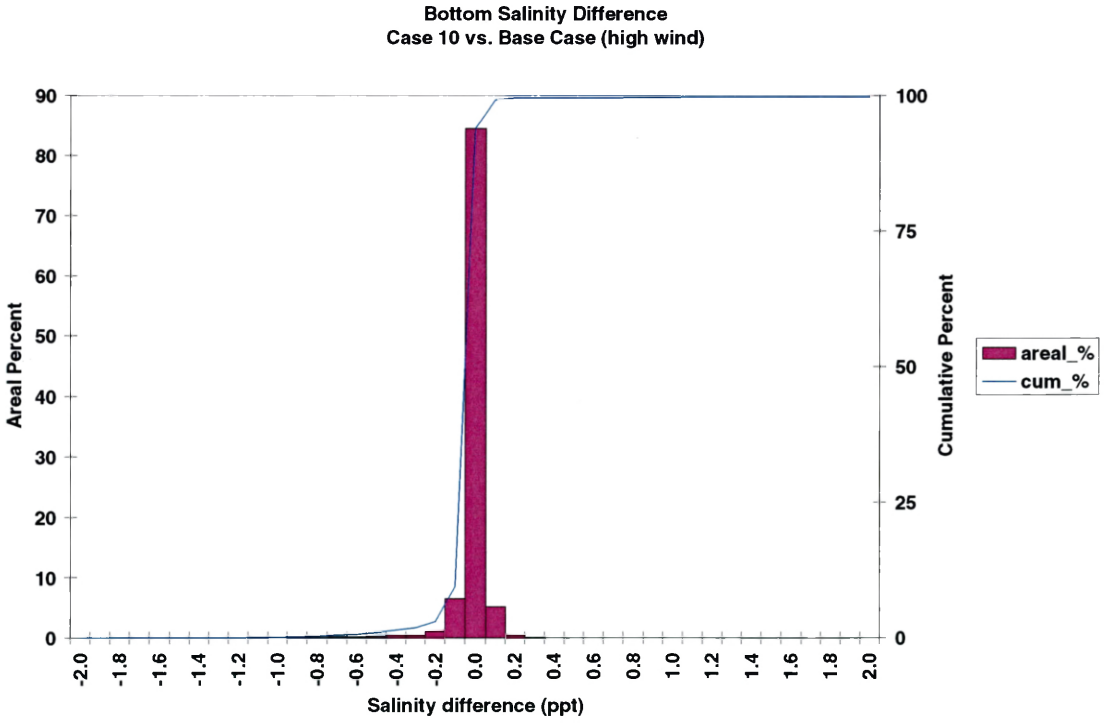

Figure 5-24. Frequency distribution of bottom salinity average difference for the Eastward and Westward Expansion (Option 7/5a, 50–foot channel) versus the Base Case during the high wind event of historical simulation.

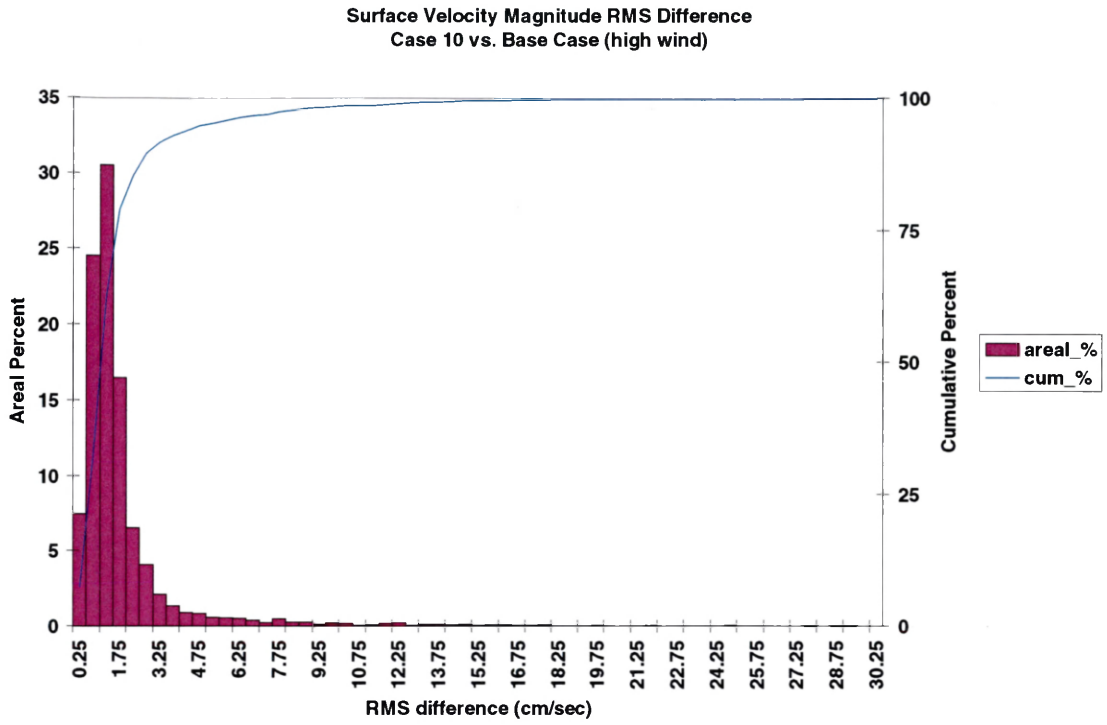

Figure 5-25. Frequency distribution of surface velocity RMS difference for the Eastward and Westward Expansion (Option 7/5a, 50–foot channel) versus the Base Case during the high wind event of historical simulation.

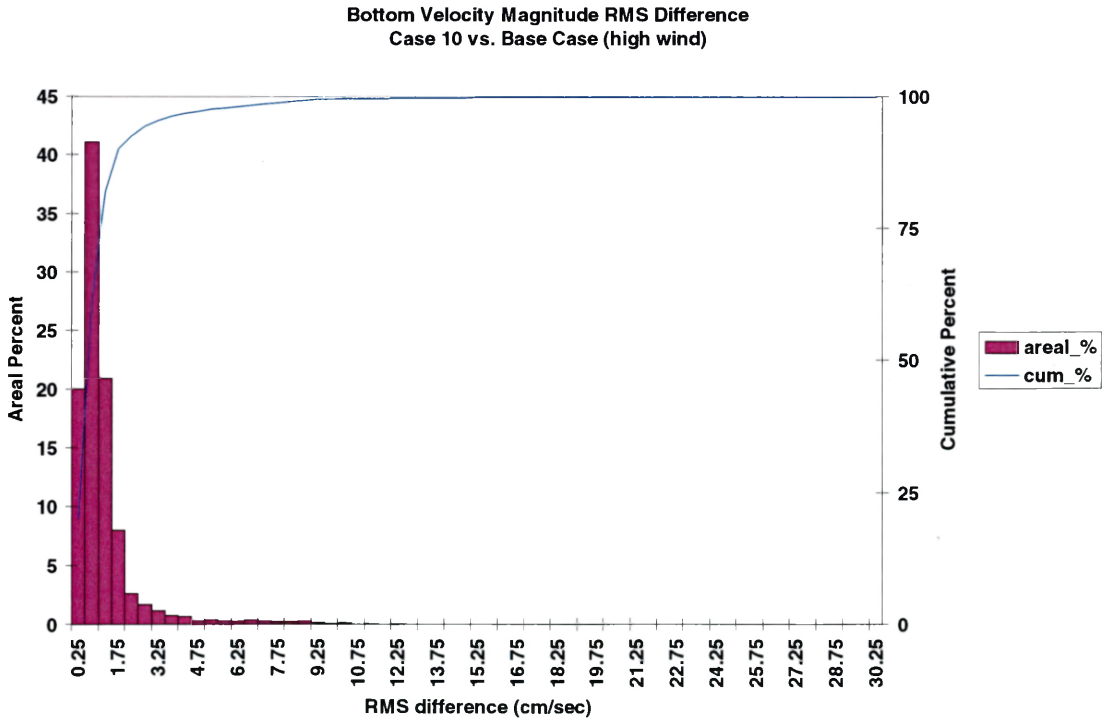

Figure 5-26. Frequency distribution of bottom velocity RMS difference for the Eastward and Westward Expansion (Option 7/5a, 50–foot channel) versus the Base Case during the high wind event of historical simulation.

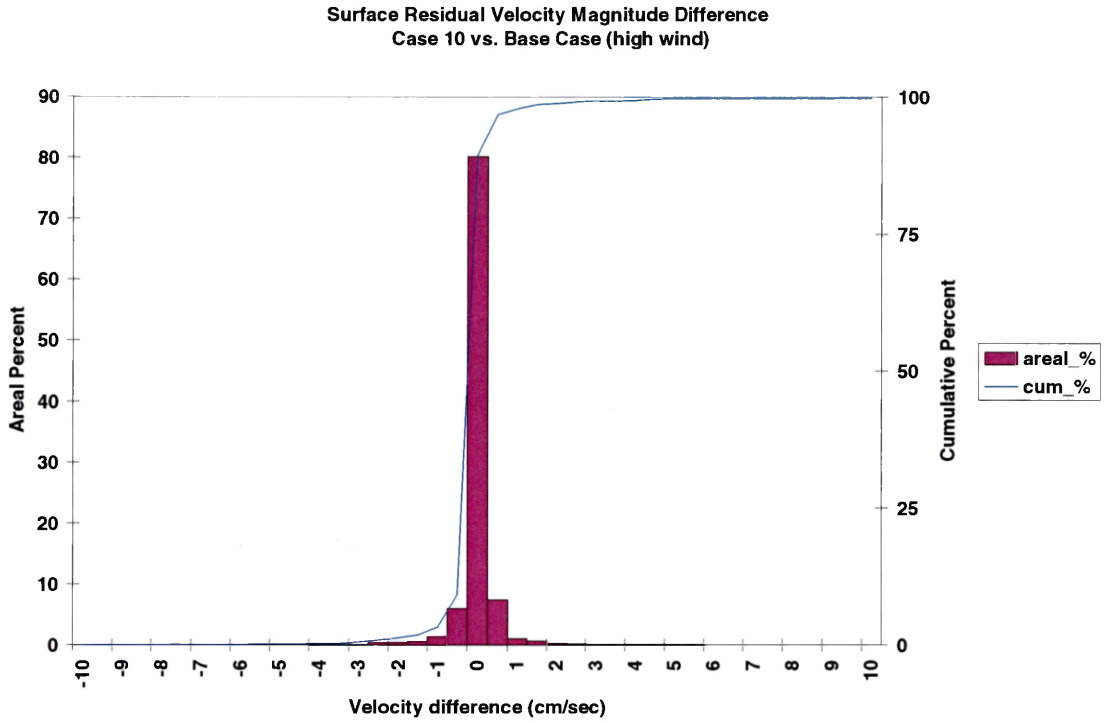

Figure 5-27. Frequency distribution of surface residual velocity magnitude average difference for the Eastward and Westward Expansion (Option 7/5a, 50–foot channel) versus the Base Case during the high wind event of historical simulation.

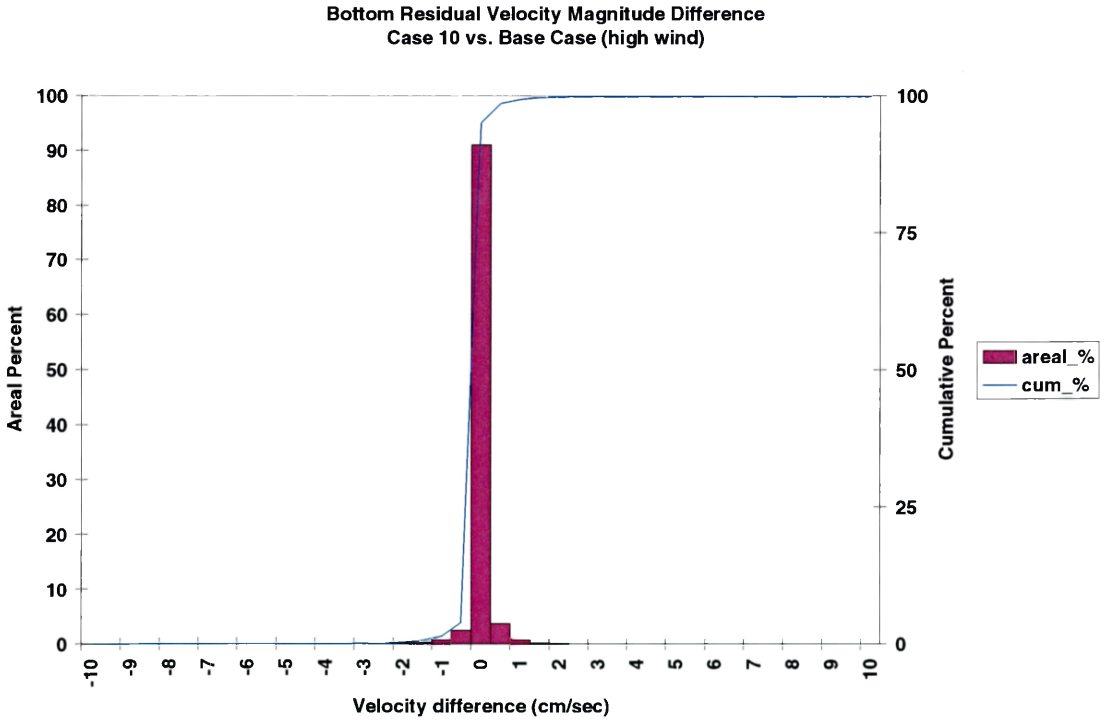

Figure 5-28. Frequency distribution bottom residual velocity magnitude average difference for the Eastward and Westward Expansion (Option 7/5a, 50–foot channel) versus the Base Case during the high wind event of historical simulation.

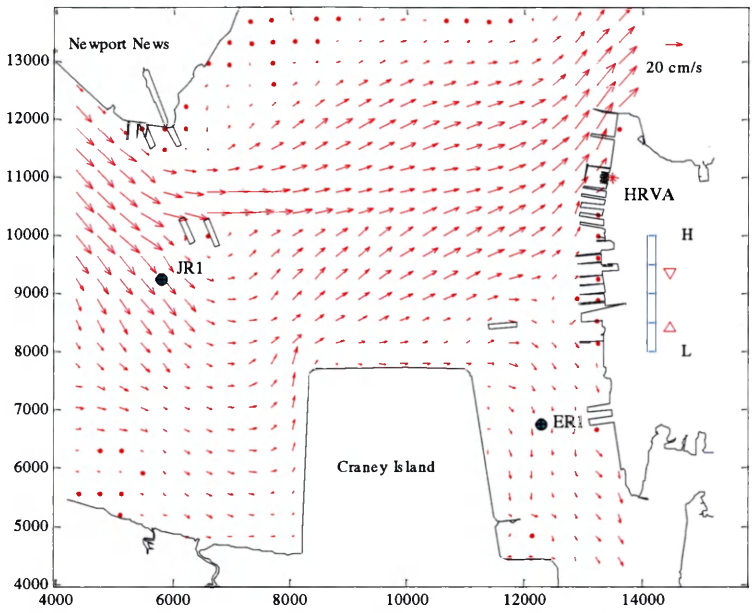

Figure 5-29. Residual surface current in Hampton Roads, April 20, 2000 (Julian Day 111). Plan view showing location of time series stations JR1 and ER1.

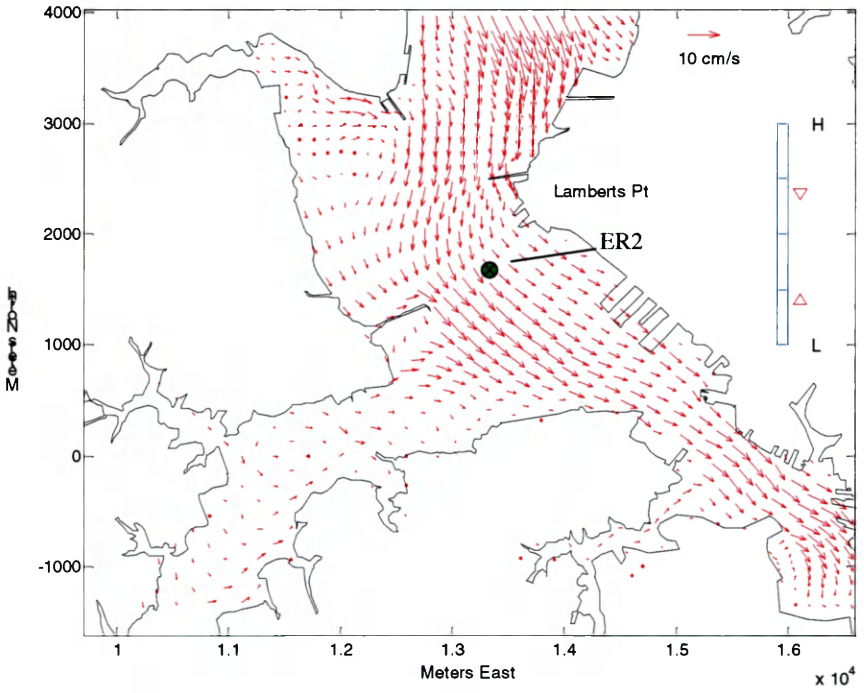

Figure 5-30. Residual surface current, Elizabeth River, April 20, 2000 (Julian day 111). Plan view showing location of time series station ER2.

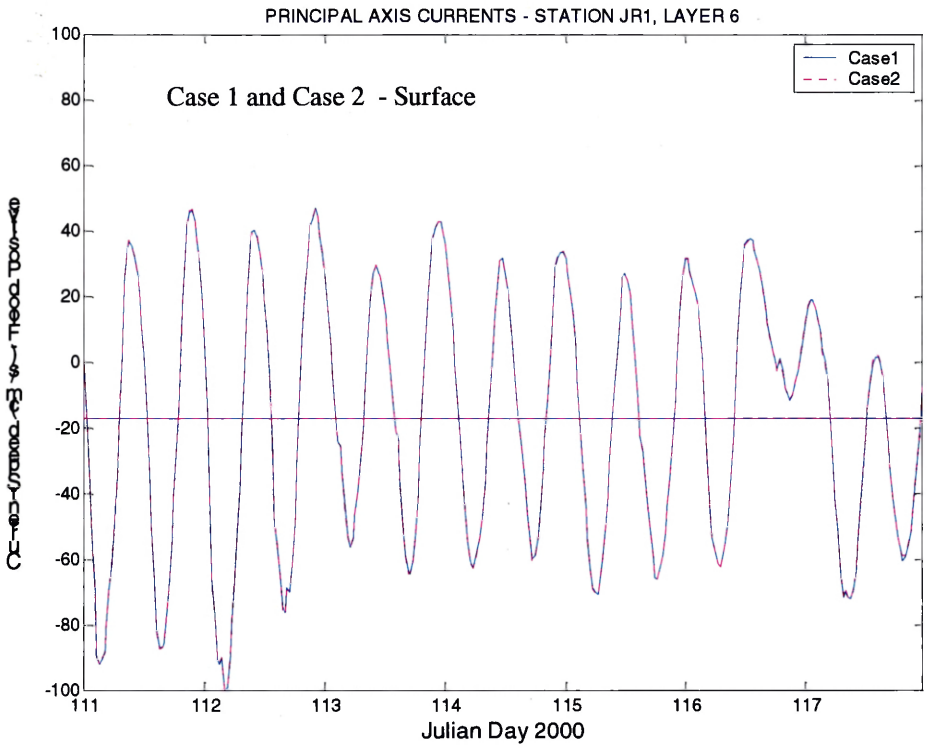

Figure 5-31. Principal axis current at Station JR1; Case 1 and Case 2 (surface layer).

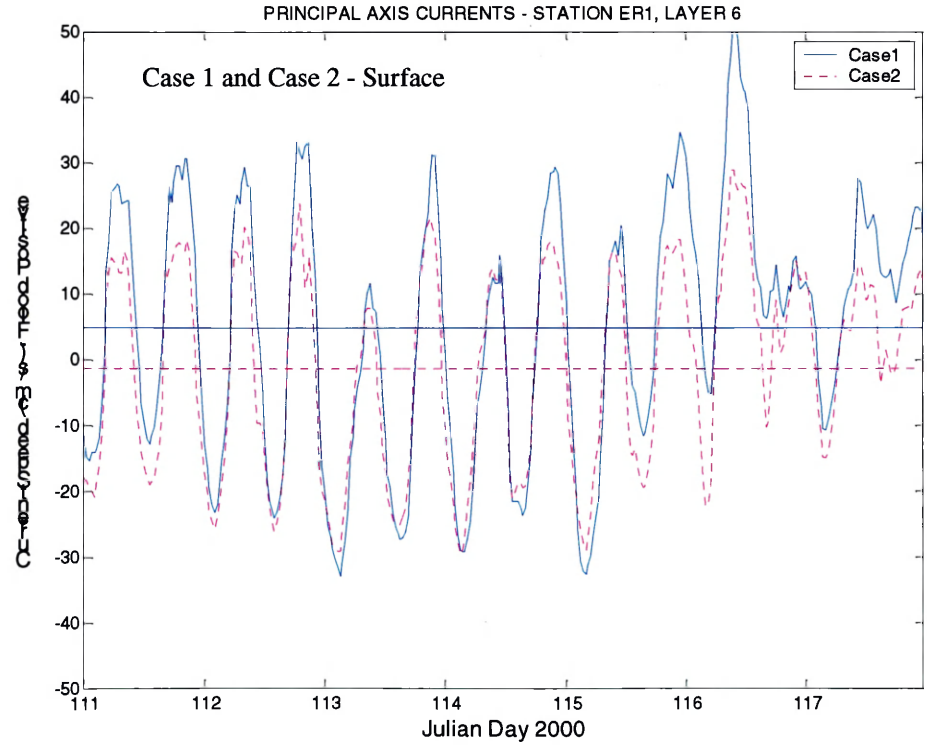

Figure 5-32. Principal axis currents at Station ER1; Case 1 and Case 2 (surface layer).

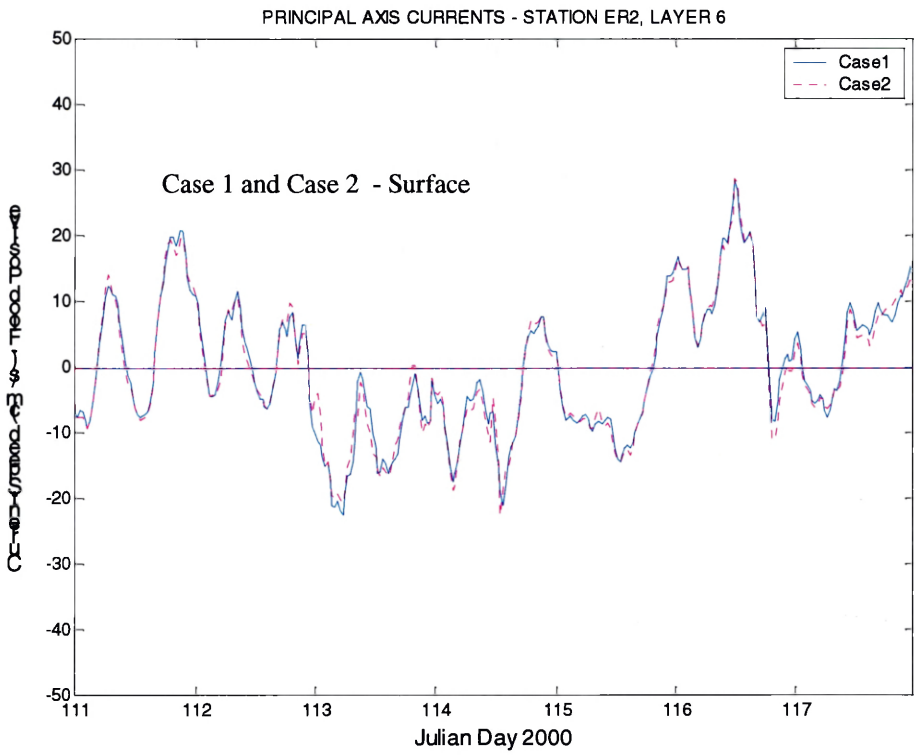

Figure 5-33. Principal axis currents at Station ER2; Case 1 and Case 2 (surface layer).

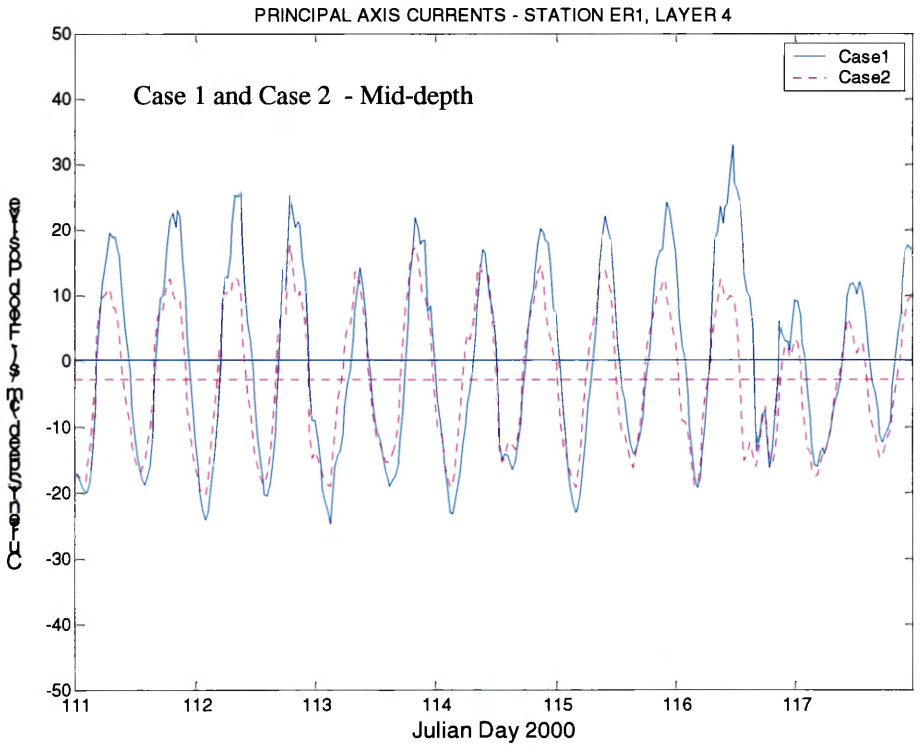

Figure 5-34. Principal axis currents at Station ER1; Case 1 and Case 2 (middle layer).

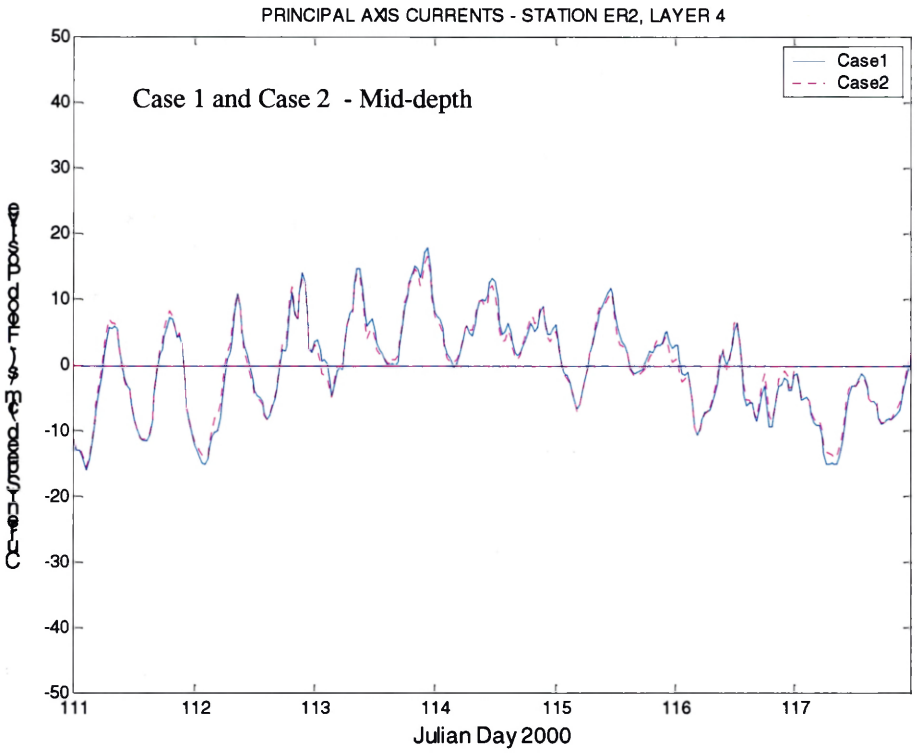

Figure 5-35. Principal axis currents at Station ER2; Case 1 and Case 2 (middle layer).

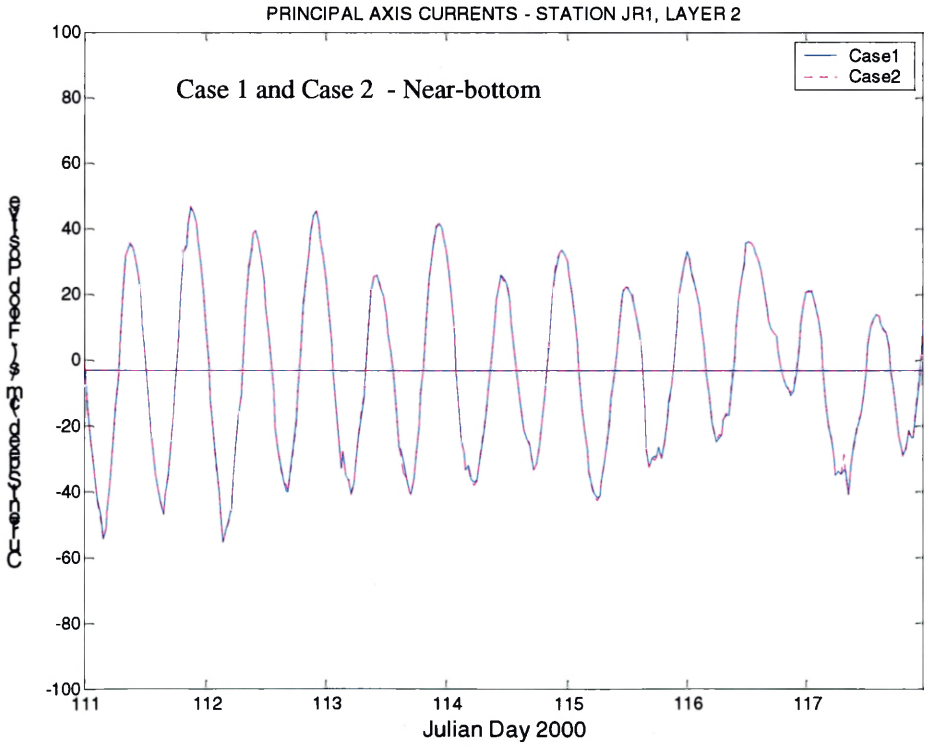

Figure 5-36. Principal axis currents at Station JR1; Case 1 and Case 2 (near bottom).

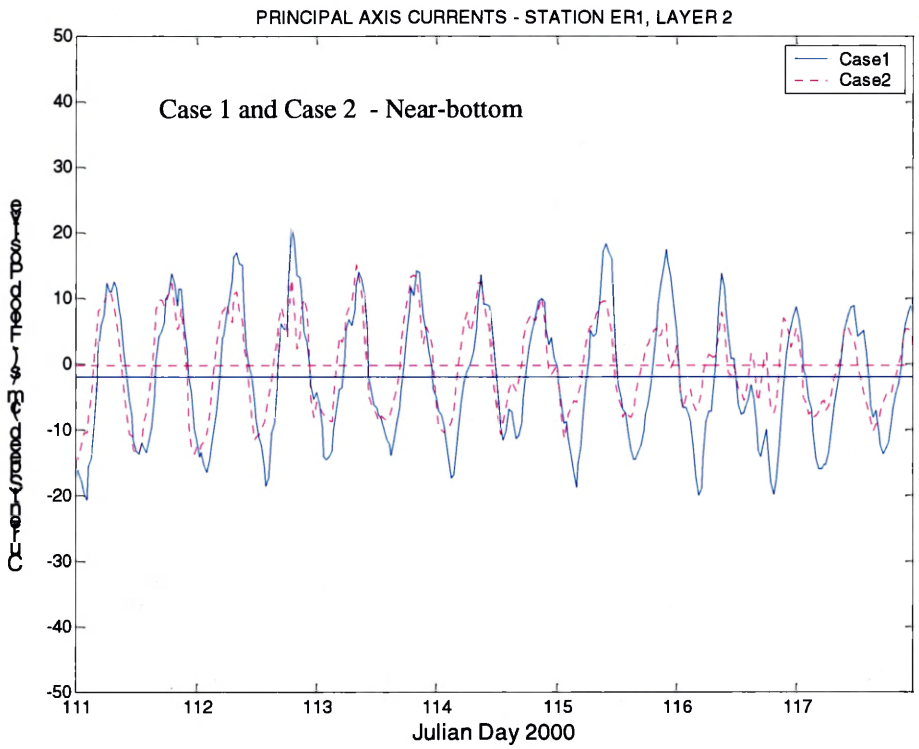

Figure 5-37. Principal axis currents at Station ER1; Case 1 and Case 2 (near bottom).

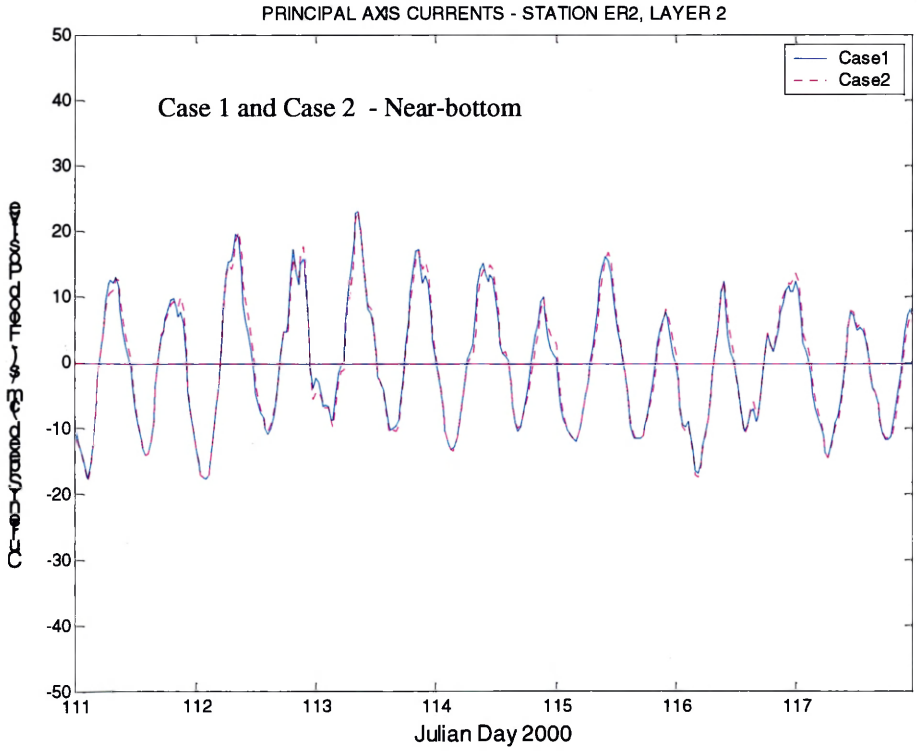

Figure 5-38. Principal axis currents at Station ER2; Case 1 and Case 2 (near bottom).

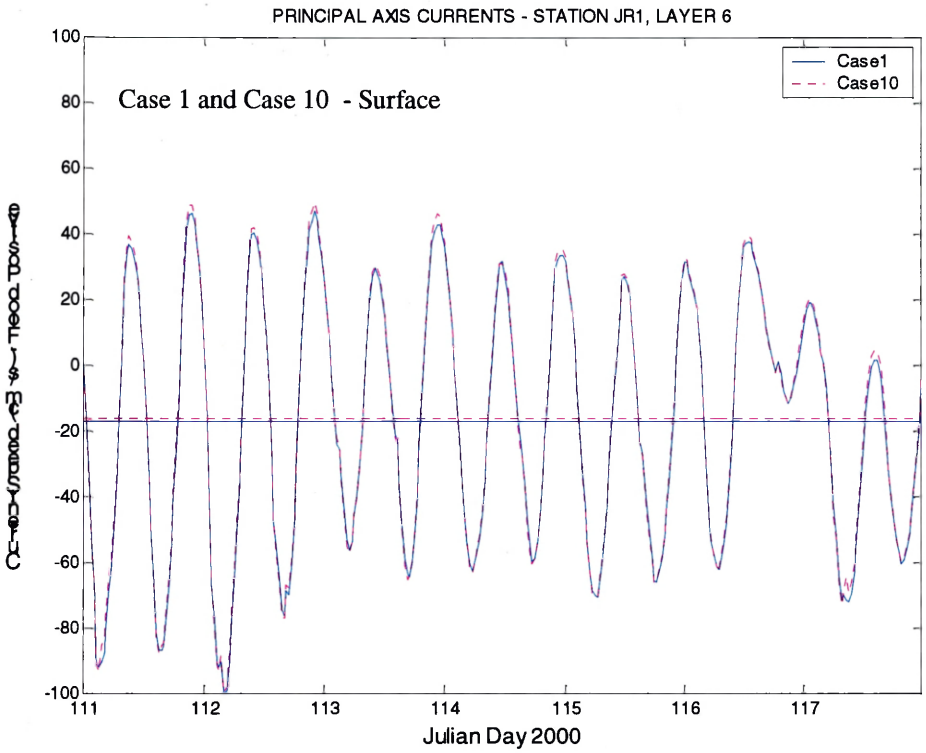

Figure 5-39. Principal axis currents at Station JR1; Case 1 and Case 10 (surface layer).

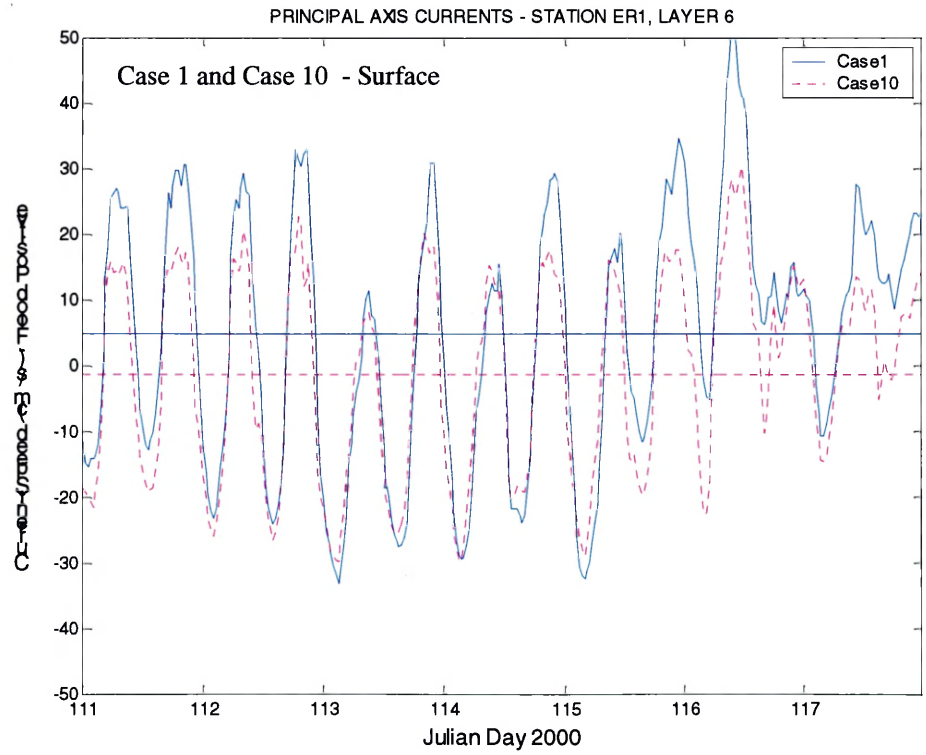

Figure 5-40. Principal axis currents at Station ER1; Case 1 and Case 10 (surface layer).

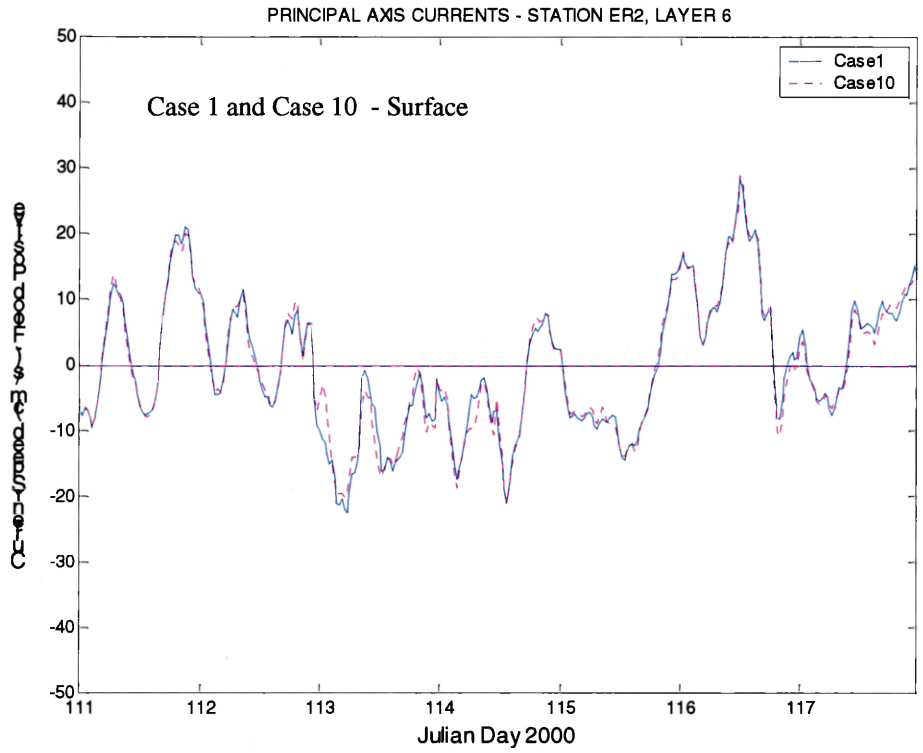

Figure 5-41. Principal axis currents at Station ER2; Case 1 and Case 10 (surface layer).

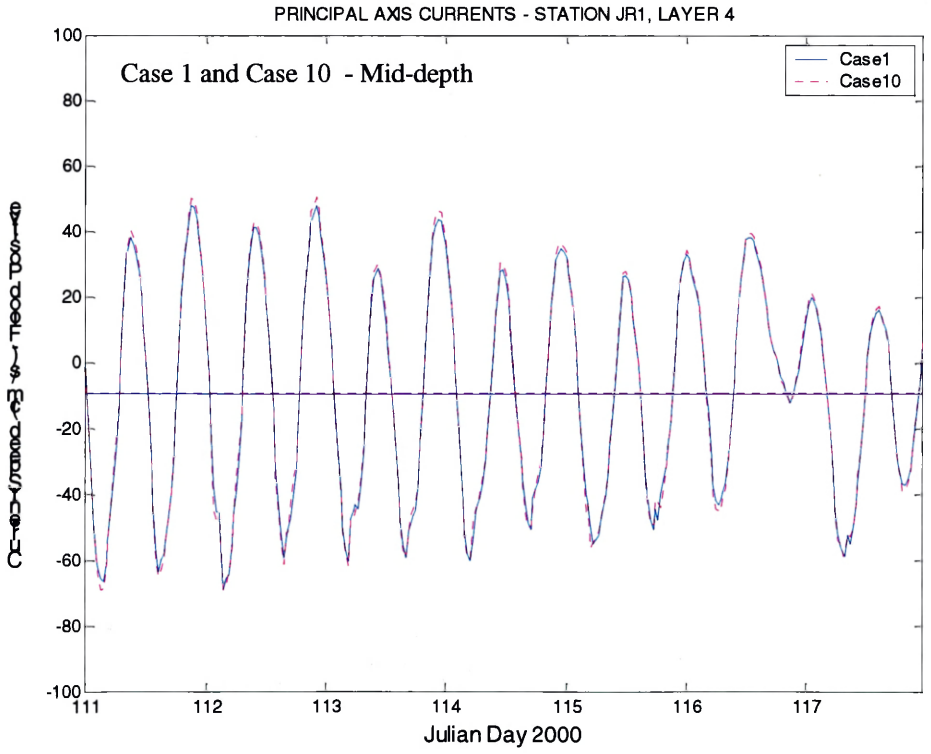

Figure 5-42. Principal axis currents at Station JR1; Case 1 and Case 10 (middle layer).

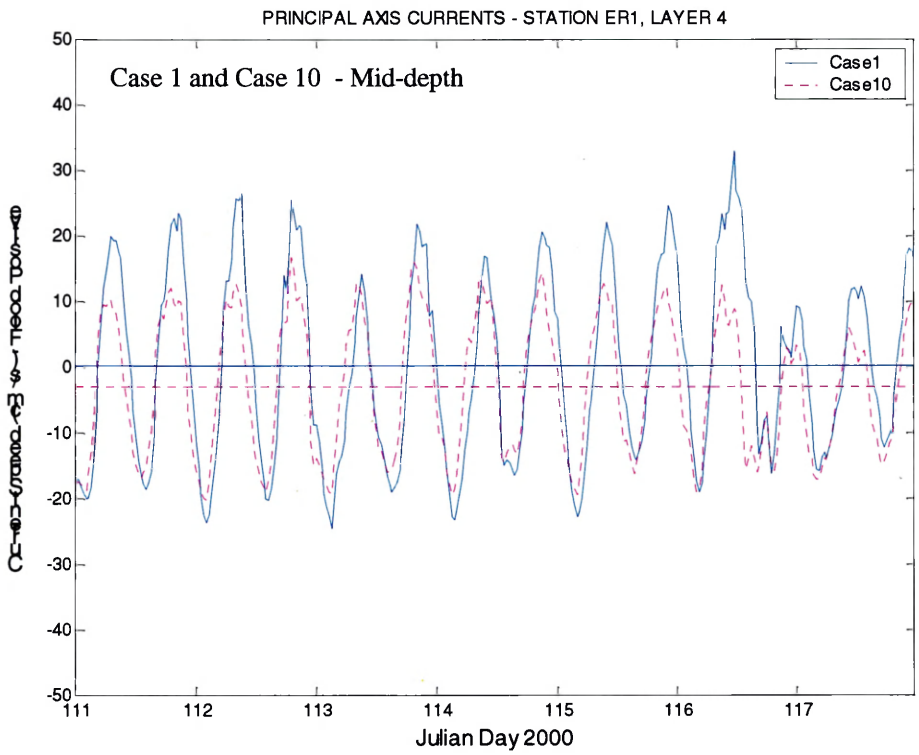

Figure 5-43. Principal axis currents at Station ER1; Case 1 and Case 10 (middle layer).

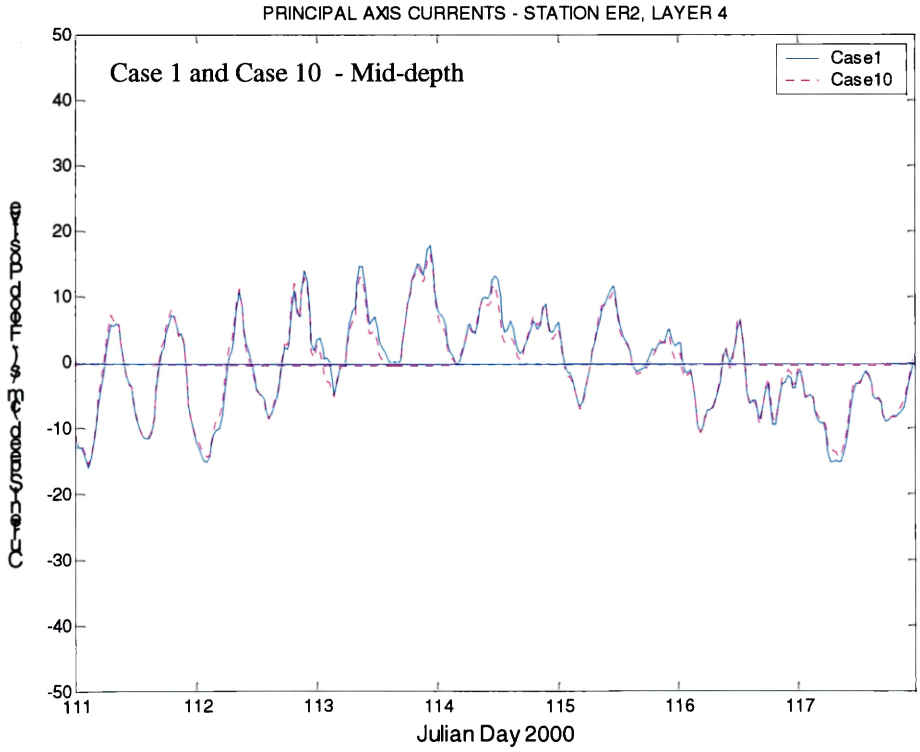

Figure 5-44. Principal axis currents at Station ER2; Case 1 and Case 10 (middle layer).

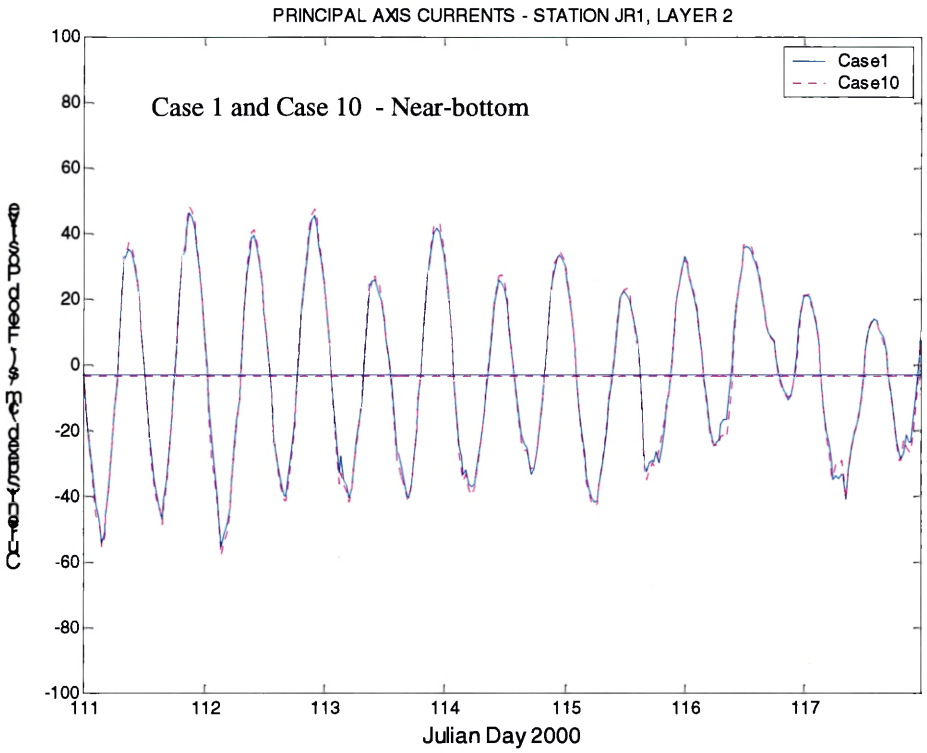

Figure 5-45. Principal axis currents at Station JR1; Case 1 and Case 10 (near bottom).

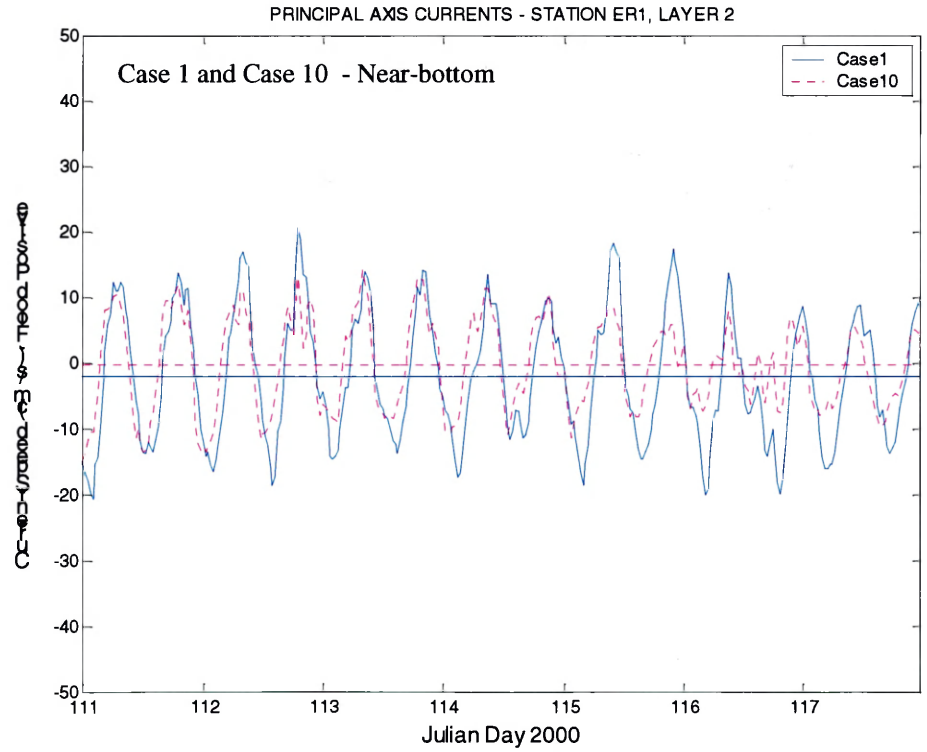

Figure 5-46. Principal axis currents at Station ER1; Case 1 and Case 10 (near bottom).

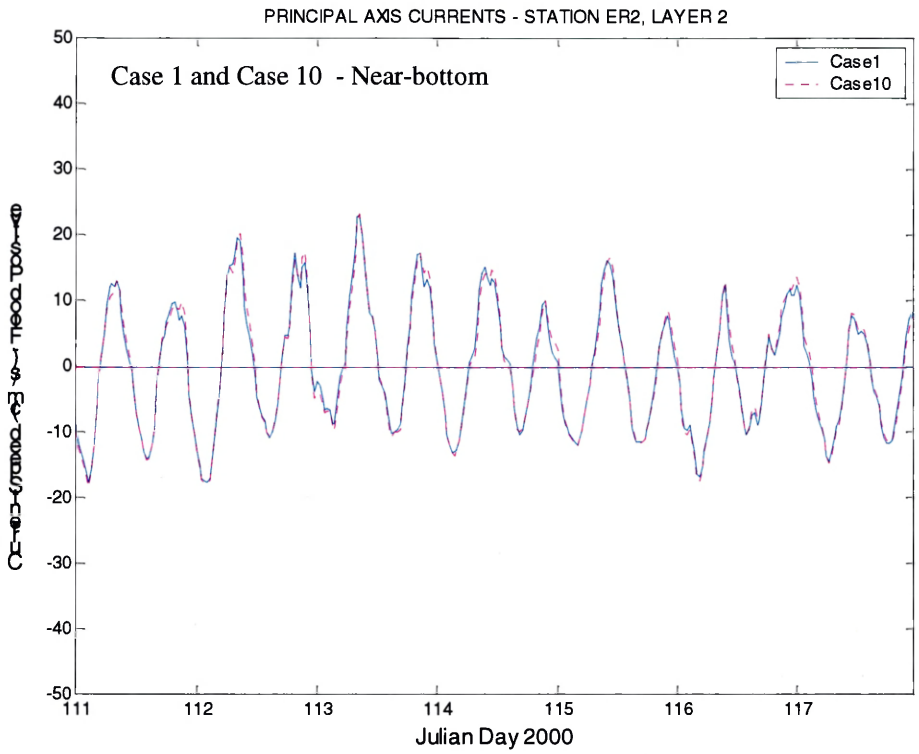

Figure 5-47. Principal axis currents at Station ER2; Case 1 and Case 10 (near bottom).

Chapter 6

Discussion and Conclusions

It has been demonstrated that wind forcing is an important mechanism in determining the water level changes, salinity distribution and current pattern in the lower James and Elizabeth River system.

Wind can raise or lower the level of surface waters and occasionally reverse the direction of flow. Longitudinal wind over a stratified water column accelerates surface water through frictional coupling. This longitudinal transport generates a sea surface slope, which in turn will accelerate bottom water in the opposite direction. A downstream wind (i.e., northwesterly/ southwesterly wind) blows surface water out of the lower James River, causing a reduction in the mean water level and setting up a surface slope from head to mouth. These were accompanied by a strengthened return flow at mid-depth and near the bottom. In contrast, an upstream wind (i.e., northeasterly/southeasterly wind) could increase the water level in the lower James and Elizabeth and reverse the direction of estuarine circulation.

Winds axial to the lower James estuarine system have the strongest effects on physical characteristics (i.e., water level, salinity distribution, and current). A downstream wind will enhance estuarine circulation, and strengthen stratification in the water column; Conversely, an upstream wind might be able to reverse the

classical estuarine circulation. For example, in the lower James, since its orientation is in the east-west direction, winds from the east, blowing upstream, drive saltier water from outside into this lower James in the upper water column. To compensate, bottom water will flow to the outside, which results in a reversed circulation pattern. While a downstream wind blows, it will drive more freshwater out of the lower James, causing more salt water to intrude into this system, which will enhance the gravitational circulation.

Wind is also a contributing factor to induce greater mixing between surface and subsurface layers, as well as leading to a less vertically stratified system. The magnitude of these effects would increase with increasing wind magnitude and duration. In time series of velocity and salinity, observed destratifications were almost invariably preceded by large wind-induced mixing. Yet a well-mixed water column by its nature tends to be highly transient and restratification usually occurs soon after the wind abates. This is because the longitudinal baroclinic pressure gradient will act to re-establish stratification as the intensity of wind mixing declines, through the mechanism of gravitational circulation. A well-mixed water column can only be maintained for prolonged periods when buoyancy input from river discharge is low and turbulence kinetic energy input from wind/tide is high. More typically in this system, a moderately stratified water column is intermittently mixed by the wind occurring during the observation period.

For the Elizabeth River system, since its orientation is in the south-north direction, wind from either the south or north will have a stronger effect on it.

Also, since it is a tributary to the lower James, there is an interaction between this 'estuary and sub-estuary system'. As an example, when the west wind blows, it will push some freshwater, driven from the upper James to the lower James, into the Elizabeth. Then, a reverse circulation pattern, even a reverse three-layer circulation, may be formed under special wind conditions (westerly).

One noteworthy point is that there is a non-tidal circulation between the Hampton Roads and the Elizabeth, which might be an important factor for the flushing characteristics of the Elizabeth River. During periods of stratification, there is a very substantial net non-tidal flow, which is set up by the density gradients, and flushing of specific water masses is enhanced. The water masses include both saltier water moving into the Elizabeth near the bottom and freshwater moving out to Hampton Roads near the surface. During periods of homogeneous or well-mixed conditions, this non-tidal flow does not exist. Therefore, the flushing of the Elizabeth is poorest during these periods and the residence time of water in the Elizabeth is increased.

In addition to the wind effects from the above description, both observation and model results show that tides and river discharge also are two important external forcing in determination of the characteristics of the lower James and Elizabeth river estuarine system. Water level, salinity/stratification, and current/circulation all have strong responses to the ebb/flood and spring/neap tidal signals. River discharge strongly affects the strength of water column stratification, but has much less influence on water level.

Wind-induced circulation is an integral part of estuarine dynamics. It generates a surface wind drift layer, which can interact with the non-tidal circulation, either reinforcing or retarding gravitational circulation. In addition, winds are associated with the surface boundary layer, which, when coupled with the bottom boundary layer, provide turbulent mixing in stratified water.

Evaluations of two proposed Craney Island Expansion Designs (Options 7 and 7/5a) under wind events were conducted using global analysis and local analysis. The Eastward Expansion (Option 7) produced less change among global analysis variables than the East/West Expansion (Option 7/5a). Local changes in the residual current field are not significant, except in the vicinity of Craney Island.

Understanding the effects of atmospheric forcing in an estuary is not only important for the hydrodynamic process, but also for the study of biological and chemical consequences. For instance, the stratified-destratified phenomenon induced by wind was reported to be responsible for the replenishment of nutrient and phytoplankton in the surface water (Webb and D'Elia, 1980; Haas et al., 1981), and the transport of oxygen in the bottom water (Kuo et al., 1991). The results presented in this thesis, thus, demonstrate the study is important for further understanding of the ecosystem process in the estuary.

LITERATURE CITED

Boon, J. D., J. M. Brubaker, and G. M. Sisson (2002): Model-assisted Comparison of Circulation Features in a Branching River Estuary. ASCE Estuarine and Coastal Modeling, Proceeding of the 7th International Conference. P384-402.

Browne, D. R. and C. W. Fisher (1988): Tide and tidal currents in the Chesapeake Bay. NOAA Tech. Rep. NOS OMA 3, 143 pp., U.S. Dept. of Commerce, Rockville, MD.

Chant, R. J., and R. E. Wilson (1997): Secondary circulation in a highly stratified estuary. J. Geophys Res., 102: 23,207-23,215.

Elliott, A. J. (1978): Observations the Meteorologically induced circulation in the Potomac estuary. Estuarine and Coastal Marine Science, 6: 285-299.

Fang, C. S., C. S. Welch, and H. H. Gordon (1972): A surface circulation study in middle Elizabeth River. Special Report in Applied Marine Science and Ocean Engineering No. 24, Virginia Institute of Marine Science, Gloucester Point, VA.

Geyer, W. R. (1993): Three-dimensional tidal flow around headlands. J. Geophys. Res., 98: 955-966.

Goodrich, D. M. (1987): Wind-induced destratification in Chesapeake Bay. Journal of Physical Oceanography, 17 (19): 2232-2240.

Goodrich, D. M. (1987): Nontidal exchange processes at the Chesapeake entrance. In: Hydrodynamic Engineering 1987, R. Ragan, editor, American Society of Civil Engineers, New York, pp. 493-498.

Goodrich, D. M. (1988): On meteorologically induced flushing in three U.S. East Coastal estuaries. Estuarine, Coastal & Shelf Research, 26, 111-121.

Haas, L. W. (1977): The effects of the spring-neap tidal cycle on the vertical salinity structure of the James, York and Rappahannock Rivers, Virginia, USA. Estuarine and Coastal Marine Sciences, 5: 485-496.

Haas, L. W., S. J. Hastings, and K. L.Webb (1981): Phytoplankton response to a stratification-mixing cycle in the York River estuary during late summer. In Estuarine and Nutrients (Neilson, B. J. and Cronin, L. E., eds). Humana Press, pp: 619-635.

Hamrick, J. M. (1996): User's manual for the environmental fluid dynamics computer code. Special Report in Applied Marine Science and Ocean Engineering No. 331, Virginia Institute of Marine Science, Gloucester Point, VA, 223 pp.

Hamrick, J. M. and M. Z. Moustafa (1995a): Development of the everglades wetlands hydrodynamic model: 1. Model formulation and physical processes representation. Water Resource Research.

Hamrick, J. M. and M. Z. Moustafa (1995b): Development of the everglades wetlands hydrodynamic model: 2. Computational implementation of the model. Water Resource Research.

Hargis, W. J. (1966): An evaluation of physical and biological effects of the proposed James River Navigation Project. Final report on results of operation James River, Virginia Institute of Marine Sciences Special Report in Applied Marine Science and Ocean Engineering, No. 7, 73 p.

Hargis, W. J. (1969): Utilization of physical and mathematical models in marine water resources research, planning and management. A report for the period 1 Sept 1967-31 Dec 1968 to the Office of Water Resources Research, U.S. Dept of Interior, Contract No 14-01-001-1597, C1214.

Haven, D. S., W. J. Hargis, Jr., and P. C. Kendall (1978): The Oyster Industry in Virginia. Special Papers in Marine Science of the Virginia Institute of Marine Science, No. 4, xlviii-1024.

Hayward D., L.W. Haas, J.D. Boon, III, K.L. Webb, and K.D. Friedland (1986): Empirical models of stratification variation in the York River estuary, Virginia, USA. Lecture Notes on Coastal and Estuarine Studies, Vol. 17: 346-367.

Hepworth, D. and A. Y. Kuo (1989): James River seed oyster bed project. Physical Data Report, I, 1984-1987, Data Rep. 31, Virginia Institute of Marine Science, Gloucester Pt., VA.

Koepfler, E. T., H. I. Kator, R. L. Wetzel, L. W. Haas, and K. L. Webb (1993): Spatial and temporal bacterioplankton dynamics during destratification of the James River Estuary, Virginia, USA, Marine ecology progress series, 102(3): 229-244.

Kuo, A. Y., R. J. Byrne, J. M. Brubaker, and J. H. Posenau (1988): Vertical transport across an estuary front. In J. Dronkers and W. van Leussen (eds.), Physical Processes in Estuaries, Springer-Verlag, Berlin, pp. 93-109.

Kuo, A. Y., R. J. Byrne, P. V. Hyer, E. P. Ruzecki, and J. M. Brubaker (1990): Practical Application of Theory for Tidal-Intrusion Fronts. Journal of Waterway, Port, Coastal, and Ocean Engineering, 116(3): 341-361.

Kuo, A. Y., K. Park, and M., Z. Moustafa (1991): Spatial and temporal variabilities of hypoxia in the Rappahannock River, Virginia. Estuaries,14: 113-121.

Kuo, A. Y., E. P. Ruzecki, and C. S. Fang (1976): The effect of Agnes flood on the salinity structure of the Lower Chesapeake Bay and contiguous waters. In the effects of tropical Storm Agnes on the Chesapeake Bay Estuarine System, CRC Publication #54. The Johns Hopkins University Press, Baltimore, MD, 81-103.

Mann, R. (1988): Distribution of bivalve larvae at a frontal system in the James River, Virginia. Marine ecology progress series, 50(1-2): 29-44.

Mann, R., R. J. Byrne, and B. M. Campos (1988): Dispersal of bivalve larvae at a front in the James River Estuary, Virginia. Journal of Shellfish Research, 7(1):124-125.

Marshall, N. B. (1954): Changes in the physiography of oyster bars in the James River. Va Proc Nat Shellfish Assoc. 45: 113-121.

Paraso, M. C. and A. Valle-Levinson (1996): Meteorological Influence on Sea Level and Water Temperature in the Lower Chesapeake Bay: 1992. Estuaries, vol. 19, No.3, pp: 548-561.

Pritchard, D. W. (1952): Salinity distribution and circulation in the Chesapeake Bay estuarine system. J. Mar. Res., 11:106-123.

Pritchard, D. W. (1954): A study of the salt balance in a coastal pain estuary. J. Mar. Res., 13:133-144.

Pritchard, D. W. (1956): The dynamic structure of a coastal plain estuary. J. Mar. Res., 15:33-42.

Proudman, J. (1955): The effect of friction on progressive wave of tide and surge in an estuary. Proc. R. Soc., London Ser. A 233:407-418.

Proudman, J. (1957): Oscillation of tide and surge in an estuary of finite length. J. Fluid Mech. Vol. 2, 371-382.

Ruzecki, E. P. and W. J. Hargis, Jr. (1988): Interaction between circulation of the estuary of the James River and transport of oyster larvae. In B. J. Neilson, A. Y. Kuo and J. M. Brubaker (eds.), Estuarine Circulation. The Humana Press, Clifton, N. J., pp. 255-278.

Roman, M. R., D. V. Holliday, and L. P. Sanford (2001): Temporal and spatial patterns of zooplankton in the Chesapeake Bay turbidity maximum. Marine Ecology Progress Series, 213: 215-227.

Sharples, J., J.H. Simpson, and J.M. Brubaker (1994): Observations and modeling of periodic stratification in the upper York River estuary, Virginia. Estuaries, Coastal and Shelf Sciences, 38: 301-312.

Shen, J., J. D. Boon, and A. Y. Kuo (1999): A modeling study of a tidal intrusion front and its impact on larval dispersion in the James River estuary, Virginia. Estuaries 22(3a):681-692.

Shen, J. and A. Y. Kuo (1999): Numerical investigation of an estuarine front and its associated eddy. Journal of Waterway, Port, Coastal, and Ocean Engineering 125(3):127-135.

U.S. Army Engineer District, Norfolk (USAED, Norfolk) (1974): The Craney Island Disposal Area- replacement or extension- report of survey investigation- Norfolk Harbor, Virginia. Norfolk, VA.

Valle-Levinson, A. (1995): Observation of barotropic and baroclinic exchanges in the lower Chesapeake Bay. Continental Shelf Research, vol. 15(13): 1631-1647.

Valle-Levinson. A., J. L. Miller, and G. H. Wheeless (1998): Enhanced stratification in the lower Chesapeake Bay following northeasterly winds. Continental Shelf Research, 18: 1631-1647.

Van De Kreeke, J. and K. Robaczewska (1989): Effect of wind on the vertical circulation and stratification in the Volkerak estuary. Netherlands Journal of Sea Research, 23(3): 239-253.

Wang, D. P. and A. J. Elliott (1978): Nontidal variability in the Chesapeake Bay and Potomac River: evidence for nontidal forcing. Journal of Physical Oceanography, 8, 225-232.

Wang, D. P. (1979a): Subtidal sea level variations in Chesapeake Bay and relations to atmospheric forcing. Journal of Physical Oceanography, 9, 413-421.

Wang, D. P. (1979b): Wind driven circulation in the Chesapeake Bay, Winter 1975. Journal of Physical Oceanography, 9, 564-572.

Wang, H. V., S.C. Kim, John D. Boon, A.Y. Kuo, G.M. Sisson, J.M. Brubaker and J.P-Y. Maa (2001): Three dimensional Hydrodynamic Modeling Study Craney Island Eastward Expansion,Lower James River and Elizabeth River,

Virginia. Special Report No. 372 in Applied Marine Science and Ocean Engineering, Virginia Institute of Marine Science, Gloucester Point, Virginia.

Webb, K. L. and C.F. D' Elia (1980): Nutrient and oxygen redistribution during a spring-neap tidal cycle in a temperate estuary. Science 207, 983-985.

Wood, L. and W. J. Hargis (1971): Transport of bivalve larvae in a tidal estuary. Proceedings, 4th European Marine Biology Symposium, edited by D.J. Crisp, pp. 29-44, Cambridge Univ., London.

Zervas, C., S. Duncar, D. Deitemyer, J. Hubbard, J. Culp, T. Landon, M. Connolly, D. Wright, and R. Bourgerie (2000): Effects of Hurricane Floyd on Water Levels. Data Report, NOAA Technical Report NOS CO-OPS 027. Silver Spring, MD.